University of Sussex

Module hierarchy and centralisation in the anatomy and dynamics of human cortex

David Samu

Submitted for the degree of Doctor of Philosophy

University of Sussex

October 2013

Declaration

I hereby declare that this thesis has not been and will not be submitted in whole or in part to another University for the award of any other degree.

Signature:

UNIVERSITY OF SUSSEX

David Samu, Master of Science

Module hierarchy and centralisation in the anatomy and dynamics of human cortex

Summary

Systems neuroscience has recently unveiled numerous fundamental features of the macroscopic architecture of the human brain, the connectome, and we are beginning to understand how characteristics of brain dynamics emerge from the underlying anatomical connectivity. The current work utilises complex network analysis on a high-resolution structural connectivity of the human cortex to identify generic organisation principles, such as centralised, modular and hierarchical properties, as well as specific areas that are pivotal in shaping cortical dynamics and function.

After confirming its small-world and modular architecture, we characterise the cortex' multi-level modular hierarchy, which appears to be reasonably centralised towards the brain's strong global structural core. The potential functional importance of the core and hub regions is assessed by various complex network metrics, such as integration measures, network vulnerability and motif spectrum analysis.

Dynamics facilitated by the large-scale cortical topology is explored by simulating coupled oscillators on the anatomical connectivity. The results indicate that cortical connectivity appears to favour high dynamical complexity over high synchronizability. Taking the ability to entrain other brain regions as a proxy for the threat posed by a potential epileptic focus in a given region, we also show that epileptic foci in topologically more central areas should pose a higher epileptic threat than foci in more peripheral areas.

To assess the influence of macroscopic brain anatomy in shaping global resting state dynamics on slower time scales, we compare empirically obtained functional connectivity data with data from simulating dynamics on the structural connectivity. Despite considerable micro-scale variability between the two functional connectivities, our simulations are able to approximate the profile of the empirical functional connectivity.

Our results outline the combined characteristics a hierarchically modular and reasonably centralised macroscopic architecture of the human cerebral cortex, which, through these topological attributes, appears to facilitate highly complex dynamics and fundamentally shape brain function.

Acknowledgements

First and foremost I am deeply indebted to my primary supervisor, Thomas Nowotny, for constant and invaluable support, as much personally as academically. This thesis would not exist without the always immediate help and encouragement I received from him in the passed three years, that I cannot thank enough. I am also grateful to Thomas for granting me the opportunity to benefit from visiting several excellent conferences.

My second thanks go to Anil Seth, my secondary supervisor, for his always spot-on scientific input, constructive criticism and invaluably supportive positive attitude. I am deeply grateful to my third supervisor, George Kemenes, for the continuous support and advices I received from him during difficult times.

I should like to thank Olaf Sporns and Patric Hagmann for making this work possible by providing me with the dataset used in this study.

For all the great conversations, the work we shared, and, equally importantly, the personal support and good times in and out of office, I would also like to thank my colleagues in the electrophysiology lab, Ildiko Kemenes, Mickey Crossley, Vincenzo Marra, Kevin Staras, Zita László and Zsolt Pirger, as well as the PhD peers in the CCNR lab, Greg Corcoran, Renan Moioli, Colin Reveley, Lucas Wilkins.

I am most grateful to the University of Sussex and the School of Informatics for accepting me as a graduate teaching assistant, and financing my research for this thesis that way. I found participation in teaching a personally rewarding activity as well, that I would like to thank to all the lecturers and students I had the opportunity to worked with.

Finally, I must express my deepest gratitude to my father, whose humanity and working morals will always be examplary for me, and whose firm belief in me persuaded me to start this work.

Contents

List of Figures

List of Tables

Acronyms

BA Brodmann area.

BOLD blood oxygenation level dependent.

CBF cerebral blood flow.

DAC directed acyclic graph.

DMN default mode network.

dMRI diffusion magnetic resonance imaging.

DSI diffusion spectrum imaging.

DTI diffusion tensor imaging.

EC effective connectivity.

ER Erdős-Rényi.

FC functional connectivity.

fMRI functional magnetic resonance imaging.

MRI magnetic resonance imaging.

rCBF regional cerebral blood flow.

ROI region of interest.

SC structural connectivity.

SF scale-free.

SN surrogate network.

SOC self-organised criticality.

Part I

Prologue

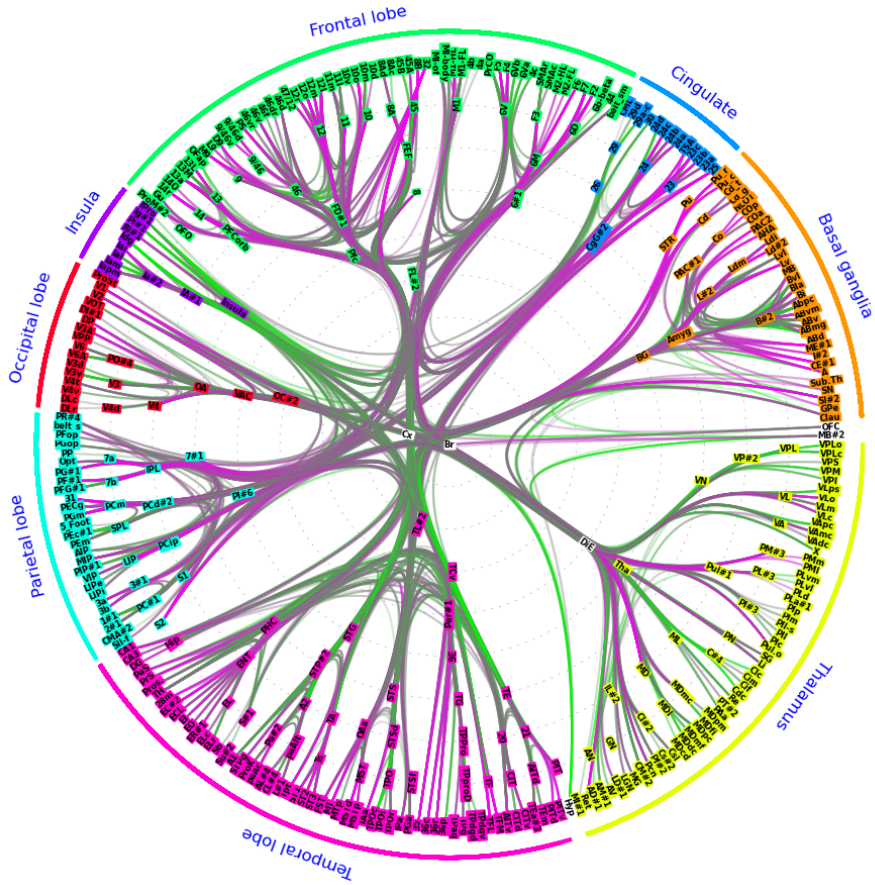

Chapter 1

Introduction to connectomics

Complex network approach in systems neuroscience

The brain is a network of extraordinary complexity on multiple spatial scales. On the macroscopic scale, local regions interconnected by a large number of white-matter projections form an intricate system: the *connectome*. Understanding the organisation principles of the large-scale architecture of the brain, how it shapes brain dynamics and how it ultimately affects function, cognition and behaviour is one of the greatest challenges faced by contemporary neuroscience (Sporns (2010)). In this introductory chapter of the thesis, we present a brief overview of the currently applied methodologies, achieved results and future research directions that are intended to unveil the extraordinarily complex organisation of the brain. At the end of the chapter, we introduce the research questions and goals proposed by the current study.

1.1 The science of complex networks

From the earliest times, mathematical geometry was developed to solve problems involving physical position and distance. In the 18^{th} century, however, Leonhard Euler took a radically different formalisation approach in resolving the famous problem of the Seven Bridges of Königsberg by abstracting away from spatial embeddedness and only taking into account the *relative relations* of the problem's entities (Euler (1736)). That publication is now generally regarded as the birth of a whole new branch of mathematics, which, complementing the traditionally space- and distance-centric view of geometry, is now known as *graph theory*.

Graphs or networks are abstract representations of real-world systems. A graph comprises

a set of nodes (vertexes) and a set of edges (connections or links). *Nodes* represent the basic elements of the system, while network *edges* define the relation between pairs of nodes. Based on the properties and attributes of the edges, graphs can be categorised into several basic types, such as weighted/binary, directed/undirected, spatial/non-spatial graphs, each one with its own application domain and analysis methods (Newman (2003), Boccaletti et al. (2006)).

For a long time, early graph theory was mainly concerned with the study of regular graphs (Kőnig (1936)). The first graph model to characterise complex, heterogeneous and large-scale networks was proposed by Paul Erdős and Alfréd Rényi in the 1950's (Erdös and Rényi (1959), Erdös and Rényi (1960)). The so-called *random graph* model and its statistical analysis was pioneering at its time, and shaped the emerging field of complex networks for decades (Albert and Barabási (2002)). Nevertheless, application of graph theory as a standard analytic tool dates back to the 1920's in the social sciences, that utilise complex network analysis for the quantitative description of social networks since then (Freeman (1996)). In fact, many basic concepts, such as small-worldness (Milgram (1967)), and analysis methods, such as centrality (Freeman (1978)) of modern complex network science were discovered and developed during these early studies on social networks. More recently, network representations of complex systems has prevailed in many fields of the natural sciences as well, and we are still witnessing the emergence of "the new science of networks" (Watts (2004)).

The breakthrough of complex network sciences can be attributed to two key factors. Firstly, the field has undergone considerable theoretical development in the last fifteen years, that has led to a diverse set of widely applicable analytic tools and powerful characterisations of real-world networks such as the small-world (Watts and Strogatz (1998)) and scale-free (Barabási and Albert (1999)) properties[1]. Secondly, thanks to ongoing technological advancements, we are now beginning to explore and map systems of increasing size, complexity and detail from many segments of the world around us. A few examples of these "networkable" systems include the Internet (Faloutsos et al. (1999)), the World Wide Web (Huberman (2001)), gene regulatory networks (Jeong et al. (2001)), social networks (Scott (2000)), semantic associations (Dorogovtsev and Mendes (2001)), ecological food webs (Bascompte et al. (2006)), metabolic pathways (Stelling et al. (2002)) and synaptic connections (Chen et al. (2006)). The fact that all these systems can be represented, analysed and better understood as complex networks of simple nodes and edges has contributed to the rise of complex network sciences, and has led to the notion that the complex network framework is a universal scientific approach (Barabási (2011)).

[1] Although see Keller (2005) for some cautious criticism on the interpretation of these results.

1.2 Complex networks in the neurosciences

1.2.1 Premises and difficulties

The advantages of utilising the framework of complex networks in the neurosciences, just as in any other applied scientific field, lays in the abstraction power of network theory. Representing the nervous system as a network or graph enables the researcher to omit some potentially irrelevant variability of the brain, such as size and surface shape, providing a necessary level of abstraction for longitudinal (Yap et al. (2011)), cross-subject (Alexander-Bloch et al. (2012)), cross-modal (structural, functional, effective) (Honey et al. (2009)) or even cross-species (Sporns and Kötter (2004)) comparison with respect to canonical local or global architectural features that govern brain function, and therefore ultimately shape cognition and behaviour. Complex network science thus offers a principled and systematic framework for system neuroscience to study the structure and function (or dysfunction) of the brain (Bressler and Menon (2010)).

Along with all these promises, the fundamental question of *"What are the networks of the brain?"* remains to be answered. According to the neuron doctrine, one can regard the neurons and their synaptic connections as the nodes and edges of the ultimate network of the brain. Assembling such a neural map from the human brain, however, poses enormous technological and theoretical challenges. It has also been argued that this micro-level description, being highly variable and redundant, is not only unnecessary but also inappropriate to represent the human brain as a network, and an integrative, multi-scale approach is favourable instead (Sporns et al. (2005)).

In the future, we need to continue and further extend and integrate the multi-scale analysis of complex brain networks, as potentially all levels contribute to the emerging dynamics of the whole system (Sporns (2010)). Within the limited resources of the current research project, this work also presents a multi-level study by investigating nodal or regional attributes at the lowest resolution of the investigated brain network, properties of greater structural and modular elements at the meso-scale, as well as global characteristics of the entire network.

1.2.2 Current acquisition techniques and connectivity types

Numerous techniques have been developed to map connectivity networks in the brain. On one end of the spectrum there are highly invasive *in-vitro* and *post-mortem* methods, such as serial block-face scanning electron microscopy (Kleinfeld et al. (2011)), that provide the most direct and highest resolution map of the neural network by entirely reconstructing the neuronal tissue in three dimensions. On the other end, we find various imaging techniques, such as diffusion magnetic resonance imaging (dMRI) (Hagmann et al. (2010a), Yendiki et al. (2011)), which, due to their non-

invasive nature, are compatible to be applied on living human subjects. However, they come with the trade-off of providing only indirect and inaccurate information about the brain network under study, and thus their resolution, reliability and completeness are limited (Jbabdi and Johansen-Berg (2011)). Nonetheless, thanks to the many recent and ongoing developments in novel brain mapping methodologies (reviewed in Leergaard et al. (2012) and in Van Essen and Ugurbil (2012)), the huge gap between these microscopic and macroscopic scales might be filled by new technologies during the coming decades, bringing along a whole new era of mapping the networks of the brain.

Next to the so far discussed structural (anatomical) networks of the brain, the highly dynamic nature of the nervous system necessitates the identification and analysis of other connectivity types describing various aspects of its operation. *Functional connectivity* (FC) measures deviations from statistical independence between distributed neuron populations, and is believed to reflect dynamical couplings between these populations (Friston et al. (1993), Friston (1994)). It is usually calculated as correlation, spectral coherence or phase locking of EEG, MEG or fMRI time series, resulting in a symmetric connectivity measure. As opposed to that, *effective connectivity* (EC) describes the directed, causal network of interactions between neural elements (Friston (1994)), and is usually derived by some complex data processing and modelling technique (Büchel and Friston (2000)). These two non-physical connectivity modalities complement the traditional structural connectivity by providing a network representation of the dynamical interactions between the neuron populations. Consequently, unlike SC, FC and EC are highly time and stimulus dependent and often statistically non-stationary.

1.2.3 Traditional and current research themes

Early studies on the large-scale characterisation of brain networks were largely limited to the nervous system of model animals, such as the *Caenorhabditis elegans* (White et al. (1986)), the rat (Burns and Young (2000)), the cat (Scannell et al. (1999)) and the macaque (Felleman and Van Essen (1991), Young (1993)). These datasets were laboriously accumulated by a large number of research groups through years or even decades, from thousands of animal subjects, and by various invasive means, such as serial electron microscopy and staining methods. In spite of the tremendous amount of labour and the state-of-art techniques of the time that the acquisition of these datasets required, they are limited to the representation of a 'standard' or 'idealised' brain of an animal species (Bezgin et al. (2012)), which, due to applied methodology, is necessarily incomplete and inherently inconsistent (Modha and Singh (2010)).

Recent advancement of non-invasive anatomical (Conturo et al. (1999), Mori et al. (1999)) and functional (Huettel et al. (2009), Pan et al. (2011)) imaging techniques, along with the development

of automated, high throughput post-processing techniques (e.g., Cammoun et al. (2012)), have opened a whole new era in brain network research and brought to the realm of comparative human subjects studies (Bressler and Menon (2010)). Recently, comparative connectome analysis has proved to be an indispensable methodology in unveiling fundamental organisational differences in the large-scale architecture of the brains of various subject groups. The focus of these diverse set of studies include development, maturation and ageing of brain connectivity (eg. Fair et al. (2008), Meunier et al. (2009a), Fair et al. (2010), Homae et al. (2010) Hagmann et al. (2010b), Homae et al. (2010), Yap et al. (2011), Zuo et al. (2011), Tomasi and Volkow (2012)), gender specific connectome differences (Hagmann et al. (2006), Duarte-Carvajalino et al. (2011), Zuo et al. (2011)), alteration in brain connectivity due to practise, personality and intellectual abilities (van den Heuvel et al. (2009b), Chiang et al. (2009), Adelstein et al. (2011), Jang et al. (2011), Hasenkamp and Barsalou (2012)), connectomical correlates of neurological disorders (for a review, see Guye et al. (2010)), in particularly in schizophrenia (Bassett et al. (2008), Lynall et al. (2010), van den Heuvel et al. (2010), Zalesky et al. (2011), Alexander-Bloch et al. (2012), Bassett et al. (2012)), and task dependent reconfiguration of functional connectivity (Fries (2005), Bassett and Bullmore (2006), Kitzbichler et al. (2011)).

The scientific employability of the complex network approach in the neurosciences, even in describing the inherently spatial and highly dynamic networks of the brain, has been demonstrated by numerous studies that successfully linked brain structure and function to cognition and behaviour. For instance, van den Heuvel et al. (2009b) showed that higher intellectual performance (IQ) is accompanied by higher functional efficiency (shorter path lengths in resting state functional connectivity [rsFC]). In practical terms on the other hand, perhaps one of the most attainable, but nonetheless extremely beneficial, application of complex network analysis of the brain would be its medical utilisation in detecting topological markers of neuropathological diseases (Nucifora et al. (2007), Reijneveld et al. (2007), Bullmore and Sporns (2009)), which is currently one of the most active and promising research area of the field.

1.2.4 Current challenges and future research directions

Given the various spatial and topological scales (such as nodal, node group, global) and the large number of partially inter-related analysis tools and models one can apply, both the scientific research and future medical applications of brain network analysis faces significant data mining challenges. To that end, several promising multi-scale and multi-method techniques have been formulated and tested with the aim to develop a comprehensive, standard framework for the analysis of complex brain networks (Meskaldji et al. (2011), Echtermeyer et al. (2011a), Echtermeyer et al.

(2011b)). However, due to the ongoing technological and theoretical progression, the field is still largely on the move, and the matured theoretical consensus and the long-awaited breakthrough towards medical applications have yet to appear.

Realising the fundamental need for data sharing among research groups, several global initiatives have been launched recently with the aim to accelerate scientific progress in the field by cooperation of distant and otherwise independent research groups. The 1000 Functional Connectomes Project[2] sets out the goal of establishing an open-access database for the fMRI community (Biswal et al. (2010)). To date, the project has successfully aggregated over a thousand resting-state fMRI scan datasets from human subjects around the world, and has made them publicly available for the research community.

Another initiative, the Human Connectome Project[3] (Toga et al. (2012)), aims to "provide the foundation for the detailed mapping of the human connectome". The main goals of the project include the collection and dissemination of connectomic, behavioural, and genotype data of normal subjects, using novel, sophisticated data acquisition methods and a web-based informatics infrastructure. The project has already generated over 50 publications to date, and holds a great potential to develop and establish future routes to the research of human connectomics.

1.3 The scope of the thesis

Recent development in the theory and analysis tools of the complex network sciences has led to the discovery of numerous organisation principles in the large-scale structural anatomy of the brain. The most prominent of these features are the brain's small-world (Sporns et al. (2000)), hierarchical (Bassett et al. (2008)) and modular architecture (Hilgetag et al. (2000)), as well as its strong structural core (Hagmann et al. (2008)) and rich-club organisation (Van den Heuvel and Sporns (2011)). However, despite the increasing number of such findings, integrative studies on singular datasets to date are largely missing, thus the relation, relative significance and potential functional implications of these concepts on the brain are still unclear.

In this work, we perform a systematic series of analyses on the human cortical connectome with the aim to comparatively assess and relate some of its fundamental organisational principles. Our goal is to integrate the obtained results into a coherent description of the large-scale network architecture of the human brain, and then to relate the found structural properties to the dynamics and function of the cortex. The importance of such comprehensive framework is underscored by numerous recent studies able to relate a wide range of brain disorders to some fundamental

[2] http://fcon_1000.projects.nitrc.org/

[3] http://www.humanconnectomeproject.org/

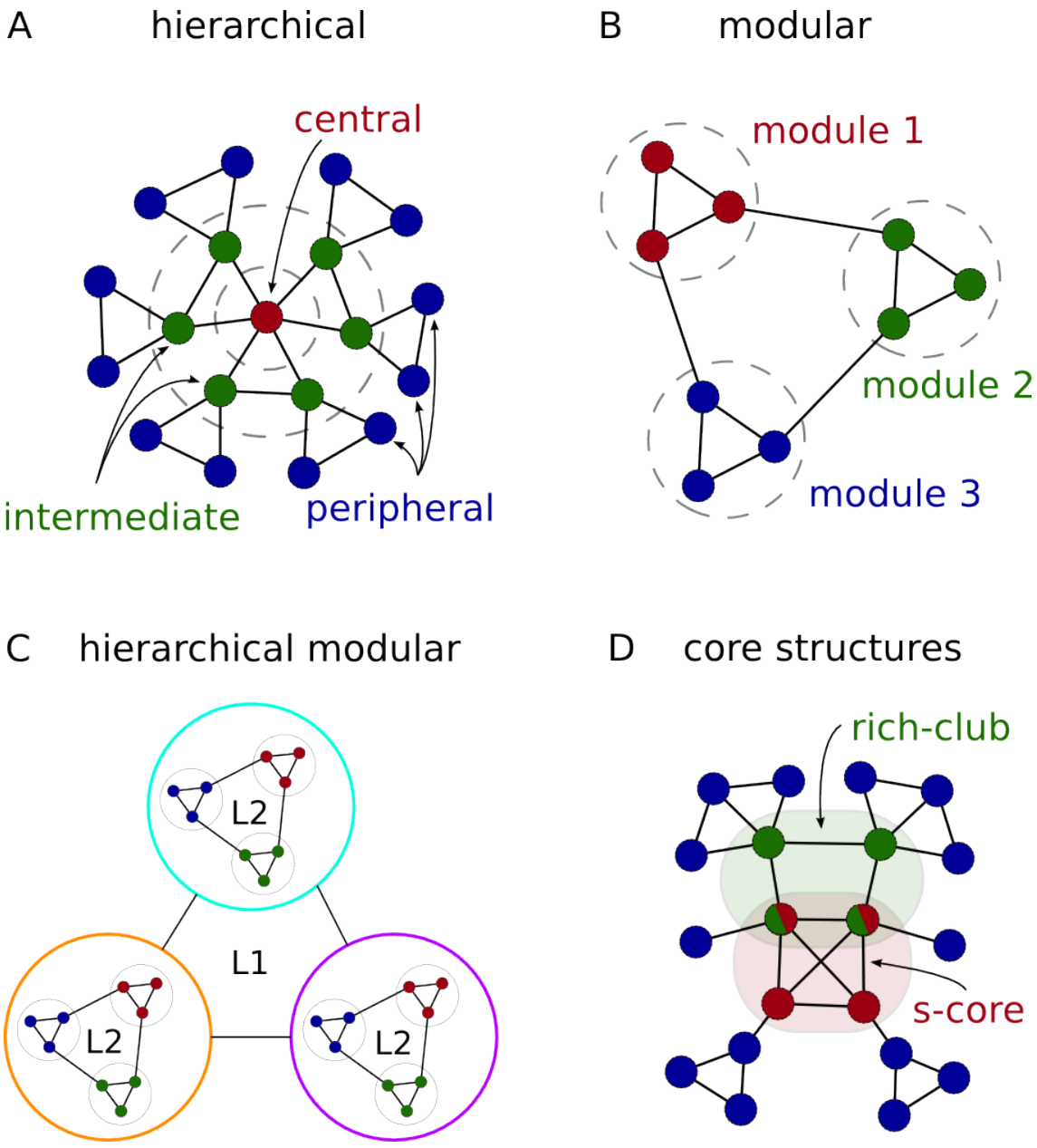

Figure 1.1: **Illustration of network organisation principles investigated in the current study.** (A) A three-level hierarchical network architecture composed of a central, an intermediate and a peripheral layer. (B) Modular structure composed of a set of highly intra-connected but sparsely inter-connected group of regions (modules, clusters or communities). (C) A hierarchical modular network architecture. Modules of the network (on level L1) are themselves composed of smaller modules (on level L2). (D) Two candidate core structures of a network: rich-club (highest degree regions) and s-core (most densely intra-connected regions). Notice the overlap between the two structures.

deviation in its large-scale structural architecture (eg. Bassett et al. (2008), Verstraete et al. (2010), Zalesky et al. (2011), Alexander-Bloch et al. (2012)). Thus, apart from promising us new insights into the organisation and operation of the healthy human brain, such a network level description may prove to be invaluable in understanding the pathogenesis of, as well as developing new treatments to, common neurological and psychiatric brain disorders, such as Alzheimer's disease, Parkinson's disease, amyotrophic lateral sclerosis, autism, schizophrenia and epilepsy (Bullmore and Sporns (2009)).

The organisation of the thesis is the following. We will begin with introducing the cortical connectivity dataset (Chapter 2) and the null-hypothesis (surrogate) networks (Chapter 3) to be used during the study. After that, we shall investigate a number of earlier findings on the organisation of the connectome, such as its integration and segregation properties and small-world architecture (Chapter 4), modular, core, rich-club and hub structures, as well as some of its widely assumed, but yet relatively unexplored features, such as its hierarchical and hierarchically modular architecture (Chapter 5). Some of the organisation principles to be investigated are illustrated on Figure 1.1. Along the way, we shall assess to what extent each of these features is the direct consequence of the basic topological and spatial properties and constraints of the cortical connectivity, in order to identify those features that are presumably the results of some higher organisation principles of the cortical connectivity, and hence may possess higher functional relevance. This analysis will be performed on the full resolution of the high resolution cortical dataset of Hagmann et al. (2008).

After the purely structural analysis of the cortical connectome, we shall turn our attention to the exploration of the relation between network anatomy, dynamics and function. The nature of the dynamics facilitated on fast time scales by the large-scale cortical topology will be explored by simulating a minimal model, composed of coupled oscillators on the anatomical connectivity of the cortex (Chapter 7). Specifically, we shall investigate the cortex' synchronizability and dynamical complexity facilitated by its anatomical connectivity, along with the role of some topologically distinguished cortical areas in these processes. Additionally, taking the ability to entrain other brain regions as a proxy for the threat posed by a potential epileptic focus in a given region, we shall also evaluate which cortical areas are the most effective in propagating synchronous activity, thus posing higher epileptic threat during white-matter mediated cortico-cortical spread of epileptiform seizures.

To assess the influence of macroscopic brain anatomy in shaping global resting state dynamics on slower time scales, we shall compare empirically obtained functional connectivity data with data from simulated dynamics on the structural connectivity of the cortex (Chapter 8). As a more detailed analysis of the structure – function relation in the human cortex, we shall also investigate

the resemblance of structural organisation features in both the empirical and simulated functional connectivities in order to gain further insight into the relation between more general features of brain structural and function.

We finish with discussing the obtained results and pointing to potential directions of future research (Chapter 9). The appendix of the thesis contains the mathematical definitions of some common complex network measures, the brief summary of the analysis of a diverse set of brain networks, and various technical information related to the conducted research.

Chapter 2

The human cortical connectome

In the first chapter, we discussed how the analysis of any brain network crucially depends on the nature of nodes and edges. With this in mind, in this chapter we introduce the structural connectivity to be used throughout this work. First, we describe the applied acquisition method and discuss its strengths and limitations. Then, we provide an introduction to the basic properties of the obtained cortical network by discussing its parcellation scheme, anatomical hierarchy, resolution and some fundamental topological features.

2.1 Introduction of the cortical connectivity dataset

Since its introduction, diffusion magnetic resonance imaging (dMRI) has revolutionised non-invasive imaging of human brain anatomy (Mori and Barker (1999)). Recently, a novel and powerful brain mapping technique has been developed in Lausanne, Switzerland by Patric Hagmann and his colleagues, combining cutting-edge brain imaging and post-processing tools. The detailed description of the technique's processing pipeline was first published in Hagmann et al. (2007), which was shortly followed by a research paper unveiling the structural core of the cerebral cortex (Hagmann et al. (2008)).

The method aims to provide a comprehensive map of the large-scale connectivity of the human brain, the *connectome* (Sporns et al. (2005)), by tracing the white matter projections linking pairs of cortical brain sites. The technique produces a compact network representation of cortical gray matter regions as network nodes, and their interconnecting white matter fibre bundles as edges. In this section, due to its prime importance to the forthcoming analysis, we provide a brief introduction to the technique's construction procedure and the basic attributes of the connectivity networks it yields.

2.1.1 The acquisition technique

Network construction

The construction method of Hagmann et al. proceeds through several intermediate stages to the final structural connectivity network (Hagmann et al. (2007), Cammoun et al. (2012)). At the first step, a set of cortical areas, the regions of interest (ROIs), is determined by partitioning the brain's white matter-gray matter boundary firstly into 66 anatomical subregions, and then further dividing each subregion into a number of ROIs. This iterative procedure results in a complete, hierarchical and non-overlapping partitioning of the cortical surface into approximately equal size ROIs, the nodes of the network. Independently of this step, the so-called *diffusion map* (voxel-wise water diffusion intensity) of the brain is calculated from diffusion spectrum MRI (DSI) scanning (Wedeen et al. (2005)). Harnessing the fact that white matter bundles shape the primary direction of local water flow in the brain (Schmahmann et al. (2007)), this diffusion map is then used to track cortico-cortical white matter projections by a tractography algorithm (Conturo et al. (1999)).

In the final step, the cortical regions and the tracked fibres (typically around three million pieces) are aggregated into a network by taking each region pair and bundling all fibres connecting the two ROIs into a single cortical projection. Each one of these final, aggregated bundles, represented by an edge in the network, possesses two important attributes: a connection length, which is the average trajectory length of the fibres composing the bundle, and a connection weight or density, which is the average of the number of fibres per cortical surface unit on the two target sites of the bundle. The result of the entire procedure is an undirected, weighted and hierarchical network that represents the large-scale white matter connectivity between cortical gray matter regions of the brain.

Reliability and robustness

Proving the reliability and accuracy of a new measurement technique always requires verification by already established methods (Bland and Altman (1986)). While numerous early assessment tests pointed to the fidelity of the above acquisition technique (Hagmann et al. (2008)), Cammoun et al. (2012) carried out an extensive validation test on the procedure. In that work, the authors showed that known fibre tract bundles with various length and projection properties (eg. homotopic, or longitudinal) are readily identifiable in the connection matrices at essentially every resolution (i.e., n = 66, 133, 241, 483 and 998 ROIs).

Additionally, the robustness of the technique was also assessed by a three-step repeatability test: i) by running the processing pipeline twice on the same dataset (scans), ii) by scanning and

processing the same group of subjects twice, and iii) by assessing the pairwise intervariability between a group of 20 subjects. The test results verified the robustness of the technique with considerably high correlation values (between 0.745 and 0.998), and showed at the same time two, fairly intuitive trends: mean correlations decline with higher measurement variability from test i) through ii) to iii) (.977, .874 and .745 at n=998 nodes), and from lower to higher resolution (0.998 and 0.977 for test i)). The latter trend points to the importance of the resolution of investigation, which should be carefully chosen in accordance with the requirements of the specific application, and kept in mind throughout the analysis (Fornito et al. (2010), Bassett et al. (2011)).

Cross-validation of the DSI method with more direct, classical anatomical techniques is an essential, but difficult step for establishing its reliability. Due to the lack of available anatomical tract tracing data for the human brain, researchers have been restricted to carry out DSI validation studies in model animals, such as the rat, mini-pigs, or the macaque. In Schmahmann et al. (2007), DSI mapping was shown to reconstruct the major features of the long-range association tracts of the macaque brain obtained by histological tract tracing, thus providing indirect support for the validity of diffusion imaging data obtained from the human brain. Another cross-technique validation test was carried out by Hagmann et al. (2008), who compared DSI data of the macaque brain with tract tracing data in the CoCoMac database (Kötter (2004)). Their results revealed a high degree of overlap between DSI and classical tract tracing anatomy, with 79% of the DSI connections matched with identified connections from the CoCoMac database, a further 15% were placed in positions from which information was unavailable in CoCoMac, and only 6% of the obtained DSI connections were reported to be absent in CoCoMac.

Methodological advantages and limitations

The above methodology and its technical realisation come with several advantages, currently unmatched by any other brain mapping technique (Hagmann et al. (2010a)). Firstly, the procedure produces a reasonably high resolution network of the entire living human brain in a non-invasive manner, making it compatible with future medical applications (Reijneveld et al. (2007), Bullmore and Sporns (2009)). Secondly, the parcellation of each subject's brain is registered uniformly with a generic labelled mesh template (Fischl et al. (2004)), allowing for direct cross-modal (structural and functional) comparison (Honey et al. (2009)) as well as for inter-subject cross-comparison (Hagmann et al. (2008)) on the same (i.e., equivalent) set of brain regions, rendering the technique a highly valuable scientific research tool. Thirdly, the method yields both weight and length information for each tracked fibre tract connection, enabling topological, spatial as well as hybrid, spatio-topological investigations of the connectome (Kaiser (2011), Wedeen et al. (2012)).

Fourthly, the automated nature of the technique (Fischl et al. (2004), Cammoun et al. (2012)) makes it a highly efficient and controllable acquisition procedure, in contrast with for example the traditional histological and tracer techniques (Köbbert et al. (2000)).

However, along with the numerous advantages discussed above, the procedure also comes with a number of shortcomings. The most severe ones, originating from the limitations of current DSI and tractography techniques, are *i)* the lack of directionality information on the resulting network, and *ii)* the reduced capability to track fibre crossings and wide angular changes along the trajectory of the fibre tracts (Zhan and Yang (2006)). A further deficiency of the specific network utilised in this research is its purely cortical nature, missing all subcortical areas, such as the thalamus or the brain stem, thus restricting our investigation to the human neocortex.

The lack of fibre polarity (limitation *i)* above) is an inherent shortcoming of the DSI tractography technique, originating from the indifference of water diffusion in efferent and afferent axons (Hagmann et al. (2010a)). Indeed, the availability of fibre directionality would not only enrich the forthcoming analysis of this work, but also open up entirely new research questions, such as how closely the directed effective connectivity (Friston (1994)) is related to and shaped by the polarity of its underlying structural connectivity. Promising preliminary studies have show the potential of multi-modal approaches to tackle this problem, where the locations of the fibre tracts provided by diffusion tractography are complemented by polarity measurements by some other techniques, such as magneto-encephalography (MEG) (e.g., Stufflebeam et al. (2008)). For the current work, however, we have to accept the non-directed nature of cortical network under study. Nonetheless, there are two arguments mitigating the severity of this limitation. Firstly, the majority of cortico-cortical connections in the macaque cortex were found to be reciprocal (Felleman and Van Essen (1991)), suggesting that the undirected network representation of the cortical connectivity may be a simplified, but reasonable approximation. Secondly, even at the currently investigated relatively high network resolution (i.e., millimetre scale), the high number of axons in each voxel ($\sim 10^5$, Aboitiz et al. (1992)) makes the presence of axons running in both directions in any single fibre bundle highly probable, rendering the question of polarity somewhat less critical. Nonetheless, it is of prime importance for future connectome research to find a way to incorporate the connection polarity of the large-scale brain connectivities, and thus increase network representation accuracy as well as enrich and extend connectome analysis (Jbabdi and Johansen-Berg (2011)).

The ability of diffusion tractography methods to detect and distinguish more complex axonal relations, such as crossing, fanning and bending of multiple fibres (limitation *ii)* above) has gone through significant improvements in the last decade (Jbabdi and Johansen-Berg (2011)). While the earliest standard method of diffusion MRI, diffusion tensor imaging (DTI) (Pierpaoli et al. (1996))

was restricted to capture a single water diffusion direction per voxel, diffusion spectrum imaging (DSI) (Wedeen et al. (2005)) models diffusion with a non-Gaussian distribution, making this more advanced technique capable of measuring intra-voxel diffusion heterogeneity caused by crossing neuronal tracts (Behrens et al. (2007), Wedeen et al. (2008)). Spreading or fanning of fibres, typical e.g. for the entire coronal radiata, or when tracts arrive at the cortex, is an abundant phenomenon in the brain that is still not captured adequately by current tractography methods, however, promising attempts at better modelling have been made recently (Descoteaux et al. (2009)).

Diffusion tractography, despite all the advances made in the field, still suffers from a number of serious limitation that researchers must bear in mind while working with such datasets (Hagmann et al. (2010a), Jbabdi and Johansen-Berg (2011)). One such limitation is spatial dependence, introduced by the accumulation of errors and uncertainties during the tracking process, practically making long-range connections susceptible to be under-represented in diffusion tractography mapped brain networks. Another deficiency is the likely under-representation of non-myelinated axons, as axonal myelin sheaths, facilitating the diffusion of the water molecules preferentially along their main direction, are more easily detectable by tractography.

Nevertheless, if interpreted with its above discussed flaws in mind, diffusion tractography provides powerful means for the study of human brain anatomy, and holds an enormous potential for the future of brain research and for medical applications (Bressler and Menon (2010)). The simultaneous advances in data acquisition, modelling and algorithmic methods in the field continuously increase our confidence on the reliability of mapped fibre tracts (Jbabdi and Johansen-Berg (2011)). Among these novel data acquisition developments are accelerated sequences (Feinberg et al. (2010)) and high field MRI (e.g., 7T) (Heidemann et al. (2010)), that will ultimately allow for higher orientation and spatial resolution and more complex micro-structural modelling in the near future.

In summary, we conclude that the acquisition method of the structural connectivity network to be utilised in the current study, with all its deficiencies discussed above, still provides a detailed, complete and reliable large-scale representation of the human brain's cerebral gray matter regions and their interconnecting white matter fibre bundles (Pan et al. (2011)). In the next section, we start the analysis of the cortical connectivity to be utilised in this study, first published in Hagmann et al. (2008), by looking into some of its most basic network characteristics, before proceeding to its detailed investigation by some more complex network analysis methods in the forthcoming chapters.

2.2 Attributes and basic properties of the cortical connectivity network

2.2.1 Cortical parcellation, anatomical hierarchy and network resolution

By the nature of its processing pipeline, the network originally consists of a two-level hierarchical parcellation of the cortex: it is composed of 66 anatomical regions at the higher level, and contains 998 ROI at the lower level (Hagmann et al. (2008)). The parcellation scheme of the dataset, defining these resolutions, is a core element of the constructed network. The procedure leads to a network that covers the entire cortices of both hemispheres, but no subcortical area is included.

In the first step of this multi-stage parcellation process, using the cortical surface construction software Freesurfer (Dale et al. (1999)), Hagmann et al. divided the surface of the cortex into 66 non-overlapping regions (33 on each hemispheres), identified by ”clear anatomical landmarks”. Then the individual brain of each subject was registered on this labelled mesh template, leading to a standardised parcellated representation of each of the five participants' brains on an ”average” brain surface.

In the second step, each of these 66 cortical regions were subdivided on the Freesurfer average brain into a set of small and compact, approximately equal size (about 1.5cm^2) subregions, leading to 998 ROIs at the highest connectivity resolution. For a detailed introduction of this subdivision algorithm, see Hagmann et al. (2007) and Cammoun et al. (2012). In the resultant sub-parcellation every ROI belongs to one and only one of the 66 anatomical region, and each one of the 66 regions is fully covered by its ROIs in a non-overlapping manner, hence defining a multi-level hierarchical connectivity network.

Several previous studies have chosen to lower the resolution of the 998-ROI network to the 66-region level, and performed analysis solely on that computationally less demanding, coarser network (e.g., Honey et al. (2010), Cabral et al. (2011), Shanahan and Wildie (2012)). This approach, however, while generating spatially compatible results with those of earlier low resolution studies (e.g., Sporns and Kötter (2004), Sporns et al. (2007), Honey et al. (2007), Deco et al. (2009)), omits the available finer (higher-resolution) of the connectivity, which is likely to affect the outcome of complex network analysis (Wang et al. (2009), Fornito et al. (2010), Zalesky et al. (2010)). Therefore, in order to obtain the most accurate and detailed results the dataset allows for, we carry out all analysis on the high resolution, 998-node anatomical connectivity network in the present study. This also applies to the meso-scale, structural level and macro-scale, global analyses, for which properties of groups of nodes will be derived (averaged or summed) from single-node results.

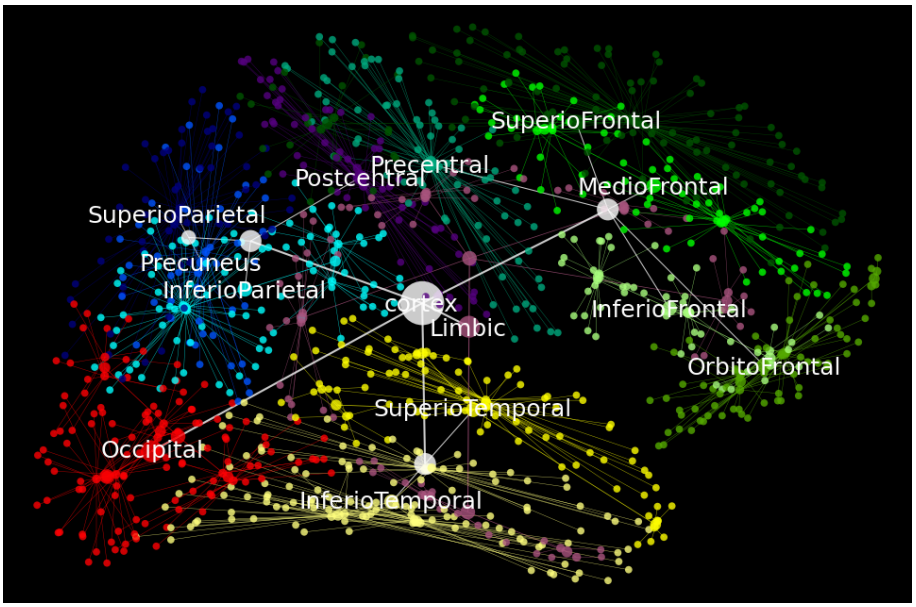

Figure 2.1: **Network hierarchy in anatomical space, coronal projection.** Labels of main anatomical structures are placed onto the 'centre of mass' of their constituting regions. Every node of the hierarchy network is connected to its parent node, 'cortex' in the centre is the root node of the network hierarchy.

Multi-scale investigations on different levels of the network hierarchy has proved to be a valuable approach in exploring the topological (eg. Van den Heuvel and Sporns (2011)) and functional (eg. Bassett et al. (2012)) properties of brain networks. With this in mind, we further extended the network hierarchy with additional greater anatomical structures, in order to gain more flexibility in multi-scale analysis. Our final network possesses a five level deep, unbalanced hierarchy, shown in Figure 2.1 and 2.3, with the following main anatomical structures: the frontal lobe is divided into *inferio-frontal*, *medio-frontal*, *orbito-frontal*, *superio-frontal* and *precentral* areas, the parietal lobe to *inferio-parietal*, *superio-parietal*, *precuneus* and *postcentral* areas, the temporal lobe is split into *inferio-temporal* and *superio-temporal* areas, and finally the *occipital* lobe and the *limbic* system are both kept as anatomical structures on their own. In the forthcoming research, we shall use these thirteen, bi-hemispherically organised anatomical structures to carry out comparative meso-scale analysis.

2.2.2 Basic network properties

The structural network at its highest resolution consists of 998 nodes, each representing an area of the cortical surface of approximately 1.5cm^2 size (in the following: region), and possesses 17865 undirected and weighted connections with additional fibre tract length information. This results in

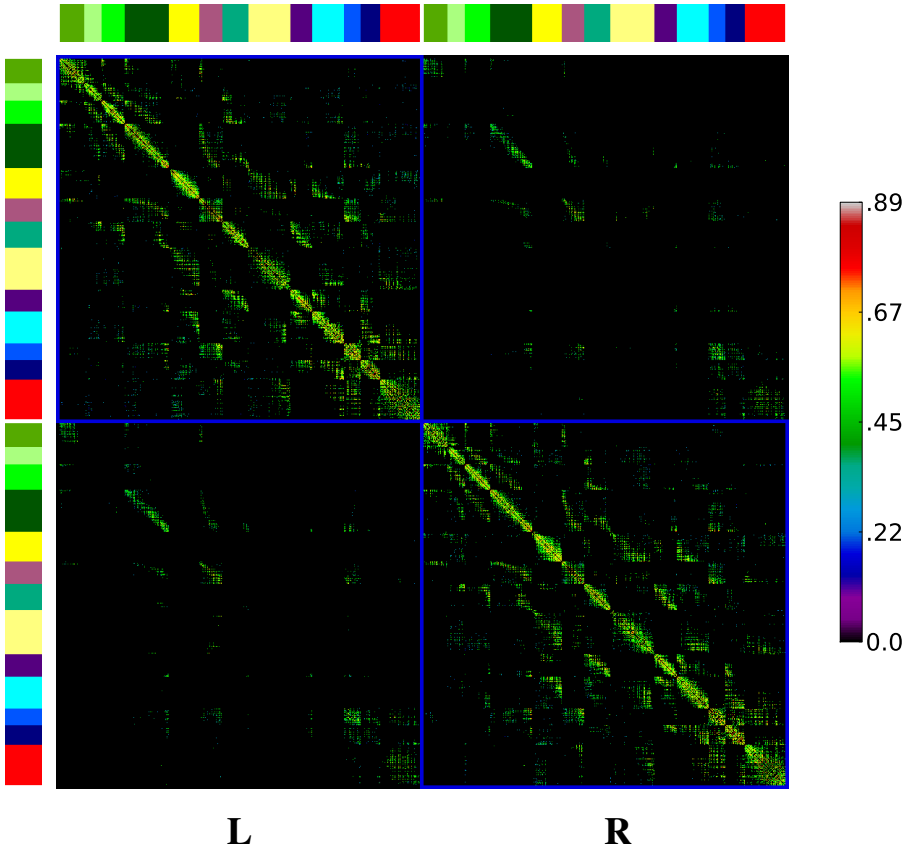

Figure 2.2: **Structural connectivity matrix.** Cortical regions are organised by hemisphere (top left sub-square is left, bottom right is right hemisphere), grouped by their containing anatomical structures (left and top colour stripes, for structural colour code, see Figure 2.3), and ordered by their spatial positions along the fronto-caudal axis (after Cammoun et al. (2012)). Matrix values represent connection weights, colour code is shown on colour bar on the right side.

a sparse, 3.59% connection density network with 35.8 mean degree of the nodes.

Out of the 998 nodes, nine (five limbic, three superio-temporal and one inferiotemporal) regions (0.9%) do not possess any connections, rendering them disconnected from the connected part of the network. However, while presumably being only weakly connected, it is unlikely that these nine regions have no white matter fibre tracts connecting them to the rest of the cortex. Instead this disconnectedness most probably originates from the above discussed limitations of the acquisition process, and warns about the inevitable incompleteness of the dataset.

For the remainder of the current study, these nine unconnected nodes will be discarded from the analysis due to their topologically separatedness from the rest of the network.

2.2.3 Network visualisation

The connectivity matrix of the network is shown in Figure 2.2. To illustrate the importance of a well structured connectivity matrix visualisation in gaining insights into the network's basic organisation properties, we follow the region ordering applied in Cammoun et al. (2012). In Figure 2.2, regions are firstly grouped by hemisphere (top left sub-squares is left, bottom right is right hemisphere), then by main anatomical structures (see colour stripes on left and top sides), and finally ordered along the fronto-caudal axis in anatomical space.

This ordering of the connectivity matrix enables us to verify some of the known anatomical features of the large-scale cortical network solely by visual inspection. Specifically, the predominantly local and iso-hemispheric connectivity of the cortex (Braitenberg and Schuz (1998)) is readily identifiable in the higher connection densities along the matrix's main diagonal in top left and bottom right sub-squares. Inter-hemispheric connectivity is contained in the bottom left and top right sub-squares of the matrix. More frequent projections between ipsilateral region-pairs is observable by the higher connection densities around the main diagonal of these subsquares. Furthermore, the structural ordering of the connectivity matrix also allows us to detect structure specific differences in ipsilateral connection densities: while there is a marked level of cross-connectivity between the left and right parts of the *occipital*, *superio-parietal*, *precuneus*, *limbic*, *superio-frontal* and *orbito-frontal* cortices, we can see no such connection within the *inferio-temporal* and *superio-temporal* cortices. This is consistent with the more medial position of the former structures and the highly lateral location of the latter group.

Figure 2.3 shows the cortical network on an abstract hierarchical radial layout (Holten (2006), Appendix E) as well as on projections in anatomical space. For clarity, only 10% (n=1786) of the strongest (highest weight) connections are shown. Both visualisations demonstrate that these strongest connections are well-distributed throughout the cortical network. However, it is also noticeable on the radial layout that the 18 parahippocampal regions in the limbic system have no such strong connection, while regions in the fusiform (FUS, in *inferio-temporal* cortex) contain only a few of those strong connections, suggesting weaker weighted connectedness of these structures compared to the rest of the network. At this point, however, just as in the case of the nine completely disconnected regions (see above), we also have to bear in mind the imperfect nature of the dataset originating from the limitations of diffusion tractography (Section 2.1.1). Specifically, due to their inferior and lateral locations, both the parahippocampal gyrus and fusiform cortex are likely to be connected to the rest of the cortex through predominantly long-range and possibly highly curved fibre bundles, the tracking of which is currently error-prone in diffusion tractography. Lower or non-myelinated axons of these regions can also cause their low connectedness in the

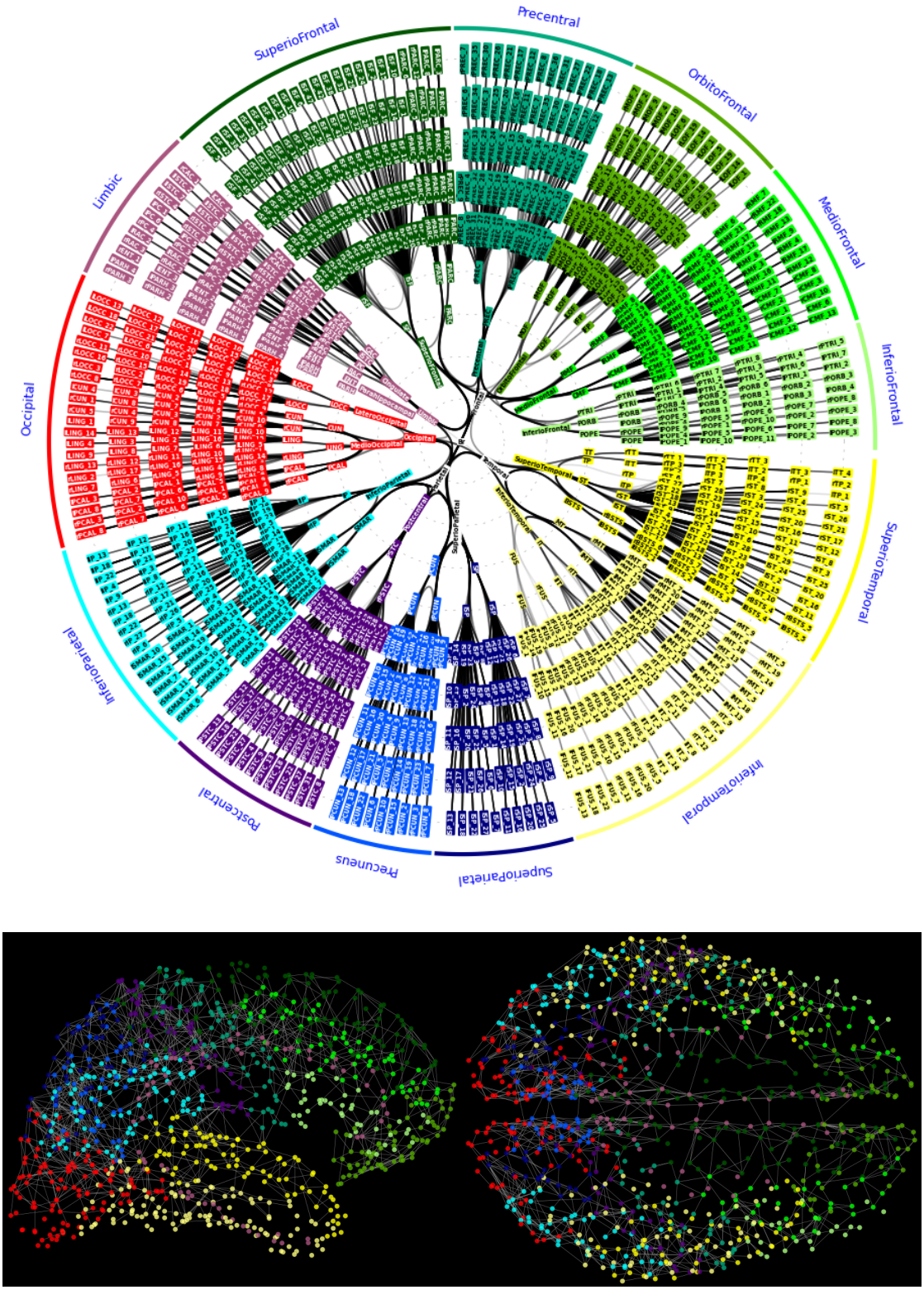

Figure 2.3: **Visualization of structural connectivity on radial layout and projections.** Top: all 998 cortical regions (5 outermost circles) along with their 72 hierarchically embedded container structures (5 innermost circles) placed on radial layout (Appendix E), grouped by main structures (see sectors at perimeter). Bottom: coronal (left) and horizontal (right) projections. On all three subfigures, only the strongest 10% (n=1786) of the connections are shown for clarity.

current dataset. All the above possible cases need to be carefully checked before drawing any further conclusions about the extraordinarily low connectedness found in these regions.

In this chapter we qualitatively introduced and visually illustrated some of the basic properties of the large-scale connectome of the human cortex. It is easy to recognise, that further characterisation of this highly complex network requires advanced network analysis methods. In the forthcoming chapters, we shall systematically uncover the topological and spatial organisation features of the cortical connectome at macro-, meso- and micro-scale with the aid of quantitative complex network analysis tools.

Chapter 3

Surrogate networks

In this chapter, we introduce our surrogate or null-hypothesis networks, that play a crucial role in the forthcoming analysis. After describing their purpose, properties and generation method, we will evaluate the generated surrogate networks against a set of validation tests in order to verify their suitability for the current research.

3.1 Need for a null-hypothesis

Measures of complex networks are highly influenced (i.e., quantitatively biased) by more fundamental properties of the network, such as its number of nodes and edges (Rubinov and Sporns (2010), Zalesky et al. (2010)). This network-specificity renders the interpretation and comparison of results of complex network measures non-trivial. For example, how should one compare the efficiencies of a 100-node and a 1000-node network just by looking at their individual global efficiency values?

A common approach to test the significance of some network property is the so-called surrogate or null-hypothesis comparison (Rubinov and Sporns (2010)). According to this analysis technique, the set of *a priori* chosen surrogate networks represent a null-hypothesis of the investigated network property by preserving some a priori chosen basic features of the network under investigation, but, at the same time, lacking its "higher" organisational characteristics. Direct quantitative comparison with, or normalisation by, these "basically similar" surrogate networks enables the researcher to draw conclusions on how significant a specific topological property of the network is with respect to the chosen basic properties.

Additionally, surrogate comparison also makes quantitative and qualitative cross-comparison between fundamentally dissimilar networks possible. For example, considering their sizes and connections densities, the segregation of network A can be more significant than that of network

B, in spite of their individual global segregation indices alone suggesting the opposite. Surrogate network comparison, as it will be used in the current study, also enables researchers to test if some basic network properties induce, or at least contribute to, the expression of some other, more global and complex organisation features of the network under study.

3.2 Surrogate network generation

3.2.1 Choosing the appropriate surrogate types

Traditional approaches

Traditionally, in determining the appropriate surrogate networks, the most widely used null-hypothesis properties are the *size* (number of nodes), *connection density* (number of edges) and *degree distribution* (the number of connections of each node) of the network. This approach has proved to be sufficient for the topological investigation of many abstract, not spatial-embedded networks, for example the World Wide Web, food-webs, gene-regulatory or metabolic networks (Milo et al. (2002)), Boccaletti et al. (2006)), and are also routinely applied in the analysis of neural and brain networks in order to demonstrate that some global, "higher-order" organisation features of the brain maps, such as modularity or small-worldness, are not the direct consequence of their basic network properties (e.g., Hilgetag et al. (2000), Bassett et al. (2008), Zamora-López et al. (2010)).

Physical networks like the brain are, however, embedded into three dimensional space which imposes additional fundamental constraints on their basic characteristics which random surrogates do not share. These surrogates hence represent a rather loosely constrained null-hypothesis set for these spatially embedded networks. Specifically, random surrogates tend to possess a large number of long-range connections because they "smooth" local inhomogeneities of physical networks. They thus form highly and rather homogeneously integrated networks, while at the same time lacking the high segregation of predominantly local connectivity, which is one of the most prominent features of brain networks (Braitenberg and Schuz (1998)). Therefore, when comparing the architecture of the brain to random surrogates, properties may appear significant to the brain's architecture even though they are predominantly only caused by the spatial constraints of its embedding into the physical world.

To address this problem, the so-called lattice surrogates have been introduce and applied in numerous studies (Sporns and Kötter (2004), Sporns (2006), Sporns et al. (2007), Honey et al. (2007), Rubinov and Sporns (2010)), which preserve (or rather increase) the high segregation of brain networks. However, the motivation behind lattice surrogates, originating from the Watts-

Strogatz small-world model (Watts and Strogatz (1998)), is to represent a lattice-like, topologically over-segregated (and thus under-integrated) surrogate network type, the counterpart of random surrogates, and to compare the studies network with these two extreme null-hypothesis types. This is reflected in the commonly applied generator algorithm for lattice surrogates (only replacing connections closer to the main diagonal of the connectivity matrix, see e.g. Sporns and Kötter (2004)), which is only indirectly linked to physical distance through some arbitrary spatial ordering of the network nodes, and is therefore only partially appropriate to provide a null-hypothesis network set for physical wiring constraints of the network under study. Furthermore, these lattice surrogates are designed to reduce, rather than preserve, the connection lengths of the studied network, therefore they are prone to loosing some brain network properties during that optimisation of spatial wiring.

Spatially preserving null-hypothesis networks

As it has been discussed above, the structure of spatially embedded physical networks, like brain networks, is usually heavily influenced by additional organisation constraints, such as the tendency of connections to be formed locally (Braitenberg and Schuz (1998)). Spatial embeddedness is one of the most fundamental factors shaping the evolution and development of the brain (Kaiser and Hilgetag (2004b)). More generally, every materially realised network faces basic physical constraints, such as the number, density and lengths of network connections (Kaiser and Hilgetag (2004c)). Comparative complex network studies have long pointed to fundamental organisation differences between 'geographic' or spatial networks, such as power grids or the Internet, and non-spatial networks, such as semantic networks or the WWW (reviewed in Newman (2003), Boccaletti et al. (2006) and Sporns (2010)).

One of the primary considerations in the physiological efficiency of brain networks is the metabolic cost their structure and operation requires (Laughlin et al. (1998), Laughlin and Sejnowski (2003)). The fact that longer synaptic connections are more expensive, both in terms of material cost and energy consumption, is likely to be a fundamental 'design' principle during the evolution and development of brain networks towards conserved wiring lengths (Kaiser and Hilgetag (2004b), Kaiser (2007)). While a small fraction of metabolically non-optimal, long-range projections is necessary for maintaining high network efficiency (Kaiser and Hilgetag (2006)), the human brain is a spatially extremely conservative network with the majority of the connections being local, even when considering the cortico-cortical white matter projections only (see Section 3.3.3).

In the current work, we introduce a new class of surrogates, spatial surrogate networks, which

preserve more of the actual embedding of the brain network into physical space than random surrogates do, and hence are a better baseline to investigate whether the particular arrangement of regions in the brain may induce some of the properties of the connectome. Specifically, as opposed to the rather abstract, minimally constrained random surrogate networks, our novel spatial surrogates additionally incorporate the physical feature of the brain to favour spatially local connections. Additionally, in order to follow the standard analysis framework of the field, as well as to be able to compare the cortex with a set of surrogate network sets with varying degree of spatial constraints, we also perform null-hypothesis analysis against a set of traditional, spatially non-restricted random surrogate networks.

3.2.2 The rewiring algorithm

Both types of surrogate networks were generated by the widely applied iterative rewiring algorithm (Maslov and Sneppen (2002), Milo et al. (2002), Sporns and Kötter (2004)), the basic variant of which proceeds as follows. Starting from the original cortical network, in each iteration, two edges, (n_1, n_2) and (n_3, n_4), are randomly chosen. After making sure that no self-connections or parallel edges (multiple links between two nodes) would be created, the two original edges are rewired to (n_1, n_3) and (n_2, n_4).

The above basic variant is used to generate random surrogate networks. In our spatially constrained variant of the rewiring algorithm, we incorporated the following additional rule: each rewiring step is only executed if the resulting total connection length of every node would not exceed that of the node in the original cortical network[1]. In the current study, the procedure terminates when each edge is rewired 20 times on average (10*17865=178650 rewiring steps, as each step rewires two edges). For both surrogate types, we generated n=20 networks. The pseudocode of the algorithm used to generate the two surrogate network types is presented in Alg. 1.

The rewiring algorithm, while randomising (shuffling) network edges between nodes, preserves not only the number of nodes and edges of the cortical network, but also its (non-weighted) degree distribution (number of connections of each node). The reason for this latter property follows from the fact, that, during the generation of a surrogate network, every 'atomic' rewiring step of the entire rewiring procedure preserves the degree of all four regions being rewired (each one looses a connection and at the same time gains another one). Therefore the binary degree distribution of every intermediate network generated during the rewiring procedure equals to that of the original cortical network, hence so does that of the final rewired surrogate network (see Figure 4.1, top left

[1]Due to losing the actual, DSI tractography-derived lengths of the projection trajectories during the rewiring procedure, connection lengths in this case were approximated by the sum of Euclidean distances between the positions of each connected node-pair, both for cortical and for surrogate networks.

Algorithm 1 Pseudocode of the surrogate network generator algorithm

Surrogate network generator method

input: C cortical network
r boolean for surrogate type
True: random, False: spatial
output: S surrogate network

▷ initialise
$n_{rewsteps} = 10 * C.number\_of\_edges()$
$S = C$
$i = 0$
while $i < n_{rewsteps}$ **do**
▷ choose two edges randomly
$n_1, n_2 = S.get\_random\_edge()$
$n_3, n_4 = S.get\_random\_edge()$
▷ avoid self-loops
if $n_1 \neq n_3$ and $n_2 \neq n_4$ **then**
$nbrs_1 = S.get\_neighbours(n1)$
$nbrs_2 = S.get\_neighbours(n2)$
▷ avoid parallel edges
if $n_3 \notin nbrs_1$ and $n_4 \notin nbrs_2$ **then**
▷ extra spatial condition
see right column for method s
if r or $s(C, S, n_1, n_2, n_3, n_4)$ **then**
▷ rewire edges
$w_1 = S.get\_weight(n_1, n_2)$
$w_2 = S.get\_weight(n_3, n_4)$
$S.delete\_edge(n_1, n_2)$
$S.delete\_edge(n_3, n_4)$
$S.add\_edge(n_1, n_3, w_1)$
$S.add\_edge(n_2, n_4, w_2)$
$i = i + 1$
end if
end if
end if
end while
return S

Extra condition for spatial surrogates

(method s from left column)

input: C cortical network
S surrogate network
n_1,n_2 nodes of first edge
n_3,n_4 nodes of second edge
output: evaluated spatial condition
True: passed, False: failed

▷ get nodes' total connection lengths
originally in cortical network
$ct_1 = C.get\_total\_conn\_len(n_1)$
$ct_2 = C.get\_total\_conn\_len(n_2)$
$ct_3 = C.get\_total\_conn\_len(n_3)$
$ct_4 = C.get\_total\_conn\_len(n_4)$
▷ get nodes' total connection lengths
currently in surrogate network
$st_1 = S.get\_total\_conn\_len(n_1)$
$st_2 = S.get\_total\_conn\_len(n_2)$
$st_3 = S.get\_total\_conn\_len(n_3)$
$st_4 = S.get\_total\_conn\_len(n_4)$
▷ get distances of node pairs
$d_{12} = get\_dist(n_1, n_2)$
$d_{34} = get\_dist(n_3, n_4)$
$d_{13} = get\_dist(n_1, n_3)$
$d_{24} = get\_dist(n_2, n_4)$
▷ True, if original connection length
would not be increased for any node
if $st_1 - d_{12} + d_{13} \leq ct_1$ and
$st_2 - d_{12} + d_{24} \leq ct_2$ and
$st_3 - d_{34} + d_{13} \leq ct_3$ and
$st_4 - d_{34} + d_{24} \leq ct_4$ **then**
return $True$
else
return $False$
end if

subfigure).

Additionally to these properties of random surrogate networks (identical network size, number of connections and degree distribution), spatial surrogates also conserve the regional total connection length distribution of the cortical connectivity, thereby satisfying our null-hypothesis requirements on connection proximity. Also, note that in all surrogate networks degrees and connection lengths (the latter only for spatial surrogates) are not only globally preserved, but also on a per node basis. This makes comparison feasible not only at the macro-scale of the entire network, but also at the micro-scale of individual regions and, by consequence, at the intermediate meso-scale of region subgroups.

In summary, comparison of complex network metrics between the cortical network and its two surrogate types allows for assessing cortical characteristics that are not (solely) the consequences of the size, connection density and degree-distribution of the cortex, in case of random surrogates, and for assessing cortical characteristics that are not (solely) the consequences of the size, connection density and degree-distribution of the cortex *and its local connectivity*, in case of spatial surrogates. Due to the additional, connection length constraint, we expect spatial surrogate networks to better approximate cortical network properties than random surrogates do.

3.3 Surrogate network verification

The rewiring algorithm outlined above is given several constraints to comply with during the randomisation of the cortical connectivity. In order to assess that, in spite of these constraints, sufficient randomisation is achieved for the forthcoming surrogate analysis, we verify the resulting surrogate networks below.

The averaged connectivity matrices of the obtained surrogate network groups are shown in Figure 3.1. By sole visual inspection of the matrices, we can note that a homogeneous randomisation was achieved across random surrogates, indicated by the blurred purple colour of their average connectivity matrix. The average connectivity matrix of spatial surrogates on the other hand noticeably resembles characteristics of their original cortical counterpart (see Figure 2.2): the concentration of high values along the main diagonal indicates that they preserved the predominantly local connectivity of the cortex to a large extent. In the forthcoming analysis, we shall quantitatively assess the similarity between the cortical network and its surrogate groups.

3.3.1 Cortex – surrogate distances

We start the assessment of the generated surrogate networks by evaluating their similarity to the cortical connectivity. Numerous indices have been devised to measure similarity between two

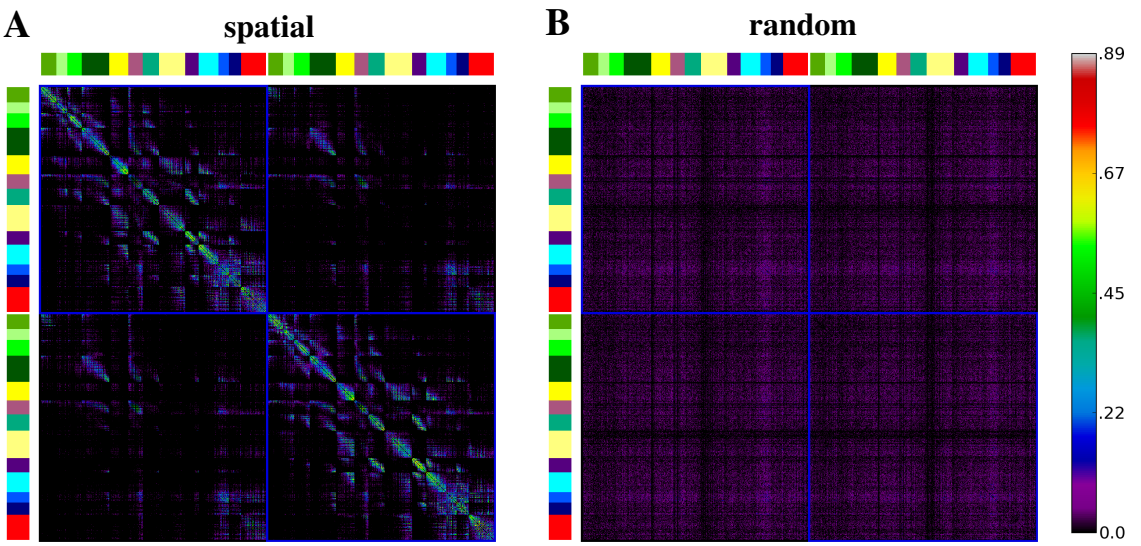

Figure 3.1: **Average connectivity matrices of surrogate network groups.** Averaged connection matrices (projection strength weighted frequencies of connection occurrences) of spatial (A) and random (B) surrogates. See colour bar on right for scale of both matrices. All matrices are symmetric due to the undirected nature of the networks. For colour code and ordering of regions (left and top strips) see Figure 2.2 and Figure 2.3. For comparison with the original cortical connectivity matrix, see Figure 2.2.

datasets. The Damerau–Levenshtein distance (Damerau (1964)) and its Levenshtein or "edit distance" variant (Levenshtein (1966)) were developed to measure the distance between two character strings as the minimum number of some discrete operations required to transform one to the other. These similarity indices are most commonly applied in bioinformatics to measure the variation between DNA sequences, in which basic steps of mutation can be represented by considered discrete operations (Jones and Pevzner (2004)). However, these metrics are less suitable for measuring our main interest here, i.e., the global dissimilarity between different networks, as they are designed to investigate the process itself that leads to those differences.

Another two metrics for measuring the similarity between two sets of data are the Jaccard index J (Jaccard (1901)), and the closely related Sørensen similarity quotient QS (Sørensen (1948)). Both measures are based on the quotient of the intersection and the union of the two sets, making them more suitable for our purpose, that is, for measuring the global (dis)similarity or relative overlap between the connection sets of networks defined on the same set of nodes. Here, we use the Sørensen distance, which is equivalent to the Bray–Curtis dissimilarity (Bloom (1981)), modified to calculate distance on (connectivity) matrices, and we call that modified measure the normalised distance δ. Specifically, the distances of each surrogate network S from the cortical network C is

calculated by the Sørensen distance of their weighted connectivity sets:

$$\delta(C,S) = 1 - QS(C,S) = 1 - \frac{2\,|C \cap S|}{|C| + |S|} = \frac{|C| + |S| - 2\,|C \cap S|}{|C| + |S|} = \frac{|C \triangle S|}{|C| + |S|} =$$

$$= \frac{\sum_{i,j \in N} |C_{ij} - S_{ij}|}{\sum_{i,j \in N} C_{ij} + \sum_{i,j \in N} S_{ij}} = \frac{\sum_{i,j \in N} |C_{ij} - S_{ij}|}{2 * \sum_{i,j \in N} C_{ij}}, \tag{3.1}$$

where $A \triangle B$ is the symmetric difference between sets A and B, N is the set of regions in the networks (the same for the two compared networks in our case), and M_{ij} is the connection weight between nodes i and j in network $M \in \{C, S\}$ (zero if the two nodes are not connected). With the above definition, δ measures the *ratio of dissimilarity* between the weighted connectivities of two networks C and S, that are defined on the same set of nodes and possess the same total connection weight sum. Normalised distance is 1 if the networks share no common connection (maximal distance), and it is 0 if the networks are equivalent, that is, they are composed of exactly the same set of weighted connections (zero distance).

We calculate the mean normalised distances $\overline{\delta}(C,S)$ for the two surrogate sets. For random surrogates, we obtain $\overline{\delta}(C,S_R)$ = 0.95 $\pm$ 0.002, indicating their almost completely different connection sets from that of the cortical network. For spatial surrogates, we obtain the much lower $\overline{\delta}(C,S_S)$ = 0.52 $\pm$ 0.002, confirming that conservation of the connectional locality of the cortical regions indeed lowered the achievable degree of randomisation. Nonetheless, even the spatial surrogates are substantially, more than 50% different in their connectivity from the cortical network, rendering them appropriate to represent a set of reasonably randomised, spatially constrained surrogate networks of the cortex.

3.3.2 Surrogate – surrogate distances

The $\delta(C,S_R)$ and $\delta(C,S_S)$ values obtained above demonstrate only some very insignificant deviation from their respective means. This can be the combined consequence of the sufficiently long edge shuffling process and the relatively large size of the network, according to the law of large numbers. Another possibility, however, is that the low deviation originates from an adversely low variation within the generated surrogate groups, each being composed of highly similar networks.

To determine which one of the above two cases is true, we calculate the pair-wise normalised network distance between every surrogate network pair in each of the surrogate groups. Mean intra-group distance values and their standard deviations are $\overline{\delta}(S_R,S_R)$ = .95 $\pm$ .001 for random surrogates and $\overline{\delta}(S_S,S_S)$ = .55 $\pm$ .003 for spatial surrogates, confirming that the intra-group distances are significantly non-zero, and invalidating the second scenario above.

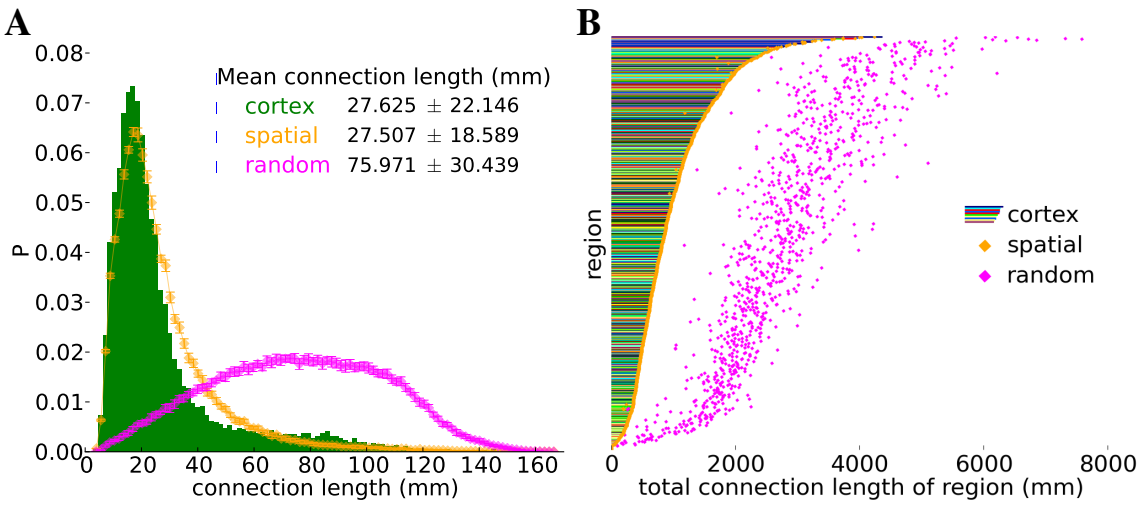

Figure 3.2: **Connection lengths of the cortical connectivity and its surrogate network groups.** (A) Connection length (distance between linked region pairs) distribution of the cortical network (bars) and its surrogates (diamonds), with mean ± standard deviation values indicated in legend. Whiskers on diamonds denote the standard deviation between networks within each surrogate group. Note the highly similar, but somewhat shorter tailed connection length distribution of spatial surrogates, and the shift of the connection length distribution of random surrogates towards much higher values, reflected in their mean and standard deviations (see figure legend). (B) Histogram of total connection length of regions (sum of distances from all neighbours). Each row corresponds to a single region, bars represent values in the cortex and are coloured to the anatomical structure colour of the region (see Figure 2.3). Diamonds denote mean of total connection lengths of regions within each surrogate groups (see legend). Note that total connection length of not only the entire network (as shown in A), but also of each individual region is preserved in spatial surrogates (orange diamonds, apart from some exceptions, match with bar values in B), while they have been increased in random surrogates.

Interestingly, the low deviations in both the $\delta(S_R, S_R)$ random-random and the $\delta(S_S, S_S)$ spatial-spatial distances indicate that in each surrogate group there exists a characteristic or natural distance, $\overline{\delta}(S_R, S_R)$ and $\overline{\delta}(S_S, S_S)$, between any two members of that group. In addition to that, we see that the mean distance of the cortical network from its surrogate groups is analogous to these characteristic distances of the groups ($\overline{\delta}(C, S_S) \approx \overline{\delta}(S_S, S_S)$ and $\overline{\delta}(C, S_R) \approx \overline{\delta}(S_R, S_R)$), and furthermore with only a very low deviation. This finding renders the cortical network a generic member of each group in terms of its basic region-region connectivity, measured by δ.

3.3.3 Connection lengths

The connection length distribution and total connection length of each region (sum of distances to all neighbours) in the cortical network and its surrogates are shown in Figure 3.2. Consistent with the predominantly local connectivity of the cortex (mean cortical connection length l^C = 27.625 mm), random rewiring of cortical connections has nearly tripled the average connection length (mean $\pm$ standard deviation of random surrogate network means: l^R = 75.971 $\pm$ 0.164 mm). For this reason, that is, due to the natural tendency of randomly swapping links to increase the lengths of the originally short cortical connections, the applied simple condition during spatial surrogate generation (i.e., 'not to exceed the original total connection length of the cortex', see Alg. 1) has been sufficient to achieve conservation of connection lengths in spatial surrogates (l^S = 27.507 $\pm$ 0.120 mm), with a similar profile, but slightly narrower connection length distribution (standard deviation of connection lengths: cortex: $\sigma(l^C)$ = 22.146 mm $\rightarrow$ spatial surrogates: $\sigma(l^S)$ = 18.589 mm) and shorter tail (see Figure 3.2 A).

This latter alteration renders the distribution of the length of the *individual cortical connections* significantly different from those of both of its surrogate groups (Wilcoxon two-sided rank-sum test for identical distribution: $p < 10^{-4}$ both for random and spatial surrogates). On the other hand, as it can be seen in Figure 3.2 B, the total connection lengths of the *individual cortical regions* have been successfully preserved in spatial surrogates (cortex minus spatial surrogate mean: -2.374 $\pm$ 5.521 %, Wilcoxon two-sided rank-sum test for identical distribution: $p = 0.898$), while random surrogates have significantly increased these regional connection lengths (cortex minus random surrogate mean: +227.5 $\pm$ 114.0 %, $p < 10^{-4}$). These results verify our novel spatially constrained surrogate network generator algorithm, as well as the obtained null-hypothesis networks, in terms of conserving not only topological, but basic spatial properties of the cortical connectivity, that are largely lost in traditional random surrogates.

3.4 Overview of results

In this chapter, we introduced and verified the robustness of the surrogate generator algorithm, and gave validity to the forthcoming surrogate comparison analysis. Specifically, we have confirmed that our spatial surrogates successfully preserved not only the basic topological properties (number of regions, connections and degree distribution) of the cortical connectivity network, but also some of its basic spatial "wiring" properties (total connection length of individual regions and the entire network). This enables the utilisation of spatial surrogates to test the significance of certain organisation features of the cortical network against the individual wiring constraints of its

regions.

We also note, however, that, although they reasonably approximate its profile, even spatial surrogates were not able to fully conserve the connection length distribution of the cortical network at the level of *individual connections*, due to having lost some of the longest-range connections of cortical connectivity. Nevertheless, while keeping the above point in mind, the conservation of the total wiring length as well as the individual wiring length of the cortical regions enables us to use spatial surrogates as null-hypothesis networks that estimate these latter aspects of the cortical wiring constraints.

With the combined utilisation of traditional random surrogates and our novel spatially preserving surrogates, we are able to distinguish in our analysis those significant topological features of the cortical network that are derivable from its predominantly local, spatially segregated connectivity (in case both the cortical network and its spatially preserving surrogates differ from random surrogates) from those that are the consequences of some primarily not spatially constrained, potentially functionally more relevant organisation principles of the cortical connectivity (in case the cortical network differs from both its spatially conservative and random surrogates).

In the forthcoming survey of analyses, we shall utilise the obtained surrogate groups with that purpose, that is, to gain insight into the *global* relevance of each investigated network organisation feature, before turning our attention to the analysis of how that feature is *internally* expressed and facilitated by various parts of the cortical topology.

Part II

From structure to function through dynamics

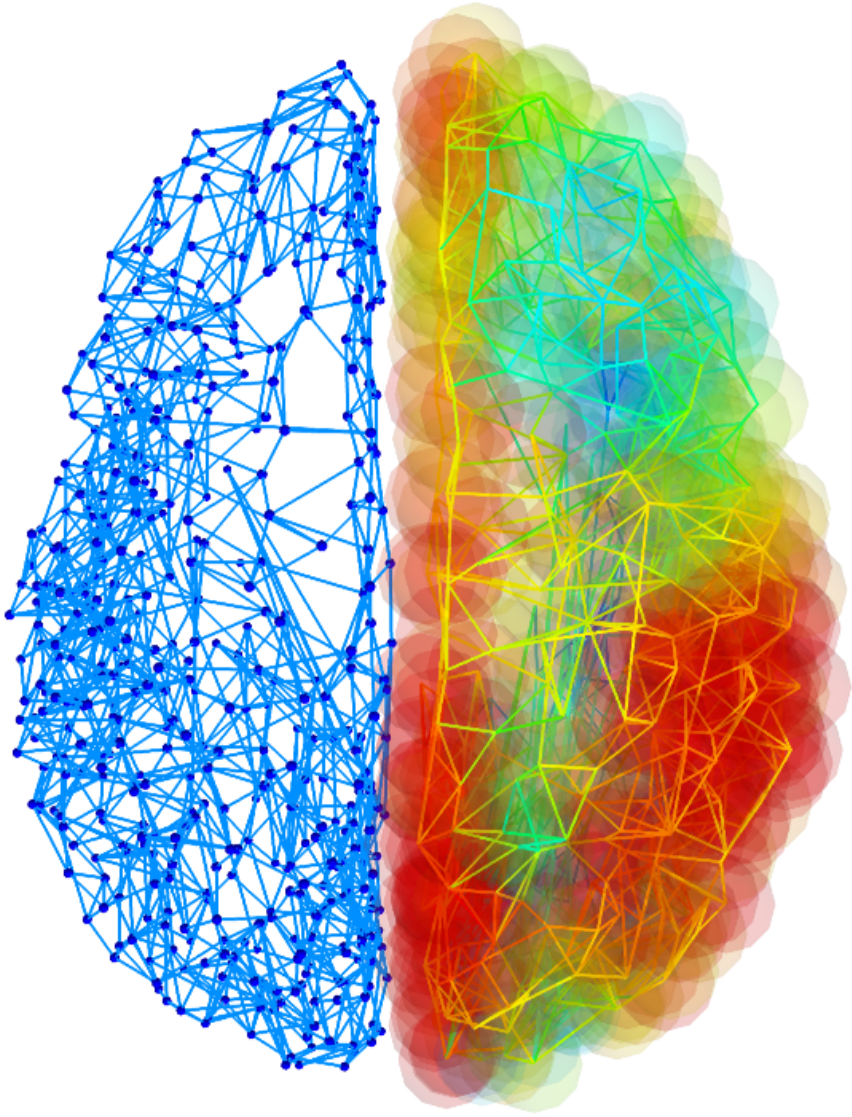

Chapter 4

The small-world of the brain

Topological basis of functional integration and segregation in the cortex

4.1 Introduction

In this chapter, we start the topological analysis of the cortical structural connectivity by assessing whether it exhibits one of the most prominent features of many real-world complex networks, the so-called small-world organisation (Watts and Strogatz (1998)). Informally, a network is called *small-world* if it is relatively sparsely and locally connected, but, at the same time, is able to maintain short path lengths between its nodes.

In practical terms, these criteria usually translate to both relatively high segregation and high integration, properties that reflect the kind of information processing the network is capable of (Tononi et al. (1998)) and are important topological aspects to be investigated on their own. Therefore, by utilising an assorted set of complex network measures, we carry out a detailed multi-scale analysis on the segregation and integration properties of the cortical network first, then, using those results, we draw conclusions on the small-world organisation of the cortex.

Beyond characterising the global integration and segregation properties of the cortical connectivity, we shall also seek for internal differences in the topological integratedness and segregatedness among the individual cortical regions, and thereby characterise potential specialisation in their functional operation. We shall also investigate the relation of integration and segregation by contrasting the regional expression of two, naturally opposing network phenomena (Tononi et al. (1998)).

It is important to note, that even in the ever-growing plethora of complex network measures

(see Costa et al. (2006), Rubinov and Sporns (2010) and Kaiser (2011) for recent reviews), there is no generally applicable ”gold standard” for the quantitative assessment of network *integration* or *segregation*. These umbrella terms should rather be regarded as qualitative characteristics with their own diverse, inter-related set of specialised measures, where each measure assesses a different aspect of the general phenomenon. The multi-scale, spatially embedded and highly dynamic nature of the brain complicates this situation further by rendering the interpretation of some measures, such as *flow* or *page-rank*, non-trivial, and necessitating the development of new measures that are able to deal with the above characteristics (Rubinov and Sporns (2010)).

For these reasons, we are necessarily restricted to work with a set of some selected, representative measures in this study. The measures following in this chapter were chosen partly due to their prior utilisation for brain network analysis, in order to work with already established, validated tools, as well as to facilitate cross-study comparison. Additionally, the importance of utilising multi-scale measures in order to capture different aspects of network integration has been demonstrated by Zuo et al. (2011). Keeping this in mind, we also attempt to use a selection of network metrics with the ability to illuminate network integration and segregation from different angles and to get a more balanced picture of the investigated general phenomena.

4.2 Integration

4.2.1 Introduction

In the context of brain networks, functional integration is ”the ability to rapidly combine specialised information from distributed brain regions” (Rubinov and Sporns (2010)). Structural connectivity of the brain gives us insight into local and global aspects of functional integration through the assumption that anatomical connections form the underlying basis of communication between brain regions. Generally speaking, topological analysis of structural connectivity builds on the notion that anatomically highly integrated regions (or groups of regions or entire networks) are able to utilise functional information present in the network in a more efficient way by requiring less time and other physical resources to access it. While the complete exclusion of the dynamical aspects of information processing from this analysis framework may seem to be an oversimplification, this approach has been adopted and widely applied in the complex network sciences as a reasonable starting point for uncovering potention for functional integration from network structure (Newman (2003), Watts (2004), Boccaletti et al. (2006), Rubinov and Sporns (2010)). Nonetheless, we will return to this basic assumption on the relation between structure and function and examine its validity in Chapter 7 in general, and in Section 8.3.2 in particular.

We investigate the integrative properties of the cortex by four complex network measures of integration: degree centrality, leverage centrality, efficiency and betweenness. Below, we first formally introduce and informally interpret all four measures, then we analyse the cortical network with respect to them.

4.2.2 Methods: Integration measures

Degree centrality

Degree centrality (or simply degree) (Rubinov and Sporns (2010)) of a node i is the number of connections the node possesses with every other network node:

$$k_i = \sum_{j \in N} a_{ij} \tag{4.1}$$

where a_{ij}=1 if there is an edge between node i and j, and 0 otherwise. Degree centrality is the most fundamental centrality measure that reflects the integratedness of the nodes by measuring their *immediate* interconnectedness with the rest of the network.

Leverage centrality

Leverage centrality (Joyce et al. (2010)) of a node i measures the relationship between its degree k_i and the degree of each of its neighbours, averaged over all neighbours N_i:

$$l_i = \frac{1}{k_i} \sum_{j \in N_i} \frac{k_i - k_j}{k_i + k_j} \tag{4.2}$$

According to the developers of the measure: "The leverage centrality of a node in a network is determined by the extent to which its immediate neighbours rely on that node for information." (Joyce et al. (2010)). A node has negative leverage centrality if its degree is less than the average degree of its neighbours, suggesting that it relies on them in communicating with the rest of the network, while the topological relation is vica versa for positive leverage centrality nodes. The correction term in the denominator of Eq. 4.2 is used to eliminate the imbalance high degree nodes would introduce to the distribution of the measure.

Efficiency

Efficiency (Latora and Marchiori (2001)) of a node i is the average of the inverse of the d_{ij} shortest path lengths between the node and every other network node:

$$e_i = \frac{\sum_{j \in N, j \neq i} 1/d_{ij}}{|N| - 1}. \tag{4.3}$$

High efficiency nodes require fewer intermediating edges to reach other nodes on average, therefore higher efficiency values represent greater potential to exchange information or exert influence on the rest of the network. Efficiency has the advantage over the more traditional average shortest path length of being computable for multi-component networks[1], and generally it is a more balanced measure due to the fact that shortest path length can be heavily effected by only a few, very long paths (Achard and Bullmore (2007)).

Betweenness centrality

Betweenness centrality (Freeman (1978)) of a node i is the fraction of all shortest paths that pass through it:

$$b_i = \frac{1}{(|N|-1)(|N|-2)} \sum_{\substack{h,j \in N \\ j \neq i, h \neq i, h \neq j}} \frac{\rho_{jh}(i)}{\rho_{jh}}, \tag{4.4}$$

where ρ_{jh} is the number of shortest paths between nodes j and h, and $\rho_{jh}(i)$ is the number of shortest paths between nodes j and h that pass through i. High betweenness centrality implies that the node contributes to many shortest paths in the network, and suggests the node's distinguished importance in supporting global, network-wide integration.

Comparison of the integration metrics

For all four measures introduced above, higher measure values suggest higher potential of the node in facilitating functional integration within the network due to its topologically more central position. From the four measures, leverage centrality can take negative values, while the other three measures are non-negative.

We emphasise, that the calculation of the four measures take an increasing extent of the network topology into account: degree centrality only counts own edges (immediate neighbours), leverage centrality considers the connectivity of neighbours, efficiency evaluates own shortest paths, and finally betweenness centrality requires all shortest paths present in the network. Consequently, the selected measures reflect the integration potential of the network nodes at various scales from local to global, thus in combination they are able to cover cortical integration processes occurring on various spatial scales.

[1] For example, the efficiency of a disconnected node degenerates to 0, while its shortest path length is infinite.

4.2.3 Results: Regional integration properties

Surrogate comparison

Distributions of regional measure results of the four integration metrics, and their pairwise relationships are shown in Figure 4.1. First, let us consider the distribution of measure values along with their surrogate tests (subfigures along main diagonal).

Degree distributions of both types of surrogate networks, by the nature of their construction (Section 3), are identical with that of the cortical network (mean: 36.0 ± 16.0). Leverage centrality distribution of the cortex is narrower around its higher mean value (network mean: L^C = -0.064) than that of its random surrogates (L^R = -0.088 $\pm$ 0.217, Wilcoxon two-sided rank-sum test for identical distribution: $p < 10^{-3}$), and is remarkably akin to its spatial surrogates (L^S = -0.064 $\pm$ 0.173, $p = 0.65$). This suggests that the predominantly short connections of the cortex link spatially close regions with similar degrees, resulting in a relative balance in functional integration within *local* neighbourhoods of regions, throughout the cortical surface.

Considering the global topological distances between cortical regions, the efficiency of the cortex is significantly lower than both of its surrogate groups (network means: cortex: E^C = 0.174, spatial: E^S = 0.214 $\pm$ 0.030, random: E^R = 0.26 $\pm$ 0.032, Wilcoxon two-sided rank-sum test for identical distribution: $p < 10^{-4}$ for both surrogate types), reflecting sub-optimality in mean regional distances. Finally, the distribution of betweenness centralities of the cortical network is more spread towards higher values (network means: cortex: B^C = 0.0021, spatial: B^S = 0.0017 $\pm$ 6·10^{-5}, random: B^R = 0.0013 $\pm$ 4·10^{-5}, $p < 10^{-4}$ for both surrogate types), indicating a more heterogeneous, possibly centralised global architecture in the cortex, with a fewer regions laying on many shortest paths, than in its more homogeneous surrogate network.

Importantly, although the cortex's integration properties, as expected, are better approximated by spatial surrogates than random networks (see mean values), in some cases the brain network is significantly different from both null-hypothesis networks (see significance tests above). Specifically, while the cortex and its spatial surrogates are locally highly similar (degree and leverage centrality), their global integration is differently organised (efficiency and betweenness centrality). This suggests that while the physical wiring constraints of individual cortical regions predominantly shape their *local* integration ability, it is likely that some other organisation principles govern the characteristics or cortical integration on the meso- and macro-scale.

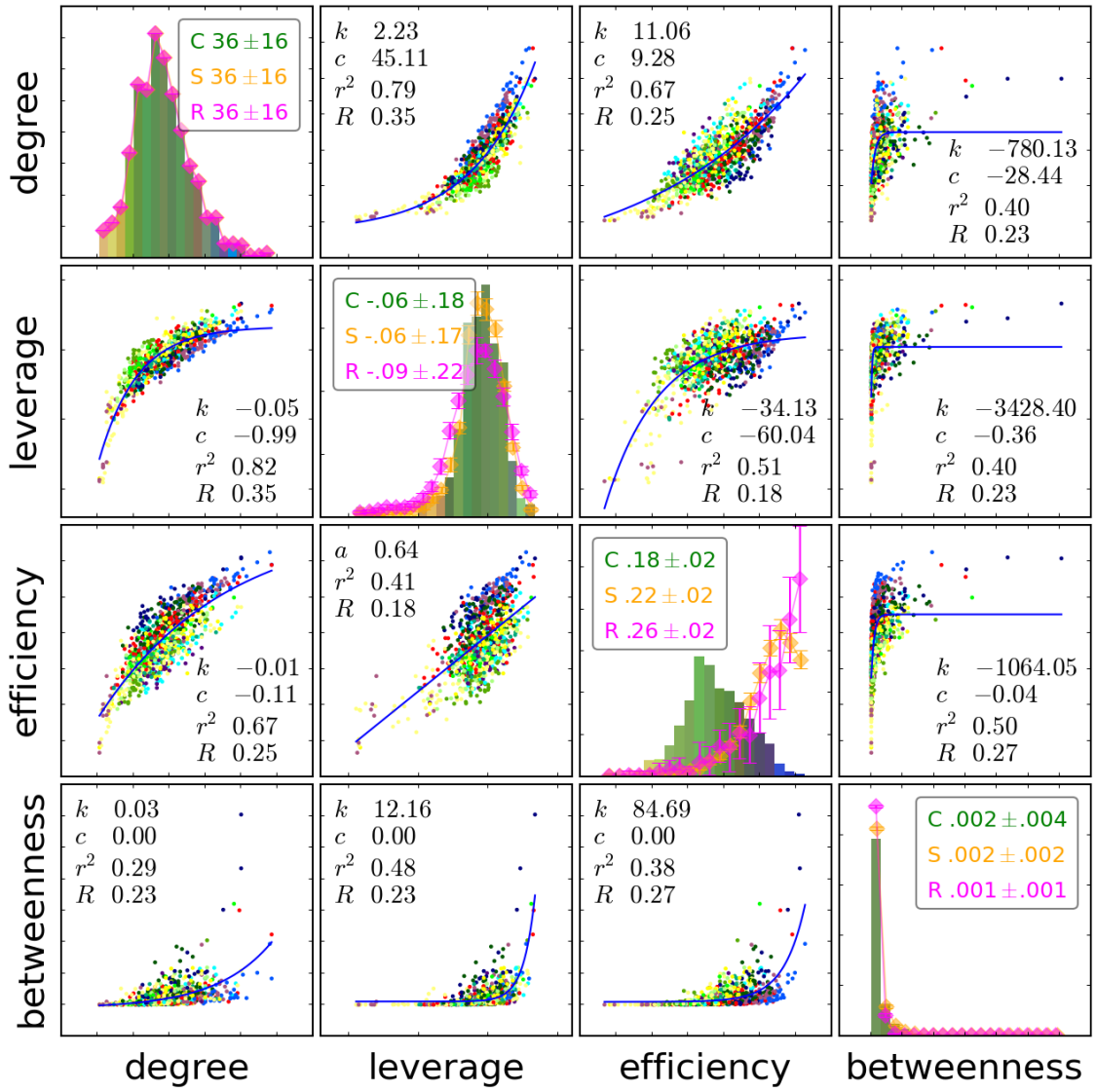

Figure 4.1: **Distributions and correlations of integration measures.** Subfigures in main diagonal: distributions of regional measure values (bars), colour coded by the mean color of comprised regions. Diamonds and whiskers show spatial (orange) and random (magenta) surrogate means and standard deviations. Legend shows mean ± standard deviation of cortical network ('C'), and its spatial ('S') and random surrogates ('R'). Off-diagonal subfigures: scatter plots of pairwise measure values of regions (dots), colour coded by their main structure. Blue line is fitted linear ($f(x) = ax + b$) or exponential curve ($f(x) = ce^{kx} + y_0$), obtained by least square fitting both models to data and choosing the one with lower r^2 value. Legends show parameters of model fit (k and c for exponential, a for linear fit), coefficient of determination ($r^2 = 1 - \sum \frac{y_i - f_i}{y_i - \bar{y}}$ (Steel and Torrie (1960))) and normalized redundancy (R) (see Appendix C). Note that although some metric pairs have a clearer trend (higher r^2 and R values) than others (lower r^2 and R values), all curve fittings indicate a generally positive correlation (co-increase) between the measures.

Inter-relation of the measures

Having calculated the four integration metrics for each region of the cortex, we are able to assess the relation of the measures to each other on the regional (network node) level of the cortical connectivity. Looking at the relationship between the integration measures (off-diagonal subfigures of Figure 4.1), we can observe positive correlations between the values of all measure-pairs: fitted curves all increase (blue curves), indicated by their positive slope a, in case of linear fitting, or identical sign (both positive or both negative) constant factor c and exponent parameter k, in case of exponential fitting. These characteristics suggest that high degree regions also tend to be influential in their local neighbourhoods (high leverage centrality), are able to reach and be reached by other regions faster and more directly (high efficiency), and are able to globally facilitate communication between many other region-pairs in the network (high betweenness centrality).

The most highly integrated regions

Regional measure values and the projections linking the regions with the highest measure values are visualised in Figure 4.2 for all four integration measure. The spatial distribution of the highest degree and most efficient regions, along with their dense inter-connections, clearly delineate a coherent central area along the caudal part of the cortical midline. Indeed, all the top 5% (n=50) highest degree and most efficient brain regions reside in only five of the 13 anatomical structures: in the precuneus, the limbic (cingulate) system, the superio-parietal, superio-frontal and occipital cortices. Furthermore, the top 10% (n=1786) of the edges connecting these regions predominantly run between regions of the former group, with only a few reaching out to areas in the temporal and frontal lobes, suggesting a high level of interconnectedness between these highly central regions. These characteristics together suggest that high efficiency regions, capable of facilitating global integration due to their topological *closeness*, are both spatially enclosed *and* form a densely interconnected subgroup in the cortex. We will directly investigate this claim in Chapter 5.

As opposed to the above centralisation of high degree and highly efficient regions, the location

---

Figure 4.2 *(following page)*: **Integration measure results on projections.** In each row, the regional measure results for an integration metric are represented on coronal (left column) and horizontal projections (right column). Regions are drawn with sizes proportional to their measure values, and are coloured to their main anatomical structure colour. On all projections, only the top 10% (n=1786) of the connections are shown for clarity, the ones that connect regions with highest measure values.

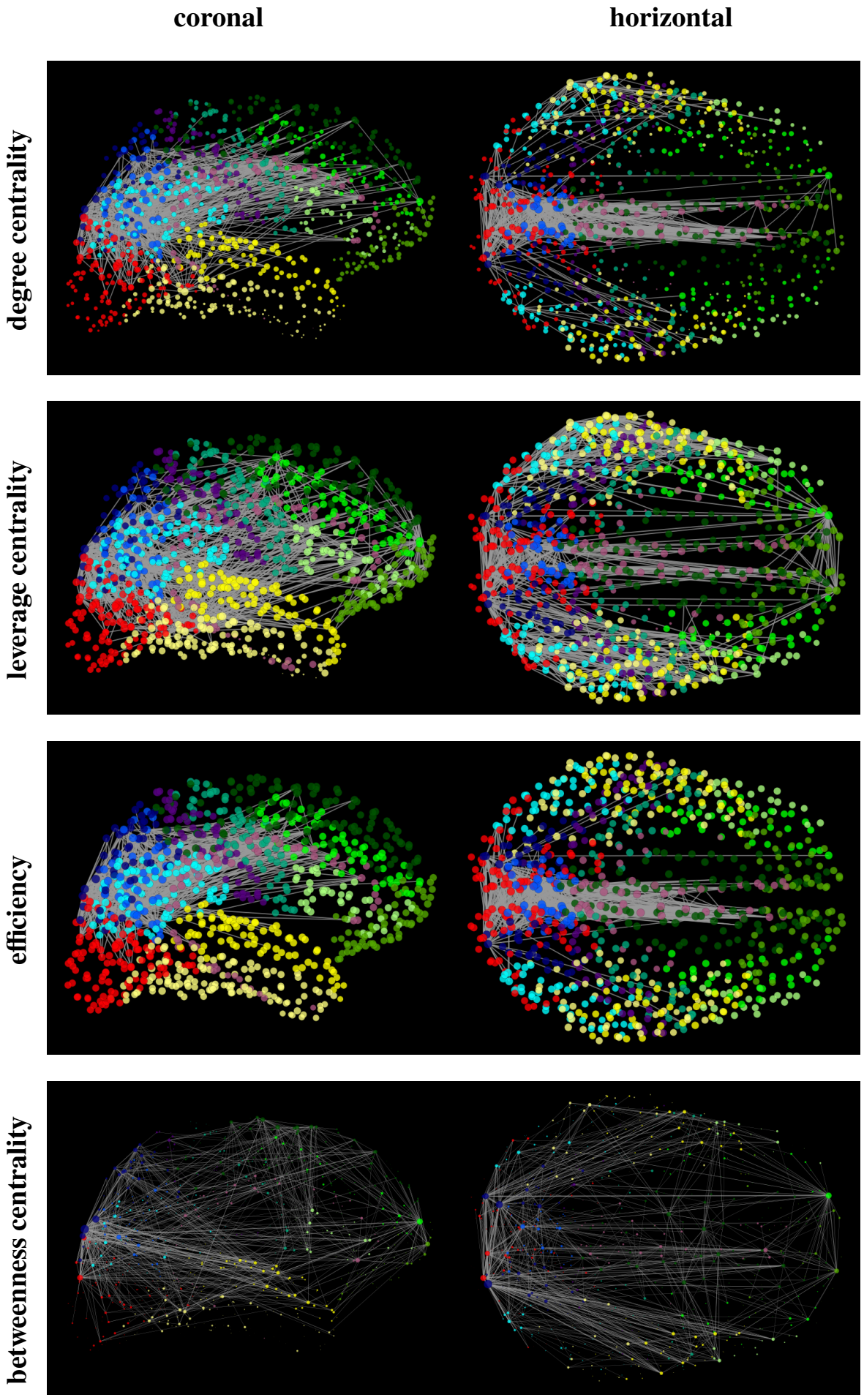
coronal
horizontal
degree centrality
leverage centrality
efficiency
betweenness centrality

of other locally and globally important integrator areas, measured by leverage centrality and betweenness centrality, respectively, exhibits a more homogeneous spatial distribution by extending to the lateral and frontal part of the cortex. As both metrics measure the potential of the regions to provide intermediating links between other regions, locally for leverage and global for betweenness centrality, their rather homogeneous spread suggests that the integration of distributed activity at various spatio-topological scales is organised around local and global hubs throughout the cortex. We will turn back to these claims in the following chapters.

4.3 Segregation

4.3.1 Introduction

In the context of brain networks, functional segregation is "the ability for specialised processing to occur within densely interconnected groups of brain regions" (Rubinov and Sporns (2010)). Similarly to the functional interpretation of topological properties in the context of integration (Section 4.2), the above definition of functional segregation is also based on the assumption that anatomical connections are the fundamental facilitators of functional interaction and specialisation. In support of this assumption, numerous studies found significant match between specialised functional areas and anatomically highly segregated parts (structural modules) in the thalamo-cortex of the cat (Hilgetag et al. (2000), Hilgetag and Kaiser (2004)) as well as in the macaque brain (Honey et al. (2007)). Nonetheless, as in the case of our functional integration analysis (Section 4.2), it is important to bear in mind that metrics of structural segregation omit the complex dynamical processes occurring on brain networks, and as such, are limited to characterise only the anatomical *potential* for functional segregation (Rubinov and Sporns (2010)). We will return to this question and investigate the relation between structural metrics and functional interaction in Chapter 7 in general, and in Section 8.3.2 in particular.

In the following analysis, we assess segregation in the cortex by two structural measures: clustering and normalised clique size. After formally defining and interpreting them, we present the results of their utilisation on the cortical connectivity.

4.3.2 Methods: Segregation measures

Clustering coefficient

The clustering coefficient (Watts and Strogatz (1998)) of node i is the fraction of triangles around it:

$$cc_i = \frac{t_i}{m_i} = \frac{\sum_{j,h \in N_i} a_{jh}}{|N_i| * (|N_i| - 1)}, \tag{4.5}$$

where N_i is the set of neighbours of i, $a_{jh} = 1$ if there is an edge between node j and h, 0 otherwise, and $t_i = \frac{1}{2} \sum_{j,h \in N_i} a_{jh}$ is the actual number of triangles, while $m_i = \frac{1}{2}|N_i| * (|N_i| - 1)$ is the maximum possible number of triangles around i, given its number of connections (cc_i = 0 for $|N_i|$ < 2) (Rubinov and Sporns (2010)).

The clustering coefficient of a node is 1 if all of its neighbours are also connected pair-wise, and it is 0 if none of its neighbour-pairs are connected. Clustering coefficient, reflecting the local density of inteconnectivity on network topology, is the basic measure of segregation.

Normalised clique size

As an alternative segregation measure to the standard clustering coefficient, we introduce a related, but slightly modified metric: normalised clique size. The normalised clique size of node i is the fraction of its neighbours that, taken together with i, form the largest complete subgraph or clique (Luce and Perry (1949)):

$$cs_i = \frac{\omega_i - 1}{|N_i|}, \tag{4.6}$$

where N_i is the set of neighbours of i, and ω_i is the clique number of i, which is the size of largest complete, i.e., fully connected, subgraph that i is the member of (Eblen et al. (2012)).

Normalised clique size reflects the level of segregation by measuring the size of the largest completely connected functional ”subunit” (topological clique) relative to the local level of interconnectivity. The normalised clique size of a node is 1, if all of its neighbours are fully connected (total segregation), and it is 0, if there is no connection between any of its neighbours (null segregation). While these extreme cases also apply to clustering coefficient, normalised clique size differs from the former by measuring local segregation in a more concentrated (the single largest clique), rather than distributed sense (all triangles around a node).

As a technical note, we mention that in the extreme case of a fully connected network (in which there exists an edge between every node-pair), all network nodes take the value one for both clustering coefficient and normalised clique size, despite the fact that such networks are normally not considered segregated. However, as, generally, real-world networks tend to have rather sparse connectivity (see e.g. the review of Albert and Barabási (2002)), and, particularly, the connection

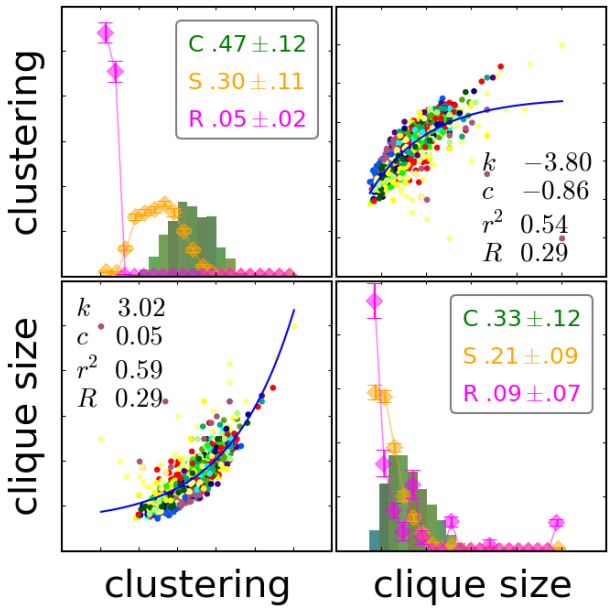

Figure 4.3: **Distributions and correlations of segregation measures.** Subfigures along main diagonal: bars denote distribution of cortical values ('C' in legend), diamonds and error bars show spatial (orange colour and 'S' in legend) and random (magenta colour and 'R' in legend) surrogate means and standard deviations. Off-diagonal subfigures: scatter plots of pairwise measure values of regions (dots), colour coded by their main structure. For further figure explanation, see Figure 4.1.

density of the analysed cortical connectivity network is 3.6%, we can safely ignore the above deteriorating aspect of the considered segregation measures.

4.3.3 Results: Region-level results

Segregation measure results are presented in Figure 4.3. The characteristically high segregation of the cortex is salient: its mean clustering coefficient and normalised clique-size (CC^C = 0.464, CS^C = 0.331) are multiple times higher than those of its random surrogate networks (CC^R = 0.048 $\pm$ 0.001, CS^R = 0.087 $\pm$ 0.002, Wilcoxon two-sided rank-sum test for identical distribution: $p < 10^{-4}$ both for measures). The cortex also has about 60% higher segregation level according to both measures than its spatially constrained surrogates (CC^S = 0.298 $\pm$ 0.004, CS^S = 0.211 $\pm$ 0.004, $p < 10^{-4}$ both for measures). As expected, spatial surrogates approximate the cortical network much closer than random test networks, reflecting the importance of spatially short connections in shaping the level of structural segregation in the cortex.

The specific values of the measures are also noteworthy: the 46% global cortical clustering coefficient means that more than almost every second neighbour-pair of each cortical region is also

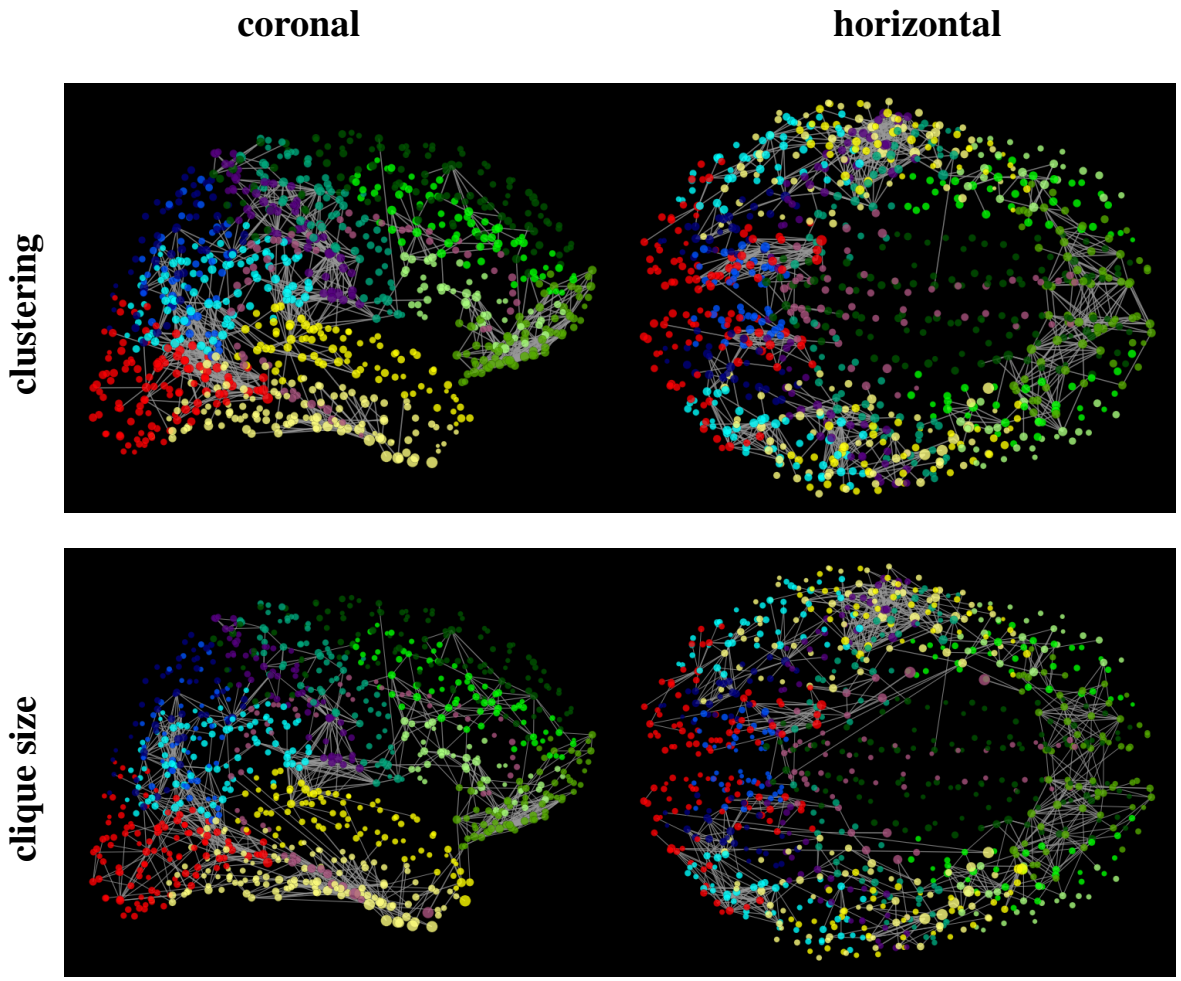

Figure 4.4: **Segregation measure results on projections.** In each row, the regional measure results for a segregation measure are visualised on coronal (left column) and horizontal projections (right column). Regions are drawn with sizes proportional to their measure values, and are coloured to their main anatomical structure colour. On all projections, only the top 10% (n=1786) of the connections are shown for clarity, the ones that connect regions with highest highest measure values.

connected on average (4.8% or 1:20 for random, and 30% or 1:3 for spatial surrogates), while the 33% mean cortical normalised clique-size indicates that each region forms a clique with as much as one third of its neighbours on average (8.7% or 1:11 for random, 21% or 1:5 for spatial surrogates).

Comparison of the two measures (Figure 4.3, off-diagonal subfigures) shows a high and strong positive correlation between them, reinforcing the intuitively expectable tendency of high clustering coefficient regions to form large relative cliques around themselves.

The most highly segregated cortical regions and their interconnectivity, are shown in Figure 4.4. The widespread spatial distribution of these regions, according to both measures, and the ”patchy” formations of their local interconnections are salient, especially in contrast with the high

centralisation of the highest degree and most efficient regions (Figure 4.2), and generally is in agreement with the interpretation of highly segregated regions to form small clusters of densely interconnected local processing units (Rubinov and Sporns (2010)).

4.4 Specialisation between integration and segregation

4.4.1 Introduction

We have seen in Figure 4.1 and 4.3, that groups of complex network metrics, measuring various aspects of integration and segregation of the brain regions, are in positive correlation, and that collectively they are capable of providing a broad, multi-scale assessment of network phenomena they gauge. Furthermore, cross-relation between these metric groups, shown in Figure 4.5, indicates negative correlation between all measure pairs. This finding supports the intuitive notion that integration and segregation are in competition with each other for the limited resources present the cortical network, e.g., for the metabolic energy the structure and operation of the connections require (Laughlin et al. (1998), Laughlin and Sejnowski (2003)). It hence appears, that individual cortical regions express one of them at the expense of the other. In this section, we attempt to characterise this regional specialisation between integration and segregation.

4.4.2 Methods: Measure for specialisation

The negative correlation between the two measure groups enables us to categorise individual brain regions by being either in an integrator or rather in a segregated position in the cortical network. To quantify this phenomenon, we introduce a metric for measuring regional specialisation between integration and segregation. Given the sets of all investigated integration and segregation measures, I and S, we order the regional results of each measure m ascending (smallest first), resulting in a rank ordered list of the regions r_m. Then we calculate the following average for each region i on its rank indices $r_m(i)$ across all m measures:

$$U(i) = \frac{\sum_{m \in I} r_m(i)}{n|I|} - \frac{\sum_{m \in S} r_m(i)}{n|S|}, \tag{4.7}$$

where n=989 is the number of regions in the cortical connectivity network, and $|I|$ = 4 and $|S|$ = 2 are the number of integration and segregation measures, respectively.

The above formula, resulting in a number in [-1, 1], evaluates the potential information processing role of each brain region in the network on a continuous scale. Regions with more positive U values are more highly ranked in integration measures, while at the same time have low segregation measure ranks, resulting in a rather integrator role in the cortical network. Conversely,

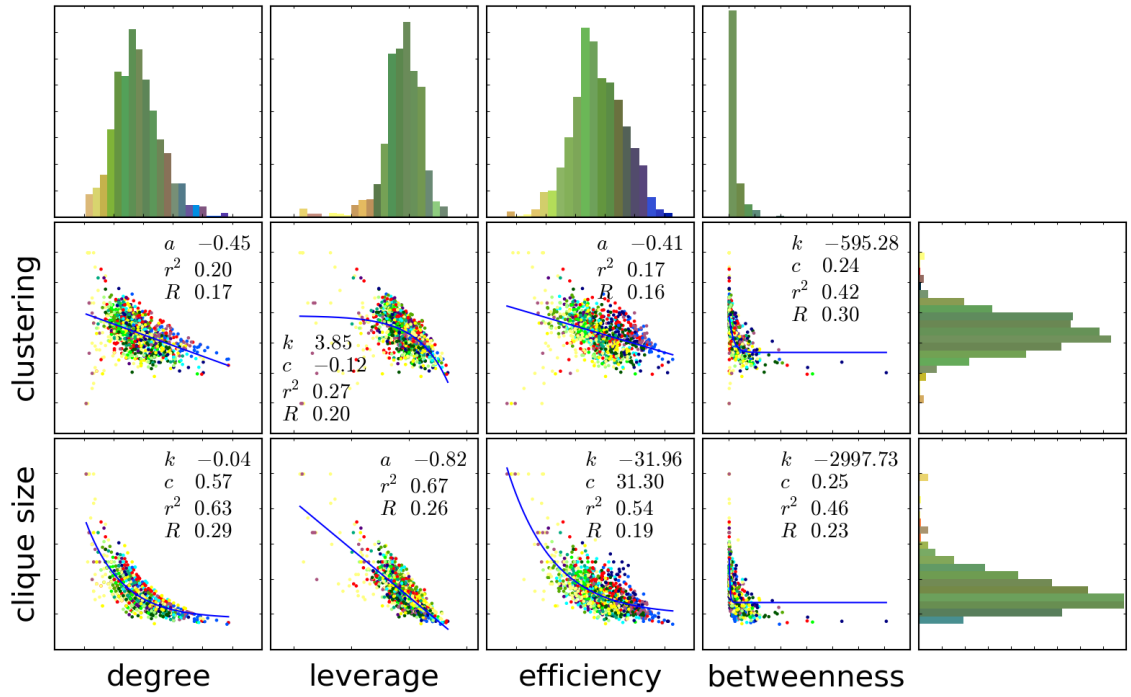

Figure 4.5: **Correlations of segregation and integration measures.** Top and right sides: distributions of regional measure values (bars), colour coded by the mean colour of comprised regions. Center: scatter plots of pairwise regional measure values (dots). Regions are colourcoded by their main structure. Blue line is fitted linear ($f(x) = ax + b$) or exponential curve ($f(x) = ce^{kx} + y_0$), obtained by least square fitting both models to data and choosing the one with lower r^2 coefficient of determination value. Legends show parameters of model fit (k and c for exponential, a for linear fit), coefficient of determination ($r^2 = 1 - \sum \frac{y_i - f_i}{y_i - \bar{y}}$) and normalized redundancy (R) (see Appendix C).

more negative U indices indicate the inverse relationship between the measure values, and therefore a topologically rather segregated information processing position of the node. Cortical regions have U values close to zero if they possess average values (ranks) in both measure groups, consequently being specialised neither as effective integrators nor as highly segregated areas.

The rationale behind using measure *ranks*, rather than normalised measure *values* directly, is to ensure a more balanced competitiveness among the regions by minimising the adverse effect of outlier regions usually having very low degrees, at the cost of loosing any additional information carried by the shapes of the measure distributions.

4.4.3 Results: Regional specialisation

Analysis results of the above U index, aggregating all the integration and segregation measures, are shown in Figure 4.6. Distribution of the regional values (Figure 4.6A) shows that the cortical network has a broader regional distribution than its random surrogates, but it is about equally wide to its spatial surrogates (mean $\pm$ standard deviation of regional values: cortex: U^C = 0.00 $\pm$ 0.49 , spatial: U^S = 0.00 $\pm$ 0.49, random: U^R = 0.00 $\pm$ 0.41). This result suggests that spatial wiring constraints, specifically, the formation of short-range connectivity accompanied by a small set of long-range connections, facilitates regional specialisation in the cortical architecture.

Anatomical structure level analysis (Figure 4.6B), although with a large intra-structural variation (see error bars), points to the *precuneus*, *superio-frontal* and *limbic* areas as the structures specialised to high integration capacity, and indicates greatly segregated information processing potential of the *orbito-frontal*, *postcentral* and *inferio-temporal* cortices. Indeed, the difference between the anatomical structures *within* each of these groups is found statistically insignificant (two-sample unpaired *t-test*s between the regional U values of pairs of anatomical structures are all $p > 0.05$, not assuming identical variances), while anatomical structure pairs from different groups (between structures having low and high mean regional U values) are all found to be statistically significantly different (all p-values are $p < 10^{-5}$).

Region level results visualised on projections (Figure 4.6C) show that highly integrative and segregated regions are well-spread throughout the cortical surface. Nevertheless, the clusteredness of colours at some cortical locations shows a tendency towards consistent local specialisation, for example the *precuneus* and its neighbourhood and the cortical midline appears to be more integrated, while the *inferio-temporal* and *orbito-frontal* structures are rather segregated. The elevated specialisation values of these greater anatomical structures suggest their excessive capability to carry out global functional integration (consistently high U values, red colour) or segregated information processing (constantly low U values, blue colour).

Positive correlation between various integration measures, and negative correlation between integration and segregation measures have been found in earlier studies. Sporns et al. (2007) investigated the hub regions of the anatomical connectivity of both the cat and the macaque brain, and found these regions to possess consistently high integration metric values (degree centrality, closeness centrality and betweenness centrality) but low segregation indices (clustering coefficient). Van den Heuvel and Sporns (2011) found similar characteristics for the high degree hub nodes in a low-resolution anatomical connectivity network of the human brain. Our results extend the validity of these findings by showing that the above relations between integration and segregation measures in general are held when considering all the regions to the entire human

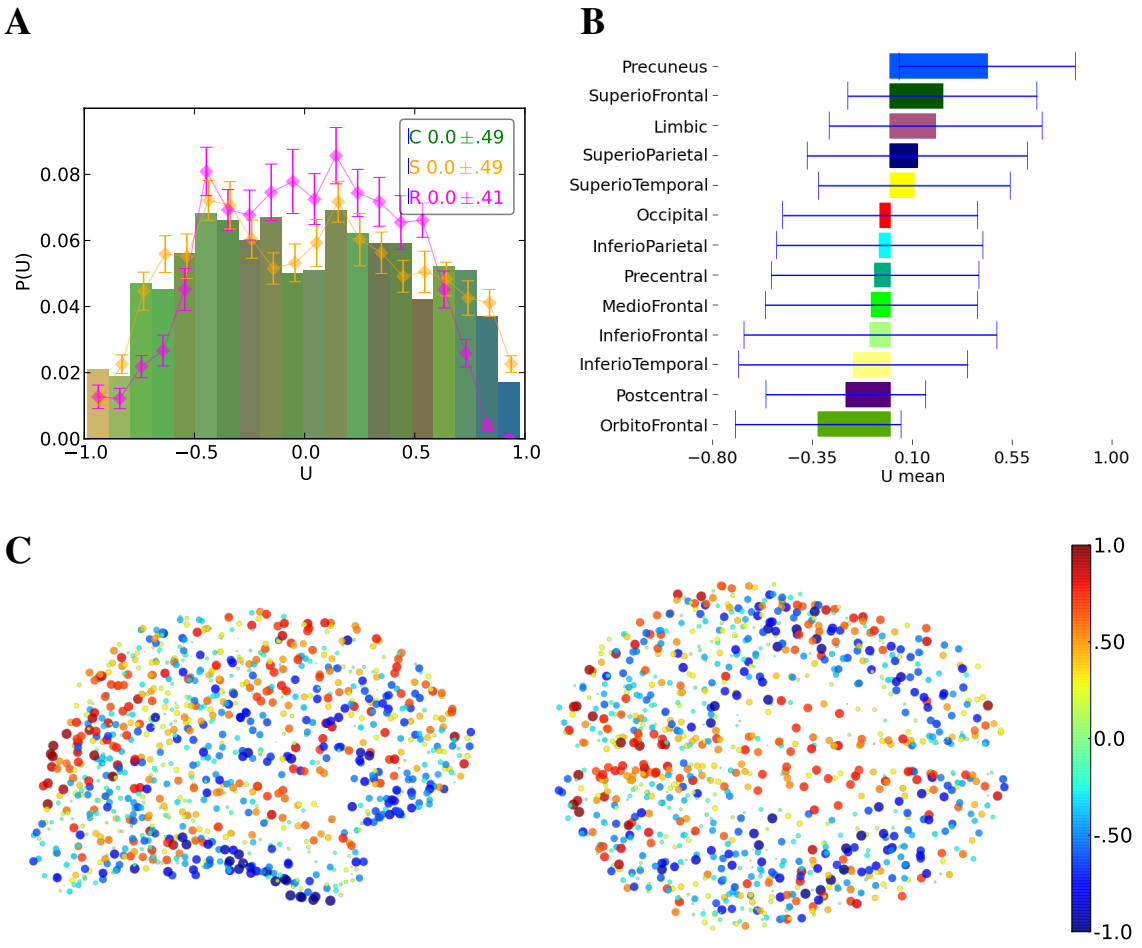

Figure 4.6: **Regional specialisation between integration and segregation.** (A): distribution of U values of the regions in the cortical network (bars and 'C' in legend) and its surrogates (spatial surrogates: orange colour and 'S' in legend, random surrogates: magenta colour and 'R' in legend). Bars are colour coded by the mean structural colour of the contained regions (see B). Error bars show standard deviation of each surrogate network type. (B): structural averages of regional results (bars) and their regional standard deviations (error bars). (C): regional U values on coronal (left) and horizontal (right) projections. Regions on projections are colour coded by their $U(i)$ index (see colourbar on the left side), and drawn with size proportional to the $|U(i)|$ absolute value of their indexes. Red: integrator regions, blue: segregated regions.

cortex.

4.5 Small-worldness

4.5.1 Introduction

The need for the simultaneous presence of integration and segregation poses opposing demands for the 'design' of a network architecture (Tononi et al. (1994)). A network possessing this balance between being too strongly integrated and too strongly segregated is called a small-world network. Small-worldness was found to be one of the most fundamental organisational property in a broad range of natural, social and technological networks (Watts and Strogatz (1998)) including neural (Humphries et al. (2006)) and brain networks (Sporns and Honey (2006), Bassett and Bullmore (2006), Bassett et al. (2006)).

In their seminal paper, Watts and Strogatz (1998) devised a simple network model that explains the development of small-world architecture by interpolating between random and lattice graphs. This model, emphasising the heterogeneous nature (neither entirely regular, nor fully random) of small-world topologies, still remains the basic model for the notion of small-worldness. Utilising the Watts-Strogatz model, Sporns (2010) intuitively explains the abundance of small-world architecture by the necessity of real-world complex networks to possess such heterogeneous topologies to a varying degree, as opposed to the idealised, homogeneous models of random and regular lattice networks.

In this section, we will assess the degree of small-worldness of the cortical connectivity.

4.5.2 Methods: The small-world index

For the quantitative assessment of small-worldness, the network's high integratedness is usually translated to relatively short path lengths (comparable to random, and exceeding lattice surrogate networks), while strong segregation is measured by a high level of clustering (comparable to lattice, and exceeding random surrogate networks) (Sporns (2011)). From the several formulae developed to assess the degree of small-worldness of a complex network (eg. Latora and Marchiori (2001), Humphries and Gurney (2008)), we use an altered version of Humphries and Gurney's small-worldness index (Humphries and Gurney (2008)), modified in the following way:

$$SW = \frac{C}{C_{rand}} * \frac{E}{E_{rand}} \tag{4.8}$$

where C and C_{rand} is the mean clustering coefficient of the network and its random surrogates, while E and E_{rand} is their efficiencies, respectively. We note, that Humphries and Gurney (2008)

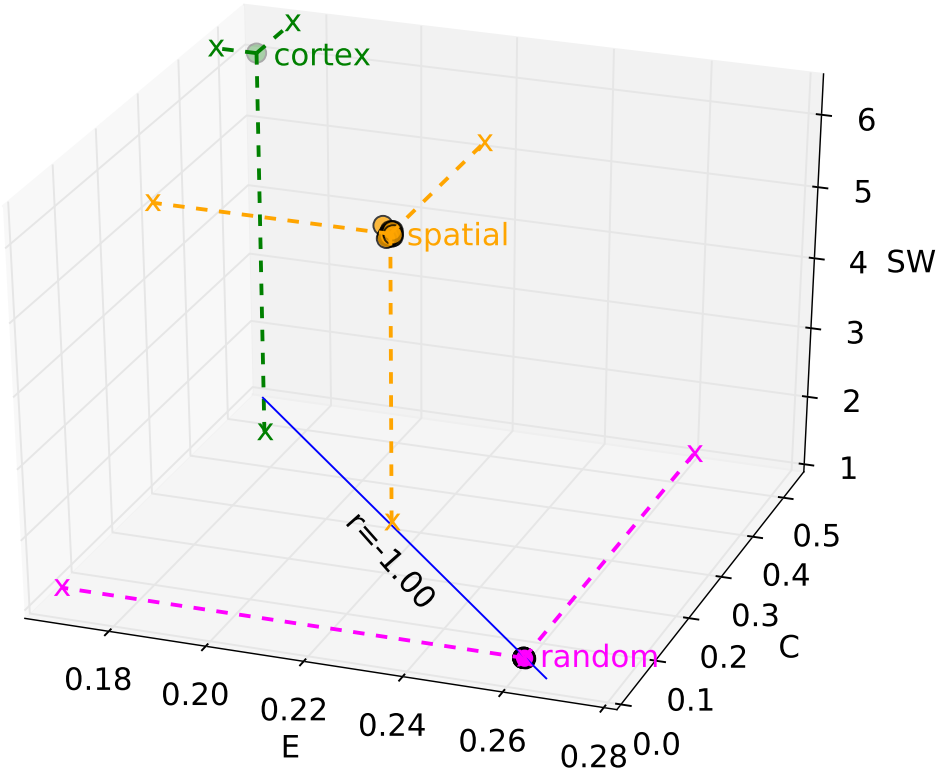

Figure 4.7: **Small-worldness evaluation.** Relation between clustering coefficient, global efficiency and small-world index in cortical connectivity and its surrogate networks. Each coloured circle represents a network, with dashed lines guiding the eye to their projections on side panes. Random surrogates lay on the E – C pane with small-world index SW=1 by definition. Note the remarkably similar values for all three measures within each surrogate group. Blue line shows correlation between clustering coefficient and global efficiency across all the investigated cortical and surrogate networks with r correlation coefficient indicated. E: global efficiency, C: clustering coefficient, SW: small-world index, r: Pearson correlation coefficient.

use average path lengths instead of efficiency. A network is said to be small-world, if it has $SW \gg 1$.

4.5.3 Results: Small-worldness of the cortical network

When considering the global integratedness and segregation of the cortical network compared to its surrogates, shown for the utilised two measures in Figure 4.7, we find that the cortex, both in terms of its global efficiency and clustering coefficient, significantly differs from both its lattice and random surrogates (cortex: $E^C = 0.174$, $C^C = 0.464$, spatial surrogates: $E^S = 0.214 \pm 0.001$, $C^S = 0.298 \pm 0.004$, random surrogates: $E^R = 0.260 \pm 0.001$, $C^R = 0.048 \pm 0.001$, one-sided

significance test assuming normal distribution of surrogate means: $p < 10^{-5}$, for both surrogate groups and both measures). Considering that the total connection length of each region in the cortical network is the same as in its spatial surrogates, these results indicate that the long-range cortico-cortical connections of the connectome are distributed in a topologically sub-optimal way for high integration (efficiency). Furthermore, the clustering coefficient indices demonstrate an excessive tendency of the cortex to form topologically segregated neighbourhoods of groups of regions, much beyond what would be expected from the spatial wiring constraints of its individual regions. Therefore, not only when compared against spatially non-constrained random surrogates, but also when taking into account the number and total lengths of the connectivity of each cortical region, the cortex appears to strongly favour topological segregation over integration.

The presence of an extremely high level of clustering in the cortex (C^C/C^R = 9.67), that naturally comes with some cost in its efficiency (E^C/E^R = 0.67), indicates a small-world cortical topology. In order to quantify the degree of small-worldness of the cortical network in comparison with its spatial surrogates, we calculate the above introduced small-world index SW to these networks. We obtain a fairly high SW_C = 6.442 small-world index for the cortical network assessed against its random surrogates, indicating the well-expressed small-world organisation of the cortex. In comparison, we obtain a significantly lower SW_S = 5.098 $\pm$ 0.029 small-world index for spatial surrogates assessed against random surrogates (one-sided significance test assuming normal distribution of surrogate means: $p < 10^{-4}$). Random surrogates have a small-world index SW_R = 1 by definition. The comparable magnitude of the small-world indices of the cortical network and its spatially constrained surrogates indicates that the physically predominantly local connectivity of the cortex plays a crucial role in shaping the characteristics of its gross architecture on the large scale. However, the significantly higher cortical small-world index also highlights that the cortex, due to its increased local segregation, exhibits the small-world property beyond what is implied by its local connectivity, despite its decreased global efficiency.

Utilising the original version of Humphries' small-world index (Humphries et al. (2006)), small-world attributes of this dataset have been found in Hagmann et al. (2008) (see their supplementary materials). Several other studies have also reported the small-world organisation of the structural connectivity of the human brain (Hagmann et al. (2007), van den Heuvel et al. (2010), Van den Heuvel and Sporns (2011)). Our results extend the findings of these studies by showing that spatial wiring constraints account for a large extent, but not for all, the small-world characteristics of the human cortex. We hypothesise, that the excess "small-worldness" of the connectome can be explained by the functional relevance of this prominent organisation pattern, specifically, by the widely accepted property of small-world architectures to naturally foster a balance between

functional integration and segregation (Bassett and Bullmore (2006), Sporns and Honey (2006)).

4.6 Overview of results

In this chapter, we carried out a detailed assessment of the functional integration (Section 4.2) and segregation (Section 4.3) abilities of the cortical connectivity by a set of relevant complex network measures for each phenomenon. Globally, we found a significantly increased functional segregation and decreased functional integration capability (especially in global efficiency) in the cortical connectivity compared to both of its surrogates groups. This decreased cortical integration capability is further underscored by the fact that the spatially similarly constrained spatial surrogates in fact possess less long-range connections than the cortex does (see Section 3.3.3), which should naturally render them topologically less integrated. We shall further assess the functional consequences and potential benefits of the topologically lowered global integratedness of the cortex in Chapter 7.

Internally, we found that while high segregatedness, both spatially and topologically, is a rather homogeneous property of the entire cortex, there is considerable deviation in the regional integration efficiency across the cortex. In particular, our results indicate, that the topologically most capable regions in carrying out functional integration are spatially centralised around the caudal part of the cortical midline, comprising most of the *precuneus*, the *cingulate cortex*, and some *superio-parietal*, *occipital*, *superio-frontal* areas.

Contrasting regional integration and segregation capabilities revealed a higher than topologically expected specialisation of the cortical regions, which was nevertheless attributable to its spatially local connectivity (Section 4.4). While the location of these extreme integrator/segregated regions are well distributed throughout the cortical surface, some degree of consistent specialisation at the level of greater anatomical structures is noticeable. Specifically, we detected the *precuneus*, the *superio-frontal* and the *limbic* areas as the main integrator structures, while large *frontal*, *precentral* and *postcentral* areas demonstrated a significantly segregated topological positioning.

Finally, we extended earlier results on the small-world organisation of the cortical structural connectivity by showing that the spatial constraints of forming predominantly local white-matter connections is a fundamental, however, not exclusive, facilitator of the significantly strong small-world architecture of the cortex (Section 4.4).

In this chapter, we gained some preliminary insight into the properties of integration, segregation and small-worldness on the micro- (region-region) and macro-scale (global network mean). However, our findings so far provide only limited information on the architecture of the cortex. For

example, with the algorithm of Watts and Strogatz (1998) one can construct networks with high clustering and small-world architecture that are not separable to modules, while modular small-world networks can also be easily created by the algorithm of Sporns (2006). We shall therefore turn to the investigation of the cortical architecture on the meso-scale in the next chapter, and assess the expression of some generic network organisation principles in the cortical connectome.

Chapter 5

Modularity, hierarchy and centrality

Organisation features of the modular architecture of the cortex

In the previous chapter we have found that many of the individual cortical regions, the micro-elements of the network, have a tendency to adopt either an integrator or segregated topological position, and how this regional specialisation leads to a small-world architecture on the global scale of the heterogeneous cortical topology. In between of these two extremes of brain network organisation scales, however, is the intermediate level of meso-scale, where groups of regions may form internally tightly integrated, but globally (i.e., from the rest of the network) segregated modules (Kaiser (2011)). The potential functional significance of these modular elements lays in their topological capability to carry out specialised information processing tasks, and thus collectively act as a single functional unit of the network (Sporns (2010)). Beyond the actual identity of the modules, the particular way by which these modules combine their specialised activity, presumably at least partially determined by their anatomical relations, is also of high importance in describing how information is globally processed in the brain, and may be pivotal in understanding how higher level cognitive capacities emerge (Bressler and Menon (2010)).

In this chapter, our investigations are organised around the module formation of the cortical connectome on its meso-scale. We will attempt to characterise the large-scale organisation of the cortical topology emerging from its meso-scale structure, that is, the relation between its network modules. For that end, we assess the level of centralisation, as opposed to distributedness, among the modules by evaluating the expression of two basic network organisation principles: hierarchical architecture and core formation.

Hierarchical architectures can be defined in multiple ways (Kaiser et al. (2010)) of which we

shall investigate two specific types. Firstly, utilising the basic idea of Ravasz and Barabási (2003), we shall assess the globally centralised topological positioning of high degree regions, which is indicative to their hierarchically distinguished role. Secondly, after finding evidence for the global modular organisation of the cortex, we shall attempt to characterise cortical hierarchy in terms of an iteratively embedded, hierarchical formation of module components at multiple scales, as it was introduced in Sporns (2006).

The detailed analysis of the obtained hierarchically modular architecture will be followed by the assessment of centralisation among the found cortical modules. Specifically, we shall compare two potentially significant central substructure of the cortical connectivity: its rich-club (Van den Heuvel and Sporns (2011)) and s-core formation (Hagmann et al. (2008)), by contrasting their topological significance and positioning. Finally, we shall end the chapter by assessing the level of centralisation in the cortical connectome.

5.1 Hierarchical organisation of the cortex

5.1.1 Introduction

Hierarchical organisation is believed to be one of the most central architectural features of various complex social networks or the World Wide Web (Ravasz and Barabási (2003)). Hierarchical aspects of network architectures can fundamentally affect their evolution, development, adaptability and efficiency on multiple scales. Despite the importance and wide acknowledgement of the phenomenon in brain sciences, the question of hierarchical organisation has not yet been analysed in large-scale whole-brain networks as comprehensively as for instance the concepts of modularity or regional centrality (Kaiser et al. (2010)), partly due to a lack of consensus over the formal definition and assessment of this rather informal notion. To our best knowledge, so far there has been no attempt to characterise the hierarchical aspects of the topological organisation of the entire human cortex on the large scale. In this section, we begin the analysis of hierarchical module structure of the cortical network by assessing its global hierarchical characteristics.

5.1.2 Detecting global hierarchical organisation

Taken the intuition, that high degree nodes should occupy a topologically central position in a hierarchical network, as a starting point of their measure, Ravasz and Barabási (2003) introduced the simple but elegant hierarchy coefficient β for assessing hierarchical features of scale-free network. After the authors observed a distinctively exponential relation between the nodal degrees and clustering coefficients for various synthetic and real-world scale-free networks, they proposed

that the β exponent of the relation quantifies the tendency of high degree nodes to be linked with a sparsely intra-connected neighbour set (themselves hence having low clustering), thus they effectively serve as connector nodes between segregated parts of the network (Figure 5.1A).

Unfortunately, the human cortical network under study exhibit an exponential, rather than scale-free degree distribution (Hagmann et al. (2008)), and the nodal degree – clustering relation does not show a clear exponential relation for the direct application of the β index. Nevertheless, as the general idea of Ravasz and Barabási (2003) remains valid irrespective of the specific shape of the degree – clustering relation, we attempt to detect traces of the above type of hierarchical organisation by observing the trend between degree – clustering in the cortex and in its surrogates. Specifically, in sparsely connected and locally highly clustered networks, such as the connectivity of the cortex (see previous chapter), if high degree nodes of a network possess a lower than average clustering coefficient, then they are in position to connect segregated parts of the network, suggesting a hierarchical type architecture with these high degree nodes being in the centre (Figure 5.1A). As opposed to that, the equal or higher then average clustering coefficient of high degree nodes indicates a more homogeneous architecture and the lack of that hierarchical organisation pattern in such a network.

Importantly, by taking into account all network nodes, the degree – clustering relation is capable of indicating graduality in the multi-level hierarchical organisation of a network (layers with different colours in Figure 5.1A), in which lower degree nodes (blue nodes in Figure 5.1A) may correspond to locally more cohesive (i.e., highly clustered) lower hierarchical levels, while higher degree but less clustered nodes integrate more segregated, greater parts of the network at higher levels of the network hierarchy (green and red nodes in Figure 5.1A).

5.1.3 Hierarchical organisation results

In their seminal work, Ravasz and Barabási (2003) detected well-expressed hierarchical structure in all investigated non-spatial (non-geographical), real-world networks, but not in the spatial ones (the power grid network and the Internet). This supports the intuition that the high cost of establishing physically long connections substantially limits the type of topology spatial networks can exhibit. In a study of a 104-region structural network of the human cortex, however, Bassett et al. (2008) reported some, although restricted, hierarchical properties in the brain when finding significant hierarchical structure among multimodal cortical regions, but not within unimodal and transmodal regions.

Following the basic idea of Ravasz and Barabási (2003) (see above), we calculated the average clustering coefficients of groups of cortical region with similar degrees, relative to the global

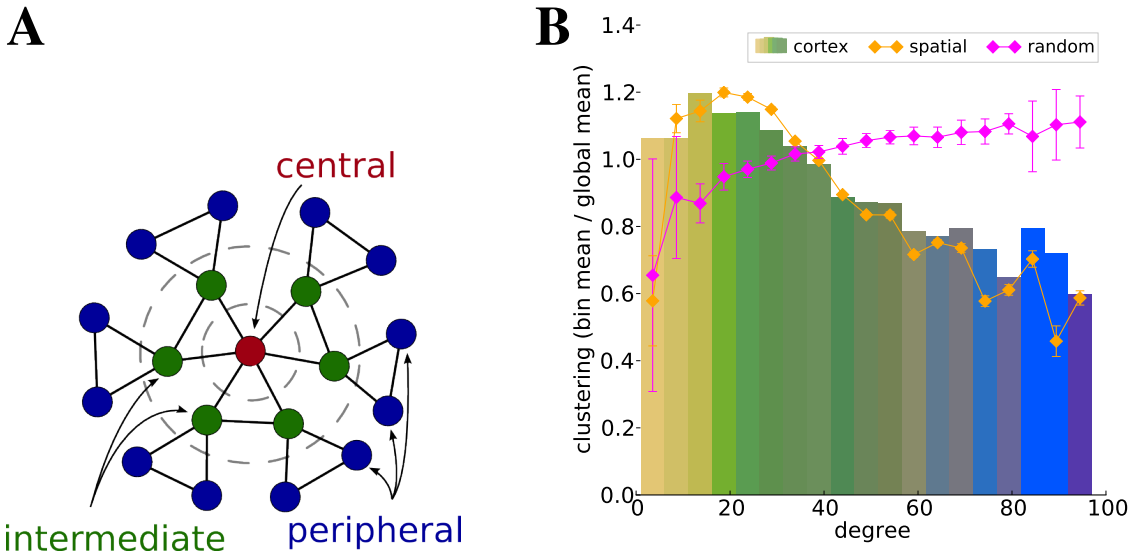

Figure 5.1: **Illustration of investigated hierarchical organisation and analysis results.** (A) A three level hierarchical structure composed of a central (high degree – low clustering, red), an intermediate (medium degree – medium clustering, green) and a peripheral layer (low degree – high clustering, blue). (B) Relation of nodal degree and clustering coefficient. Regions are binned by degree (x axis), and plotted against the average clustering coefficient of the bin normalised by the global average clustering coefficient of their network. Bars correspond to cortical results and are colour coded to the mean of the colours of the contained regions (see sector names in Figure 2.3). Diamonds and error bars represent surrogate mean values and standard deviations (see legend). Note the negative correlation in the cortex and the spatial surrogates, suggesting their hierarchical organisation, as opposed to the positive correlation in random surrogates.

clustering coefficient of the network (Figure 5.1B). We observe a steep decline in its mean clustering – degree relation (see bars), indicating that the cortex possesses the type of hierarchical organisation illustrated in Figure 5.1A. This finding confirms the general notion of a hierarchically organised brain (Kaiser et al. (2010)), despite the tendency of spatially embedded, physical networks not to develop such an architecture due to the basic spatial (geographical) constraints acting on them (Ravasz and Barabási (2003)). Furthermore, we observe highly similar tendencies for the spatially constrained surrogates of the cortex, but not for its spatially unconstrained random surrogates, in which clustering actually increases with region degree. This remarkably high robustness of the clustering – degree relationship indicates that the individual wiring lengths and positioning of high degree regions in the cortex is such that the globally hierarchical organisation naturally arises from these basic network features alone.

Furthermore, the colours of the bars in Figure 5.1B provide some insight into the role and positioning of various parts of the cortex in the found hierarchical organisation. Specifically, we

can observe the abundance of temporal regions (yellow bars) at low degrees, corresponding to more peripheral, lower hierarchy levels. Medium degrees, that are associated with intermediate hierarchy levels, are dominated by frontal regions (greenish bars). Finally, at high degrees, corresponding to the most central, highest hierarchy levels in our model, we find the abundance of parietal (blue), limbic (magenta) and some occipital (red) regions. This structural differentiation across degree range is held for spatial and random surrogate networks as well due to the identical degrees of their regions, but with markedly different clustering – degree trend in the case of random surrogates, in which high degree regions in the latter structures have lost their relatively low clustering.

In summary, utilising a simple measure to find traces of hierarchical patterns in the cortical architecture, our results indicate the presence of a globally hierarchical network organisation in the cortical connectome, in which high degree regions are capable of connecting segregated parts of the cortical network. In the following sections, we shall give further evidence to our findings in this section, and a more detailed characterisation of the cortical hierarchy.

5.2 Modules of the cortex

5.2.1 Introduction

It has been widely acknowledged that most real-world networks have a characteristic topology that allows for their separation into some relatively densely intra-connected and weakly inter-connected subgroups (Newman and Girvan (2004), Boccaletti et al. (2006)). These subgroups, illustrated in Figure 5.2, are usually referred to as the modules (or clusters, communities) of the network.

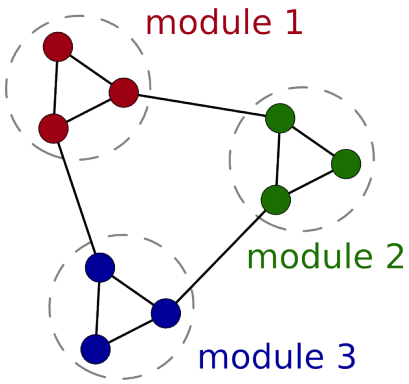

Figure 5.2: **Illustration of modular network architecture.** A modular structure composed of a set of highly intra-connected but sparsely inter-connected group of regions (modules, clusters or communities).

Recent studies all reported highly modular architecture of the human brain in its structural (Chen et al. (2008), Hagmann et al. (2008), Van den Heuvel and Sporns (2011)) as well as in its functional connectivity (Valencia et al. (2009), Meunier et al. (2009b), He et al. (2009)). Furthermore, studying the effect of ageing on the brain's modular structure, Meunier et al. (2009a) pointed out marked differences in the composition and putative topological roles between the modules in the rsFC of younger (mean: 24 years) and older human subjects (mean: 67 years).

Our motivation in investigating the modular architecture of the cortex lays in the fact, that, due their high internal connectedness and relative separateness, modules naturally have the capability for increased internal information exchange and cooperation and thus may serve as candidates for the *functional units* of the brain.

5.2.2 The modularity measure

Interestingly, despite the prevalence and salience of the phenomenon of modularisation, its general formalisation has proved to be so difficult that no widely accepted formal definition (let alone identification) for a modular architecture exists in complex network sciences.

However, from the large number of accumulated approaches (Boccaletti et al. (2006), Costa et al. (2006)), the so-called modularity index proposed by Newman (2004), is emerging as the most commonly used measure for assessing the *modular strength* of a given partitioning of a network (Danon et al. (2005), Rubinov and Sporns (2010)). Here, we will use its weighted, non-directed variant, which is formally defined as follows. Given a set of node groups (modules) M, that fully partition the network without overlaps, the modularity index Q of that partition is

$$Q = \sum_{u \in M} Q_u = \sum_{u \in M} \left[e_{uu} - \left(\sum_{v \in M} e_{uv} \right)^2 \right] = \sum_{u \in M} \left[\frac{\sum_{i,j \in u} w_{ij}}{l^w} - \left(\frac{\sum_{i,j \in u} k_i^w k_j^w}{l^w} \right)^2 \right], \tag{5.1}$$

where Q_u is the modularity index of module u, e_{uv} is the *proportion* of all weighted connections w_{ij} between modules u and v in the network, l^w is the sum of all weights in the network, and k_i^w is the sum of all connection weights of node i.

From the above definition, modularity is the difference between the ratio of intra-cluster edges (sum of weights) in the actual (positive term in Eq. 5.1) and in a fully randomised network (negative term in Eq. 5.1), the latter essentially serving as a null-hypothesis value (Newman (2006)). Therefore, intuitively, modularity assesses how much more intraconnected the modules of a given partition are than it would be expected based on the individual connection strengths of their nodes. Taking its values from the [0,1] interval, the modularity index of a strong community structure approaches 1. However, it typically does not exceed 0.8 for real complex networks even if they have a well-pronounced modular structure (Newman and Girvan (2004)).

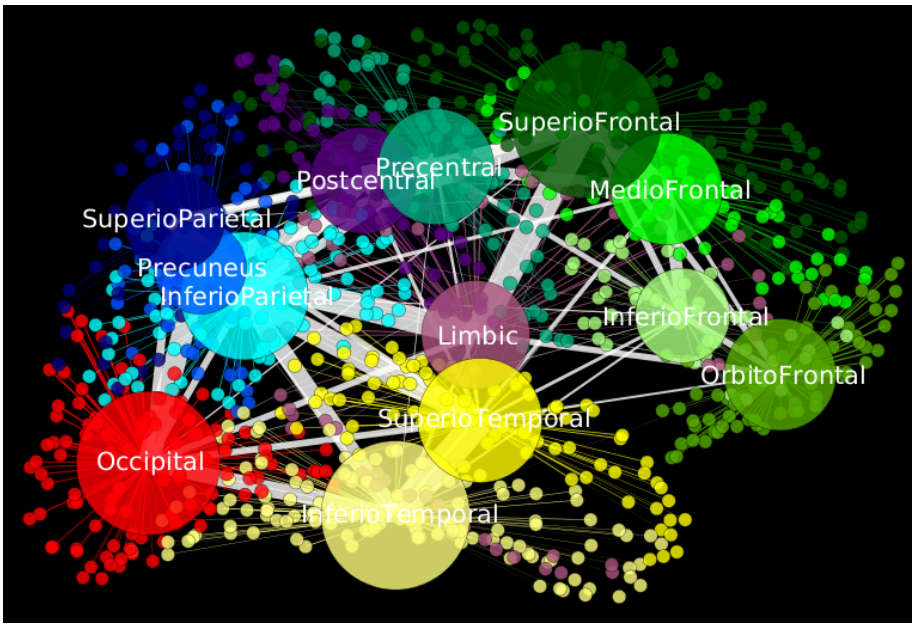

Figure 5.3: **Modular properties of anatomical structures.** Anatomical structures as modules on coronal projection. Structures, represented by large circles, drawn at the mean position of the contained regions, and with radius proportional to their size (number of regions). Inter-structure edge widths are proportional to the total strength of the interconnecting links.

5.2.3 Modular strength of the anatomical structures

Being capable of assessing the ”strength” or ”quality” of a certain community division with Q in Eq. 5.1, as an initial analysis, let us first investigate how strong community partitioning is formed by the anatomically (and not topologically) defined main structures of the cortex. The anatomical structures, their contained regions and interconnectivity strengths are shown in Figure 5.3. Modularity index calculation of the anatomical structures in the cortical network results in a fairly high Q_C = 0.41 value, while the same anatomical partitioning in its randomised networks yields Q_R = 0.0008 $\pm$ 0.002 and Q_S = 0.32 $\pm$ 0.003 values for random and spatial surrogates, respectively. The somewhat trivial quasi-zero Q_R value simply verifies that connection proximity, absent in random surrogates, provides the basis of spatially local module formation in the cortex. The higher than random, but still significantly lower than cortical structural modularity of spatial surrogates (one-sided significance test assuming normal distribution of surrogate means: $p < 10^{-4}$) suggests that the anatomical structures of the cortex are more modular (encapsulated) than what is expected from the degrees and connection lengths of their regions alone.

Having found a reasonable modular segregation of the main anatomical structures of the cortex, let us find that set of cortical region groups that exhibit the highest modular segregation in the

network, i.e., that collectively possess the highest modularity index. The best such partitioning of the connectome defines the topological modules of the cortex, that are important network elements due to their increased ability to carry out segregated information processing and thus realise specialised functional areas of the brain (Rubinov and Sporns (2010), Kaiser (2011)).

5.2.4 The module detection algorithm

The Q modularity index has proved to be a highly accurate and powerful indicator of the modularity strength of a given partitioning of a complex network (Danon et al. (2005), Boccaletti et al. (2006)). However, finding the best such partitioning, i.e., the partitioning with the highest Q modularity index, requires some further analysis tools. For example, we have seen that the anatomical structures represent a fairly strong cluster partitioning with a moderately high Q index. However, having been identified according to large-scale anatomical landmarks (sulci and gyri), they are by no means guaranteed to form the optimal modular division (partition with maximal Q modularity index) of the cortical structural connectivity.

Numerous algorithms have been developed to recover the modular structure of complex networks (for reviews, see Danon et al. (2005), Boccaletti et al. (2006)). In fact, many of them utilise Q as a 'fitness' measure to be optimised by some means. In this study, we use the simple and elegant spectral based algorithm developed by Mark Newman (Newman (2006)). Starting from the entire network as a single module, this algorithm splits each module into two in each iteration step. The procedure finds the optimal division of a module by utilising a so-called "modularity matrix" derived from the networks connectivity matrix. The leading eigenvector of this modularity matrix determines the node composition of the two submodules of each module to be split. The algorithm stops where no more increase in the global Q modularity index can be achieved by any more split.

Newman's procedure comes with a number of benefits over the formerly applied stochastic optimisation approaches (such as simulated annealing or genetic algorithms, e.g. Hilgetag et al. (2000)). Firstly, the procedure is a divisive technique that leads to a nested module hierarchy carrying potential extra information (Newman (2006)). Secondly, the technique is deterministic, thus reproducible and analytically more tractable. Thirdly, it is computationally cheap, therefore applicable to nowadays large networks (Danon et al. (2005)). And fourthly, it is fairly naturally generalisable to weighted and directed networks (Newman (2006), Leicht and Newman (2008)).

Two disadvantages of the method, however, are that it is unsuitable for detecting overlapping clusters, and, just like any other multi-resolution technique relying on a global null model, that the procedure suffers from scale limit issues in resolving the finest community organisation of large networks (Fortunato and Barthélemy (2007), Lancichinetti and Fortunato (2011)). It is also

worth noting here that the optional fine-tuning extension of the above introduced basic method, also proposed by Newman (2006), proved to be highly valuable. The utilisation of the extension resulted in a 5-10% increase in the final Q modularity values over the ones obtained by the basic version of the procedure, hence provided a higher 'quality' partitioning that the basic method alone could detect.

5.2.5 The global cortical modules

Utilising the above discussed algorithm of Newman on the cortical network, we obtain a module partition with a considerably high, Q_C = 0.65 modularity index and with N_C = 8 discovered modules, shown in Figure 5.4. As opposed to that, spatial surrogates only reach a significantly lower (one-sided significance test assuming normal distribution of surrogate means: $p < 10^{-4}$), but still relatively high level of modularity: $\overline{Q}_S$ = 0.55 $\pm$ 0.005 (random surrogates, as expected, express almost no modularity: $\overline{Q}_R$ = 0.15 $\pm$ 0.001) and $\overline{N}_S$ = 5.95 $\pm$ 0.22 number of spatial surrogate modules (random: $\overline{N}_R$ = 4.50 $\pm$ 0.59). The difference between the modularity index of the cortex and those of its spatial surrogates shows that the spatial constraints on the length of cortico-cortical white-matter connections is a fundamental, but not exclusive factor in increasing the higher than expected strength (Q_C) and granularity (N_C) of the cortex's global modular architecture.

Outstandingly, the eight modules found retain 77.1% (n = 13769) of the cortical projections internally, while only 22.9% (n = 4098) of the connections run across module boundaries. This results in an average of 22.1% intra-module and 0.95% inter-module connection density, indicating that while more than every fifth intra-module region-pair is linked, this ratio is down to 1:100 between region-pairs from different modules. In comparison, the global connection density of the network is 3.6%.

5.2.6 Comparison with previous results

Module detection on the 66-node lower resolution derivative of the cortical connectivity dataset used in this study has been previously performed by Hagmann et al. (2008) and by Cabral et al. (2011), both studies reporting only six global modules. Nevertheless, their modules are in close correspondence with the ones found here: the two, rather large lateral modules of the above studies are each refined into two submodules in our results (into M3 and M4, and into M5 and M6 in Figure 5.4), while the other four modules are quasi identical. Apart from the obvious resolution differences, this discrepancy can also originate from, or at least be amplified by, the utilisation of the basic, non-weighted version of the module detection algorithm as well as by the lack of Newman's fine-tuning extension (Newman (2006)), that the other studies do not report

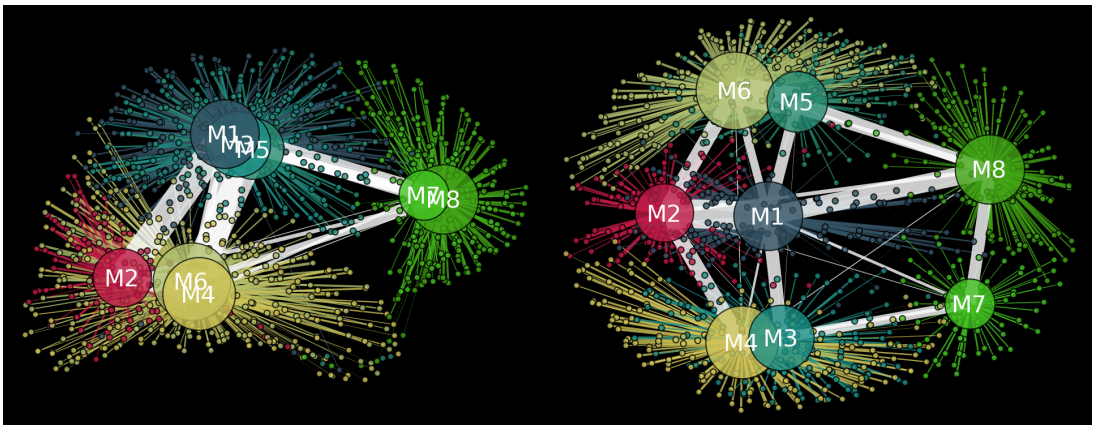

Figure 5.4: **Global cortical modules on projections.** The eight cortical modules, identified by applying Newman's module detection algorithm on the entire network, are represented by large circles, drawn at the mean position of the contained regions, with radius proportional to their size (number of regions), and are coloured by the average anatomical structure colour of the regions contained (for colour code, see Figure 5.3). Regions (smallest circles) are connected to their modules, and drawn with the colour of their modules. The widths of inter-module edges (gray lines) are proportional to the total strength of the interconnecting links. Note the lack of interconnectivity between the lateral modules on the right (M3 and M4) and left hemispheres (M5 and M6).

to have incorporated. Furthermore, Hagmann et al. (2008) also reports that "Recovering the modularity structure using high-resolution connection matrices produced similar results [to their low resolution ones] (unpublished data)", which directly points to the importance of applying the fullest variant of the module finding algorithm in order to detect the highest quality, most precise module partitioning. For the defence of the basic variant of the module detection algorithm, we note that the δQ increment achieved by the split of these lateral modules were rather insignificant ($\delta Q_{M3,M4}$ = 0.006 and $\delta Q_{M5,M6}$ = 0.009) when compared to the overall modularity index of the entire network (Q_C = 0.65), nevertheless, the detection of even these minor increments can lead to large differences between the module configurations of two partitionings (six modules versus eight modules).

A significantly different modular organisation is found by Van den Heuvel and Sporns (2011) in a 82-node structural network of the human brain, including subcortical areas. In that study only four global modules are detected, one located at the anterior and one at the posterior parts, on each hemisphere. Because the module partitioning algorithm used in that study is the same as that of Hagmann et al. (2008) and similar to the one used here, it is likely that including subcortical areas into the structural network of the brain alters its global module configuration. This claim was not

addressed in Van den Heuvel and Sporns (2011), therefore direct comparison between the cortical connectivities utilised in these studies, or even a consistent, higher-resolution dataset incorporating cortical and subcortical areas, is needed to provide evidence for or against this claim.

Confirming earlier results, we found in this section that the cortical connectome can be partitioned into a number of highly separated modules. Given their relatively large size in the current resolution of investigation, what kind of internal organisation these modules themselves have? In the next section, we shall try to answer this question.

5.3 Hierarchical modularity in the cortex

5.3.1 Introduction

Hierarchical modularity ('decomposability') has long been recognised as a potentially universal organisation feature of a wide range of complex systems in nature (Simon (1962)). The evolutionary and adaptive advantages of this architecture lay in the reduced risk any segregated module component impose on the entire system during its functional adoption, effectively accelerating the emergence of complex systems from simpler building blocks (Koch and Laurent (1999)). More recently, numerous computational studies have confirmed the generic tendency of complex networks to evolve towards such modular topology under a wide range of dynamical and functional selection pressures (Sporns et al. (2000), Gong and van Leeuwen (2004), van den Berg and Van Leeuwen (2004), Kaiser and Hilgetag (2007), Rubinov et al. (2009)).

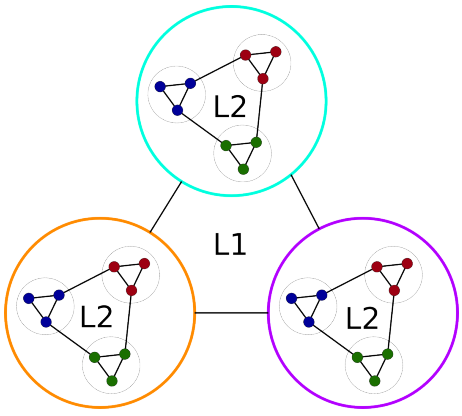

Figure 5.5: **Illustration of hierarchical modular network architecture.** Modules of the network (on level L1) are themselves composed of smaller modules (on level L2). The figure only depicts two hierarchical levels (L1 and L2), but of course this iterative pattern can continue to deeper hierarchical levels.

In particular, a widely acknowledged property of the cortex, and perhaps one of its most

fundamental 'design' principles, is its hierarchically embedded, multi-scale modular organisation at essentially all levels: from the micro-level of small neuron populations (Szentágothai (1983)), through the mesoscale of cortical columns (Mountcastle (1997), Somogyi et al. (1998)), up to the global macroscale of brain regions and greater structures (Hilgetag et al. (2000)) we are presently dealing with. However, in Section 5.2.5 we only retrieved eight, fairly large, global cortical modules (mean size: n=125 regions, 12.5%), and were unable to detect any further subclusters in any of the modules. This result contradicts the notion of multi-scale, hierarchical modularity of the cortex.

As we noted above, the Q modularity index, although it is technically capable of it, has difficulties in finding the fine modular structure in large networks (Fortunato and Barthélemy (2007), Lancichinetti and Fortunato (2011)). Indeed, as Fortunato and Barthélemy (2007) report about all the five biological networks they investigated: "The communities found through modularity optimisation are in fact clusters of smaller modules". In this section, we attempt to overcome the scale-limit effect of Newman's module detection algorithm and find the modular hierarchy of the cortex to the finest level our dataset allows for.

The hierarchical modular organisation we seek to discover here is similar to the fractal-like neural architecture proposed in Sporns (2006). In that study, the synthetic networks, composed of self-similar elements at each hierarchy level, were found to possess highest small-world index, 'functional motif' counts (Sporns and Kötter (2004)) and complexity (Tononi et al. (1994)) at a coinciding, intermediate value of the parameter governing the distribution of intra- versus inter-module connections, and furthermore in a scale-invariant manner (i.e., independently of the number of hierarchy levels). These properties, also characteristic of real brain networks, support the hypothesis of the presence of fractal-like patterns in the neuroanatomical connectivity of the cortex.

5.3.2 Methods: Fine-scale hierarchical module detection

In order to be able to assess the cortex's modular organisation at lower scales of the cortical connectivity network, we attempt to overcome the above algorithmic limitation by iteratively applying Newman's module detection procedure on readily identified modules. Potentially, this iterative approach allows for the progressive construction of a hierarchically embedded module structure at several predefined scales. At each scale, as it is shown in Figure 5.6, we essentially increase our resolution of investigation by zooming onto a specific group of regions, previously detected to form a module at that scale, and seek for submodules inside that region group.

In order to be able to investigate the modules globally at various resolution levels, we aim the detection procedure to return with a coherent set of modules with reasonably similar sizes at each specific resolution, by requiring a minimum number of regions forming each submodule.

These lower limits, also defining our scales (resolutions) of investigation, are the following: supermodules: 150 regions (15%), modules: 50 regions (5%), submodules: 15 regions (1.5%), minimodules: 5 regions (0.5%), micromodules: 2 regions (0.2%). It is important to note upfront, that the above procedure by itself does no guarantee any degree of approach of the module sizes to their corresponding minimum limit, as will be discussed in details shortly.

Technically, the subgraph partitioning approach proposed above has partially been applied in Hagmann et al. (2008), as an illustrative example that the visual and the frontal cortex are divisible into known anatomical substructures. However, neither did Hagmann et al. (2008) attempt to systematically uncover the cortex modular hierarchy, nor did they try to compensate for the scale limit issues of the Q modularity index, also utilised in their study.

5.3.3 Results: The cortical module hierarchy

Result illustration

Figure 5.6 demonstrates the method outlined above on the found module hierarchy of the cortex by zooming onto micromodule 'M21412' (second supermodule → first module → fourth submodule → first minimodule → second micromodule, see red subsquares in Figure 5.6). This micromodule is composed of three *precentral* and three *postcentral* regions and is located on the left hemisphere. In the progression of travelling through the six hierarchy levels, we can visually observe the formation of modules with increasing internal connection densities (Figure 5.8, fifth column). The concentration of a high proportion of the strongest edges of the parent module into, and not in between, its submodules is also salient at every level, complying with our informal definition of a module (highly intraconnected – weakly interconnected node group).

Figure 5.6 *(following page)*: **Module hierarchy of the cortex.** Zooming to micromodule M21412 (second supermodule, first module, fourth submodule, first minimodule, second micromodule) through the module hierarchy, from left to right, top to bottom. Matrix entry colours code connection strengths from black (no link) to red (strongest link). Colour stripes on the left and top of each matrix correspond to anatomical colorcodes (see Figure 5.3). Blue and red subsquares delineate modules at current hierarchical level, each red module is expanded on consecutive subfigure.

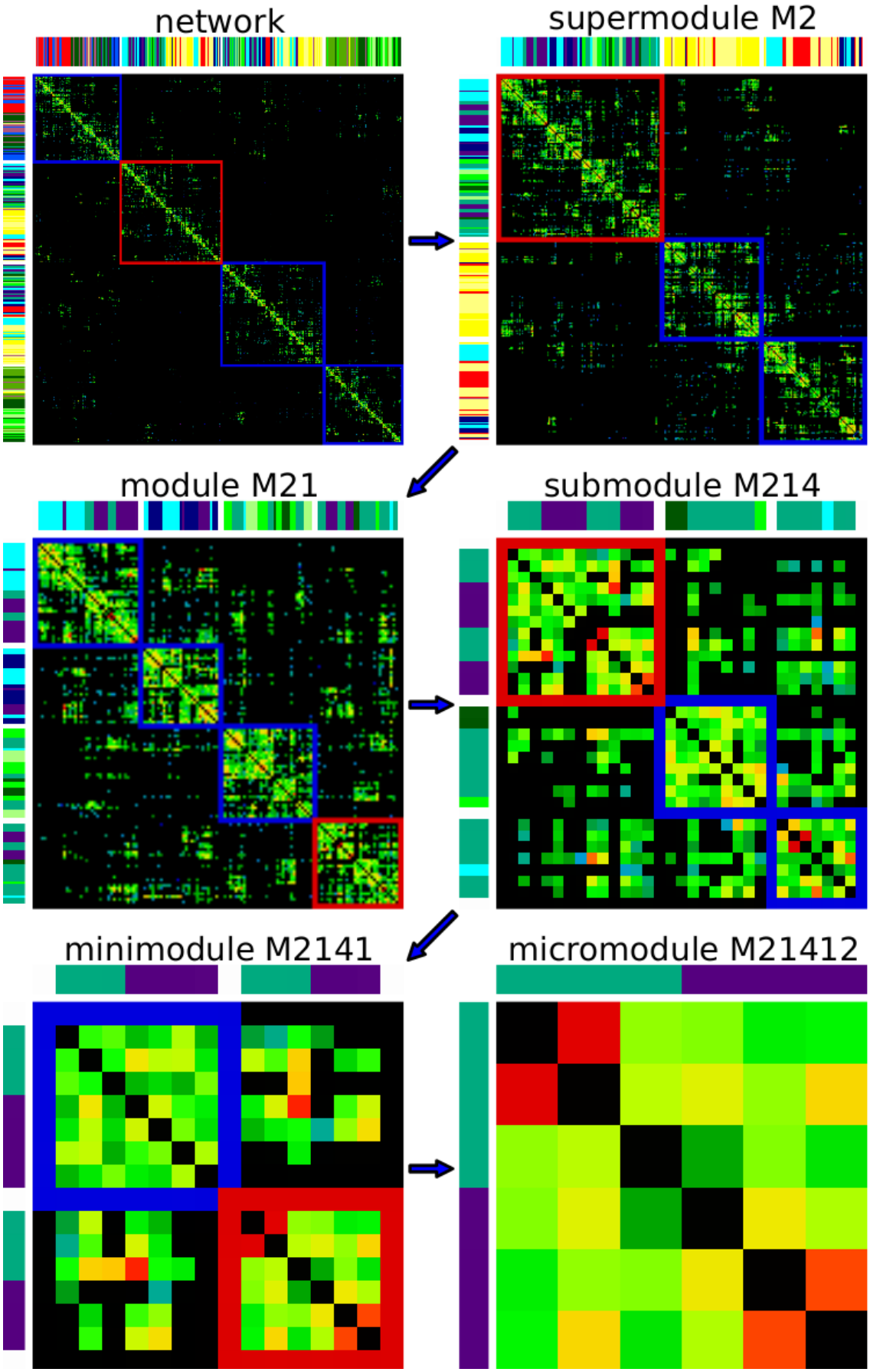
network
supermodule M2
module M21
submodule M214
minimodule M2141
micromodule M21412

Result verification

As Fortunato and Barthélemy (2007) point out, submodule partitioning of a network module by the iterative utilisation of Newman's algorithm is a *per se* unsafe approach in the modularity framework. Indeed, by neglecting all external links of the module towards the rest of the network, the detected submodules are not guaranteed to satisfy the modularity condition globally, that is, to have positive modularity index when considering the entire network (Q_u terms in Eq. 5.1). For this reason, it is also important to quantitatively validate the found submodules by calculating their individual Q_u modularity index in the whole network.

For every detected module on all hierarchy levels, we find that all modularity indexes are indeed positive, that is, their internal connection density is higher than what their global degrees alone suggest (random null hypothesis). This finding confirms that, according to the modularity framework (Newman (2004)), the detected modules are indeed valid submodules not only of their respective parent module, but also of the global network.

We note that the above discussed scaling limit of Q is observable in our results in the decrease in global Q modularity index on lower hierarchy levels (Figure 5.8 third column). This tendency, being in agreement with Fortunato and Barthélemy (2007), demonstrates why the 'flat', single-run application of the module detection algorithm in Section 5.2.5 was unable to find the finer modular elements of the network while maximising Q.

Intra- and inter-connectivity of modules

The most fundamental characteristic of the module hierarchy is an increase in both intra- and inter-module connection densities from higher to lower levels of the hierarchy (Figure 5.8 fourth and fifth column). Both trends are inevitable in any hierarchically modular network, otherwise at any given hierarchy level, one could find no more higher intra- than inter-connected submodules within the modules (see Sporns (2006) for a modelling example).

The increasing concentration of internal connections in turn result in saturation in the number of modules at the lowest, micromodule hierarchy level. As shown in Figure 5.8 (first and second columns), the first four iterations (network $\rightarrow$ supermodules $\rightarrow$ modules $\rightarrow$ submodules $\rightarrow$ minimodules) are able to increase the number of modules (and consequently to decrease average module size) by about a factor of three each. In contrast to that, at the level of minimodules, further splitting into micromodules is unsuccessful in more than 30% of the minimodules. This saturation is exactly the factor that limits our investigation on the utilised dataset, and forces the iteration of the module partitioning algorithm to stop at the level of micromodules (6.7 regions/module on average). The identification and analysis of submodules presumably present at finer hierarchy

levels would require the mapping of higher resolution whole-brain connectivity networks.

The strong discrepancy observable between internal and external connectedness (Figure 5.8 fourth and fifth columns), especially towards lower hierarchy levels, can be misleading in determining the amount of connectivity between the modules at the various hierarchy levels. We get more shaded picture if we also consider the number of connections in absolute terms. For example, an average micromodule possesses as much as 93% of its possible internal connections, but only 2.8% of its possible external links exist, and yet 83% of all connections ($n \approx 15000$) are between micromodules, and only 17% ($n \approx 3000$) within micromodules.

Thus the overall picture confirms the traditional notion about a predominantly locally concentrated cortical connectivity, with large, spatially distant parts of the cortex being largely unconnected (as can be seen on the interconnectivity between supermodules or modules in Figure 5.6), while at smaller scales spatially close cortical areas become increasingly tightly coupled (as can be seen in the inter-connectivity between minimodules or micromodules in Figure 5.6), granting increased potential for inter-module communication among miniature cortical neighbourhoods (sub-, mini- and micromodules).

Modules as functional units

The high internal connection density of the mini- and micromodules points to their capability to act as separate functional units in the cortical network (Section 4.3, Rubinov and Sporns (2010)). However, it has also been proposed, that the connectional fingerprint (set of all neighbours) of any brain region fundamentally determines the functional role it can play in a network (Passingham et al. (2002)).

In order to assess that phenomenon in the found module hierarchy, we measure the mean

---

Figure 5.7 *(following page)*: **Modules of the cortex in anatomical space.** Recovered modules at all five hierarchical levels are shown row-wise on horizontal (left) and coronal (right) projections. Modules, represented by large circles, are drawn at the mean position of contained regions, with radius proportional to their size (number of regions), and are coloured by the average anatomical structure colour of the regions contained (see Figure 5.3). Regions (smallest circles) are connected to their modules, and drawn with the colour of their modules. The widths of inter-module edges (gray lines) are proportional to the total strength of the interconnecting links. Note the lack of interconnectivity between the lateral supermodules (first row, light green circles). Strong coupling between the sub-, mini- and micromodules along the caudal part of the cortical midline is also observable.

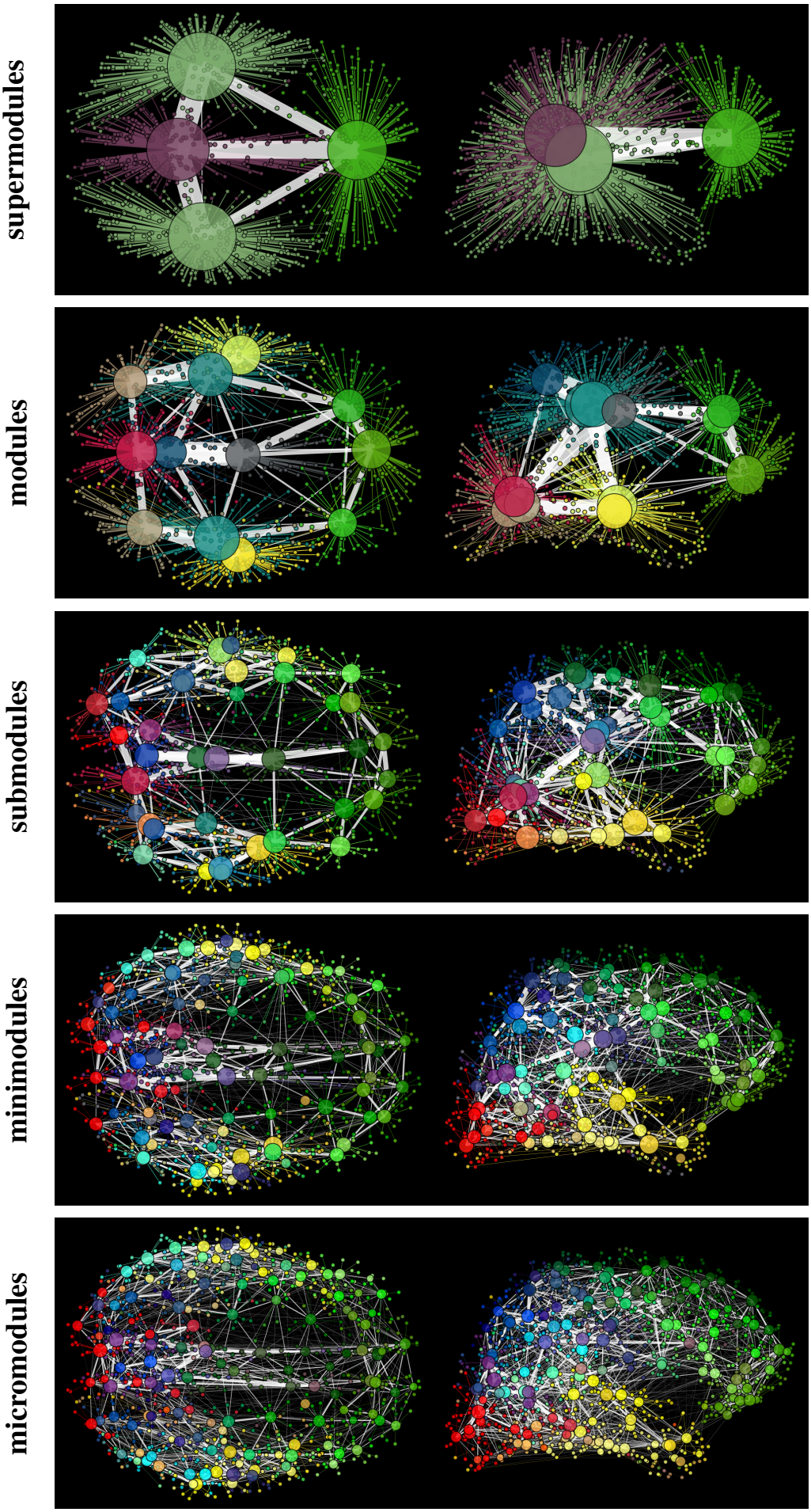
supermodules
modules
submodules
minimodules
micromodules

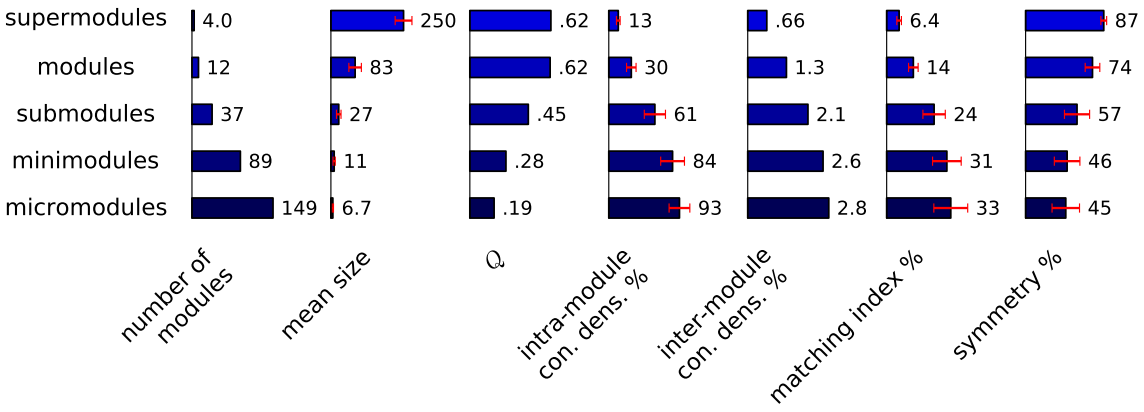

Figure 5.8: **Properties of the module hierarchy.** Mean module size: mean number of contained regions. Q: modularity index (Eq. 5.1). Intra-module connection density: mean internal connection density of modules (number of actual over number of possible links). Inter-module connection density: external connection density among modules. Matching index: mean ratio of overlap of connectivity (set of all internal and external neighbours) of every node pair *within* each module. Symmetry: mean ratio of overlap with hemispherically 'homologous' module, averaged over all modules. The homologous module of a module is identified as the module containing the largest number of homologue region pairs of the regions of the original module, and can be identical to itself (to deal with modules positioned along the cortical midline, such as the red module in the second row of Figure 5.7). Red error bars indicate standard deviation across individual module data.

similarity between the connection fingerprints of the cortical regions within the same modules at each hierarchy level by averaging the ratio of overlap between the individual neighbour sets of each region pair in every module (matching index, Zamora-López et al. (2010)). We obtain 30% and 33% average matching index values at the mini- and micromodule levels (Figure 5.8, sixth column), meaning that on average, each region shares about every second of its (both external and internal) neighbours with any other region from the same module on these hierarchy levels. These highly similar connectivity profiles provide further evidence for the high functional segregation or encapsulation of the smallest modules at the lowest hierarchy levels.

Spatial aspects: symmetry, encapsulation and anatomical composition

Figure 5.7 shows the detected modules at each resolution level on horizontal and coronal projections. It is noticeable, that while the modules are hemispherically highly symmetric on the large scales of supermodules and modules, this symmetry appears to break down as the resolution is increased. Quantitative evaluation of this characteristic in Figure 5.8 (last column) confirms, that,

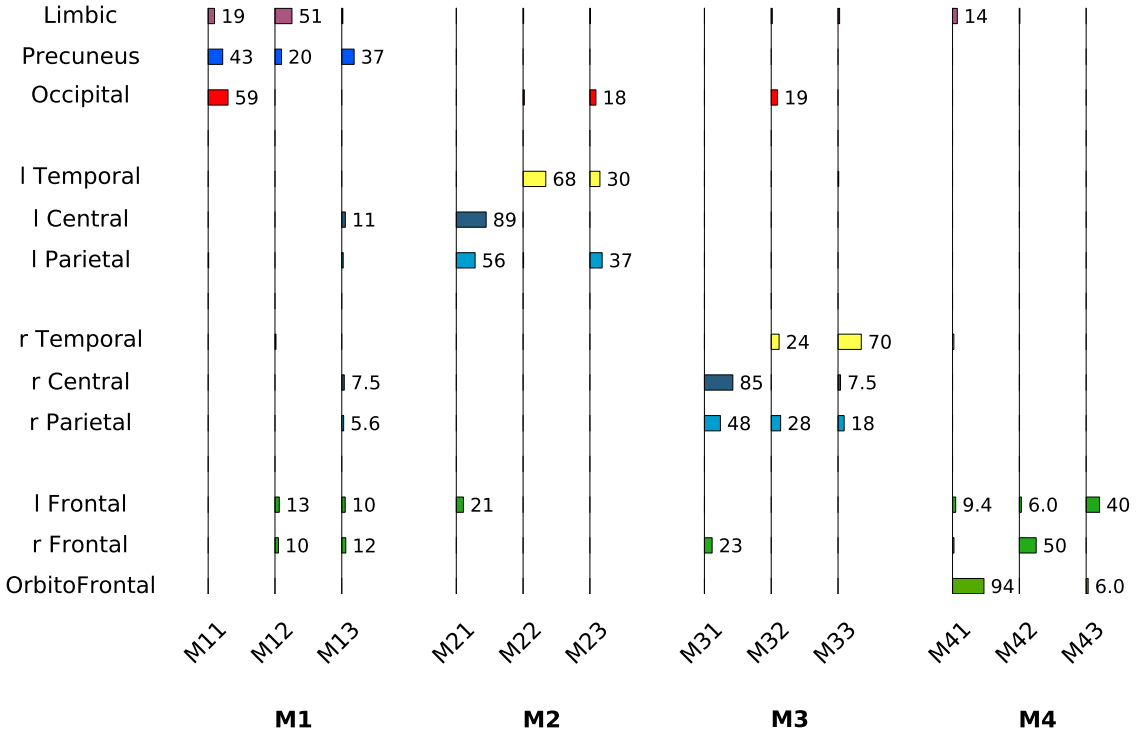

Figure 5.9: **Module composition of anatomical structures.** Each row shows the distribution of an anatomical structure in % across network modules (from M11 to M43), grouped by supermodules (M1 to M4). Higher than 5% overlaps are indicated by text labels. Supermodules: M1: medial, M2: left lateral, M3: right lateral, M4: frontal (see Figure 5.7). Anatomical structure prefixes: 'l': left, 'r': right, no prefix: unsplit medial structure.

as lower and lower hierarchy levels are considered, the cortical modules indeed gradually loose their initially almost complete hemispheric symmetry (ANOVA test for equal symmetry means on all module hierarchy levels: $p < 10^{-15}$). This steady increase in asymmetry from the supermodule to minimodule level saturates at the level of minimodules and micromodules at about 45% symmetry value (two-sample unpaired *t-test*s between pairs of module levels are all $p < 10^{-3}$ between supermodule, module, submodule and minimodule symmetries, not assuming identical variances, but $p = 0.45$ between mini- and micromodule symmetry values).

Even though the anatomical structures are far from being the optimal cortical modules (Section 5.2.3), there is nevertheless a rather high correspondence between the anatomical and modular partitioning. Modular composition of the anatomical structures is presented in Figure 5.9. The concentration of anatomical structures into only a few modules, and vica versa, is salient. The medial M1 supermodule contains the whole *precuneus*, and the majority of the *occipital* lobe and the *limbic* areas. The two lateral supermodules, M2 and M3, largely match with the temporal, pre- and post-central and parietal cortices on the left and right hemispheres. The frontal M4

supermodule contains large part of the frontal lobe and no other major structure. Furthermore, there is a remarkably high correspondence between the M41 module and the *orbito-frontal* cortex, suggesting a topologically high segregatedness of the whole *orbito-frontal* cortex from the rest of the network. The found correspondence provides credibility to the traditional anatomical partitioning of the brain from the perspective of its underlying structural network.

It is worth re-emphasising here that the module detection algorithm utilises only the topology of the cortical connectivity, no spatial information is incorporated. Therefore, the remarkably high level of symmetry, even at higher resolutions, the high spatial integrity (encapsulation) of the detected modules, as well as their relatively high anatomical correspondence, are all the exclusive consequence of the local, segregated connectivity of the cortex, and not of some *a-priori* knowledge of the module detection procedure. Furthermore, broad agreement between the anatomical and functional subdivisions and the topological modules have been previously reported in the cat and macaque brain (Hilgetag et al. (2000), Hilgetag and Kaiser (2004)), providing support for the potential anatomical and functional relevance of topological module partitioning technique in general.

5.3.4 Discussion

Recently, Ferrarini et al. (2009) and Meunier et al. (2009b) showed that the functional connectivity network of the human brain exhibits hierarchical modular organisation patterns. However, despite its wide acknowledgement (Sporns (2010), Stam and van Straaten (2012)), such finding has not yet been reported, to our best knowledge, on the anatomical connectivity of the human brain. One possible reason for this is that the analysis of multi-level, hierarchical modularity requires high resolution connectivity networks which have only recently become available for the living human brain.

Kaiser and Varier (2011) attributes the appearance of hierarchical modular organisation in the human brain to the increase in topological complexity of brain networks on evolutionary time scales, which is a natural consequence of evolutionary divergence and the specialisation of life forms. As it has been discussed in the introduction of this section, hierarchical modularity is also believed to accelerate evolutionary adaptation under selection pressure, increase the robustness against injury, and enables adaptive reconfiguration of the system (Simon (1962)). In the neurosciences, another functionally advantageous characteristic of hierarchical modular brain networks is their increased complexity (Tononi et al. (1994), Sporns (2006)), which we shall investigate in Chapter 7.

In the next section, we continue the characterisation of the meso-scale organisation of the

cortical connectome by assessing the level of centralisation (versus distributedness) in the cortex. We start that analysis by detecting the global core of the cortex.

5.4 The cortex's central core

5.4.1 Introduction

In the last section we have detected the hierarchically modular organisation of the cortex, its composition of a number of relatively tightly intraconnected but loosely interconnected clusters or modules essentially at all resolutions of the structural connectivity. In this section we investigate what topological relationship of these modular elements can tell us about the nature of functional cooperation among them. Specifically, we search the answer to the question: Do the putative functional processing units of the cortex hold equal roles in a topologically homogeneously distributed system, or rather, is there topological evidence that their activity might be coordinated by some "central executor" or "global workspace" (Dehaene and Naccache (2001), Baars (2002))?

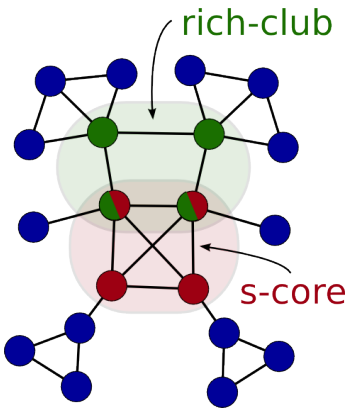

Figure 5.10: **Illustration of rich-club and s-core network structures.** Two core structures of a network: rich-club (highest degree regions, green regions) and s-core (most densely intra-connected regions, red regions). Note the overlap of the two structures.

The *core* of a network is a set of 'elite' nodes, that are topologically centrally positioned, forming a highly intra- and inter-connected global centre (Shanahan and Wildie (2012)). Figure 5.10 illustrates this type of network organisation with two such groups of nodes, the network's rich-club and s-core. The existence of such formations in network topology indicates the presence of centralisation in the network's dynamics and functional operation, which is fundamentally different from that of a homogeneous network architecture composed of distributed, identically segregated units (see Figure 5.12).

Core formation in the brain

Realising the importance of the phenomenon, numerous studies have investigated the core structure of various brain networks, utilising a range of analysis tools. In a series of studies, Zamora-López and his colleagues, utilising rich-club analysis (see Section 5.4.2), reported a highly connected, yet distributed core in the modular architecture of the cat thalamo-cortical network (Zamora-López et al. (2009), Zamora-López et al. (2010)), and pointed to the dynamical implications of this centralisation on the synchronisation and potential functional operation of the network (Gómez-Gardeñes et al. (2010)).

A remarkably tightly connected inner-core of the macaque brain is reported in Modha and Singh (2010) by k-core decomposition (see Section 5.4.2). Hagmann et al. (2008) utilise k-core and s-core decomposition (see Section 5.4.2 to recover the structural core of the same cortical network of the human brain that is used in this study. The results of both techniques, combined with other measures of integration, pointed to the posterior medial cortex as a highly central part of the human brain.

In a more recent work on a relatively low-resolution network of 82 cortical and subcortical regions of the human brain, a wide spectrum of network analytic tools were utilised to establish the prominent rich-club organisation of the large-scale structural connectivity of the human connectome (Van den Heuvel and Sporns (2011)). The results at low-resolution were in qualitative agreement with their exploratory high-resolution analysis (1170 cortical regions) in pointing to a strong rich-club organisation of the human brain. However, while the obtained spatially rather compact low resolution rich-club was located along the cortical midline, the authors exploratory high resolution analysis revealed a more scattered distribution of the rich-club regions, pointing to the characteristic scale-dependence of the analysis technique (Fornito et al. (2010), Zalesky et al. (2010)) and to the importance of a detailed high-resolution analysis.

Despite the potential significance of, and previous findings in, the topic of core formation in the brain, no thorough comparison has been presented between the two most commonly utilised methods, k-core (s-core) and rich-club analysis, neither regarding the significance of the two phenomena nor about identity of the regions on a high-resolution cortical connectivity network of the human brain.

5.4.2 Methods: Core detection algorithms

Difference between high integration and high coreness

Due to the interrelated nature of the two phenomena, there is usually a considerable overlap between the set of highly integrated nodes and the inner core of the network (Hagmann et al. (2008), Modha and Singh (2010), Van den Heuvel and Sporns (2011)). Here we make the following conceptual difference between high level of integration and network coreness. On the one hand, individual regions possess strong functional integration potential if they have high level of global or local centrality, measured by the metrics introduced in Section 4.2. Network coreness, on the other hand, is a group-level, meso-scale property: it is necessarily defined for, and identified in, a group of regions, that are found to be in a certain relation with each other and, *as a whole*, with the rest of the network.

Nevertheless, the above distinction is not meant to separate the naturally related concepts of integration and centralisation (Rubinov and Sporns (2010)). On the contrary, we expect the network core to have a large degree of overlap with the set of individual regions with high integration capacity. The purpose of proposing these definitions for the two notions is simply to stress the necessity of using specialised centralisation or core detection algorithms over the integration measures applied in Section 4.2, as the latter are not suitable to detect any relevant relation between central network nodes.

K-core and s-core detection

The core of a network is usually unveiled by some iterative peeling algorithm. These algorithms, in each step, remove ('peel off') a set of 'shell' or 'crust' nodes , with the aim to progressively focus on the more and more centralised ones. In this context, centralisation is assessed by some *coreness* condition.

The *k-core* of the network (Seidman (1983)), for a given degree k, is the set of nodes that are connected to at least k other nodes in the core. The *k-coreness* index of a node is then the highest k degree whose core the node is still the member of. Similarly, the weighted variant k-core, the s-core of the network (Hagmann et al. (2008)) is the group of nodes in which each one has a total connections strength of at least s towards the rest of the s-core. The tightest or innermost s-core of the network (simply s-core from here and on) is the set of remaining nodes at the highest strength threshold that still yields a non-empty s-core.

Rich-club: introduction

Another analysis related to the notion of centralisation assesses the so-called *rich-clubness* of the network. The rich-club phenomenon is the tendency of high degree nodes to be preferentially connected to each other (Zhou and Mondragón (2004), Colizza et al. (2006)). The phenomenon, like many others in complex network sciences, has been first observed in social networks, in which highly central individuals with *rich* connectivity tend to form a highly interconnected *club* (McAuley et al. (2007)). The degree of rich-clubness is usually measured by the $\phi(k)$ *k-density* function of the network, which is the internal connection density among all nodes with degree larger than k.

Let us note here the fundamental difference between obtaining the most centralised nodes by the two introduced methods. While rich-club counts all connections of the central nodes with every other network node, k-core and s-core decomposition only considers core-internal edges. As we shall see below, this difference makes k-core and s-core a more "elitist" core over the rich-club.

Rich-club: weighted version

A possible weighted variant of the rich-club measure, as introduced in Opsahl et al. (2008), evaluates the tendency of the highest connection weights to be distributed among high degree (*rich*) nodes. However, this variant, due to normalisation by the number of edges, results in a connection density independent index, which renders it unsuitable for measuring edge centralisation. As both phenomena are of interest here, that is, both connection *and* weight centralisation, we propose another weighted version of rich-clubness metric below, which is capable of capturing both tendencies.

We define weighted rich-clubness as the internal weighted connection density $\phi^W(k)$ of the set of nodes with degrees larger than k, $N_{>k}$, which is the ratio between the sum of connection weights $W_{>k}$ among the nodes in $N_{>k}$ and the maximum of their possible weight sum $W_{>k}^{max}$:

$$\phi^w(k) = \frac{W_{>k}}{W_{>k}^{max}} = \frac{W_{>k}}{\sum_{l=1}^{E_{>k}^{max}} w_l^{ranked}}, \tag{5.2}$$

where $E_{>k}^{max} = |N_{>k}| * (|N_{>k}| - 1)/2$ is the maximum possible number of edges among the nodes in $N_{>k}$, and w_l^{ranked} is the lth strongest (highest weight) link in the network.

With the above ϕ^w we define a normalised coreness measure function, which takes its value from [0, 1] for each k degree. ϕ^w is 1 only in the extreme case if $N_{>k}$ is fully connected by exactly the strongest connections of the network. In general, ϕ^w measures the fraction of interconnection strength within $N_{>k}$ relative to this theoretical maximum, given the set of weighted edges present in the network.

Let us note that in Eq. 5.2 the denominator is not calculable if $E_{>k}^{max}$ is greater than the number of edges E present in the network. This condition renders the interpretation domain of ϕ^w dependent on the connection density of the investigated network, and makes ϕ^w applicable for weighted rich-clubness measurement only for a fraction of the highest degree nodes $N_{>k_{min}}$. Specifically, for undirected graphs, the number of these nodes $|N_{>k_{min}}|$ cannot be larger than the real solution of the quadratic equation

$$E = \frac{x(x-1)}{2} \quad \Longrightarrow \quad x^2 - x - 2E = 0. \tag{5.3}$$

Eq. 5.3 finds the largest number of nodes x that can still be fully interconnected by the existing number of edges E in the network. The cortical network under study has $E = 17865$ connections, thus we get $|N_{>k_{min}}| = 188$ nodes as the largest assessable rich-club size. This size makes up about 20% of the nodes in the network, and renders $\phi^w(k)$ the domain of $k \in [k_{min}, k_{max}]$, where $k_{max} = 97$ is the largest node degree, and $k_{min} = 49$ is the degree of the 188th node in the rank ordered node list.

In summary, the novel ϕ^w metric introduced above (Eq. 5.2) unifies the earlier unweighted (Zhou and Mondragón (2004)) and weighted (Opsahl et al. (2008)) rich-club variants, and is hence capable of measuring the weighted concentration of edges among the rich-club regions, relative to the connection strength distribution of the network.

5.4.3 Results: Comparison of the cortex' s-core and rich-club measures

Coreness evaluation of the cortical connectivity network is performed by the above introduced two methods, s-core and weighted rich-club analysis (Figure 5.11). First, we examine the global degree of centralisation in the cortical network in comparison with its surrogates, and then we examine the core cortical regions the methods yield.

Figure 5.11 *(following page)*: **S-core and rich-club analysis results.** Top: core sizes (solid lines) and $\phi^W(k)$ weighted k-densities (dashed lines) of the cortex and its surrogates for the two core detection algorithms. Rich-club sizes (green) are the same for all networks due to their identical degree distribution. Colour-filled regions delineate surrogate ranges by their minimum and maximum values. Middle and bottom: n=100 (10%) strongest s-core and rich-club regions and their connections visualised on coronal and horizontal projections (middle row), and on abstract hierarchically radial layout (Holten (2006)) (bottom row).

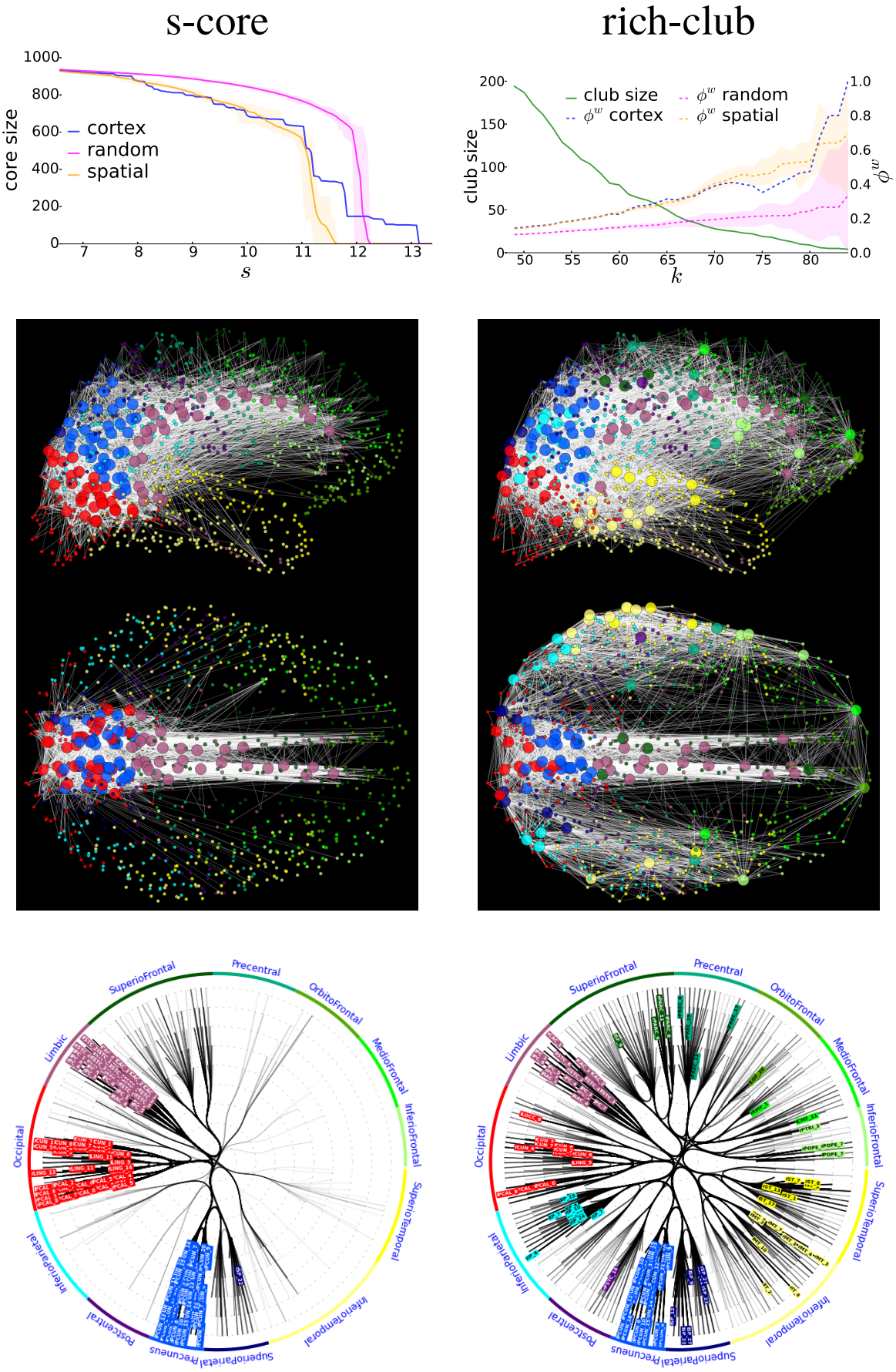
s-score
rich-club
core size
cortex
random
spatial
s
club size
club size
ϕ^w cortex
ϕ^w random
ϕ^w spatial
ϕ^w
k
Precentral
OrbitoFrontal
MedioFrontal
InferioFrontal
SuperioTemporal
InferoTemporal
SuperioParietal
Precuneus
Postcentral
InferoParietal
Occipital
Limbic
SuperioFrontal

S-core significance

Generally speaking, s-core analysis assesses a network's tendency to form a densely intra-connected inner core by measuring the size of, and overall connection strength within, the most strongly inter-connected group of nodes. We identify the s-core of the cortical network through a peeling procedure that iteratively removes less connected regions from a candidate s-core (see Methods). Examining the evolution of the s-core decomposition of the cortical network and those of its surrogates (Figure 5.11 top left) during the peeling procedure, we can identify two characteristic phases. In the early phase of the crust peeling process, that is, for relatively low strength thresholds (s<11), random surrogates are able to keep a significantly higher number of their nodes in the (weak) core than the cortical network or its spatial surrogates. This is clearly the consequence of the highly integrated and poorly segregated connectivity of random surrogates (Section 4.2), granting them higher resistance against the destructive peeling process in this low strength threshold regime.

This longer early phase then transitions into an unstable phase (s>11), in which the s-cores of both surrogate types diminish and vanish suddenly. The cortical network, on the other hand, continues to sustain a substantially sized s-core of n=100 regions (9.98%) for much longer. This s-core eventually collapses at a significantly higher strength threshold (s^C = 13.095) than its counterparts in the random (s^R = 12.055 $\pm$ 0.078, one-sided significance test assuming normal distribution of surrogate means: $p < 10^{-4}$) or spatial surrogates (s^S = 11.433 $\pm$ 0.124, $p < 10^{-4}$).

The fact that the s-cores of the connection length restricted spatial surrogates all vanish prior to that of random networks demonstrates the surprising tendency, that the specific spatial constraints of the cortical regions by themselves hamper the formation of a strong s-core in the cortex. This finding further accentuates the significance of the strong cortical s-core, and suggests that the white-matter "wiring" of the cortical network may be optimised towards the formation of a significant global s-core, which is much stronger than its connection length constraints alone would suggest.

Rich-club significance

An alternative measure of core formation in a network is the assessment of its rich-club index (Zhou and Mondragón (2004), Colizza et al. (2006)). Our rich-club index variant, ϕ^w, measures the tendency of high degree nodes to be both densely and strongly interconnected. Comparing the evolution of ϕ^w in the cortical network and in its surrogates (Figure 5.11 top right), we can see a slightly counter-intuitive outcome in the light of the s-core results: spatial surrogates reach substantially higher ϕ^W values than random networks for the whole valid range of the measures, and even keep up with the cortical network. However, in combination with the s-core results, this in fact indicates that while the cortex possesses a densely intraconnected internal core (strong s-

core), that core is not exclusively composed of the highest degree regions, because they are not more strongly interconnected than their spatial counterparts for any reasonable core size (for n>9 regions $\rightarrow$ k<80).

It is important to note that previous studies (Zamora-López et al. (2010), Van den Heuvel and Sporns (2011)) used random surrogates exclusively for assessing the rich-club property of the cat and the human brain networks, according to which the cortical network under study also expresses a highly developed rich-club (magenta versus blue line). However, our spatial surrogate result extends this picture by showing that this property originates from the relatively low variance in the spatial locations of highly connected regions (Figure 4.2), which, in combination with the highly clustered, local connectivity of the cortex, naturally results in a tendency for strong rich-club formation.

This observation is supported by the r *assortativity coefficients* of the networks. Degree assortativity is a global metric measuring the tendency of high degree nodes to be preferentially connected to other high degree nodes (Newman (2002)), and is thus highly interrelated with the phenomenon of rich-club formation. We obtain positive assortativity coefficients for the cortex (r = 0.29) which is highly similar to those of its spatial surrogates (r = 0.28 $\pm$ 0.004, one-sided significance test assuming normal distribution of surrogate means: $p = 0.10$), while almost no degree assortativity is found in random surrogates (r = 0.05 $\pm$ 0.005, $p < 10^{-4}$).

This preferentially mutual connectedness of high degree regions, resulting in the detected strong rich-clubs in both the cortex and its spatially constrained surrogates, indicate that the found rich-club formation tendency of the cortex naturally arise from the location of these cortical hubs and the spatial wiring constraints of the network.

Comparing the s-core and the rich-club

Let us now examine the detected s-core and rich-club of the cortex in detail. In order to be able to compare the two, we take an equal size group of the most central regions provided by each procedure. We choose the size of the final non-empty s-core for this, containing a reasonable proportion, n=100 (9.98%) regions, of the entire cortex.

The s-core and rich-club regions selected by the two methods (Figure 5.11) are largely consistent with those found by Hagmann et al. (2008) and Van den Heuvel and Sporns (2011) on lower resolution cortical networks. Our s-core (n=100 regions in final, non-empty core) and rich-club regions (n=100 highest degree regions) exhibit a considerable, exactly 50% (n=50 regions) overlap between the two groups. However, while we can observe a high level of spatial encapsulation of the s-core around the caudal part of the cortical midline, formed by the

precuneus, the *cingulate cortex* and the superior part of the *occipital lobe* (*cuneus*, *lingual gyrus* and *pericalcarine cortex*), this centralisation is, although also present, much less pronounced, in the cortex' rich-club, as about one third of it extends to the lateral and frontal parts of the cortex. Our finding on the spatially dispersed cortical rich-club is consistent with earlier studies reporting both spatially and modularly distributed rich-clubs of the cat thalamo-cortex (Zamora-López et al. (2010)) and in the entire human brain (Van den Heuvel and Sporns (2011)).

Additionally, as expected from their detection methods and is shown in Figure 5.11, the spread of arborization of the two cores are also markedly different. The more numerous (n=5662, 31.7%) projections of the rich-club establishes direct connectivity with almost the whole of the rest of the cortex (n=795, 88.5% regions). At the same time, the s-core possesses a smaller, as well as more internally directed, connection set (n=3921 edges, 21.9%), which connects it directly with only one third (32.7%, n=294 regions) of the rest of the network.

These differences, originating from the definitions of the s-core and rich-club structures, demonstrate the more distributed nature of the cortex' rich-club, as opposed to the rather encapsulated, but spatially and topologically central position of the s-core. Furthermore, unlike its rich-club structure, the s-core of the cortex appears to be optimised even against its physical wiring constraints, which suggests high functional relevance to that core structure, and renders it an appropriate candidate for some sort of putative central, global coordinator substructure of the brain (Baars (2002)).

Due to its above found spatial and topological properties, in the forthcoming analysis, we will consider the above detected s-core as the global core of the cortical network. Additionally, we hypothesise that the spatially rather scattered cortical rich-club is more suited for fulfilling the role of a set of distributed cortical hub regions, predominantly connecting their local neighbourhoods with distant parts as well as with the core of the cortex. Nevertheless, the large (50%) overlap between the s-core and rich-club regions suggests a great extent of functional cooperation between these highly intertwined core structures.

5.4.4 Topological location of the core in the cortex's modular architecture

Modular centralisation of the cortical s-core

In the last section, we have seen the spatially highly centralised anatomical structure composition of the s-core along the medio-caudal part of the brain. In Section 5.2 we have also found that the actual module organisation of the cortex is highly related, but not identical, to its anatomical division (Section 5.2.3). An important question regarding the topological positioning of the core at this point is whether it is evenly distributed among the modules of the network, and resembles

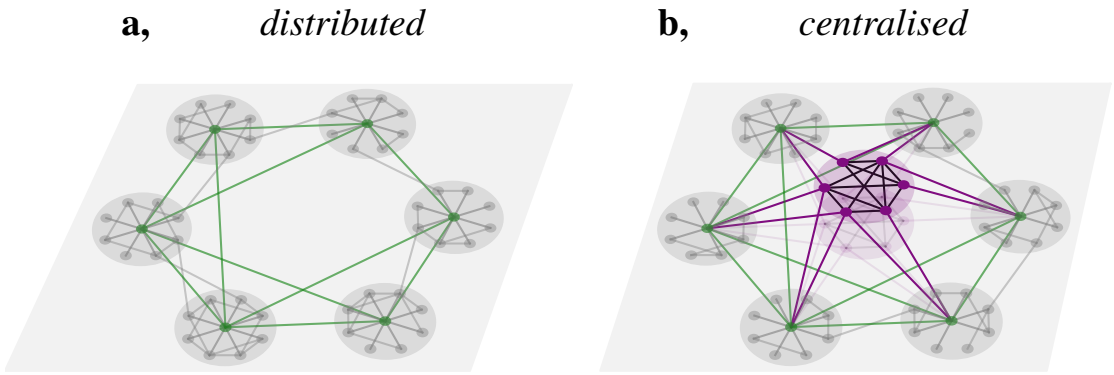

Figure 5.12: **Schematic diagrams of distributed and centralised modular architectures.** *a*: distributed organisation of an aggregation of segregated modules (large gray disks), capable of acting as specialised functional units, and cooperating predominantly via inter-module links of their high degree module hubs (green disks). *b*: in a centralised architecture, the densely intraconnected and topologically central network core (magenta) is in the position to effectively integrate information from the otherwise sparsely interconnected, but densely intraconnected, segregated modules (gray).

a highly interconnected multi-module hub structure, or whether it is positioned in a centralised manner by residing in a (small set of) central module(s). In this section we carry out a series of investigations to decide between the two, radically different, architecture types illustrated in Figure 5.12.

Considering the position of the core with respect to the modules of the cortex, we find that the entire s-core resides in a single supermodule out of four (25%), 90% of it is located in two modules out of 12 (17%), and 80% of the s-core is further concentrated in only three submodules out of 37 (8%). Conversely, the s-core makes up 42% of its supermodule, more than 50% of the two mentioned modules, and almost 70% of its three main submodules. The concentration of s-core into these module components clearly renders them a distinguished topological role, and provides support for the centralised, rather then distributed network organisation type (Figure 5.12*b*). In the rest of this chapter, our main aim will be assessment of this hypothesis by further analysis.

Connection centralisation towards the cortical s-core

Having established the modular concentration of the cortical core regions, let us now investigate the degree of *direct* centralisation of the connectivity of cortical modules towards the network core. To that end, we compare the average inter-module and inter-supermodule connection densities (actual over possible number of connections) with the connection density between the network core and the modules/supermodules. For a clear comparison, the three modules (one supermodule) in which

the network core resides (total of n=234 regions, 23.4%), are discarded from this analysis, in order to eliminate the overlap between the core and the modules [1].

We obtain 0.82% connection density between the core and the non-core both at the level of modules and supermodules (the values are the same, because the same connections are considered at both hierarchy levels). Less than half of this, only 0.38% of the possible connections exist between non-core supermodules at the supermodule hierarchy level, indicating the topologically central location of the core among the otherwise very loosely coupled supermodules of the cortex. As opposed to that, non-core modules are pairwise interconnected with a 50% higher, 1.2% connection density, due to many of them residing in the same supermodule, demonstrating no direct centralisation of the rather intra-supermodularly interconnected cortical modules towards the core.

In conclusion, the core appears to be an important *immediate* way station in between peripheral supermodules, however, in accordance with the found hierarchical modular architecture, the strong internal organisation of these supermodules lessens the importance of the core as a central communicator starting from the module level and on lower levels of the hierarchy. We note, however, that the above analysis only considered *direct* centralisation in the modular organisation of the cortical connectivity towards its network core, which we will extend by utilising more general complex network measures in the forthcoming analysis.

5.4.5 Intra-module organisation: local s-cores in supermodules

Introduction

Considering the findings on the relation between the cortex's global core and its module hierarchy found so far in this section, a possible scenario is that the cortex possesses a number of densely intraconnected and globally equally important 'local cores', presumably one within each of its supermodules. Indeed, the crust peeling procedure of the s-core algorithm is an extremely elitist strategy: it necessarily yields only one, the most strongly intraconnected group of nodes, even if multiple such groups are present in the network with comparable strength. Intuitively, an indicator of this scenario is a sudden drop in the core size at a certain threshold value, where one such alternative core is detached ('peeled off') from the somewhat more strongly interconnected remainder. Examining Figure 5.11 (top left subfigure), this is exactly what we see at $s \approx 11$ and $s \approx 12$. Furthermore, the fact that the global s-core resides in its entirety in only one of the four supermodules calls for the investigation of the *local s-cores* of the other three supermodules.

In Section 5.4.4 we have seen how the centralisation towards the cortical core, present at the

[1] We also note, however, that this in turn introduces a slight bias towards lower core-module connections densities.

supermodule level, is suppressed at the module level by the dominating internal connectivity of the supermodules. In the following, we investigate the nature of this internal organisation by assessing the local core formation tendency within these modular elements.

Methods

We perform s-core detection within each individual supermodule, that is, within the cortical sub-network formed by the regions and internal projections of each supermodule. Local organisation features and global significance of these intra-supermodular s-cores are evaluated by calculating their strength, size and centrality, both relative to their own supermodule and in absolute terms in the entire cortical network. We emphasise here, that the comparison of these local s-cores also assesses them with respect to the global s-core, because, as we have already seen in Section 5.4.4, the global s-core happens to be one of the supermodular s-cores.

Global and relative strengths are measured as the ratio of local s-core strength (final s-threshold) to mean global node strength and intra-supermodule node strength, where the latter only considers internal connections. Likewise, we assess global and relative size of supermodular s-cores as the proportion of contained regions with respect to the entire network and to their own supermodules only.

Centrality and contribution to network integration are measured by two means: i) as the ratio of mean betweenness centralities of regions of the local s-core and of regions network wide (betweenness, see Section 4.2), and ii) as loss in mean network efficiency after removing all s-core regions and their projections (vulnerability, Albert et al. (2000), Crucitti (2003)).

In order to gain further insight into the individual organisation of the local s-cores, we assess their dispersion at one hierarchy level lower, at the level of modules. We define the modular dispersion of supermodular s-core s as:

$$\delta(s) = 1 - [max(P(s)) - min(P(s))], \tag{5.4}$$

where the vector P contains the proportion of s-core regions in each module of the supermodule. $\delta(s)$ is 1 if s is evenly distributed across its modules ($P(s)$ is uniform $\rightarrow$ maximal dispersion), 0 if s is contained by a single module (one element of $P(s)$ is 1, the other elements are 0 $\rightarrow$ zero dispersion), and otherwise a value in between indicating the degree of dispersion of s across its modules.

Results

Figure 5.13 visualises the local s-cores of the four supermodules, while their quantitative assessment is presented in Figure 5.14. As we discussed it in Section 5.4, the caudal-central M1 contains

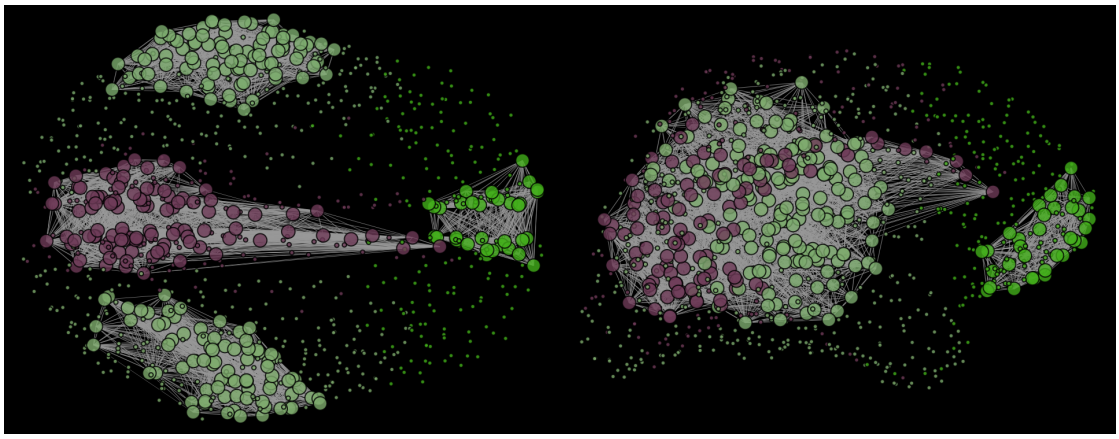

Figure 5.13: **Local s-cores in anatomical space.** Local s-cores (larger, interconnected circles of the same colour) of each supermodule are shown on horizontal (left) and coronal (right) projections. Regions (circles) are coloured to the colour of their supermodules (Figure 5.7).

the global s-core, while M2, M3 and M4 are the left lateral, right lateral and frontal supermodules, respectively.

Firstly, let us consider the strengths (final threshold of the peeling process) of the supermodular s-cores. In the two lateral and the frontal supermodules (M2, M3 and M4), we find local s-cores that are weaker in global terms (in comparison with the network average connection strength, first column), but similarly strong or, as in the case of the frontal M4 supermodule, even stronger in local terms (in comparison with their internal mean connection strength, second column) than the global s-core of M1.

Secondly, examining the extent of the local s-cores, both in relative (third column) and in absolute terms (fourth column), we find relatively small size local s-cores in both lateral supermodules (79 and 85 regions). Remarkably, the size of the s-core of the frontal supermodule is much smaller (33 regions), only one third of the size of the global core (100 regions). This, along with the extreme relative strength of this frontal s-core (second column), is a potential indicator of a high level of internal centralisation within the frontal lobe, with the majority of the peripheral nodes being only very loosely coupled to the extremely strong local core. We also note that the global s-core of the cortex is composed by close to half of the caudal-central supermodule M1 (third column), making up 10% of the whole network. This indicates an extraordinary extent of tight connectivity within that supermodule, which, as we have shown before, contains two thirds of the highest degree regions with a strong tendency to be mutually connected (see Figure 5.11).

To further investigate the topological centralities of the local s-cores in the cortical supermodules, we assess their global and intra-supermodule integration capabilities (fifth, sixth and seventh columns in Figure 5.14) by evaluating their betweenness, the vulnerability of the network to their

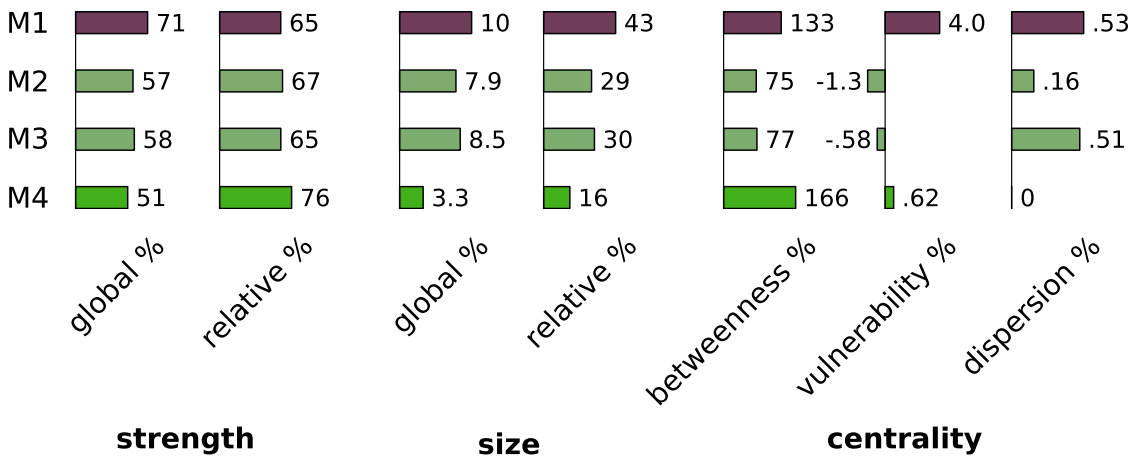

Figure 5.14: **Organisation of local s-cores in supermodules.** Global/relative strength: ratio of s-core strength (final s-threshold) to mean global/intra-supermodule node strength (sum of internal connection weights only). Global/relative size: proportion of contained regions in entire network/own supermodule. Betweenness: % of mean betweenness of regions in s-core to network mean. Vulnerability: % of loss in mean network efficiency after removing all s-core regions (and their projections). Dispersion: % of dispersion of s-core across modules of supermodule.

loss (deletion), and their degree of dispersion across the modules of their supermodule. Firstly, the lateral s-cores, in M2 and M3, exhibit very low mean betweenness values: they lay on about 25% less shortest paths than an average network region. This global segregatedness in fact provides them with such a level of isolation that their removal from the network actually increases global network efficiency, as indicated by their negative network vulnerability index. At the same time, the global and frontal s-cores in M1 and M4 possess high betweenness values, and contribute positively to the efficiency of the cortical network, with the global s-core being significantly more pivotal however.

Finally, let us consider the modular composition of the supermodular s-cores (seventh column in Figure 5.14). While the central and right lateral s-cores, in M1 and M3, demonstrate a relatively high level of modular dispersion, each residing in multiple modules of their own supermodule, the left lateral s-core in M2 exhibits a very low level of modular distribution. Even more remarkably the M4 frontal s-core is entirely concentrated into a single one of the three modules of the frontal supermodule. This module is M41, which, as we have seen in Section 5.3.3, consists of 94% of the *orbito-frontal* cortex (Figure 5.9), complementing the extremely high internal integratedness (modularity) of the *orbito-frontal* cortex by pointing to its not only spatially, but also topologically central role within the frontal supermodule and in the frontal lobe.

In summary, we found comparably sized, but more weakly intraconnected and highly isolated local s-cores in the two lateral cortical supermodules, and a very tightly integrated and locally

remarkably central, but small size and globally insignificant local s-core in the orbitofrontal cortex of the frontal supermodule. Based on these findings, we conclude that the global s-core in M1 occupies not only an anatomically, but also topologically central position in the cortical connectivity. However, our results also indicate that the highly segregated, modular and hierarchical nature of the cortex limits this centralisation to the largest topological scales: to its inter-supermodule connectivity.

5.5 Overview of results

In this chapter, we turned to the investigation of the cortical architecture on the meso-scale, and evaluated the expression of some generic network organisation principles in the cortex, such as hierarchical, modular, and centralised organisation patterns.

With the utilisation of a simple model for network hierarchy, we detected the presence of a globally hierarchical organisation in the cortical connectivity (Section 5.1). After that, we confirmed the previously reported highly modular architecture of the cortex, however, with some variation in the actual identity of the modules compared to earlier results (Section 5.2.5). These differences can be attributed to the resolution difference of the utilised datasets, as well as to the inclusion/exclusion subcortical brain areas in the analysis.

We tested the hypothesis that the cortical connectivity possesses hierarchical organisation patterns in its modular structure. The resolution of the network under study allowed us to detect an iterative pattern of submodule formation up to five hierarchically embedded levels, with significant connectivity saturation at the fifth level (6.7 regions/micromodule, 93% internal connection density). Spatially, the modules are highly compact at all hierarchy levels and hemispherically symmetric at higher levels. Increasing capability of the submodules at lower hierarchy levels to operate as individual functional units is indicated by the increase not only in their internal connection density, but also in their modular matching indexes, reaching as high as 33% at the lowest hierarchy levels. In summary, topological analysis of the large-scale anatomical connectivity of the cortex confirmed its characteristic organisation feature of being composed of relatively loosely coupled subunits (modules), in a repetitive manner across multiple levels.

In any modular architecture, such as the one found in the cortex, network modules on the global level can engage in two fundamentally different topological relations, and thus functional cooperation: in a distributed (Figure 5.12 *a*) or in a centralised (Figure 5.12 *b*) architecture pattern. While the exponential degree distribution (Hagmann et al. (2008)) and globally hierarchical organisation (Section 5.1) already suggested the latter type of architecture, we explicitly examined which, if any, parts of the cortex is topologically able to fulfil that putative central coordinator role

and thus potentially operate as the global workspace of Baars (2002) (Section 5.4). Confirming previous results of Hagmann et al. (2008), the most densely intra-connected group of regions, the s-core of the cortex, was found to be spatially encapsulated at a medial-caudal location, composed by the *precuneus*, the *cingulate cortex* and the superior part of the *occipital lobe*. Furthermore, surrogate comparison detected an elevated level of internal integratedness (intra-connection strength) in the cortex's s-core, indicating the existence of a spatially compact and topological significant network core.

As opposed to that, the existence of another candidate central structure, the rich-club formation of the cortex (Van den Heuvel and Sporns (2011)), while exhibit a denser than random intra-connectedness, was also found in its spatial surrogates, thus can largely be explained by the spatial embedding and wiring constraints of the cortex. Furthermore, the rich-club of the cortex was found to be formed by a relatively loosely coupled, spatially not significantly strong, and both spatially and topologically rather dispersed set of regions, as it was found in the cat thalamo-cortex (Zamora-López et al. (2010)) and in the entire human brain (Van den Heuvel and Sporns (2011)). These properties, as opposed to the even spatially highly significant and well-confined cortical s-core, render the rich-club a less appropriate candidate for a putative central cortical core, and more suited for fulfilling the role of a set of distributed cortical hub regions, predominantly connecting their local neighbourhoods with distant parts of the cortex. Nevertheless, the large (50%) overlap between the s-core and rich-club regions suggests a great extent of functional cooperation between these highly intertwined core structures.

In order to further investigate the putative role of the detected core in the network, we assessed how much topologically centralisation is actually expressed by the network towards its core. To that end, we evaluated the level of local centralisation within each supermodule by detecting the 'local s-cores' in each of them, the global network core itself being one of them (Section 5.4.5). We found that these local s-cores, while being the main integrator substructures within their respective supermodules, are significantly smaller in size and weaker in terms of intra-connectedness than the global core, and furthermore they are in a rather segregated position from the other supermodules, as opposed to the global s-core, which itself is one of these supermodular s-cores due to its modular encapsulation. These results place the network core to a global inter-supermodule integrator position: a spatially and topologically central structure capable of integrating and coordinating the otherwise highly segregated lateral parts of the two hemispheres.

Using the anatomical connectivity map they collated using the CoCoMac database (Kötter (2004)), Modha and Singh (2010) also reported the presence of a strong k-core in the brain of the macaque, which, however, was found to be a "deeply nested", highly centralised and integrated

structure of the macaque brain. While this and our results are in general agreement regarding the significance of the network cores, the more centralised manner of the macaque brain of Modha and Singh (2010) may arise from the lower strength of the modularity structure of that connectivity map, that was not assessed in Modha and Singh (2010).

Having established the hierarchical modular and reasonably centralised architecture of the cortical connectivity around its significant strength s-core in this chapter, in the next chapter we shall investigate the topological position of another functionally potentially highly significant group of regions, the hubs of the cortex.

Chapter 6

Hubs of the cortex

Having found a reasonable level of modular centralisation in the cortex around its significant s-core in the last chapter, in this chapter we shall attempt to characterise the topological properties of another potentially functionally significant set of cortical regions, the hubs of the cortex (Sporns et al. (2007)). Specifically, we will evaluate their topological positioning and integration capabilities with respect to the features of the cortical network architecture unveiled so far, in order to gain further insight into the organisation features of the cortex. After that, we shall also evaluate and compare the kind of stereotypical functional operations the core and hubs regions of the cortex are specialised to at the micro-structure level by performing a detailed network motif analysis (Milo et al. (2002)). Throughout this chapter, our main goal will be to further characterise and compare cortical hub and core regions in terms of their topological integratedness, centralisation and potential functional cooperation.

6.1 Introduction

6.1.1 Overview of results up to this point

In the previous chapters, we have found a highly modular organisation in the cortex (Section 5.2), with high global, but low local centralisation towards its s-core structures at the various levels of its module hierarchy (Section 5.4.5). The prominent global s-core of the cortical connectivity is both spatially and topologically central and well-confined. Specifically, rather than being distributed among the high-degree nodes of the network modules, the global s-core takes a highly concentrated position with respect to the underlying hierarchically modular cortical architecture by residing in just one of the four supermodules (Section 5.4.4). Furthermore, we have also shown by surrogate tests that the s-core, as opposed to the rich-club, is far more tightly connected than the degrees, locations and connection lengths of its constituting regions would suggest (Section 5.4).

Based on the above findings, we propose that the cortex has a centralised, rather than distributed, and yet modular architecture, schematically illustrated in Figure 5.12 *b*. Nevertheless, our results so far do not allow us to clearly categorise the cortical network either as a centralised and fractal structure, empirically found in Ravasz et al. (2002) and theoretically studied in Ravasz and Barabási (2003), or as a hierarchy of module agglomerations, studied for example in Shanahan (2008) and in Shanahan (2010). While it is most likely that, being a complex, spatial network, the cortex combines organisational elements of both architectures types, in this section we explore the question by investigating the topological positioning of a pivotal region group, the *hubs* of the cortex.

6.1.2 Hubs in complex networks

Taken the proposed architecture scheme in Figure 5.12 *b*, the question we ask is: *Are there distinguishable nodes in the cortex that facilitate interaction between the individual modules and the network core? If so, which ones are they?* (green nodes in Figure 5.12) These nodes have traditionally been referred to as the *hubs* of the network, and usually simply identified by their high degree (Boccaletti et al. (2006)).

Recognising the characteristically modular architecture of most biological and brain networks, as well as the two fundamentally different topological positionings a hub can take with respect to a given module partitioning, it has become a standard in systems neuroscience to further differentiate between *provincial* (intra-cluster) and *connector* (inter-cluster) hubs (eg. Guimerà and Nunes Amaral (2005), Bassett and Bullmore (2006), Sporns et al. (2007), Hagmann et al. (2008)). Provincial hubs, tightening intramodule connectivity by their mostly internal links, reside in the topological centre of a single module. Connector hubs, on the other hand, are maintainers of inter-cluster connectivity due to their links being highly distributed among network modules.

6.1.3 Hubs in the brain

By their informal definition, hub nodes are the primary integrators in complex networks. Accordingly, the identification of hub regions in various large-scale brain networks have generated considerable interest (Sporns et al. (2007), Rubinov and Sporns (2010)).

In the original analysis of the cortical connectivity dataset investigated here, Hagmann et al. (2008) have reported that connector hubs are concentrated in the posterior medial and parietal cortex, while the majority of provincial hub areas are located in the frontal, temporoparietal and occipital modules. Other studies carried out on directed brain networks identified 'driving' hubs and 'driven' hubs, according to the significantly elevated number of their out- and in-degrees,

respectively (Yan and He (2011)).

Having found a strong hierarchical modular organisation and a spatially and topologically centrally positioned structural core in the cortex, in this chapter we investigate the topological position and properties of the hub regions of the cortex. Specifically, we shall assess their relation and relative significance to the global network core with the aim to gain further insight into their putative functional role in the cortical architecture as characterised so far (Figure 5.12b).

6.2 Global topological properties of hub regions

6.2.1 A novel hub categorisation scheme

In Section 5.4.4 we have found a very low interconnection density ($\sim$ 1%) between the cortical modules, which places connector regions into a distinguished topological position. Furthermore, in Section 5.4, we have found that one half of the top n=100 (9.98%) highest degree nodes, the rich-club nodes, are contained in the spatially and topologically confined, highly intra-connected global s-core of the network, a prominent central element of the cortical network. These observations lead us to propose an alternative categorisation to the above connector/provincial hub types. We distinguish between *core hubs* and *module hubs*, depending on whether they reside within the network core, or in a module outside of the core.

The traditional connector and provincial hub types are determined solely by taking a known module configuration of the network (Sporns et al. (2007)). As opposed to that, our alternative core hub/module hub categorisation first characterises hub regions with respect to network core, and only then the uncovered module configuration is taken into account to evaluate their putative functional role by their structural location in the modular topology (Figure 5.12 *b*).

In this section, we shall attempt to uncover topological differences between the above two, alternative hub groups with the aim to find evidence for the potentially different functional role they are able fulfil in the cortical connectivity. Specifically, we shall search for topological specialisation in the positioning of the hub groups that may support or weaken the significance of the cortical organisation found in the last chapter, i.e., the hierarchically modular cortical architecture that is reasonably centralised around its strong s-core. For this comparative analysis, we will use the non-hub regions of the cortex as a baseline population.

This section of the chapter, we start our investigation by the global topological properties of the hub groups by several complex network measures on the macro-scale. In the next section, we extend these results and investigate the micro-structural characteristics of the hub groups on the lowest levels of the cortical connectivity by a detailed motif spectra analysis.

6.2.2 Methods

All cortical regions are categorised into one of the following groups: core hubs, module hubs and non-hub regions. We analyse the three groups by assessing them against various integration and segregation measures in order to gain further insight into their topological position and potential functional role in the discovered network architecture.

In order to measure the general integration ability of the above three node groups, we take the mean of their contained regions for each of the four basic integration measures, applied in Section 4.2: degree, leverage centrality, efficiency, and betweenness centrality. The selected metrics, in the above order, measure the integration potential of the network nodes from local to more global topological scales (degree centrality: own neighbours, leverage centrality: neighbours of own neighbours, efficiency: own shortest paths, betweenness centrality: all shortest paths), thus in combination they are able to address a whole spectrum of integration processes of the cortex allowed by resolution of the dataset.

The collective contribution of specific region groups to network-wide integration efficiency is evaluated by calculating the vulnerability (loss in mean efficiency) of the cortex to the removal of each region group (Albert et al. (2000), Section 5.4.5). For direct comparability of the vulnerability of the above three groups of different sizes, we normalise the obtained efficiency losses by the number of regions removed.

We also assess inter-module integration ability of the three node groups directly by calculating the mean participation coefficient of their regions (Guimerà and Nunes Amaral (2005)). Participation coefficient, used to distinguish between connector and provincial hubs, measures the connection distribution/concentration of a node among the network modules (see Appendix A for definition).

We are also interested in the general clusteredness and internal integration ability of the three region groups. At single region level, mean clustering coefficient of the groups' regions is calculated to measure local regional segregation. For assessing group-level integratedness, which is indicative of increased internal cooperation and global segregation, we calculate the internal connection densities of the groups.

6.2.3 Results: Global positioning of module hubs and core hubs

Visualisation of the two hub groups, along with their topological features, are presented in Figure 6.1. Due to the relation of the s-core and rich-club of the cortex (Section 5.4.3), the number of hub regions inside the core (core hubs) is equal to the number of hubs outside of the core (module hubs) (n=50, 5% of the entire cortex), making the two groups directly comparable in the following

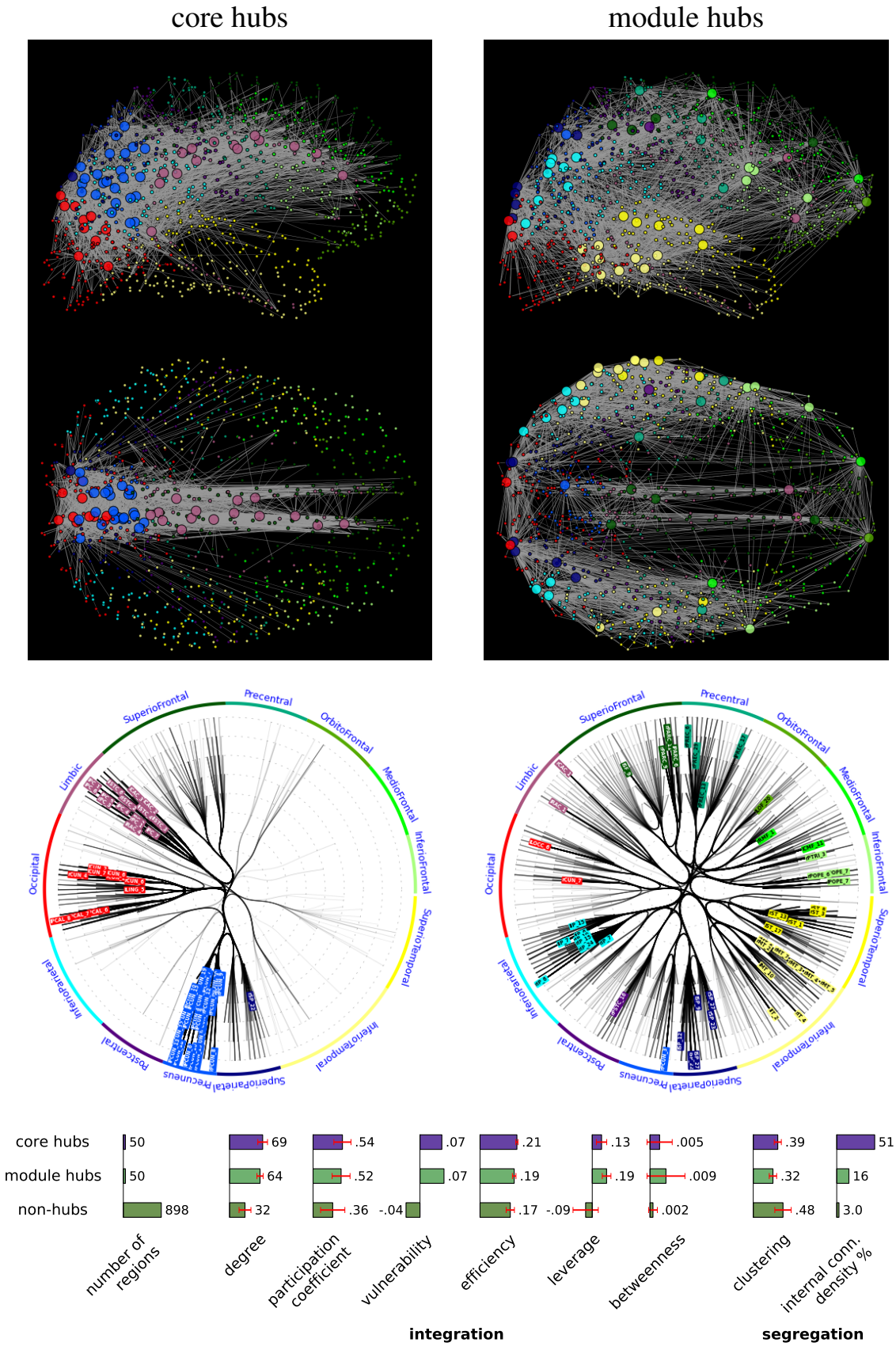

Figure 6.1: **Analysis of core hubs and module hubs.** Core hub (left) and module hub (right) regions and their connections on coronal and horizontal projections (top row), and on radial layout (middle row). Bottom: metric results of the two hub and the non-hub region groups.

analysis.

The presented visualisation suggests marked differences in the spread of connectivity of the two hub groups. While module hubs possess 17% of the cortical connections (n=2996) and have direct links to 85% of the rest of the network, core hubs, with about the same number of links (n=2842, 16%), are only connected to 2.5 times less, 34% of the network, and concentrate more than half (53%) of their connections inside the network core, that consists of only n=100 regions (10%). This basic difference in their topological positioning suggests fundamentally different functional roles for the two hub groups. In the following, we shall further characterise this difference by the above introduced complex network measures.

We assess the integration capability of the various hub and non-hub region groups by a number of complex network measures (Figure 6.1 second to seventh columns). Firstly, all metrics confirm that non-hub regions, making up 90% of the cortex, are significantly poorer integrator areas than the two hub groups, as expected from their definitions (for all integration measures between non-hub and core hub, and non-hub and module hub regions: $p < 10^{-4}$ for two-sample unpaired *t-test*, not assuming identical variances). Secondly, looking at the two hub groups, one can observe no marked difference between their average degree, participation coefficients (spread of connections across modules) and vulnerability (loss of global network efficiency caused by their collective deletion).

However, we obtain a significantly higher mean efficiency of hub regions in the core (E^{CH} = 0.21 ± 0.006) than in module hubs ($E^{MH} = 0.19 \pm 0.010$), compared to the baseline efficiency of non-hub regions ($E^{NH} = 0.17 \pm 0.023$, Wilcoxon two-sided rank-sum test for identical distribution: $p < 10^{-5}$ between all group pairs), which shows that core hubs are in a more central position in the cortex, that is, topologically they are located closer to an average region in the entire cortical network than module hubs are. Importantly, the applied core detection algorithm does not utilise centrality metrics *per se* (Section 5.4.2), thus the found central topological position of the core was not *a priori* guaranteed, but rather it is an independent feature of the cortical connectivity, supporting the found centralisation in the cortical connectome (Section 5.4.4).

In addition to the direct centralisation described above, we also detect that module hubs appear to possess a somewhat higher group average than core hubs with respect to two specific integration metrics: leverage centrality and betweenness centrality. The difference between the two hub groups is significant in the case of leverage centrality ($p < 10^{-6}$ for two-sample unpaired *t-test*, not assuming identical variances), but not for betweenness centrality ($p = 0.049$). Both measures quantify how much a given node facilitates the integratedness of other nodes, locally in the case of leverage centrality and globally in the case of betweenness centrality (Section 4.2). On the

one hand, the mean leverage centrality of module hub regions being significantly higher than non-hub regions is intuitively expected from their exceedingly high degrees within their local modules. This finding, being consistent with both architecture schemes in Figure 5.12, reinforces the putative role of module hubs as the main local integrators of their neighbourhood. On the other hand, the elevated betweenness centrality of modules hubs over core hubs would indicate their heightened global importance in establishing short communication channels (paths composed of chains of white-matter connections) between their local neighbourhood and distant cortical areas. The almost half as low mean betweenness centrality of core hubs is suggestive, but inconclusive in this case, and has to be assessed in combination with the vulnerability results of the two hub groups. Together the two metrics seem to indicate that, while the *individual* regions of the highly intraconnected core are effective substituters of each other by facilitating alternative pathways between distant brain regions (intermediate betweenness of individual core regions), they are at the same time *collectively* equally important integrators of the cortex as the local module hubs (equally high vulnerability for collective removal of the module hub and core hub regions).

Along with their integration capacity in the cortical network, we also investigate the degree of segregation of the hub region groups, both at the level of individual regions as well as for the entire hub groups as a whole, in order to unveil their potential for functional specialisation and collective cooperation, respectively (Rubinov and Sporns (2010)). We measure the former by the mean clustering coefficients of the region groups (Figure 6.1 eighth column), and the latter by their internal connection density (Figure 6.1 ninth column). The obtained intermediate clustering values of core hubs (C^{CH}=0.39) presumably originate from their high intra-connectedness: more than every second possible connections exist between these core cortical regions. On the other hand, module hubs demonstrate the lowest individual clustering coefficient (C^{MH}=0.32), indicating their lower functional specialisation within their local neighbourhood. At the same time, however, considering their spatial scatteredness and the low, 3% connection density of the rest of the network, module hubs exhibit a relatively high, 16% intra-connectedness among themselves, which, being in line with the rich-club organisation of the cortex (Section 5.4), supports the notion that spatially remote hub regions possess increased potential for functional cooperation.

Inter-connectivity of the presented region groups provides additional information on their mutual relationship in the network architecture. Consistently with their position in the modular organisation of the cortex, module hubs, directing 85% of their connections towards non-hub regions, are much more important network elements in terms of their potential in directly collecting and disseminating local information than core hubs, that share only 41% of their connections with non-hub regions outside of the core (85% of the network). Module hubs possess an about equal

number of connections (6%) between themselves and towards core hubs, maintaining similar level internal and pro-core connectedness. As opposed to that, core hubs retain almost four times more, 22%, of their connections internally, forming a much more tightly integrated group.

Considering the strong modular organisation found in the cortex, an important question is how much the two hub groups contribute to inter-module integration. We find that both groups keep about 70% of their connections inside their own module, and contribute about equally, with 12.5%, to inter-module connectivity, placing neither hub group above the other in facilitating inter-module communication. Furthermore, the low ratio of internally kept connections of module hubs (6%), and comparison of their connection density in the cortical network (16%) and in its surrogates (random: 12%, spatial: 17%) provides evidence against the notion that module hubs would form a separate functional unit acting collectively as a group of global integrator regions among various segregated parts of the cortex.

These results together are consistent with the found significant rich-club organisation and high assortativity in Section 5.4.3, and provide further evidence for the remarkably high internal integratedness and global centrality of the network core, as well as for a lower, but still relatively high level of cooperation between cortical hubs in even distant modules, as illustrated in Figure 5.12.

6.2.4 Discussion

In this section we investigated the *hubs* of the cortical connectivity with respect to the previously found organisation features of the network. First, we identified the hubs of the network as its one hundred most highly connected regions, that is, its rich-club (Section 5.4.3). We found that 50% of the hubs are also part of the core. Then, based on this 50% overlap between the core and rich-club of the cortical network (Section 5.4.3), the set of hub regions was split into two equal size (n=50 regions, 5% each) groups: hubs inside the network core, or *core hubs*, and hubs outside network core, or *module hubs*.

This way, in the first group we obtained a set of centrally located and highly intra-connected hubs, the *core hubs*, along the caudal part of the cortical midline, mainly containing regions from the *precuneus*, along with some visual and *limbic* (cingulate) areas. The second group outside of the network core mainly is comprised of more lateral regions in the *temporal lobe*, *parietal lobe*, as well as some *precentral* and frontal areas.

Originating from their topological and spatial positioning, we have found core hubs to be highly concentrated, and module hubs to be more dispersed, both in terms of regional location and spread of connectivity. Furthermore, analysis by various integration measures showed that core hubs are

globally central integrator regions of the cortex, while module hubs are rather local integrators that effectively organise their local neighbourhoods as well as link it with more distant cortical areas (Figure 6.1).

Altogether, these results are in agreement with the existence of a globally highly central and densely intra-connected core module, mainly composed of the *core hubs* of the network (Figure 5.12 *b*). However, they also point to a lessened degree of centralisation in the cortical network by revealing a relatively strong inter-connectedness of the peripheral modules, mainly facilitated by their local hub regions, the *module hubs*.

Sporns et al. (2007) provided a detailed analysis on the topological characteristics of the hub regions in the large-scale connectivity networks of the macaque and cat brain. In accordance with our results, Sporns et al. (2007) found that high degree nodes generally exhibit high integration and low segregation measure values, making them capable of acting as functional links between segregated subsystems of the brain.

Hagmann et al. (2008) investigated the spatial distribution of hub regions in the current dataset using the traditional connector/provincial hub categorisation scheme, with regard to their slightly different module partition (see Section 5.2.6). They found that most of the connector hubs are located along the anterior–posterior medial axis in the cingulate cortex and the precuneus, as well as in the parietal cortex. Similar results were found by Van den Heuvel and Sporns (2011). These areas largely coincide with the cortical core, underscoring the core's significance in global, intermodule integration. Furthermore, prominent provincial hubs, the facilitators of local integration, were found in the temporal module by Hagmann et al. (2008), reinforcing our findings about the extremely high internal integratedness of that module (Section 5.4.5).

In this section we have established the distinguished global topological position of the high degree hub regions in the cortical connectome. We found that hubs in the network core (core hubs) and outside of the core (module hubs), while being similar to each other in some basic hub properties (degree, participation coefficient, vulnerability), differ significantly in some other, potentially functionally important features (betweenness, clustering, internal connection density). In the next section, we attempt to further characterise this difference by comparing the kind of stereotypical functional operations the core and hubs regions of the cortex are specialised to at the micro-structure level of the current resolution of the cortical connectome.

6.3 Motifs spectrum differences as a proxy for function of hub regions

6.3.1 Introduction

Network motifs

Network motifs are miniature subgraphs abundant in the network (Milo et al. (2002)). Comprised of only several nodes which arranged in characteristic formations, network motifs are regarded as putative functional atoms of the network at its finest level, that are capable of carrying out certain stereotypical computational tasks (Holland and Leinhardt (1974)). The deviation of the motif distribution of a network from that of its set of null-hypothesis networks carries information on the functional and evolutionary constraints of the network (Milo et al. (2002)). Furthermore these deviations tend to be characteristic to groups of networks, the so-called "superfamilies", originating from seemingly unrelated domains, such as social and engineered networks (Milo et al. (2004b)).

However, it has been argued that inappropriately chosen null-hypothesis networks can lead to ill-posed deductions about the adaptive and/or evolutionary value of observed motifs. In some cases, the abundance (or scarcity) of certain miniature subgraphs may be readily explained by some more elementary principles, such as local clustering or network growth constraints (Artzy-Randrup et al. (2004)), not addressed by simple null-hypothesis networks. Nonetheless, careful and comprehensive motif analysis provides a generic framework that is potentially able to advance our understanding on the topological characteristics, stereotypical functional elements and evolutionary processes of complex networks (Milo et al. (2004a)).

Motifs in brain networks

In the context of neural networks, motifs can be regarded as the 'canonical' processing circuits of the network (Douglas and Martin (2004)). In one of the earliest comprehensive studies on the motifs in the neurosciences, Reigl et al. demonstrated the descriptive power of the technique by exploring the network motifs in the neuronal wiring of *C. elegans* (Reigl et al. (2004)). They found several symmetric, densely connected, and feed-forwardly coupled motif forms of size two, three and four (but none of size five). These motif forms reflect some of the most fundamental organisation features of *C. elegans* nervous system of being bilaterally symmetric, highly clustered, approximately three-layered (motor, interneuron and sensory layers) and of having evolved essentially to carry out information processing (as opposed to the rather sensory nature of transcription networks or the information storing of social networks (Milo et al. (2004b))).

A comparative study on the network motifs of various brain networks was carried out by Sporns and Kötter, who investigated the motif spectrum of cortical brain networks of the macaque monkey and the cat, as well as the invertebrate nervous system of *C. elegans* (Sporns and Kötter (2004)). They found that the cortical networks possess motif distributions that are markedly different from those of invertebrate brains, which led the authors to propose that cortical networks form a distinct *superfamily* (Milo et al. (2004b)) to invertebrate nervous systems in terms of significant network motifs. However, as the study compared the macaque cortex with the entire *C. elegans* nervous system, the question of whether the found difference is also present between the cortex and the spinal cord of the macaque, or indeed between the entire nervous systems of the macaque and the *C. elegans* would require further investigation, as well as it raises the problem of resolution difference (brain regions versus single neurons) when comparing various brain networks (Rubinov and Sporns (2010), Kaiser (2011)).

Furthermore, Sporns and Kötter (2004) optimised the topology of synthetic networks to maximal number of ”functional” motifs (sub-motifs within traditional structural motifs), but not to maximal number of ”structural” (traditional) motif, and found characteristically similar evolved networks to the cortical networks with respect to several topological measures, such as complexity (Tononi et al. (1994)), clustering coefficient, shortest path length, and therefore small-worldness (Section 4.5). In combination with previous results (Sporns et al. (2000)), these findings quite strikingly suggest that efficient integration and segregation through global network architecture can be achieved by several, possibly interrelated criteria, such as high small-world index, high complexity, or certain motif distributions (Sporns and Kötter (2004)).

In a subsequent study, Sporns and colleagues included motif spectrum analysis into their survey of structural measures during an attempt to find and characterise hub regions of the large-scale cortical networks of the macaque and the cat brain (Sporns et al. (2007)). Interestingly, a specific 3-node subgraph, the reciprocally connected V-shape was found at significantly elevated numbers at the putative, high-degree and highly central hub regions. Furthermore, principal component analysis (PCA, Pearson (1901)) pointed to this specific motif as a highly significant component in the regional motif spectral distribution in the cortical connectivities of both species. Preliminary investigations on the positional motif spectra of these regions suggested that they are indeed located at the ”apex” (central position) of the motif form with a much higher ratio than it would be expected, leading to low clustering coefficients at these regions and reinforcing their role as intermediating way stations in the network topology. Utilising these finding, increased contribution to the same reciprocal V-shape motif form was taken as an indicator of individual nodes to serve as network hubs in Honey et al. (2007).

Interpretation and generalisation of network motifs

Regarding the interpretation of motif analysis results, one can consider the evolutionary and adaptive benefits of subgraphs found overabundant in various biological networks. It has also been proposed that motif forms with higher structural stability, due to their higher reliability in a noisy environment/system, might have generally been favoured contrary to motifs that are less stable to perturbations in their connection strengths and polarity (Prill et al. (2005)). However, as the authors admit, the hypothesis that motifs can be regarded as independent dynamical units, able to act and evolve relatively uninfluenced from the global state of the complex network they are embedded in, renders the theory less appealing for the more tightly integrated and simultaneously active neural and brain networks than, for instance, for transcription networks composed effectively of on–off switchable molecular elements.

The general notion of characterising and grouping individual nodes of a brain network (neurons, cortical columns or anatomical regions) with respect to a certain set of network measures was first proposed and studied in Passingham et al. (2002) and in Kötter and Stephan (2003). By specifying such a set of measures, each network node can be given a set of according attributes, which are collectively called the node's "fingerprint". These fingerprints are not restricted to the spectra of small-size subgraph the nodes participate in. Instead, they generalise the notion of network "motifs" to characteristic vectors describing topological properties of individual nodes along a combination of complex network metrics, including for example integration or segregation measures (Section 4.2 and Section 4.3).

Although preliminary studies of Passingham et al. (2002) and Kötter and Stephan (2003) were carried out on relatively small networks (up to about 100 brain regions) of the macaque brain, and used rather simplistic network measures (connection fingerprint, density, symmetry and transmission), they were able to point out the potential value of applying network measures at the single node level to identify groups of nodes with similar topological and thus presumably functional characteristics. This approach, at its time of introduction, departed from the traditionally applied, global network measures that only provide characteristic descriptions of the whole network, and it was one of the first techniques to put emphasis on the internal organisation differences of brain networks at the regional (node) level.

A recent extension of the fingerprinting technique proposes a framework for automatic identification of network nodes that are "special" in the sense of being outliers from the trend followed by the majority of the nodes (Costa et al. (2009), Echtermeyer et al. (2011a)). Focusing the investigations on these "motif nodes", the virtue of the technique was demonstrated in Echtermeyer et al. (2011b), in which the authors carried out for the first time a comparative analysis among a

spatio-temporally diverse set of structural connectivities of the human cortex, obtained from more than 50, 12 to 23 year old children and young adults, at three different spacial resolutions (at about 400, 800 and 1600 ROIs). Their results showed that along both dimensions (subject age and brain network resolution), node motifs as well as overall network characteristics differ in several, partly previously already reported, topological and spatial aspects, such as fibre tract length distribution, motif diversity or significance profile.

Motif node spectrum as a proxy for the function of individual network regions

We further investigate and contrast the putative functional role of the hub and core regions by analysing their motif spectra. In the forthcoming analysis, it is important to carefully distinguish between the terms *motif node* and *network node*. The abstract term *motif node* refers to a node of a motif graph, which is different from a node of the brain network, a concrete cortical region, that can take the role of a motif node in many motif graphs.

Previous studies used motif analysis mainly to investigate the dominant (and significant) type of information processing the network under study, *as a whole*, is capable of or adapted to, by analysing the motif distribution of the entire network (see introduction). Here, instead, we carry out a more detailed analysis, and look for the putative functional role of *various parts* of the cortical network by their individual motif fingerprint. To this end, we generalise the approach of Sporns et al. (2007), who reported that hub regions appear at a certain position of a specific motif form, at the apex of the V-shape motif, with increased probability. Specifically, we investigate the dominant "canonical processing function" of each cortical region by examining how often the region takes place at each specific location of every subgraph, that is, at each *motif node*.

Based on their connectivity within their motif forms, we categorise each node of every three- and four-node motif form into one of three types: integrator, terminus and clustered. Informally, we define these categories in the following way. *Integrator* motif nodes are central nodes of the motif that create indirect links between nodes that are not directly connected. As opposed to that, *terminus* motif nodes realise a start/end point of the motif by being connected to the rest of motif by a single link only. Finally, *clustered* motif nodes, being neither in central nor in peripheral position, are topological equal (symmetrically connected) members of some densely connected motif form.

The classification of each motif node to be investigated is shown in Figure 6.2. With the above categorisation, we seek to unveil the dominant functional role of cortical regions by analysing the distribution of how often they participate at particular positions in network motifs.

This analysis, just like most techniques of the field of complex network sciences, is interrelated to, but not equivalent with, some of the already applied analyses. Specifically, a dominantly

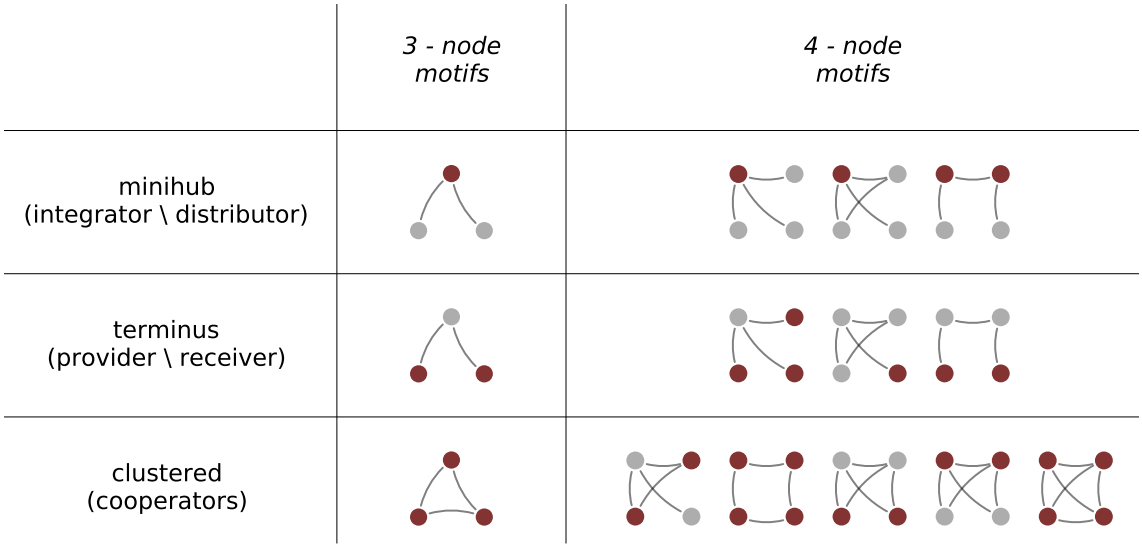

Figure 6.2: **Motif node types investigated in this study.** There are two three-node and six four-node undirected (and connected) motif forms. All of their motifs nodes are first grouped by isomorphism (red coloured nodes in a single motif graph) and then classified into one of the three types: integrator, terminus or clustered, based on their connections with the rest of the motif graph nodes.

clustered motif node spectrum necessarily correlates with high clustering coefficient (Section 4.3), while integrator/terminus motif node spectra are expected to be related to low clustering coefficient and to high/low degree in particular, as well as to high/low integration measures in general (Section 4.2).

We use the outlined analysis framework specifically to find differences in the motif spectra of four previously investigated parts of the cortex, delineated by the core and the hub structure of the network. Both the core and the crust (non-core) parts of the network are divided into two subgroups: hub regions inside the core (core hubs), non-hub regions inside the core (non-hub core), hub regions outside of the core (module hubs) and non-hub regions outside of the core (non-hub crust). The last group, non-hub crust, makes up the majority of the network (848 regions, 85%) and can be regarded as the baseline population of the cortical regions, while the first three, topologically rather distinguished groups, consist of 50 regions each (5%).

We investigate the individual motif fingerprint of the core and hub regions of the cortical connectivity network in order to gain additional insight into their putative functional roles from the micro-connectivity perspective of motifs. Our hypothesis is that the above four region groups, due to the difference in their topological properties, also significantly deviate in their *motif node* spectra from each other, suggesting their different characteristic functional roles in the canonical

processing units of network motifs. For example, cortical regions found predominantly in integrator motif node positions are likely to play a functional integrator role between specialised topological neighbourhoods, while regions located mainly in terminus motif node positions are likely to act as functionally highly specialised receivers or providers within the cortical network.

6.3.2 Methods

Motif node counting algorithm

In order to count the occurrences of network nodes at each individual position of the motif forms, we developed our own specialised motif counting algorithm. Motif counting is an algorithmically challenging task due to its high computational cost on large networks. For the complete motif counting on the entire cortical network, even for only the six four-node undirected motif forms, the 'brute-force' approach of examining all the possible node-quartets in the network is computationally not feasible[1]. However, exploiting the sparseness of the network, one can radically reduce the computational cost by only considering the existing edges of the network. To this end, a modified and extended version of the algorithm of Batagelj and Mrvar (2001) has been implemented, with the generalisation of being able to deal with both directed and undirected motifs of any size. We used that algorithm to count the motif node spectra of each individual region in the cortical network and in its surrogates, as well as to obtain the global motif graph distributions of these networks.

Motif node counts and spectra

We count the global occurrence number C_m of each m motif (k node subgraph) in the entire network. The motif spectrum of each individual region is determined on a per $C_{m,n}$ *motif node* basis in the cortical network and in its surrogates, for each node n of each motif m. Occurrences of isomorphic nodes within each motif form (red nodes of the motifs in Figure 6.2) are dealt with by averaging. Aggregating these region level spectrum results, the motif node spectrum of a group of regions is calculated by summing up the motif node occurrences at the individual regions in the group. To be able to make comparisons between these group spectra, they are normalised by the total number of contained motif nodes, yielding an occurrence probability $P_{m,n}(G)$ of each node n of each motif m within a certain group of cortical regions G.

[1] Even in our intermediate size, 998-node network, there is about 41 billion of such node-quartets.

Z-score

In statistics, the Z-score of a given observation indicates how many standard deviations that observation is above or below the mean (Larsen and Marx (2010)). Mean z-scores or standard scores of the region groups for each motif node are calculated against both surrogate network types as the average of the individual z-scores of each region contained in region group G:

$$z^S_{m,n}(G) = \frac{\sum_{r \in G} z^S_{m,n}(r)}{|G|}, \tag{6.1}$$

where $z^S_{m,n}(r)$ is the z-score of region r against surrogate type S for node n of motif m:

$$z^S_{m,n}(r) = \frac{C_{m,n}(r) - \mu(C^S_{m,n}(r))}{\sigma(C^S_{m,n}(r))}, \tag{6.2}$$

where $\mu(x)$ and $\sigma(x)$ are the mean and standard deviation of value set x. This way, $z^S_{m,n}(G)$ indicates the significance of motif node spectrum deviation of the cortical regions from their surrogate correspondences.

6.3.3 Results

The occurrences of all three- and four-node undirected and connected motifs were counted in the cortical network and on its two surrogate network sets. The undirected nature of the network under study limited our investigation to undirected motif analysis. While technological (computational) barriers prevent the analysis of larger motifs in practise[2], 'functional' interpretation of motif forms also becomes less and less straightforward with the increase of size (Reigl et al. (2004)), thus reducing the potential virtue of motif analyses at greater size.

Three-node motifs

Figure 6.3 shows the results of the three-node motif analysis. The cortical network contains about half a million pieces of the two three-node (undirected) motifs forms in total (Figure 6.3 *a*). In absolute terms, the linear form, due to the low connection density of the cortex, occurs more than four times more frequently than the clustered triangle. Nonetheless, high z-scores of this latter form against both surrogate sets reassure previous segregation results by indicating the overabundance of clustered triplets in the cortex in relative terms (Section 4.3).

Absolute motif node counts of the four region groups are plotted in Figure 6.4, group averaged motif node spectra and z-scores are shown in Figure 6.3 *b*. Firstly, the higher probability of the

[2]For example, to count the occurrences of all the 21 five-node undirected motif forms, one is required to perform the computationally expensive isomorphism check between all of these motif forms and each one of the billions of 5-node subgraphs of the network.

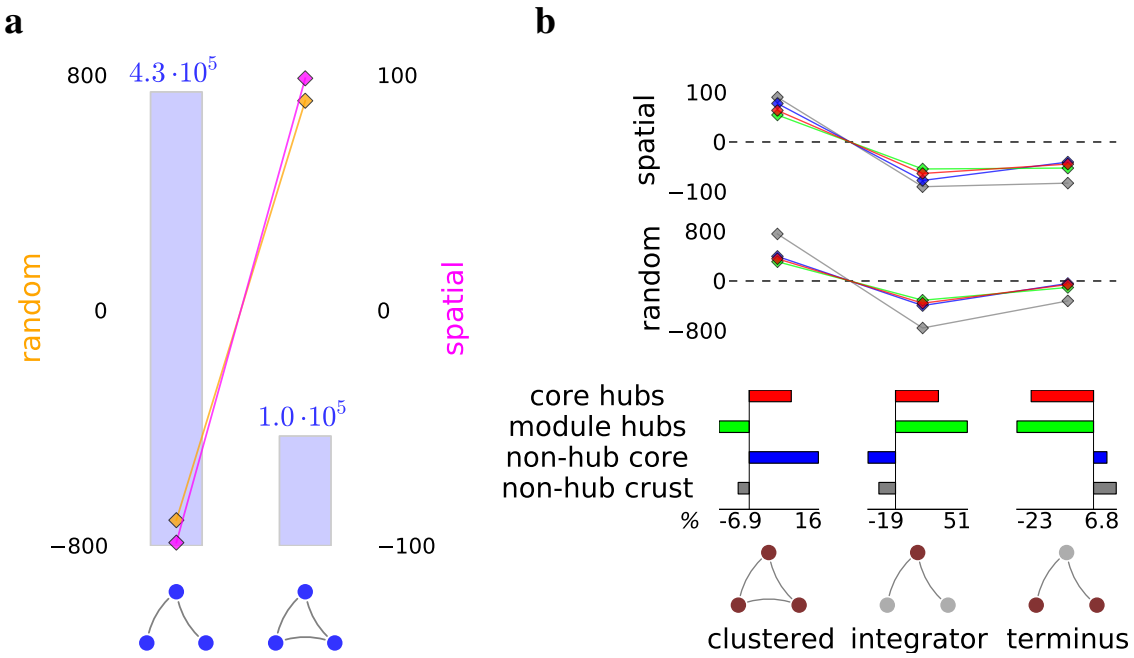

Figure 6.3: **Three-node motif results.** *a*: absolute motif counts (bars) and random (orange) and spatial (magenta) z-scores (diamonds) of the two three-node undirected subgraphs. Numbers on top of the bars indicate absolute motif counts, scales on the two sides indicate z-score values. *b*: z-scores of the three motif node types, clustered, integrator and terminus (top plots), and deviations of normalised spectra (bars in the middle) of the three motif node types, clustered, integrator and terminus, of the two hub and two non-hub groups, from that of the network mean. Colour codes of z-scores on top match that of spectrum deviations at the bottom.

triangle motif in the network core indicates that the core is generally more clustered than non-core regions (Figure 6.3 *b*, first column). Along with that, both core and module hub regions fulfil their integrator role (second column) by creating connections between, and thus collecting information from, both non-hub region types, which themselves are more frequently found in terminus position (third column). Furthermore, this finding is reinforced by a higher random z-score value of the integrator motif node in the cortical core and hubs than in the non-hub network crust. This less negative z-score value indicates a centralisation in the distribution of those motif positions towards the core and hub regions, thus a higher than expected integration capacity of these cortical areas. However, as the z-score difference is much less pronounced for the spatial surrogates, this centralisation can partially be accounted for by the length distributions and physical locations of the core and hub regions.

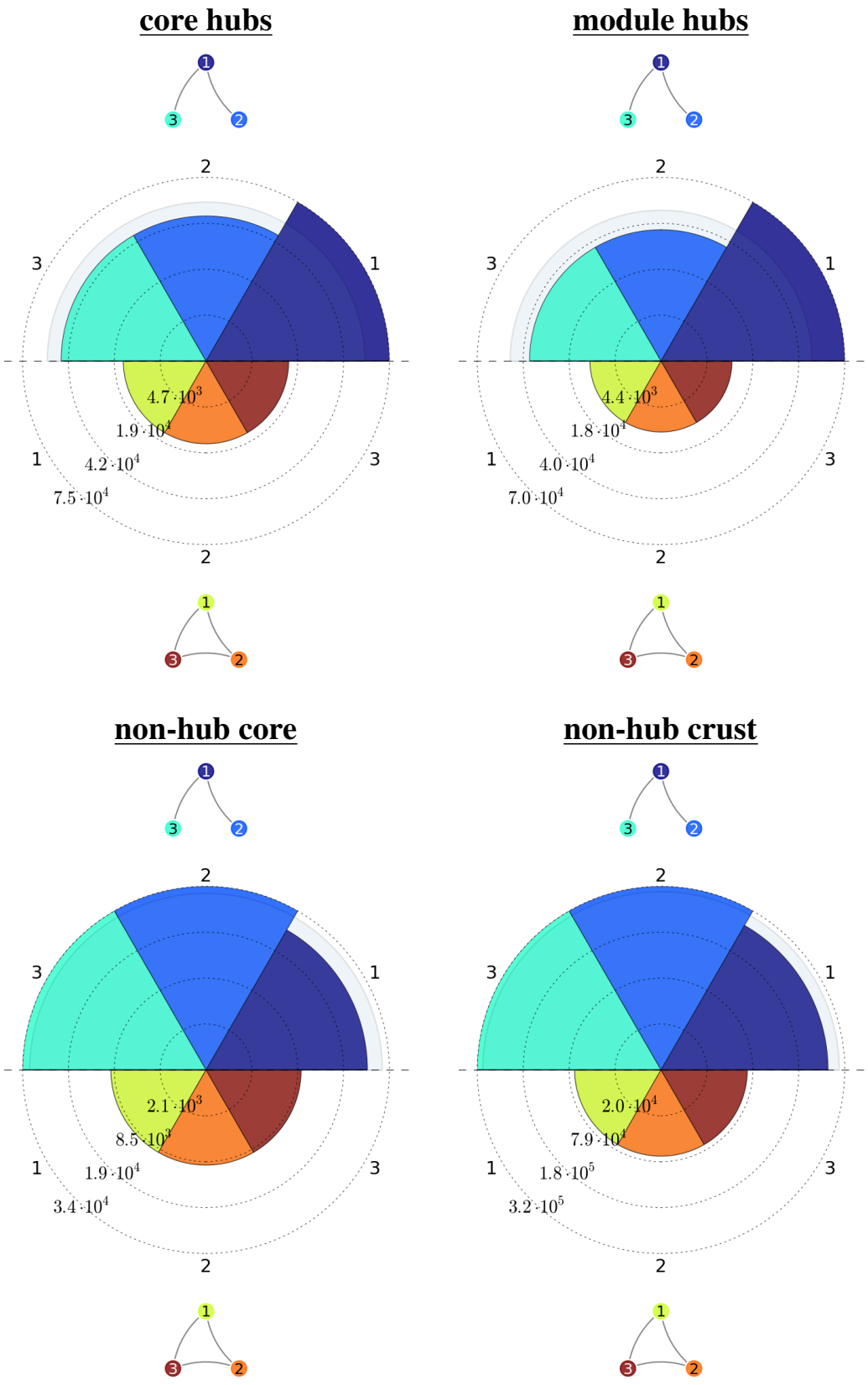

Figure 6.4: **Three-motif node fingerprints of the two hub and two non-hub groups.** Each sector corresponds to a motif node by its index (see motif forms on periphery). Sector areas (and not radii) are proportional to motif node occurrences (see motif node occurrence number indicators on dotted circles).

Four-node motifs

Figure 6.5 shows the results of the four-node motif analysis. The cortical network contains about 20 million of the six four-node motif forms in total (Figure 6.5 *a*). In absolute comparison, the 'linear' four-node subgraph (form 2) significantly outperforms the other five shapes, with more then 10 million (∼50%) occurrences, pointing to the predominantly linear (possibly edge-wise two-way) information processing scheme among the sparsely connected cortical regions. Furthermore, the 'fan' (form 1) and 'crossed fan' subgraphs (form 3) are also represented significantly in the network, with about 2.8 million (∼14%) and 5.1 million (∼25%) instances, respectively. These two forms suggest a completely different, rather distributive and/or integrative communication scheme among the contained node quadruplets, one of them possessing the special role of being a central 'mini-hub' of the formation in each case.

Surrogate comparison with both surrogate groups (Figure 6.5a) results in positive z-score values for all clustered motif forms (motifs that contain at least one triangle, i.e., form 3, 5 and 6), and negative z-score values for all non-clustered motif forms (motifs without any triangles, i.e., form 1, 2 and 4), demonstrating the dominating effect of the high clusteredness of the cortical network on the gross signature of its miniature 'functional units'.

Beside the effect of its extremely high clustering, another fundamental topological property of the cortical network,its low connection density, provides further understanding of the found four-node cortical motif distribution. Indeed, in comparing the six four-node motif forms, the three with the highest absolute occurrence number, form 1, 2 and 3, are the ones containing the lowest number of edges (3, 3 and 4, respectively) and the greatest number of linear (non-triangular) node triplets (3, 2, 2). The low expression of motif form 5 (∼6%) and 6 (∼2%) conforms well with this trend: with them possessing 5 and 6 edges, they are the most densely connected motif forms, and they contain only 2 and nil linear node triplets.

Interestingly, form 4, the rectangular subgraph, is an exception from the above rule: it is made up of only four edges, all four of its node triplets are linear, and yet, with only about two hundred thousands occurrences (∼1%), it is the most under-represented four-node subgraph in the cortex, its anti-motif. However, the sparse and yet highly clustered connectivity of the cortex provides a straightforward explanation to this apparent discrepancy: the scarcity of the rectangular formation simply indicates the extremely low probability of any two regions in the cortex to be indirectly linked by two other (unlinked) regions, while not being directly connected to each other. In other words, if there exists at least two two-step long independent paths between any two cortical regions, they are almost always directly connected as well.

Let us analyse now the group averaged motif node fingerprints of the three investigated cortical

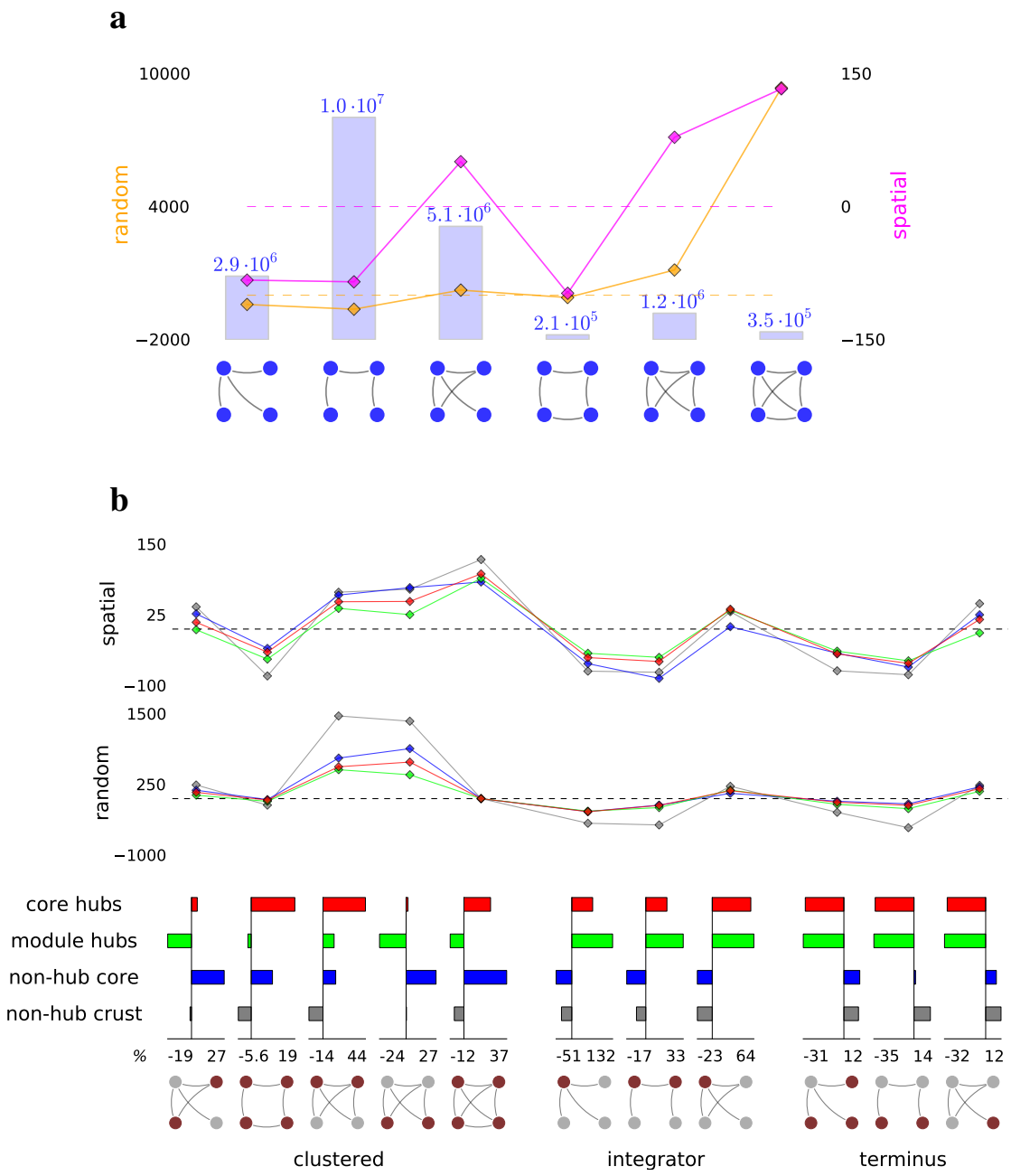

Figure 6.5: **Four-node motif results.** *a*: motif counts (bars) and random (orange) and spatial (magenta) z-scores (diamonds) of the six four-node undirected motifs. Number of top of the bars indicate absolute counts of subgraphs, scales on the two sides indicate z-score values. *b*: z-scores (top plots) and normalised spectrum deviations (bars in the middle) of the three motif node types, clustered, integrator and terminus, of the two hub and two non-hub groups, from that of the network average. Dashed lines indicate zero z-score levels. Due to its relative (but not absolute) over-representation by the cortex (random z-score between 5000 and 12000), random z-scores of the last clustered subgraph (the complete graph) was manually set to zero to fit to scale.

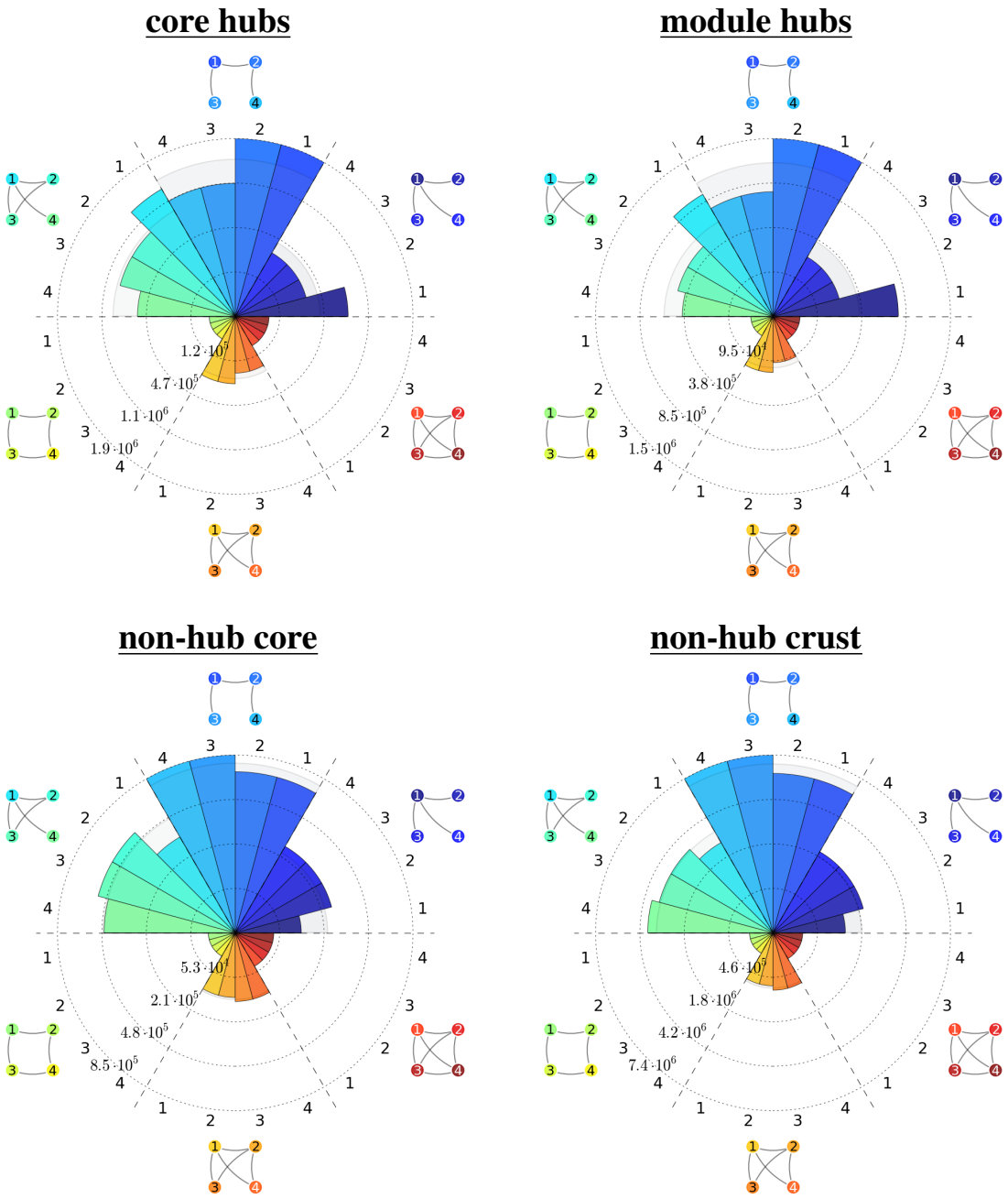

Figure 6.6: **Four-motif node fingerprints of the two hub and two non-hub groups.** For figure explanation, see Figure 6.4.

region groups (core hub, module hub, non-hub core) and that of the baseline, non-hub crust group (Figure 6.5b). Firstly, the motif node spectra of the various region groups clearly demonstrate uniformly positive or negative deviation within each motif node types (clustered, integrator and terminus). These consistent trends confirm that our predefined motif node classes, although all contain nodes from various motif forms, are indeed groups of corresponding motif nodes whose over- or under-expressions correlate for the four investigated cortical region groups. Furthermore, the actual functional capabilities suggested by the spectrum deviations of the three distinguished region groups are consistent with the ones indicated by our earlier analysis, thus verifying that motif node categorisation is a viable analysis technique for investigating the putative functional roles of certain cortical regions or region groups.

Spectrum deviations of the four region groups at the different motif node groups types are consistent with what was found for the three-node motif form distribution. Specifically, we find that both hub groups occur at terminus motif nodes with decreased, and at integrator motif nodes with elevated frequencies, indicating their high functional integration potential over the rest of the cortical network. Additionally, the fact that module hubs surpass even core hubs in integrator motif node count indicates that module hubs are the most capable regions in the cortex to act as 'mediator' regions between two otherwise unconnected regions in the cortical connectivity. We also find that both sub-groups of the core, hubs and non-hubs in the core, tend to be found at high degree clustered motif nodes more frequently, which is in line with our earlier findings on their dense, mutual inter-connectedness, and grants them a remarkable internal integration potential at the topological centre of the cortical network.

Absolute motif counts of the four region groups, plotted in Figure 6.6, also demonstrate significant differences in their motif fingerprints. Most notable is the overabundance of integrator motif nodes at the two hub groups, the increased occurrence of high degree clustered motif nodes at the two core groups, and the increased relative frequency of terminus motif nodes at non-hub crust regions, each one confirming previously found properties of the four node groups.

6.3.4 Discussion

In this section, we investigated the characteristic processing role of various topologically relevant groups of cortical regions within its 'canonical functional units', the network motifs. To this end, we divided the cortex into four region groups, core hubs, module hubs, non-hub core and non-hub crust, and analysed their three- and four-node motif spectra on a per motif node basis.

We started off our motif analysis by counting the 3- and 4-node motif spectrum of the cortical network globally (Section 6.3). Due to its low connection density, we found an overabundance of

sparsely connected (low edge number) motifs in the cortex in *absolute* terms. However, surrogate analysis also unveiled the *relative* overabundance of more clustered (high edge number) motif forms, attributable to the extremely high local segregation present in the cortex. These results are broadly in agreement with those found by Reigl et al. (2004) and Sporns and Kötter (2004) in the neural network of the *C. elegans* and in the macaque visual cortex, pointing to overall similar characteristics of the motif spectra of various brain networks at different scales, originating from their common properties of having a sparse, but relatively clustered connectivity.

On the global level, we found that low edge number, sparsely connected subgraphs dominate in the cortex in absolute terms, due to its overall sparse connectivity. However, in relative terms, more densely connected motifs are overabundant in the cortical network in comparison with both of its surrogate types, providing the previously detected high clusteredness to the cortex. Furthermore, in the particular case of four node motifs, we found the circularly connected rectangle subgraph formation to be highly under-represented in the cortex, pointing to the extremely low probability of any two unconnected regions to be indirectly connected through at least two other regions. This finding suggests the relative lack of parallel information processing along short (two-step-long) parallel pathways in the cortex compared to other stereotypical functional blocks, such as linear or fanned motifs, at least at the currently investigated resolution.

Considering the various topological parts investigated, we found that each one of the four region groups specialised to different motif node types. Highly clustered motif nodes are characteristic in only the two core groups, providing high internal integration capability to the core as a whole, compared to the rest of the network. In general accordance with the results of Sporns et al. (2007), regions from both hub groups can be found in integrator motif node positions with significantly increase frequency, while, on the contrary, regions of both non-hub groups appear to favour terminus motif node positions. The found typical motif node fingerprints provide further evidence for the topological specialisation of the investigated region groups, and suggests functionally different roles during cortical information processing.

Due to the undirected nature of the currently utilised dataset, we are not able to test the intriguing finding of Sporns et al. (2007) about the characteristic and strong preference of hub regions in the cat and macaque brain networks for the appex position of the two-way connected V-shape motif form. That motif node is one of the integrator motif node types in our categorisation scheme, which was found to be favoured by both cortical hub groups, providing indirect support for the validity of the finding of Sporns et al. (2007) in the human cortex. Nonetheless, future, directed versions of the human cortical connectivity will significantly enrich our motif analysis by being able to detect such direction-specific differences in the motif node spectra of various cortical

region groups.

6.4 Overview of results

In this chapter, we analysed the topological properties of a functionally potentially highly significant group of regions, the hubs of the cortex. Investigating the topological position of high-degree hub regions in the found hierarchically modular and considerably centralised cortical architecture, we found a stronger than random, spatially rather scattered rich-club structure, which nevertheless exhibits a 50% overlap with the network core (Section 5.4). This led us to depart from the traditional connector/provincial hub categorisation scheme, and to distinguish hub regions with respect to the network core, as *core hubs* or *module hubs*, depending on if they reside inside or outside of the core (Section 6).

Comparing the two, equal size groups (n=50 regions, 5% each), we found that module hubs, as opposed to hubs in the core, are spatially more distributed and topologically rather segregated from each other (only sparsely intra-connected), and furthermore they appear to contribute more to local rather than global integration. These findings suggest that, as depicted in Figure 5.12b, the rather disconnected extra-core hubs in the various cortical modules are indeed primarily specialised to coordinate and connect their local neighbourhoods to the rest of the network, reinforcing the globally central position of the network core.

The possibility that individual cortical regions may favour different *motif node* positions within the various motif graphs can result in substantial internal inhomogeneity in the motif spectrum distribution of the cortex. Furthermore, motif nodes, besides forming isomorphic groups within individual motif graphs, can be further categorised into characteristic classes according to their intra-motif connectivity *across* motif graphs. We categorised each motif node as being either in a terminus, integrator or clustered position within their respective motif form. To investigate these properties of the cortex, we assessed the motif node spectrum deviations of four, topologically distinguished region groups of the cortex: hubs in the network core (core hubs), hub outside of the network core (module hubs), non-hub regions in the core (non-hub core) and non-hub regions outside of the core (network crust)(Section 6.3).

Firstly, spectrum deviations of the various motif nodes showed systematic co-variation within the same group type across all four investigated cortical region groups, validating our motif node categorisation scheme. Secondly, we found that each cortical region group is specialised to different motif node classes. Specifically, both hub groups favour integrator, and rather than terminus motif node positions, supporting their putative functional integrator role even at the microscopic network elements of motifs. Additionally, hubs inside the core, but not hubs outside of it, can be found

in clustered position with increased frequency, in agreement with our previous results on their extraordinary internal integration capability. Furthermore, both non-hub region groups favour terminus, rather than integrator motif node positions in the three most common motif forms, with non-hub core regions also appearing in clustered positions with increased probability. Altogether, these findings are in agreement with the dominant topological characteristics of the investigated region groups, further underscoring the distinguished topological, and putative functional, role of the core and hub regions as the main collective and distributed integrators of the cortex, respectively.

This chapter concludes our purely topological analysis on the anatomical architecture of the cortical connectome. In the next chapter, we shall simulate network activity on the cortical connectivity in order to investigate the relevance of our structural findings on the dynamics of the cortex.

Chapter 7

The structural origin of cortical synchronisation

Simulations of coupled oscillators on the cortical structural connectivity

In the previous chapters, we carried out a survey of analyses on the organisation features of the structural connectivity of the human cortex on multiple scales. Using those results, in this chapter we will turn to the investigation of the properties of the dynamics the topology of the cortical architecture facilitates. We shall observe and analyse the dynamical patterns on the simulated activity of cortical regions interacting through their anatomical connectivity.

The chapter is organised around three fundamental dynamical phenomena: the emergence of synchrony, dynamical complexity, and propagation of activity. For the complete observation of the first phenomenon, we shall investigate the path of the cortical connectivity from asynchrony to complete synchrony in a physiologically non-plausible dynamical model, and assess the resemblance and significance of the various architecture features of the cortex in its emerging synchronisation patterns (synchronizability). We shall investigate the second phenomenon, dynamical complexity, by a biophysically more plausible model, in order to characterise the significance of certain topological features of the cortical connectivity in facilitating this important aspect of cortical dynamics (Shanahan (2010)), as well as to guide our parameter choices in forthcoming dynamical analysis. Finally, the third phenomenon, propagation of synchronous activity, will be investigated to gain insight into the threat posed by certain parts of the cortex in propagating and picking up epileptiform seizures. Throughout this chapter, our analysis will be organised around the topologically distinguished parts of the cortical architecture obtained in

the previous chapters, its modules, core and hub regions, in order to test their putative functional significance in the unfolding cortical dynamics.

7.1 Introduction: Synchronised oscillations in the cortex

The central challenge of the neurosciences is to uncover how the brain carries out its fundamental function: to translate sensory information to motor commands through internal information processing. Given the brain's various organisation levels, from subcellular elements through cortical columns to brain regions, and considering the wide range of information processing demands, from sub-conscious stimulus processing and motor command execution to high-level mental activities, the notion of a single, universally applied information processing strategy seems highly unlikely, which calls for a multi-scale and multi-modal approach (Dayan and Abbott (2001)).

Different kinds of information processing strategies have indeed been discovered in the brain. Sensory stimulus encoding into neuronal firing intensity and timing (Butts et al. (2007)), or specialisation of neurons to the selective representation of different colours, orientations, or spatial locations (McNaughton et al. (2006)), are only two examples of the numerous strategies possibly utilised by the nervous system.

On larger scales, synchronisation between neural assemblies (Buzsaki (2006)) has extensively found to be involved in the execution of 'higher order' cognitive tasks, such as arousal, perceptual integration, attention selection, association and working memory (Engel and Singer (2001), Melloni et al. (2007), Lakatos et al. (2008)). Additionally, abnormal neural synchrony was shown to be a pathophysiological mechanism of several neuropsychiatric disorders, such as autism spectrum disorders (ASDs), epilepsy and schizophrenia (reviewed in Uhlhaas et al. (2009a)).

In this chapter, we examine the characteristics of spontaneous and evoked oscillations emerging on the human cortical connectivity by various simulation techniques. To gain a better understanding on how the unfolding network dynamics are facilitated through the structural features of the cortical network, we carry out a detailed, multi-stage and multi-model analysis of the dynamics with respect to the cortex various topological features found in the previous chapters. Besides investigating the basic large-scale dynamical characteristics of the cortex, our primary goal throughout the analysis will be to extend our purely structural analysis results on the found hierarchically modular and considerably centralised cortical topology, and explore how these properties affect the emerging network dynamics.

7.2 Methods: The Kuramoto phase oscillator model

7.2.1 Introduction of the Kuramoto model

Originally motivated by the dynamics of chemical oscillator systems almost 30 years ago, the Kuramoto oscillator model (Kuramoto (1984)) has since been analytical investigated in great depths (Acebrón et al. (2005), Arenas et al. (2008)), and has become a widely utilised tool for the exploration of synchronisation on complex networks of different domains (see Arenas et al. (2008) for a review). In the neurosciences, the Kuramoto model is widely applied for the simulation of meso- and macro-scale dynamics of cortical networks (Honey and Sporns (2008), Gómez-Gardeñes et al. (2010), Cabral et al. (2011)). Its popularity can be attributed to its capability for addressing a wide range of dynamical phenomena and yet being simple enough to be analytically and computationally tractable, compared to the more detailed and thus more parameter-rich neural mass models (Deco et al. (2008), Deco et al. (2009), Jirsa et al. (2010)) or spiking neuron models (Gerstner and Kistler (2002), Izhikevich (2004), Izhikevich (2010)). Despite its relative simplicity, dynamical network models of coupled Kuramoto oscillators are able to incorporate such fundamentally important anatomical and physiological features of the brain as connection specific coupling strengths and transmission delays, and variance in internal region activities.

In terms of complexity, on the other end of the spectrum of models there has been an increasing interest on large-scale simulations of virtual brains composed of a tremendous number of microscopic elements: individually modelled spiking neurons (reviewed in de Garis et al. (2010)). The inherent potential of creating a unified and universal model by arching over multiple spatio-temporal scales makes these approaches highly appealing for modellers and computational researchers. However, while there has been an enormous technological progress since early studies (Lumer et al. (1997a), Lumer et al. (1997b)), the interpretability and theoretical tractability of these extremely detailed simulations is still problematic up to date, which in turn limits their scientific benefit (see Izhikevich and Edelman (2008) as a recent example of such a study). These issues, along with the motivation to focus our investigations on how network dynamics is shaped by network structure, rather than by any particular node model, supports our choice for choosing a 'minimal' model for the simulation of large-scale brain dynamics.

Our oscillatory model will closely follow the one introduced in Cabral et al. (2011), where the emerging network dynamics and functional connectivity of a 66-region downsampled version of the cortical network was studied in an intermediately synchronous, but highly metastable dynamical regime of coupled Kuramoto oscillators. In spite of utilising the same cortical connectivity network, there are two major differences between the study of Cabral et al. (2011) and the current

one regarding their simulated connectivity networks. Firstly, a network of 15 times larger in size will be investigated here, rendering the resolution of the current study to mm-size cortical regions, as opposed to the cm-size regions of Cabral et al. (2011). Secondly, at the nodal level, network dynamics of the former study was enriched by the partial directionality introduced during the downsampling process[1]. In the following, we will introduce the components and construction of the applied node and network model.

7.2.2 Detailed introduction of the model

Prior to any simulations, the cortical structural connectivity network is pre-processed in order to reach a normalised and controllable domain for the simulations (Cabral et al. (2011)). Specifically, the connectivity matrix C, containing the connections weights between the cortical regions, is normalised so that the mean strength is set to 1. The fibre tract length matrix L is transformed into a conduction delay matrix τ by choosing a conduction velocity V, resulting in a mean conduction delay $\langle\tau\rangle = \langle L\rangle/V$, where $\langle L\rangle$ is the mean fibre tract length.

In the structural connectivity network, each node (cortical region) represents a local population of excitatory and inhibitory neurons. The phase of the self-sustained (locally generated) dynamics of these neuron populations at the gamma frequency range (30-80 Hz) (Bartos et al. (2007)) is simulated by a Kuramoto phase oscillator at each network node. This particular range is chosen because slow power fluctuations of the local field potential of neural activity in this frequency range has been shown to be correlated with BOLD fMRI signal (He et al. (2008), Miller et al. (2009), Schölvinck et al. (2010)), which relation serves as the basis for our resting-state functional connectivity simulations, as well as in order to be able to compare our results with those of Cabral et al. (2011) obtained in the same frequency range.

The coupling between the oscillators are determined by the connectivity of the network, resulting in the following differential equation governing the phase θ_n of oscillator n:

$$\frac{d\theta_n}{dt} = \omega_n + k\sum_{p=1}^{N} C_{np}\, sin\Big(\theta_p\big(t-\tau_{np}\big) - \theta_n(t)\Big) + \eta_n(t), \tag{7.1}$$

where $N = 998$ is the number of network nodes, k is the network's global coupling strength, C_{np} is the relative coupling strength and $\tau_{np} = L_{np}/V = \langle\tau\rangle L_{np}/\langle L\rangle$ is the delay between node p and node n, $f_n = \omega_n/2\pi$ is the intrinsic frequency of node n, and $\eta_n(t)$ is the noise received by the local neuron population. As the C connectivity matrix contains only non-negative elements, region-region inhibition through coupling is not modelled by the above formula. This simplifying

[1]The network used in Cabral et al. (2011) was directed in the sense that two-way links between the same node-pairs were non-symmetric in their connection weights, but were still symmetric up to their presence (both exist or absent)

aspect of the model is supported by the fact, that the inhibitory cortico-cortical connections are generally absent in the macaque cortex (Deco et al. (2009)).

We note that the above formula takes three factors into account in determining the influence that one node exerts on another: their coupling strength, interaction delay and phase difference. The relative distribution of the first two of these factors are fixed by the connectivity and delay matrices, but their scaling can be varied with k and $\langle\tau\rangle$. In order to introduce regional inhomogeneity to the model, the intrinsic frequencies f_n of the nodes are drawn from a Gaussian distribution with mean f_0=60Hz and standard deviation σ_f. The $\eta_n(t)$ noise received by the local neuron population is modelled as uncorrelated Gaussian white noise with zero mean ($\langle\eta_n(t)\rangle = 0$) and σ_n^2 variance.

The four main free parameters of the model are the global coupling strength k, mean conduction delay $\langle\tau\rangle$, dispersion of natural frequencies σ_f and variance of noise σ_n received by the oscillators. The first two parameters, determining the magnitude of the strength and delay of the interaction between the oscillators, are the parameters by which the emerging dynamics is affected by the actual structure of the underlying network. The last two parameters, frequencies dispersion and noise, model phenomena that are naturally present in the brain, and are included to increase the realism of the model. Although analytical studies have pointed to the potentially significant effect of Gaussian noise in the Kuramoto model as well as in more general oscillator models (see e.g. Daffertshofer (1998), Acebrón et al. (2005)), extensive numerical exploration of the parameter space of the model to be used here, carried out by Cabral et al. (2011), showed that both frequency dispersion and noise have relatively small influence on the behaviour of the network in their plausible ranges, compared to the global coupling strength and conduction delay (Cabral et al. (2011) supplementary material). Motivated by the findings of Cabral et al., we will use their choice of $\sigma_f = 3$ and $\sigma_n = 2$ as a working point for all of our simulations, except in Section 7.3, where both parameters are set to zero.

A typical simulation run proceeds as follows. First, node phases are initialised randomly. Then, in order to accumulate sufficient pre-run node phases sufficient for the delays of the network, a non-interacting (and non-noisy) network is run until maximum delay time τ_{max}. After that, the internal noise of each node and the coupling between the node-pairs are turned on, and the actual simulation is performed until t seconds. In order to minimise the effect of initial conditions, the first t_0=2s of the simulation is discarded from further analysis, except for the synchronizability simulations. Numerical integration is performed using the Euler method with δt = 0.1ms time step.

7.2.3 Effects of the various model components

In order to find appropriate parameter choices of the forthcoming simulations, we explore the effect of the various model components on the emerging network dynamics by running partial simulations with only some of the model components enabled.

For this preliminary analysis, we are interested in measuring the temporal internal synchrony and mean phase of the entire network (N) or among a group of nodes (G). For this, we use the jointly defined phase uniformity $R_G(t)$ and group phase $\Phi_G(t)$ order parameters:

$$R_G(t)e^{i\Phi_G(t)} = \frac{1}{|G|}\sum_{n\in G} e^{i\theta_n(t)}, \tag{7.2}$$

where $\theta_n(t)$ is the phase of node n at time t and i is the imaginary unit of complex numbers (Arenas et al. (2008)). $R_G(t)$ is 0 at time t, if the nodes in G are fully desynchronized, and 1 if they are in full synchrony, that is, they are in the exact same phase.

Figure 7.1 *a* illustrates the characteristic dynamics emerging from the simulation of the simplest Kuramoto model variant: homogeneous, instantaneously interacting phase oscillators with no frequency dispersion, noise or transmission delay (applied eg. in Arenas et al. (2006) and in Gómez-Gardeñes et al. (2010)). In this most basic model variant, starting from a randomised phase distribution, both the individual modules as well as the whole network evolves into an almost fully synchronous state fairly quickly, even at this low level of coupling (k = 2).

Figure 7.1 *b* shows the dynamics of the Kuramoto model of intermediate complexity, composed of inhomogeneous and noisy phase oscillators with instantaneous transmission (zero delay). Again, starting from a randomised phase distribution, both intra-modular and global network synchrony

---

Figure 7.1 *(following page)*: **Illustration of the effect of various model components on the simulated network dynamics.** Network dynamics from three variants of the model are presented: *a*: noiseless oscillators with instantaneous interaction, *b*: noisy oscillators with instantaneous interaction and *c*: noisy oscillators with time-lagged interaction. In the top four subfigures for each variant, all 998 cortical regions are represented by dots around the circle perimeter, with angles corresponding to their momentary phases, and with regions in the same module drawn to the same distance from the origin. Synchrony, main phase and phase dispersion of each one of the 12 modules is plotted as the length, phase and opening angle of correspondingly coloured inner circle sectors. On the figures below, relative module phases (difference between mean network phase Φ_N and module phase Φ) and module synchronies R are shown as the function of time. Model parameters: noiseless (*a*): τ_m=0ms, σ_f=0, σ_n=0, noisy (*b*): τ_m=0ms, σ_f=3, σ_n=2, time-lagged (*c*): τ_m=1ms, σ_f=3, σ_n=2. For all three variants: k=2 and f_0=60Hz.

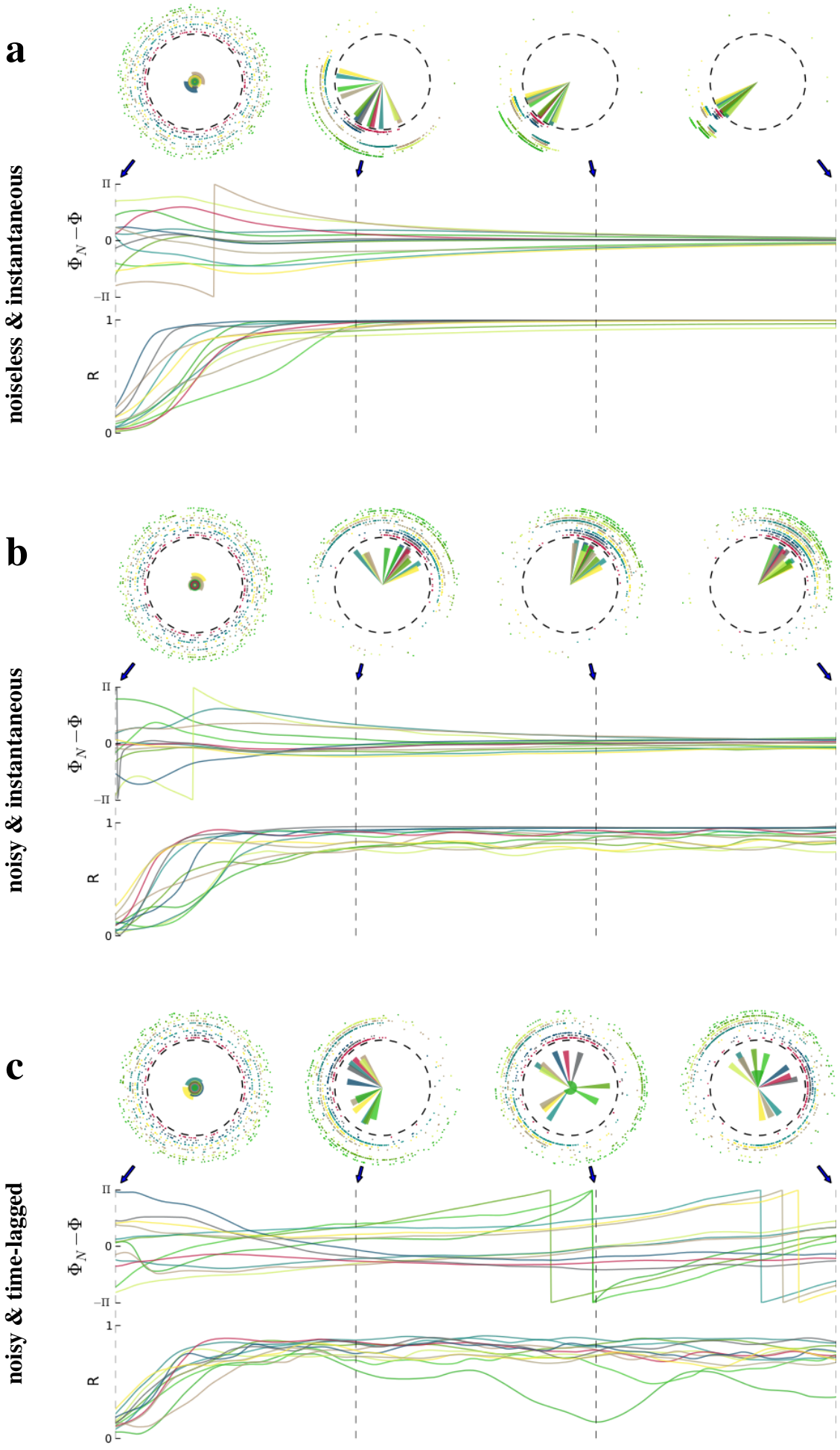
a
noiseless & instantaneous
b
noisy & instantaneous
c
noisy & time-lagged
Π
0
−Π
$\Phi_N - \Phi$
1
R
0

of this model variant are able to reach high levels too, however, a certain level of noisy oscillations appear compared to the homogeneous, noiseless case (*a*), due to the repulsive forces appearing due to the introduction of inhomogeneous frequencies and internal white noise at the nodal level.

Figure 7.1 *c* illustrates the typical dynamics of the fullest Kuramoto model variant to be used in this study: inhomogeneous and noisy phase oscillators with transmission delays (applied e.g. in Cabral et al. (2011)). Note that even the introduction of as low as τ_m=1ms mean node coupling delay results in substantially reduced mean structural and global synchrony. Specifically, the magnified oscillations in internal structural synchrony (R) is accompanied with increased decoupling among the angular movement of the structures (Φ) at the inter-group level. Thus the addition of conduction delays to the model significantly enriches the dynamics of the network on micro- (sub-modular), meso- (modular) and macro- (global) scale.

To summarise, in this section, we have seen characteristic differences in the network dynamics to the various variants of the Kuramoto model. In particular, confirming the results of Cabral et al. (2011), we have found that parameters introducing inhomogeneity to the dynamics of *individual nodes* (σ_f and σ_n), even at low global coupling strengths, cause only minor alteration to the emerging dynamics at meso- and macro-scales, and that turning on the node-node interaction affecting conduction delays is necessary to increase the complexity of the temporal dynamics of the coupled oscillator network.

We also note that the early phase of the dynamics is highly susceptible to the actual distribution of the randomly initialised phases of the network nodes. For this reason, when the dynamics of that initial period is not the interest of the analysis, we will discard the first $t = 2$s of the simulations for evaluating any temporally averaged measures.

7.3 Global synchronizability of the cortex

7.3.1 Introduction

In this section, we start the exploration of cortical synchronisation dynamics facilitated by its structural connectivity by investigating the evolution of global synchrony from initial asynchrony (random phase distribution). Specifically, we will ask the questions: *In what ways do the found topological features of the cortex organise, contribute to and participate in the emergence of cortical synchronisation?*

The simulation of synchronisation phenomena as an abstract exploratory tool has proved to be useful for the identification and analysis of various dynamically important structural substrates of complex networks (Arenas et al. (2008)). In a series of analytical investigations, Arenas and

his colleagues studied the evolution of local synchronisation patterns towards global synchrony on different stereotypical network architectures. The emergence of synchronisation on 'homogeneous' structures (such as hierarchically modular networks (Sporns (2006)) and Erdös-Rényi (Erdös and Rényi (1960)) graphs) was found to be dominated by a sequence of rather sudden transitions, each corresponding to the propagation of intra-module synchrony from a certain hierarchical level to the one above (Arenas et al. (2006), Gómez-Gardeñes et al. (2007)). As opposed to that, evolution of global synchrony on 'heterogeneous' network structures (such as scale-free graphs (Barabási and Albert (1999))) is a rather smooth process, mainly organised around and driven by the hubs of the network (Gómez-Gardeñes et al. (2007), Gómez-Gardeñes et al. (2011)).

Practical utilisation of synchronizability analysis on the structural connectivity of the cat cerebral cortex was carried out by Gómez-Gardeñes et al. (2010), who explored the emergence of synchrony within and between the modules and the modularly distributed rich-club of the network. The technique reinforced and extended previous structural (Zamora-López et al. (2009)) and linear dynamical system analysis (Zamora-López et al. (2010)) results, pointing to the significance of the rich-club structure of the cat cortex as a topologically central mediator of cerebral synchronisation.

Utilising the above techniques as some abstract analysis tools to gain insight into the significance of certain topological features in shaping network dynamics, in this section we will start investigating the dynamical significance of our findings on the structural organisation of the cortical connectome. In our first, initial set of analysis, we investigate the path followed from local to global synchronisation in the network and observe the synchronisation features of the identified topological substrates of the cortex, i.e., its modules, its network core and its hub regions.

As we discussed above, different network organisations were found to exhibit characteristically different paths to global synchrony (Arenas et al. (2006), Arenas et al. (2008), Gómez-Gardeñes et al. (2007)), and various parts of the network, depending on their topological features and global significance, can contribute to the emergence of this synchronisation by a different extent (Gómez-Gardeñes et al. (2010)). Therefore, with the initial simulations of this section we aim to extend our, up to this point, purely topological results on the cortical connectome by some preliminary analysis on their dynamical significance using the simplest Kuramoto model variant. Specifically, in order to be able to examine the evolution of total network synchrony from total asynchrony, we utilise an abstract (biophysically non-plausible), instantaneously interacting (non time-lagged) variant of the Kuramoto model, with a global coupling strength that guarantees the emergence of global synchrony.

We have to stress, that the simulation of the evolution of total network synchrony in this section is not meant to be the model of any biophysically plausible phenomenon of the brain, but rather we

utilise it as an abstract, minimal and controllable analysis tool to investigate the dynamical potential of various parts of the cortical network to cooperate and exert influence on (or drive) other parts of cortex. We will turn to biophysically more plausible investigations on the complex dynamics of the cortex in the following sections of the chapter.

7.3.2 Methods

Dynamical model and simulation parameters

In order to examine the emergence of global network synchrony, we have to use a dynamical model that is able to asymptotically approach the totally synchronous state from a random initial state. For the study of this rather abstract phenomenon (emergence of global synchrony), we use the simplest, physiologically least plausible Kuramoto network model variant, composed of instantaneously coupled (zero-time lagged), noiseless and identical oscillators (Figure 7.1 *a*). The same model variant was used for example in Arenas et al. (2006) and in Gómez-Gardeñes et al. (2010) for similar investigations.

For each analysis in this section, n=100 simulation runs are performed and averaged, which differ from each other only in the initial phases of the cortical regions. The identical and noiseless Kuramoto oscillators at each region are coupled instantaneously and with a relatively low, k=2 global coupling strength in order to observe the emergence of global synchrony with reasonable temporal resolution. Modular and global network level synchrony are measured by the R order parameter (Eq. 7.2).

Global synchronizability of the cortex is assessed against its surrogates. Besides comparing the evolution of the network-wide order parameter R for the intact networks, we also assess the resilience of cortical synchronizability against different lesion scenarios: i) against removal of n=100 random regions and ii) against removal of its n=100 hub regions. For the quantitative evaluation of the simulation results, we measure the simulation time steps needed to reach a synchrony threshold for each network (cortex and its surrogates) in each simulation scenario (intact, hub lesioned, random lesioned). In order to use a uniform threshold for all the above cases, we choose the minimum of the maximum synchrony levels reached by the end of the simulations, across all cases. This simulation case is the hub lesioned cortical network simulation, which reaches R_{th}=0.785 by the end of the simulation time.

Due to the abstract nature of the applied model in this section (zero time lag and very low coupling strength), interpretation of time dimension in absolute terms is not attempted here, instead we only assess the temporal evolution of the investigated phenomena relative to one another.

Pairwise region synchronisation matrices

Internal evolution of synchrony is examined similarly as it was in Arenas et al. (2006). To that end, synchronisation times between all region pairs are calculated, and then aggregated for certain region groups. Below, we formally introduce our analysis methods.

First, we define a continuous metric for measuring correlation between oscillator-pairs:

$$\rho_{ij}(t) = \langle cos(\theta_i(t) - \theta_j(t)) \rangle, \tag{7.3}$$

where $\langle \cdot \rangle$ is average over all n=100 simulation runs. This results in a local order parameter matrix ρ, that indicates the level of synchrony on a continuous scale ($\rho_{ij} \in$ [-1, 1]) at each time instance of the simulation (Arenas et al. (2006)).

To clearly distinguish between synchrony and asynchrony, ρ is then thresholded to get the binary D *dynamical connectivity* matrix (Arenas et al. (2006)):

$$D(t)_{ij} = \begin{cases} 1 & \text{if } \rho_{ij}(t) \geq Th \\ 0 & \text{if } \rho_{ij}(t) < Th \end{cases} \tag{7.4}$$

In our analysis, Th is set to 0.8 in order to reach a close to complete global synchrony by end of the simulation.

Finally, we unify the above time-dependent D dynamical connectivity matrices into a single, *synchronisation onset time* matrix S, each entry of which indicates the earliest time the corresponding region pair gets synchronised:

$$S_{ij} = \underset{t}{\operatorname{argmin}} \{ D(t')_{ij} = 1 \mid \forall\, t' \geq t \} \tag{7.5}$$

With that, we reach a quantified, compact representation of the synchronisation ability (synchronizability) of each region-pair.

Group synchrony assessment

Being able to assess the onset of phase synchrony between any region-pair, we use the matrix S to compare the onset of internal synchrony of various region groups of interest. As the transition from incoherent dynamics to synchrony is regarded as the dynamically critical regime of coupled oscillators (Strogatz (2000), Acebrón et al. (2005)), we weaken the total, all-to-all synchrony condition and define the onset of internal synchronisation of a group of regions as the earliest time when an average region of the group is in synchrony with at least L proportion of the rest of the group.

As a trade-off value that allows for most of the investigated groups to reach internal synchrony (not too high L) and at the same time gives high enough time resolution for the analysis (not

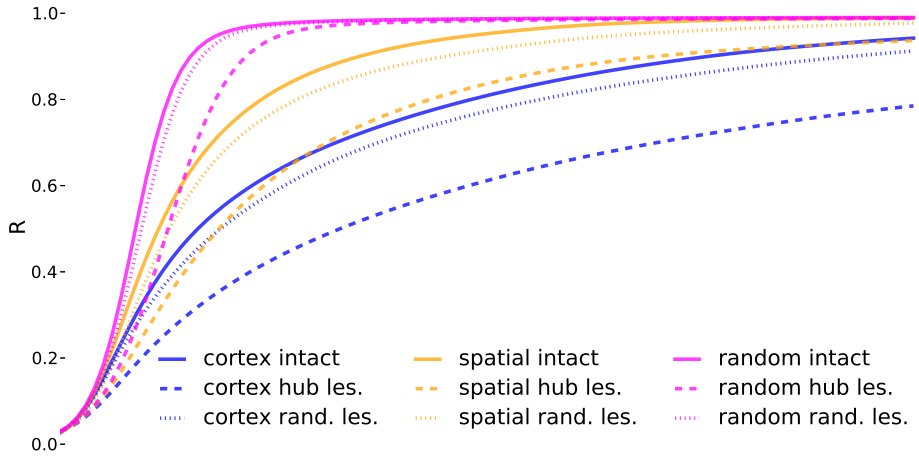

Figure 7.2: **Temporal evolution of global network synchrony.** The x axis denotes abstract (physiologically implausible) simulation time.

too low L), we found L=65% to be an optimal intermediate value for our simulations. We note here, that this reduced group synchrony condition implies, that for the remaining of this section *group synchronisation time* means the *onset*, rather than termination, of internal group synchrony evolution.

7.3.3 Results

Global synchronizability of the simulated cortex

Evolution of global network synchrony is shown for the cortex and for its surrogates in Figure 7.2 (solid lines). The simulated cortex is clearly less globally synchronizable than both of its surrogates (simulation time to synchrony threshold R_{th} = 0.785, cortex: $t^C(R_{th})$ = 45, spatial surrogates: $t^S(R_{th})$ = 22, random surrogates: $t^R(R_{th})$ = 12). These differences in the pace of global synchrony emergence presumably reflect integration and segregation measure differences of the cortex and its surrogates. Specifically, the more segregated (high clustering coefficient, Section 4.3) and less integrated (lower efficiency, Section 4.2) topology of the cortical network slows down phase synchronisation of topologically distant regions, thereby elongating the development of global, network-wide synchrony in the cortex.

For assessing the significance of hub regions in the emergence of global synchrony in the cortex, as well as in its surrogates, we assess how much global synchronizability of the intact network is affected by hub-lesion and random-lesion. All three networks largely preserve their synchronisation characteristics when losing n=100 (10%) random regions (Figure 7.2 dotted lines) (percentage of increment in simulation time required to reach threshold synchrony R_{th} = 0.785: cortex: Δt^C_{rnd}

= 16%, spatial surrogates: Δt^S_{rnd} = 18%, random surrogates: Δt^R_{rnd} = 8%). Considering the contribution of hub regions in global synchronisation, all three networks exhibit significant loss in their synchronisation times for the removal of hub regions (n=100 [10%] highest degree regions) (cortex: Δt^C_{hub} = 120%, spatial surrogates: Δt^S_{hub} = 86%, random surrogates: Δt^R_{hub} = 50%), with the cortex being the most effected by hub lesion among the investigated networks. The found increased importance of the hub regions in disseminating synchronisation globally in the cortex supports our earlier findings about the distinguished topological positioning and putative functional role of hub regions in the heterogeneous cortical architecture (Chapter 6).

Interpretation of global synchronizability results

In this section, we carried out a synchronizability analysis as a simplistic model for the internal capacity of spatio-temporally extended synchronisation in networks. The cortical connectivity, exhibiting the lowest such capacity compared to its surrogates, appears to avoid the sudden and broad emergence of such scenarios, which is in accordance with the pathological nature of these conditions to brain function (Arthuis et al. (2009)). On the other hand of course, information processing through synchronisation (Uhlhaas et al. (2009a)) requires a certain level of synchronizability. We found that hub regions contribute to the cortex' global synchronizability substantially more than random regions, suggesting that hub regions may be crucial elements of the cortical connectivity in facilitating synchrony-mediated processing in the cortex. This result reinforces our earlier findings on their increased ability as functional integrators (Chapter 6), and also warns about their potential as mediators of epileptiform network seizures (Section 7.5).

In conclusion, we consider three functional benefits of the observed reduced level of global cortical synchronizability:

- it increases the cortex's ability of carry out segregated, specialised information processing,
- it increases the dynamical complexity/metastability of the cortex, and
- it prevents hyper-synchronous neuronal activity and makes the cortex resistant against epileptic seizures.

These claims will be further investigated in the following sections.

Emergence of global synchrony through module hierarchy: overview

Looking at the internal evolution of network synchrony, firstly we investigate how the found module hierarchy affects the phenomenon. Specifically, the finding that global synchrony builds up through the modular elements of the various hierarchy levels would provide dynamical evidence

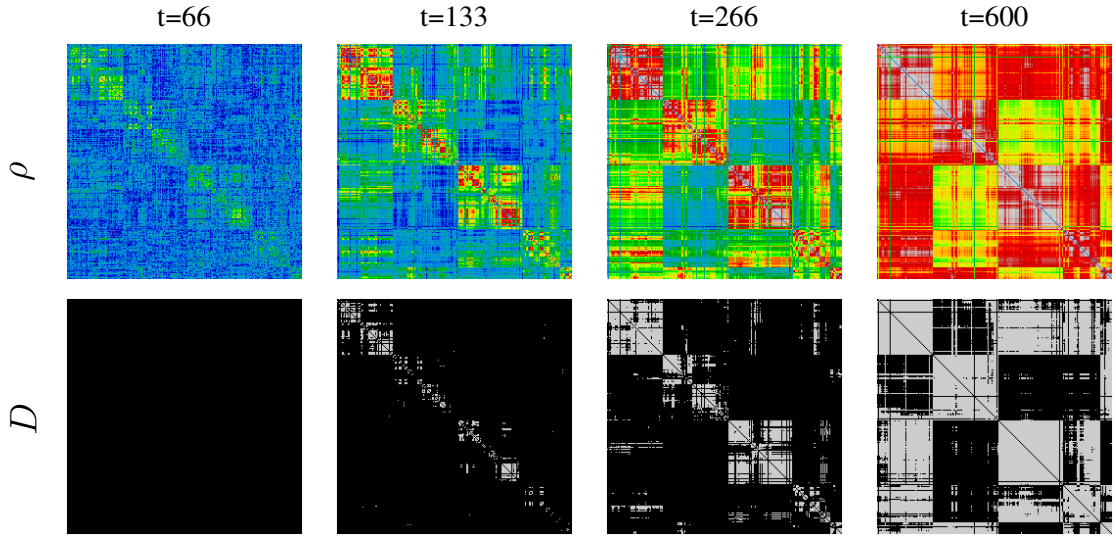

Figure 7.3: **Evolution of pairwise synchronies.** Samples of ρ (top) and D (bottom) synchrony matrices. Colour codes: ρ: from blue (asynchrony) to red and white (complete synchrony), D: black: asynchrony, grey: synchrony. In every subfigure, cortical regions are ordered according to the found module hierarchy (see Figure 5.6 top left).

for the ability of the found modules to indeed cooperate functionally (Arenas et al. (2006) Gómez-Gardeñes et al. (2010)). Additionally, we are also interested in the role in cortical synchronizability of the other topologically important parts of the cortex: its core and hub regions.

Figure 7.3 shows the evolution of both pairwise synchrony matrices, ρ and D, at four time instances of the simulations. The visually observable formation of highly synchronised sub-blocks along the main diagonal of both matrices indicates the emergence and progression of internal group synchronies from lower to higher levels of the modular hierarchy, and eventually between supermodules (by t=1000, not shown).

Before quantitatively assessing the synchronisation times of the elements of the module hierarchy, let us examine the aggregated S synchronisation times matrices of the cortex, both in its intact state and after introducing various lesion types. Following our structural analysis (Section 5.4 and Section 6), we investigate four lesion scenarios: removal of the core hubs (n=50 regions), removal of the module hubs (n=50 regions), deletion of all hub regions (n=100 regions), and deletion of the entire core (n=100 regions). We have already seen in Figure 7.2 that random region removal does not significantly affect cortical synchronizability, thus that lesion scenario is not studied here further, and simply the intact network is used as a baseline case.

Synchronisation time matrices of the intact and the four lesioned cortical network variants are shown in Figure 7.4. Block formation of highly intra-synchronizable region groups along the main

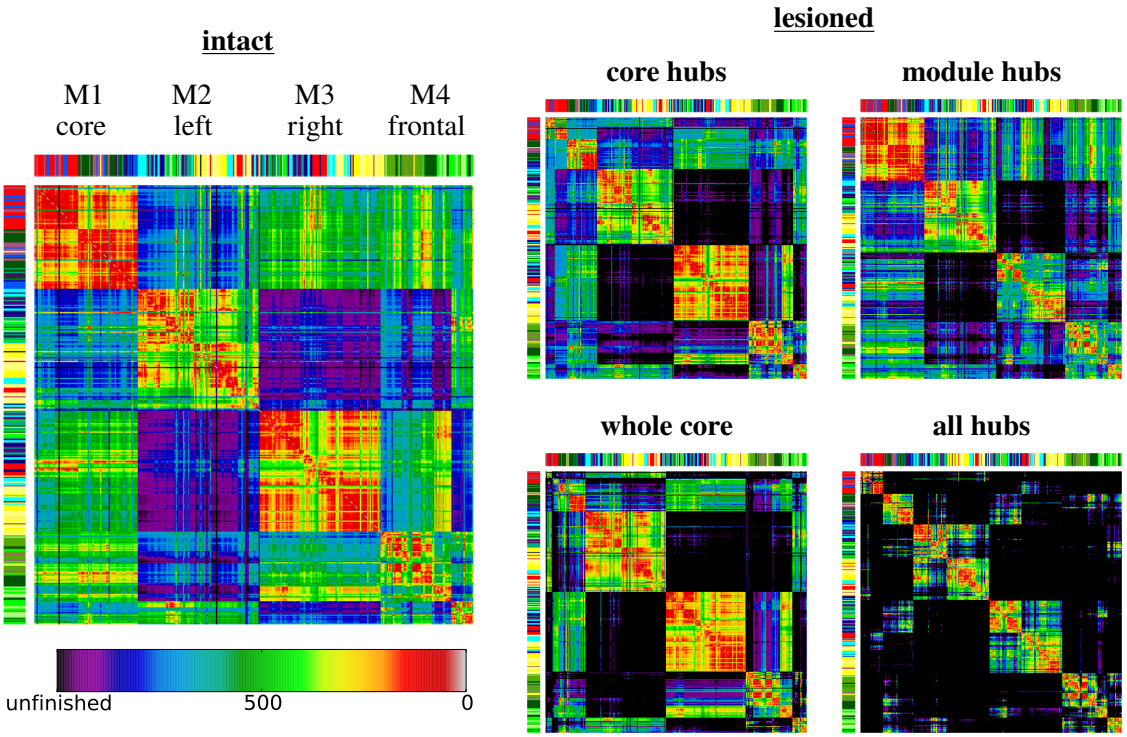

Figure 7.4: ***S* synchronisation time matrices of the intact and lesioned cortex.** Colours inside matrices code synchronisation times (see colorbar, 'unfinished': region pair did not reach synchrony threshold by the end of simulation, that is, by t=1000), left and top colour strips are anatomical colour codes.

diagonal of the intact cortex is a salient tendency, corresponding to the early intra-synchronisation of the found cortical module configuration. This characteristic modularisation in network dynamics is so strong, that it is not destroyed even in the most severely lesioned networks, after the removal of the entire core or of all network hubs. However, one can discover greatly reduced synchronizability (increased synchronisation times) inside the lesion affected modules and supermodules by plain visual inspection.

For instance, M1, which contains the network core and is located on the top left corner of the matrices, is the supermodule fastest to synchronise internally, with $\overline{S}_{M1}$ = 208 mean synchronisation time. This quick synchronisation time is only elongated by the three lesion cases that include the removal of local regions (core hub lesion: $\overline{S}_{M1}$ = 500, whole core: $\overline{S}_{M1}$ = 581, all hubs: $\overline{S}_{M1}$ = 711), but not affected when only module hubs are removed ($\overline{S}_{M1}$ = 210). On the other hand, the deletion of core regions (core hubs and whole core lesion cases) has only little effect on the intra-synchronisation of the non-core supermodules (M2, M3 and M4). This suggests a robust, relatively independent internal synchronizability of cortical supermodules and provides dynamical evidence for the topologically indicated role of the network core as mainly being involved in inter-

supermodule integration (Section 6).

To further examine this point, let us note that in the intact synchronisation time matrix, lateral supermodules (M2 and M3) are the latest to start inter-synchronisation, which process appears to happen through the intermediating central M1 supermodule, containing the network core. Inter-hemispheric synchronisation also appears to be the "weakest" point of network synchronizability: it is the slowest to occur in the intact cortex as well as the most highly affected process in all lesioned cases.

As a global measure of the significance of the lesioned parts in cortical synchronizability, we calculate the global mean $\overline{S}$ of the synchronisation time matrices S. As a baseline value, we obtain $\overline{S}$ = 576 time steps for the mean synchronisation time of the intact cortical network. While lesioning with module hubs only ($\overline{S}$ = 686) has less severe effect than the removal of core hubs ($\overline{S}$ = 705), deletion of all hub regions ($\overline{S}$ = 877) have more severe effect on cortical synchronizability than the removal of the entire core ($\overline{S}$ = 720).

We stress the fact, that lesioning of all hubs has a far more devastating effect on the synchronizability of the cortex ($\Delta\overline{S}$ = 301) than the sum of the individual effects of its two components: core hubs ($\Delta\overline{S}$ = 129) and module hubs ($\Delta\overline{S}$ = 110). Furthermore, our results are in qualitative agreement with earlier simulation studies, reporting that the removal of highly central regions exerts the most widespread as well as greatest overall effect on the functional connectivity (FC) of the remaining brain (Young et al. (2000), Honey and Sporns (2008), Alstott et al. (2009)).

Emergence of global synchrony through the module hierarchy: quantitative analysis

In the following more detailed analysis, we attempt to find out if the hub and core regions serve different roles in the emergence of intra- and inter-module synchronisations at the various module hierarchy levels. To that end we assess the change in the average intra-module synchronisation times on all module hierarchy levels after lesioning the cortical network by those region groups. The basic idea behind the analysis is that the magnitude of elongation in internal module synchronisation at a certain hierarchy level indicates the significance of the removed regions in the synchronizability of the intact network at that level.

Mean and variance of intra-module synchronisation times are shown in Figure 7.5. Firstly, we note the high variance in intra-module synchronisation times, which likely results at least partially from the highly heterogeneous intra- and inter-connectivity of the modules even in the intact cortical network (see second column). This high variance is further increased in most lesion scenarios (third to sixth columns), which can be explained by the fact that the regions removed by each lesion type, rather than being distributed homogeneously, are concentrated into only a

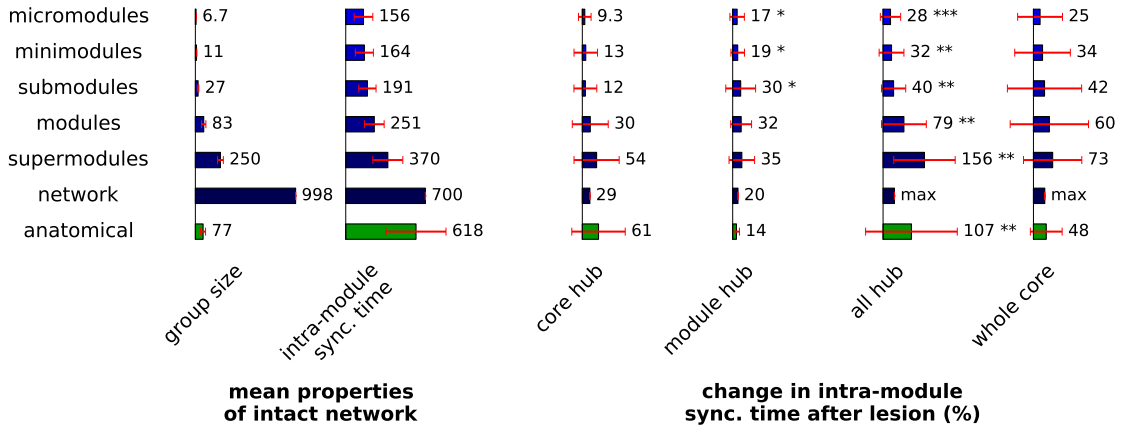

Figure 7.5: **Modular intra-synchronisation times.** Intra-module synchrony time is the time needed for the modular elements to reach the onset of internal synchronisation (65% of regions in synchrony). Bar widths denote mean values, error bars indicate standard deviation. Statistically significant changes at lesioned cases (third to sixth columns) compared to the intact network (second column), assessed by two-sample unpaired *t-test*s for identical sample means, are denoted by * if $p < 0.05$, ** if $p < 0.01$, and *** if $p < 0.001$. The label 'max' indicates that synchronisation did not finish by the end of the simulation.

few modular elements (see Figure 5.11 and Figure 6.1), therefore their removal effects (increases) intra-synchronisation in these modules much more severely than in other modules.

Considering the means of the intra-module synchronisation times, we can observe increasing mean synchronisation times of the modular elements from lower to higher levels of the module hierarchy (second column), with a very late network synchronisation time at the end (ANOVA test for identical mean intra-module synchronisation times across hierarchy levels $p < 10^{-6}$). We performed post-hoc analysis to detect significance between the individual hierarchy levels by calculating two-sample unpaired *t-test*s, not assuming identical sample variances. We found that while the increase across hierarchy levels decribed above is not statistically significant between pairs of consecutive hierarchy levels (micromodules $\rightarrow$ minimodules, minimodules $\rightarrow$ submodule, etc.), the difference is significant between hierarchy levels at least two steps away from each other (micromodules $\rightarrow$ submodules, minimodules $\rightarrow$ modules, etc) (all $p < 0.05$).

For comparison, the mean of anatomical structure synchronisation times is also plotted on Figure 7.5 (last row). Anatomical structures are very late to reach synchrony onset: in the intect case only about 10% earlier than the entire network does (one-sided significance test of network synchronisation time being significantly different from anatomical structure synchronisation times, assuming normal distribution of the latter, $p = 0.38$), and significantly

later than cortical supermodules (two-sample unpaired *t-test*: p = 0.045) or modules ($p < 10^{-3}$) synchronise, despite the fact that anatomical structures are on average smaller than cortical modules. This elongated synchronisation in anatomical structures is presumably attributable to their bi-hemispheric distribution in the topologically hemispherically largely divided cortical network.

Assessment of the lesioned cases indicate that the two hub groups coordinate intra-module synchronisation at different levels of the module hierarchy (third and fourth columns). While hubs in the core appear to be more, although not significantly more, engaged in the intra-synchronisation of modules, supermodules and the entire network (third column), this profile is shifted to lower hierarchical levels in the case of module-hubs, that appear to contribute more to the internal synchronisation of lower levels of the module hierarchy (micromodules to submodules) (fourth column), but not as much to global synchrony. These differences are even more pronounced if we consider the inevitable "cascade effect" of our analysis toward higher module hierarchy levels, making it more difficult to precisely localise the effect of the various lesion scenarios. For example, the elongation of submodule intra-synchronisation by the removal of module-hubs also necessarily adds to the synchronisation times of the modules, supermodules and the whole network on higher levels of the hierarchy.

The obtained increases in global synchronisation times for core hub and module hub lesions (29% and 20%) appear rather large, considering that each group makes up only 5% of the network, and that random removal of twice as many, i.e. 10% of the cortical regions, caused less, namely only a 16% increase in global synchronisation time (Figure 7.2).

Nonetheless, all-hub-lesion (fifth column) has an even more severe, statistically significant (see stars next to mean values), exponentially elongating effect on modular synchronisation towards higher hierarchy levels (ANOVA test for identical level of *increase* in mean intra-module synchronisation times at all hierarchy levels after removing all hub regions: $p < 10^{-5}$), which at the network level reaches our maximum simulation time. Removal of the entire network core from the cortex (sixth column) has less overall effect than all-hub-lesioning, with a steady increase in the mean intra-synchronisation times towards higher hierarchy levels, but without any statistically significant difference in the impact of lesion between these levels (ANOVA test for identical level of *increase* in mean intra-module synchronisation times across hierarchy levels after removing all core regions: p = 0.823). Nevertheless the simulation terminates before the onset of global network synchronisation would occur in this lesioning case as well, suggesting that the core may be mainly involved in organising synchronisation globally between supermodules.

7.3.4 Discussion

Synchronisation has been shown to reveal the topological scales of hierarchically modular architectures in Arenas et al. (2006). This phenomenon was observed in this section, indicating the increased ability of various modular elements across the module hierarchy to interact and cooperate as segregated functional units of the human cortex. Earlier studies on the transition towards synchronisation in the anatomical connectivity network of the cat thalamo-cortex also revealed that functional clusters of synchrony coincide with structural modules of the network (Zemanova et al. (2006), Zhou et al. (2006), Zhou et al. (2007)).

More interestingly, however, Zamora-López et al. (2010) extended these results by showing that the significant topological centralisation found the cat brain network around its strong rich-club (Gómez-Gardeñes et al. (2010)) is capable of "orchestrating" the evolution of synchronisation in the network, resulting in a transition from modular to centralised organisation of synchronisation. The characteristics of the evolution of global synchronisation we found in the human cortex is highly similarity to the above results, with the core and hub regions appear to play a central role in the coordination of inter-module synchronisation. These properties, supporting our structural analysis, make these cortical structures capable of acting as some sort of (reasonably) centralised coordinators of the dynamics at the highest levels of cortical processing.

In this section we provided evidence for the claim, that the distinguished topological properties of the core and hub regions, found in the last two chapters, result in their increased general capability of mediating synchrony across the cortical connectome. Specifically, we found that both core and hub regions seem to facilitate synchronisation both intra-modularly as well as globally, as opposed to our finding that randomly chosen regions of the network elongate network synchronisation, and that hub regions appear to have a higher and more significant impact on the emergence of synchrony, especially on lower, more local levels of the module hierarchy of the cortex. In the next section, we extend our model to investigate the ubiquitous phenomenon of metastability in cortical dynamics, and the role of various network components in its global emergence.

7.4 Metastability of the cortical network

7.4.1 Introduction

Metastability in complex systems and brain networks

In the previous section (Section 7.3), we investigated the synchronisation path of the cortex facilitated by its structure, along with the specific role certain topological features of the cortex play

in the process. While studies of these stable, synchronous states of systems of coupled oscillator have attracted particular attention (Acebrón et al. (2005), Arenas et al. (2006), Gómez-Gardeñes et al. (2010)), spatio-temporally extended synchronisation in many systems, such as the brain, is actually pathological, and is a symptom of seizures (Arthuis et al. (2009)). The need to understand more realistic dynamics of these complex systems has motivated the study of metastability of coupled oscillator networks in general (Niebur et al. (1991), Shanahan (2010)), and of the brain in particular (Bressler and Kelso (2001), Kitzbichler et al. (2009)).

Computational modelling and simulation provides an excellent scientific tool for investigating the complexity and metastability of complex dynamical networks, such as the brain, at various states (parameter regimes) (Shanahan (2010)). In a relatively early study on simulating cortical functional connectivity (FC) on the 47-node network of the macaque brain, Honey et al. (2007) combined a nonlinear biophysical node model (Breakspear et al. (2003)) with transfer entropy (Schreiber (2000)) to obtain functional connectivities emerging from spontaneous network dynamics on various time scales. They observed high structural to function correspondence on the slow time scales of minutes. At an intermediate time scale (0.1 Hz), however, significant fluctuations appeared in FC, along with the formation of anti-correlated functional clusters, also observable in simulated BOLD signals. Finally, at the fastest time scale ($\approx$ 10Hz), the authors reported high temporal metastability in network dynamics characterised by intermittent synchronisation (phase-locking) and desynchronization between brain regions.

In a subsequent study, Deco et al. (2009) applied the biophysical Wilson-Cowan model (Wilson and Cowan (1972)) on a relatively coarse, 38-node network of the macaque brain, organised around two main functional clusters (modules). In that model, nodal noise proved to be a crucial element in putting the network into such a dynamical regime, in which the transient internal synchronisation and desynchronization of the clusters alternated, resulting in spontaneous anti-correlation in their simulated BOLD signal. This led the authors to hypothesise how intrinsic noise, by rendering network dynamics to spontaneously fluctuate between multistable states, cast high competition between the various task-specific subnetworks and may thus facilitate highly tuned and responsive brain dynamics, a so-called 'active resting state' (Deco et al. (2009)).

The role of hierarchically modular structure in facilitating limited sustained network activity (LSA) was explicitly explored by Kaiser and his colleagues by simulating a simple spreading process model on different stereotypical networks (Kaiser et al. (2008)) as well as on a spectrum of parameterised, synthetic networks, approximating specific large-scale brain architectures (Kaiser and Hilgetag (2010)). They found that modular architectures, in contrast to non-modular random and small-world networks, prevented global activity spread, and supported the formation of local

and persistent activity in a large critical range, even without the presence of noise, inhibition or external stimulation. Across the different hierarchically modular networks, both increase in scale (number of hierarchy levels) and in granularity (number of modules on each level) were found to further facilitate LSA (widen the critical range). Notably, from an abstract dynamical point of view, the sustained but limited activity (LSA) investigated in these studies, which neither dies out but nor spreads globally, is akin to high temporal metastability between coupled oscillators, balancing between total synchrony and asynchrony (Shanahan (2010)).

In exploring the dynamics of the model applied in the current study, Cabral et al. (2011) obtained highest global network metastability at the regime of intermediate coupling strengths (10<k<30) and realistic mean time delays (10ms<τ<20ms). Additionally, this increased metastability coincided with the emergence of intra-module, but not global, synchrony. Most interestingly, however, this regime largely overlapped with the one in which their simulated functional connectivity best approximated the empirically obtained one. These results suggest that the structure and dynamics of the brain may be co-optimised towards (some sort of) maximal metastability, overlapping with the occurrence of intra-module synchrony.

In this section, we shall investigate the characteristics of the complex dynamics unfolding on the simulated cortical connectivity. Using a more plausible dynamical model than in the previous section and utilising several dynamical complexity metrics, we aim to explore at which parameter regimes the simulated cortical network exhibits the highest metastability in its dynamics globally as well as within and between its modules, and assess the physiological plausibility of those regimes. With hub lesioning we aim to assess the role of hub regions in facilitating the high complexity of network dynamics. Internally, we shall investigate characteristics of intra- and inter-module synchronisation in the found complex dynamical regime. Additionally, our goal is to find an appropriate, physiologically plausible regime in the parameter space of the model that results in high complexity in cortical dynamics, in order to conduct our subsequent dynamical simulations in that regime.

7.4.2 Methods

For the study of metastability in simulated cortical dynamics, we use the most complex and plausible Kuramoto model illustrated in Figure 7.1 *c*, composed of delay-coupled, non-identical and noisy oscillators. Fundamentally, our approach is to ”sweep” the parameter space of the model and assess its metastability at each value combination of the parameter set by calculating various complexity metrics on the simulated dynamics.

The four free parameters of the model variant are the global coupling strength k, mean

conduction delay $\langle\tau\rangle$, dispersion of natural frequencies σ_f and variance of noise σ_n received by the oscillators (Section 7.2.2). Due to computational limitations, only a restricted regime of the entire parameter space can be swept. However, Cabral et al. (2011) already showed that out of those four parameters, only the first two, k and $\langle\tau\rangle$, are significant in shaping network dynamics, while σ_f and σ_n have negligible effect on the emerging dynamics, also illustrated in Figure 7.1 (see also main text in Section 7.2.2). We note that this fundamental property of the model also conforms well with our primary motivation to explore how network topology influences emerging dynamics, due to the fact that the former two parameters determine node-node interactions over network connectivity, while the latter define internal dynamics of individual nodes. In fact, the above finding suggests the dominating importance of connectivity over the applied single node model in network dynamics (at least in the Kuramoto framework), and provides confirmation to the validity of our investigations, that is, to the influential role of network structure in the emerging dynamics.

Below, we formally introduce and briefly discuss the various measures we utilise for assessing the complexity and metastability of network dynamics.

Global synchrony and (nodal) metastability

We define temporal synchrony between a group of regions by the order parameter $R(t)$ (phase uniformity) according to Eq. 7.2. Its temporal mean, $\overline{R}$, is applied as an index of global synchronisation level, and its temporal standard deviation, σ_R, measures the level of metastability of the network (Shanahan (2010)).

The synchrony and metastability indices defined above evaluate global properties of synchronisation dynamics from the oscillation patterns of *individual nodes*. The following four measures on the other hand assess various aspects of dynamical complexity at the level of *modules*.

Modular metastability

Temporally averaged variance in the synchrony of a given module can be defined as

$$\sigma_{met}(m) = \frac{1}{T}\sum_{t\leq T}(R_m(t) - \langle R_m\rangle_T)^2, \tag{7.6}$$

where $R_m(t)$ is the internal synchrony of module m at time t. The mean of this variance over all modules gives the modular metastability of the network:

$$\zeta = \langle\sigma_{met}(m)\rangle_M, \tag{7.7}$$

where M is the set of all m modules (Shanahan (2010)). High ζ modular metastability indicates a temporally highly varying level of synchrony within an average network module, while ζ is zero if

the internal synchrony levels of the modules are temporally constant, including the extreme cases of total synchrony (R_m=1) and ynchrony (R_m=0).

Chimera index

Changing the order of averaging in Eq. 7.6, we can define the module averaged variance of temporal inter-group synchronies as:

$$\sigma_{chi}(t) = \frac{1}{|M|} \sum_{m \in M} (R_m(t) - \langle R(t) \rangle_M)^2. \tag{7.8}$$

The mean of this variance gives the chimera index of the network

$$\chi = \langle \sigma_{chi}(t) \rangle_T, \tag{7.9}$$

that indicates how "chimera-like" the system is on average during simulation time (Kuramoto and Battogtokh (2002), Shanahan (2010)).

Both total synchrony and total asynchrony result in σ_{met} = σ_{chi} = 0. In the intermediate dynamical regime, however, both measures take positive values. In the case of metastability measure σ_{met}, typical dynamics in this regime are composed of a series of states, in which the network is synchronised at some times, and desynchronized at other times. In the case of the chimera index, σ_{chi} is positive if some of the modules are internally synchronised at some time, while others are not. These properties make the above measures appropriate for addressing the dynamical complexity of individual network modules.

Pairwise synchrony

To measure the complexity of interaction between module pairs, first we define temporally averaged synchrony of a given module pair m_i and m_j as

$$R(m_i, m_j) = \frac{1}{T} \sum_{t \leq T} R_{m_i \cup m_j}(t). \tag{7.10}$$

The mean over all module pair combinations gives the mean pairwise synchrony of the network:

$$\psi = \langle R(m_i, m_j) \rangle_{\forall m_i, m_j}. \tag{7.11}$$

ψ, taking its values from [0,1], measures the extent by which modules are in synchrony with each other. ψ=1, if all module pairs are in synchrony for the whole simulation time (global synchrony), ψ=0 if no module pairs in synchrony at any time during simulation, and intermediate values show that some modules are in synchrony for some time, indicating more complex interplay (synchronisation and desynchronization) between modular pairs.

Coalition entropy

For assessing the variability of the exhibited metastable chimera states, whether the network only periodically returns into the same few chimera states, or, more interestingly, it has a great repertoire of different chimera states, *coalition entropy* H_C (Shanahan (2010)) is calculated:

$$H_C = -\frac{1}{log_2|S|}\sum_{s\in S} p(s)log_2(p(s)), \tag{7.12}$$

which measures normalised entropy of the entire possible set of chimera states S, using the probability (occurrence frequency) $p(s)$ of each possible $s \in S$ coalition. In this context, the term "coalition" refers to a *set of synchronised network modules*.

To be able to distinguish between synchronous and non-synchronous states among a set of modules, we apply a joint module synchrony threshold $\gamma = 0.8$, above which modules are considered to be in synchrony.

In the cortical network studied here, the number of possible chimera states, determined by its 12 modules, is $|S| = 2^{|M|} = 2^{12} = 4096$. H_C, being the *entropy* of the probability distribution of module coalitions, is bound to be between 0 and 1. H_C takes the value 0 if the network, for the whole simulation time, exhibits a single s chimera state: a certain module coalition, which includes the extreme cases of complete asynchrony as well as global synchrony. On the other hand, H_C is 1 if all possible s module coalitions are exhibited with an equal frequency (uniform probability distribution). For a more detailed discussion on coalition entropy, modular metastability and chimera index, see Shanahan (2010).

7.4.3 Results

Cortical metastability at the global level

We start our dynamical complexity analysis by assessing the *global metastability* of the cortex in comparison with its surrogates. Global synchrony index R and metastability index σ of the intact and lesioned cortex and its surrogates at a chosen, physiologically plausible point of the model parameter space (mean axonal conduction delay τ_m is 10ms, Ghosh et al. (2008)) are shown in Figure 7.6. In accordance with the found low synchronizability of the cortex (Section 7.3), the intact cortex reaches a lower mean global synchrony level than both of its surrogates. This is presumably attributable to its highly segregated (Section 4.3) and modular (Section 5.2.5) topology, because, as the more tightly integrated connectivity of random surrogates demonstrates (Section 4.2), close to global synchrony (R = 0.88) is attainable even at the investigated relatively high conduction delay (τ_m = 10ms) and low network connection density (3.6%).

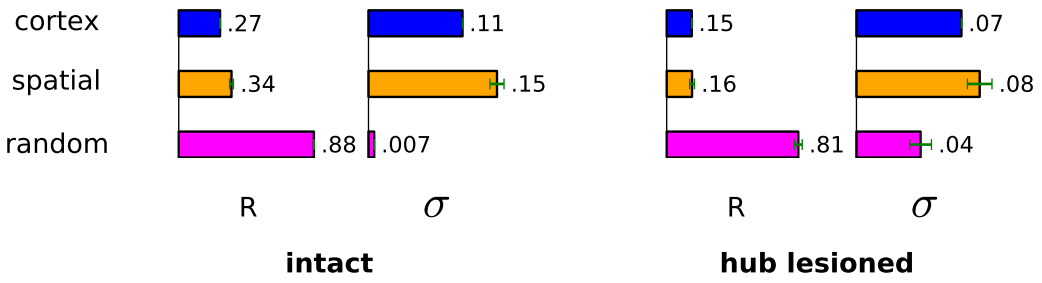

Figure 7.6: **Global synchrony and metastability of the cortex and its surrogates.** Intact: entire network, hub lesioned: network remaining after removal of all hub regions and their connections. Bars length denote mean values, error bars indicate standard deviation across surrogate network values. Model parameters: k=20, τ_m=10ms, f_0=60Hz, σ_f=3, σ_n=2.

Interestingly, spatial surrogates, that possess an intermediate level of both topological integration and segregation (Section 4.2, Section 4.3), reach significantly higher average metastability index σ than the cortex (one-sided significance test assuming normal distribution of surrogate means: $p < 10^{-4}$). This finding, however, can partly be attributed to the higher mean global synchrony level R of spatial surrogates, making their relative variation close to identical. Additionally, lesioning the cortex and its spatial surrogates with the hub regions (n=100 highest degree regions) results in a substantial reduction not only in their global synchrony level, but also in their metastability (Figure 7.6 right), equalising the above difference (p = 0.06). These results provide dynamical evidence for the notion that hub regions may play a facilitating role in the formation of transient coalitions during spontaneous cortical dynamics (Shanahan (2010)) and hence effectively enrich the dynamical regime of the cortex.

Metastability of cortical modular dynamics

We investigate the effect of regional coupling strengths and interaction delay on the complexity of network dynamics by varying the corresponding parameters of our model, k and τ_m. Results of the four module-level complexity measures are shown in Figure 7.7.

Comparing the global complexity results obtained by the four investigated metrics (Figure 7.7), all four measures seem to indicate the same apparent relation between k and τ_m. Specifically, the dynamics exhibit relatively high complexity values already at low, but non-zero coupling strengths and delays (k=5, τ_m=2ms), and approximately preserve that level of complexity with the simultaneous increase of k and τ_m. In that intermediately coupled regime ($5 < k < 40$), all four measures indicate highest dynamical complexity, because the formation of transient and partial inter-module coalitions is already facilitated between cortical modules, however, the coupling is

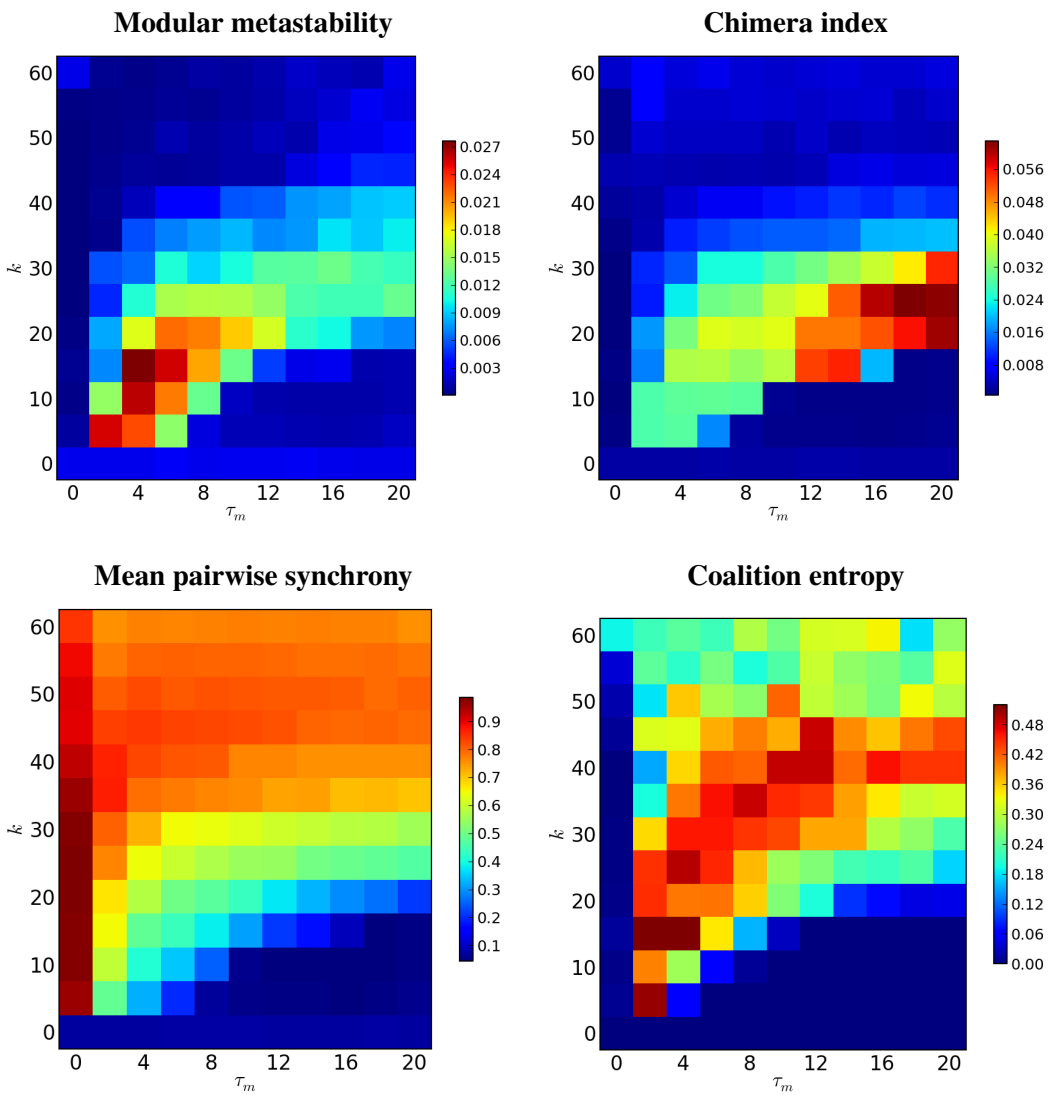

Figure 7.7: **Summary of module-level dynamical complexity measures.** Global values of dynamical complexity measures emerging from module level dynamics, as the function of mean coupling strength k and mean transmission delay τ_m. f_0=60Hz, σ_f=3, σ_n=2. Higher values indicate higher metastability, except for *mean pairwise synchrony*, where higher complexity in inter-module dynamics occurs at intermediate (green) values.

not yet strong enough to drive network dynamics into more sustained and global level synchrony against the time-lag of the interaction. Our findings are similar to the results of Shanahan (2010) and Cabral et al. (2011).

We will use these parameter sweeping results for determining the parameters of the simulations of epileptiform activity spread in the next section and for the simulation of functional connectivity in Chapter 8.

Modular dynamics at a chosen working point from regime of parameter space that facilitates the most complex dynamics is shown in Figure 7.8. The highly metastable dynamics of network

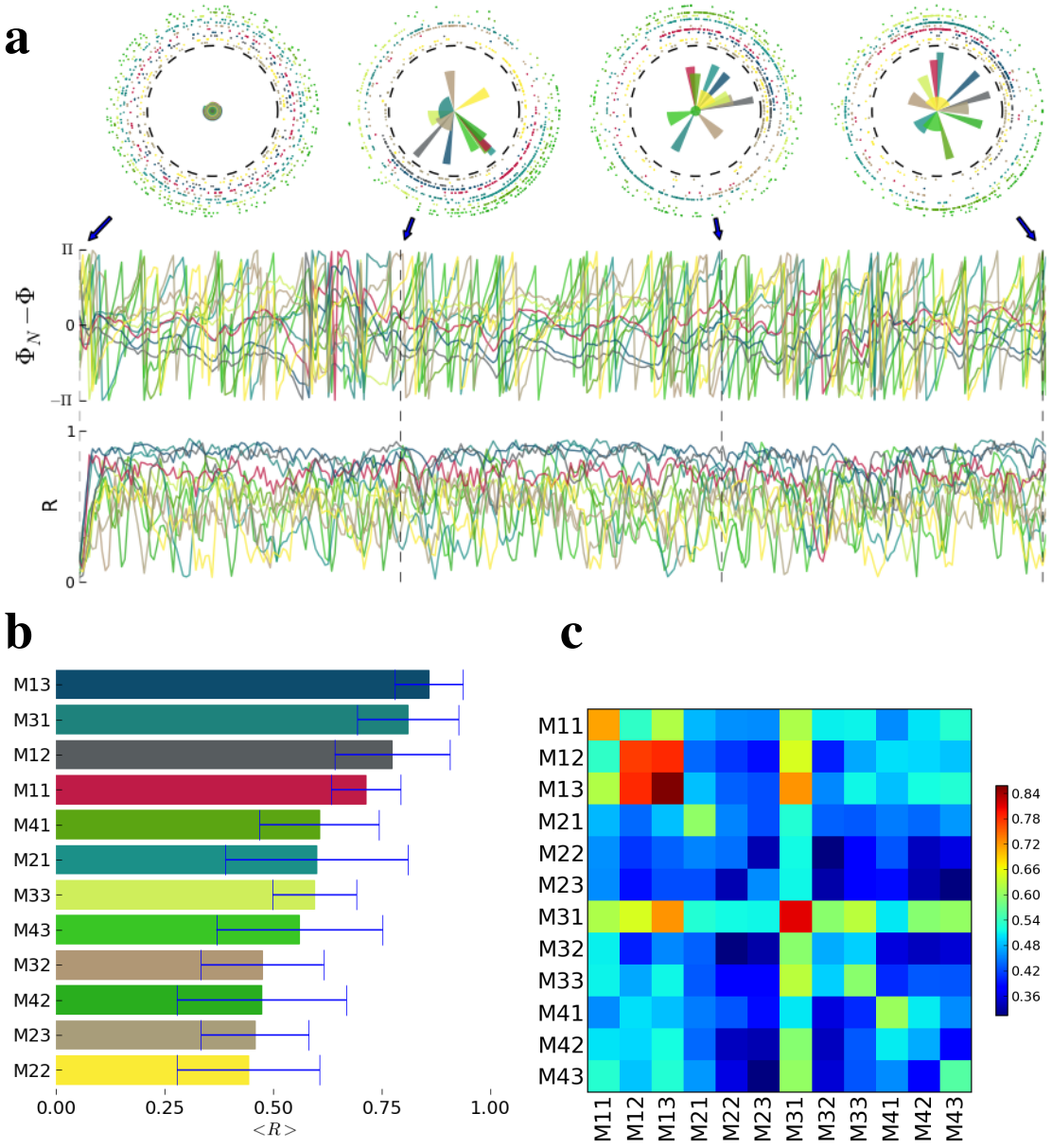

Figure 7.8: **Modular dynamics at a chosen working point of the parameter space.** *a*: a 1s sample of the dynamics, see Figure 7.1 for figure explanation. *b*: modular synchronies $\langle R \rangle$ (bars) and metastabilities $\sigma(R)$ (error bars). *c*: mean diagonal: intra-module synchronies ($\langle R \rangle$) as in *b*, off diagonal: mean pairwise module synchronies (ψ). Parameters: k=20, τ_m=8ms.

modules is observable in the great variance in their R intra-module synchrony index (Figure 7.8 *a*). We can also note substantial individual differences in intra-module synchronies, with some, mainly lateral and frontal, modules being more metastable, while the more densely intra-connected modules of the M1 supermodule, that contains the network core, exhibits more stable internal dynamics (Figure 7.8 *b*). Additionally to intra-module synchronies, we can also observe a complex, highly metastable pattern of inter-module interactions (Figure 7.8 *a*).

The pair-wise module synchrony values in Figure 7.8 *c* show only moderate mean intra-supermodule synchrony outside of the network core (M1), nevertheless with a relatively high M1-M4 core-frontal inter-supermodule synchronisation (bottom left and top right 3x3 sub-rectangles). Furthermore, the right lateral M31 module exhibits one of the highest internal and inter-module synchronisation values. The fact, that this non-core module alone, out of the nine other non-core modules (11%), contains 9 of the 50 module hubs (18%), provides further validation to to the significance of hub regions in mediating between cortical modules.

7.4.4 Discussion

Our findings on the highly metastable dynamics of the cortical connectivity, organised around its modules, are in agreement with those of Shanahan (2010) and Cabral et al. (2011), but at the same time extend them by showing that other dynamical complexity related measures possess their maximum at a coinciding parameter regime. This results in a large repertoire of dynamically forming module coalitions that engage in transient synchronisation and desynchronization during spontaneous cortical activity in our model. These transient, metastable, highly variable and "labile" dynamics of the brain are believed to mediate perception and cognition (Friston (2000), Honey et al. (2007)), and they have even been associated with behavioural performance (McIntosh et al. (2008)). These notions are supported by our findings on the maximum dynamical complexity of the cortical connectivity in the biophysically plausible parameter regime of our model (5-20 ms, Ghosh et al. (2008)).

Furthermore, our findings also pointed to the core modules (M11, M12 and M13) as central elements in the transient and metastable cortical dynamics, not only as the modules exhibiting the highest level of internal synchrony, but also as the ones most capable of engaging with other modules in transient inter-synchronisation. Altogether, these results suggest that these modules, as well as the network core residing in them, may be pivotal cortical structures in organising synchrony mediated cognition in the cortex (Friston (2000)).

Having confirmed the metastable properties of the spontaneous dynamics of the cortex, in the next section we investigate the activity propagation characteristics of the cortical topology while

being in this dynamically metastable state.

7.5 Structure facilitated spread of epileptiform activity in the cortex

7.5.1 Introduction

Transient and spatially partial synchronisation of neural assemblies is believed to be one of the fundamental mechanisms of brain functioning (see previous section), but hyper-synchronous neuronal activity is a pathological case of brain activity (Uhlhaas et al. (2009a)). Epilepsy is a diverse set of chronic neurological disorders characterised by the tendency of brain seizures to recur (Milton (2010)). It is the third most common neurological disorder, with over 50 million people worldwide suffering from it (WHO (2009)). Despite the great interest and substantial research effort made so far (Chang and Lowenstein (2003)), our knowledge is still very limited on the physiological and neuro-anatomical causes of epilepsy, let alone its unifying dynamical definition (Ullah and Schiff (2009)). Hence, experimental and computational neuroscience must continue close cooperation and find novel research methods to gain a better understanding and more effective treatments for this common neurological disorder (Milton (2010)).

The study of various spreading processes, such as rumour spread or epidemic spread of viruses in social as well as in computer networks, has provided valuable insights to the important phenomena of activity or information spreading occurring on a diverse set of complex networks (reviewed in Boccaletti et al. (2006)). However, traditional models of spreading processes assign network nodes one of the set of possible discrete states (Daley and Kendall (1964)), making them unsuitable for modelling epilepsy, which is a dynamical disease (Milton (2010)). Researching the build-up and propagation of epileptic seizures in brain networks requires continuous models (Soltesz and Staley (2008)), that are modulated by and intricately intertwined with the already extraordinary complexity of the dynamics of the intact brain. With this in mind, we shall utilise the Kuramoto model of the previous section in its highly metastable parameter regime and apply a mechanistic model for simulating the build-up of the inter-synchronisation of epileptic region group the from spontaneous network activity, in order to investigate the seizure propagation properties of the cortex globally as well as the specific role of certain parts in it.

In the nervous system, long-range cortico-cortical connections, subcortical, and brainstem structures have all been identified as important components of seizure generalisation. Specifically, subcortical and brainstem nuclei are pivotal in modulating the onset, propagation, and subsequent termination of epileptic seizures (Milton and Jung (2003)). Generally, there are three types of pathways to consider in spreading seizure activity arising from an isolated epileptic focus:

(i) intracortical spread from the epileptic focus, horizontally to the cortical surface; (ii) white matter-mediated spread via myelinated cortico-cortical axons radially to the gray matter, and (iii) subcortical nuclei-mediated spread, radially to the cortex, via myelinated axons to the underlying subcortical nuclei, with subsequent, more diffuse back-projection to the cortex (Milton (2010)).

Unfortunately the current dataset at hand excludes all subcortical and brainstem structures and their connectivity with the cortex, therefore we are unable to analyse a full model of the brain containing those epileptically important structures, and limited to model the propagation of seizures through type (i) and type (ii) connections. As a result, the analysis of this section is a rather exploratory one, that, in general, aims to investigate the characteristics of spreading processes within the cortex facilitated by its anatomical connectivity. Our main goal therefore is to extend the results of the thesis obtained so far by considering the capability of cortical regions to exert influence on the spontaneous activity of rest of the network.

In this section, we study the characteristics of synchronous activity spreading facilitated by the topology of the cortical connectivity. We shall assess the susceptibility of the cortex to be overrun by periodically recurring epileptic activity (seizures) originating from focal or distributed cortical sites. We do not address the also important and difficult question of how such seizures arise from normal brain activity, instead we restrict our investigation to the spreading characteristics of seizures through the cortical connectivity that are steadily generated and emitted from a distributed (generalised seizure) or local (focal seizure) set of regions. Additionally, in a more detailed analysis, we also seek differences in the activity spreading properties of individual cortical areas, the cortical core and hub regions and its modules, in order to assess their effectivity in influencing the rest of the cortex, as well as to gauge their potential danger as cortical propagating points of epileptiform activity.

Acknowledging the limitations of our dataset and dynamical model, we stress the experimental nature of the following analysis. Our main purpose in this section is to extend our dynamical analysis by investigating the characteristics of synchrony spreading in the cortical connectivity, and not to propose a detailed and accurate model for epileptic activity. Nevertheless, our analysis of finding the cortical regions that are topologically the most influential to others may be generalisable for more accurate investigations of epileptic phenomena in the brain.

7.5.2 Methods

In this section, our goal is to assess the strength and extent of seizures a given part P of the cortex is capable of propagating towards the rest of the network globally. Our model for assessing this phenomenon is the following. Firstly, during simulation, we let spontaneous network

activity develop for t_0 = 1s, after which time we externally force (entrain) P to oscillate in total synchrony (R_P = 1) at a specific entrainment frequency, 10Hz. This is done by setting the intrinsic frequencies of the regions in P to f_0 = 10Hz, turning off their internal noise (σ_n = 0), and allowing instantaneous, all-to-all interactions between these regions (τ_m = 0ms). At the same time, to guarantee total synchrony, we also decouple these regions from the rest of the network by turning off their afferent connections coming from outside P.

Using the above method, we let the applied dynamical model continuously build up and then sustain a synchronous 10Hz oscillation within P *mechanistically* (within the framework of the model), as opposed to introducing an abrupt, rather artificial jump in network dynamics by directly setting the output of the Kuramoto model, the phases of the entrained regions. All parameters of the regions outside P are kept unchanged, and their dynamics is only affected by the entrained regions through network connectivity.

After simulation, we assess the potential of the entrained P part of the network in propagating cortical seizures by comparing the power at entrainment frequency (10 ± 0.5Hz) in the spectrum of the spontaneous and entrained dynamics. Greater power increase indicate wider seizure spread in the frequency domain. Additionally, we evaluate the spatial extent of induced seizures by counting the number of cortical regions with power at the entrainment frequency exceeding the threshold T = 80% of their total power. In order to compensate for the size differences of the entrained areas, as well as for a clearer spontaneous-entrained comparison, the entrained region of P are discarded from spectral analysis in the entrained case.

Firstly, susceptibility to seizure spread of the entire cortex is assessed on the global scale. Specifically, power increase at the entrainment frequency in the cortex is compared with those of its surrogates in response to random focal (a random seed region and the 99 spatially closest regions to it), random non-hub (100 random regions that are not hub regions) and hub region (100 hub regions) entrainment. For each of the two random entrainment cases, n=10 simulations are run with independently chosen random seed regions. Additionally, the seizure spreading capability by various parts of the cortex is investigated in a more detailed analysis. Specifically, we entrain all 12 modules of the cortex, and compare the power of the globally induced seizures with those induced by cortical hubs and by the network core.

7.5.3 Results

Global spread and susceptibility to synchronised activity of the cortex

Spectral and spatial spread of seizures in the cortex and in its two surrogate network sets are shown in Figure 7.9 for four experimental scenarios: spontaneous (baseline) network activity, random

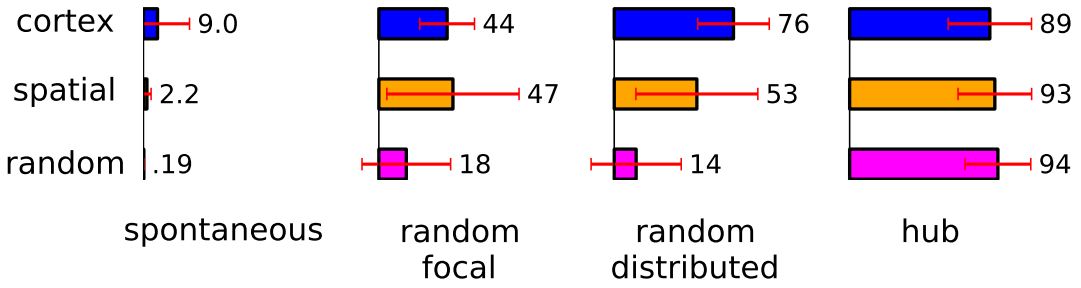

Figure 7.9: **Magnitude of global seizure spread in the cortex and its surrogates.** Bars denote mean power at the f = 10Hz entrainment frequency, averaged for all nodes, error bars indicate standard deviation across nodal powers. Spontaneous: under no entrainment, random focal: during entraining a randomly chosen seed region and the 99 spatially closest regions to it, random distributed: during entraining n=100 random regions, hub: during entraining the n=100 hub regions. Model parameters: k=30, τ_m=10ms, f_0=60Hz, σ_f=3, σ_n=2. For random entrainment cases, n=10 independent simulations were run.

focal, random distributed and hub entrained activity. Firstly, spontaneous activity confirms the low baseline spectral power around the frequency of generated seizures in all three networks.

Random focal entrainment results in intermediate mean spread of entrained seizure activity in the cortical network and its spatial surrogates (one-sided test for the cortical mean being drawn from the distribution of spatial surrogates, assuming that the latter is a normal distribution: p = 0.46), but not so much in random surrogates, yet still not significantly differently (p = 0.18). As opposed to that, we obtain higher cortical susceptibility to epileptic activity originating from distributed random entrainment sites, compared to its somewhat, but not significantly, more resilient spatial surrogate networks (p = 0.27), and the significantly more resilient random surrogates (p = 0.02). We interpret this to mean that, at the investigated parameter regime, it is the higher metastability of the cortical network, as opposed to the high level of global synchrony in surrogate networks, that makes the cortex more vulnerable to be globally overrun by seizures originating from a distributed (non-local) set of random regions.

Interestingly, however, not only the cortex, but also its surrogate networks demonstrate increased susceptibility to be invaded by synchronised activity generated at the network hubs (p > 0.4 for both surrogates). These distributed (non-focal) seizures, originating from the topologically most vulnerable points of the networks (see Chapter 6), its highest degree nodes, appear to pose increased threat to the more integrated spatial and random surrogate networks than to the highly segregated cortex, especially relative to the threat posed by random focal and random distributed propagation points (two-sample unpaired *t-test*s for identical means between random and hub

entrainments for both surrogates yield $p < 10^{-5}$, not assuming identical variances). This is in agreement with the long recognised functional advantages of modular architectures (Simon (1962), Koch and Laurent (1999)), granting a globally lower level of synchronizability (Section 7.3) and higher dynamical decomposability to the cortex in general. We hypothesise that these dynamical properties may contribute to the relative resistance against hub entrainment found in the cortex (Figure 7.9), compared to the relative vulnerability to hub entrainment of its surrogates, lacking these characteristics. Nonetheless, as we will see it in the next section, hub regions are still significantly more effective activity propagation points of the cortical connectome, than any other spatially localised (focal) parts of it.

Seizure propagation properties of cortical areas

Spectral power of all cortical regions around the entrained 10Hz frequency in response to samples of entrainment sites are shown on projections in Figure 7.10, while a summary evaluation of the entire simulation set is presented in Figure 7.11. All entrainment simulations model localised, focal seizure onsets, except hub entrainment experiments (third row), which, due to the relatively wide dispersion of cortical hub regions (Figure 5.11, rich-club column), models a distributed seizure onset targeting the highest degree regions of the cortex. Each result is the average of n=5 independent simulation runs.

In absolute comparison, hub regions proved to be the most effective areas in propagating synchronous activity by spreading the 10Hz frequency oscillations imposed on them effectively to the entire cortex, both in the frequency (89%) and spatial domains (86%) (two-sample unpaired *t-test*s for identical distribution means between hub entrainment and each of the other 14 experimental cases all yield $p < 10^{-5}$, not assuming identical variances). This also indicates that seizures originating from the cortical hub regions pose the highest epileptic threat in cortico-cortical seizure propagation. This finding is not surprising, considering the topological (Section 6) and dynamical (Section 7.3 and 7.4) significance of the hub regions. However, considering the results of Figure 7.9, it seems likely that the lower spread of the localised seizure cases (core and module entrainment) is also caused partly by the functionally favourable modular

---

Figure 7.10 *(following page)*: **Entrainment results on projections.** Colours code regional power at 10Hz derived from spontaneous dynamics (top) and from activity during entraining four cortical locations at 10Hz: the network core (focal), hubs (distributed), a lateral module (focal) and a frontal module (focal). First column: coronal projections, second column: horizontal projections. Model parameters: k=30, τ_m=10ms, σ_f=3, σ_n=2, and f_0=60Hz.

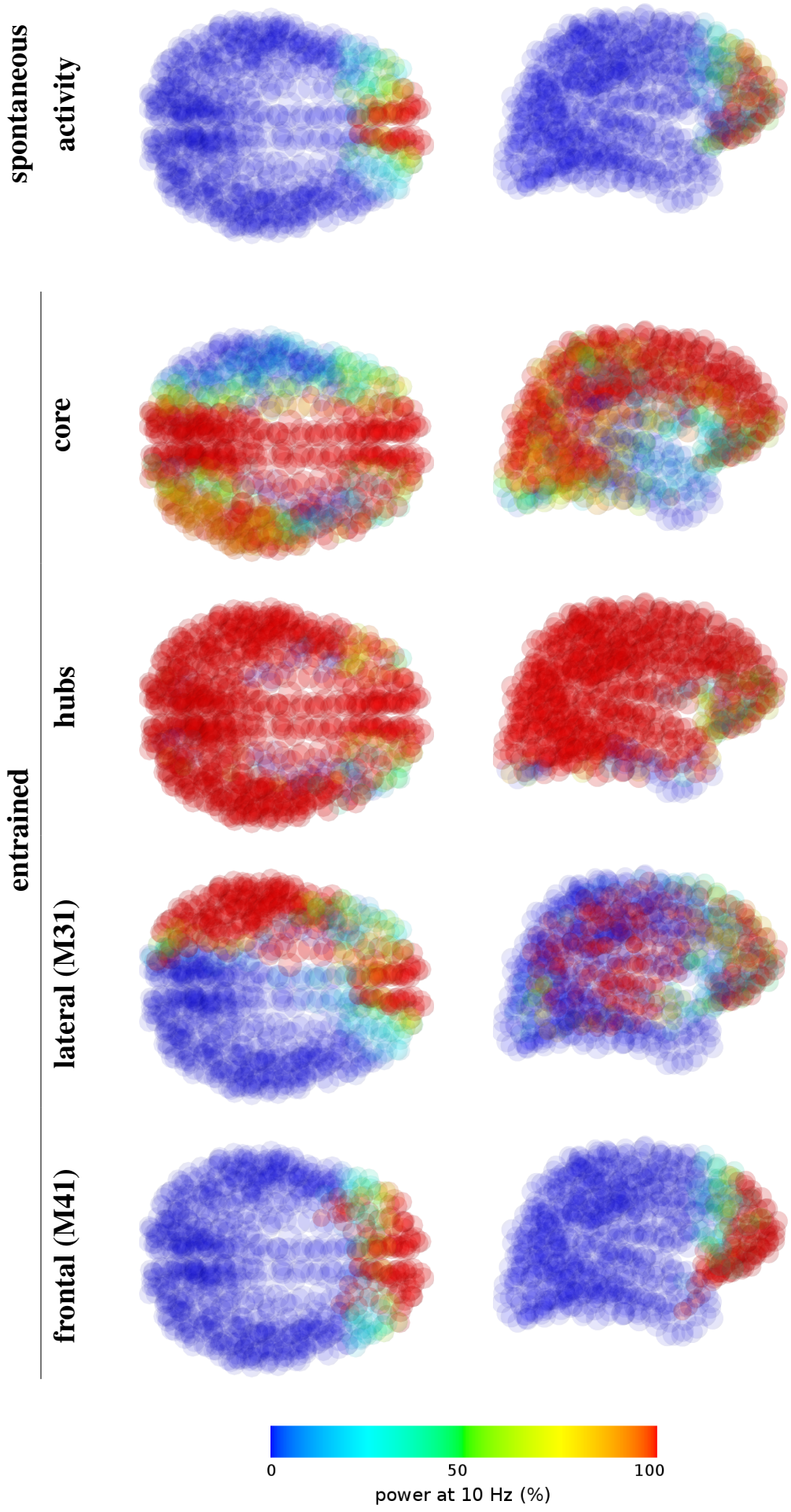
spontaneous activity
entrained
core
hubs
lateral (M31)
frontal (M41)
0
50
100
power at 10 Hz (%)

("decomposable") architecture of the cortex (Simon (1962), Koch and Laurent (1999)), effectively segregating distant cortical areas from each other and this way preventing them from being permanently overrun by incoming seizures of other modules.

From the localised (i.e., non-hub) seizure cases, the network core, presumably due to its central topological position, is the most effective area in propagating its activity (global power: 63%), and thus it may pose the highest threat as epileptic focus point (two-sample unpaired *t-test*s for identical distribution means between core entrainment and each of the other 14 experimental cases all give $p < 10^{-5}$, not assuming identical variances). The core is followed by one of its container modules, M12 (44%, all $p < 10^{-5}$), and the lateral modules, M21–M33 (∼35%). The power spectra distribution these lateral modules induce to the cortex are highly similar to each other ($p > 0.2$ for all pairs in M21–M33), but significantly different from the rest of the entrained areas (pair-wise *t-test*s between a lateral and a non-lateral module all give $p < 10^{-4}$, except for p(M11, M21) = 0.09, p(M11, M22) = 0.06, and p(M11, M32) = 0.07), suggesting their topologically highly similar seizure propagation ability. Modules in the frontal lobe, M41–M43, demonstrate the lowest potential to propagate seizures to the rest of the cortex (∼17%), which modules again induce highly similar cortical power spectra to each other (p > 0.3 for all pairs in M41–M43), but not to the rest of the entrained areas ($p < 10^{-6}$ between frontal modules and the every other areas). Results on the spatial extent of seizure spread (Figure 7.11 second column) seem to follow similar trends to the proportion of regional powers at the entrainment frequency (Figure 7.11 first column).

7.5.4 Discussion

Combining with our earlier results, in this section we have seen how the functionally advantageous high metastability of the cortex results in higher sensitivity in spreading locally generated synchronous activity, and thus higher generic susceptibility to epileptic activity, than in the less modular and thus less metastable (globally more synchronised) surrogate network of the cortex. At the same time, however, we also found the cortex to be relatively less vulnerable to seizures originating from its hub regions than its surrogates are, presumably attributable to the cortex's highly segregated and modular architecture.

The hub nodes have long been suspected to orchestrate synchronisation in complex neural networks (Gómez-Gardeñes et al. (2010)). Several computational and experimental studies have showed that hyper-connected hub neurons contribute largely to the hyper-excitability of the developing hippocampus by mediating gamma-frequency oscillations (Morgan and Soltesz (2008), Bonifazi et al. (2009), Case and Soltesz (2011), Quilichini et al. (2012)).

Detailed entrainment simulations showed that the propagation of synchronous activity from

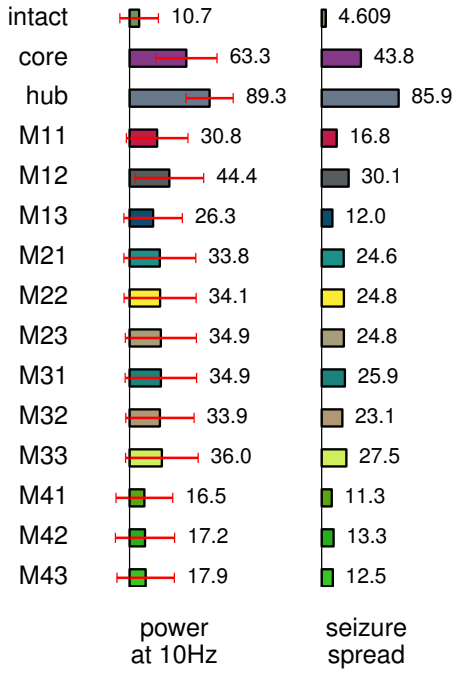

Figure 7.11: **Seizure propagation ability and susceptibility of cortical areas.** Power at 10Hz: means (bars) and standard deviations (error bars) of regional powers at 10±0.5Hz. Seizure spread: proportion of cortical regions with more than 80% of their power concentrating around the entrainment frequency (10±0.5Hz, see Methods). All values are in %ge.

focal cortical sites, the core and the modules of the cortex, are significantly less effective, and thus potentially epileptically less dangerous, then those originating from distributed cortical areas (random and hub entrainment). These characteristics are again clearly attributable to the highly segregated, modular topology of the cortical connectivity. From the localised cases, the cortical core exhibited the significantly strongest ability to wide activity spreading, reinforcing its functional importance indicated by its topological characteristics.

Notably, the results of our preliminary simulations of the highly complex phenomenon of epilepsy report the topologically central structural core as the most dangerous epileptic focus in terms of seizure spreading potential. This finding is consistent with the results of Vaudano et al. (2009), who provided evidence that the *precuneus*, a prominent substructure of the cortical core, gates generalised spike wave discharges in the thalamo-cortical network.

For the interpretation of these findings it is important to note, however, that our exploratory model was not devised to investigate the potential of cortical areas to generate epileptiform seizures, but to assess their capacity of propagating their synchronous activity and of being effected by incoming seizures. The detailed, physiologically accurate investigation of epileptic brain activity requires a more complete dataset of the entire brain including the thalamus and biophysically more

plausible dynamical models (Soltesz and Staley (2008), Milton (2010)).

7.6 Overview of results

In this chapter, we carried out a series of analyses on the structure facilitated synchronisation properties of the cortex. We started off by investigating the emergence of cortical synchrony from local to global levels in an abstract oscillatory model (Section 7.3). Globally, we found that the cortex exhibits significantly lower levels of synchronizability than its surrogates, which we attributed to its topologically decreased integratedness and increased segregatedness.

Investigation of the internal synchronisation times of various parts of the cortex indicated that modular elements on all levels of the unveiled module hierarchy are indeed possess increased capability for functional cooperation through their high synchronizability. We also assessed the ability of various topologically distinguished region groups of the cortex to facilitate this synchronisation process across the module hierarchy. Results indicate, that while hubs outside the cortical core are significantly more involved in organising synchronisation on the lower levels of the module hierarchy, hubs in the core appear to facilitate synchronisation on the higher hierarchy level of supermodules and in the entire network globally. These findings provide dynamical validation to our earlier results on the differentiated roles of core hubs and module hubs suggested by network topology (Chapter 6). We also found that the removal of all hub regions results in a significantly more devastating effect in modular and global synchronizability than the sum of the effects of its components.

The putative functional advantages of the found low level of cortical synchronizability were further investigated by simulating physiologically more plausible coupled oscillator models (Section 7.4). Firstly, we found that the low global cortical synchrony is accompanied by a relatively high metastability facilitated by the segregatedness of the network. Furthermore, this high metastability is substantially lowered after the removal of cortical hub regions, which is attributable to the decrease in inter-module connectivity.

Module level analysis revealed high agreement among several dynamical complexity measures in the parameter regime where the cortex exhibits maximal metastability, specifically at intermediate coupling strength and physiologically plausible conduction delay values (5-20 ms, Ghosh et al. (2008)). Within that regime, cortical modules, while themselves being internally highly metastable, spontaneously engage and disengage in transient coalitions of varying combinations.

In our final experiments on cortical synchronisation dynamics, we investigated the level of susceptibility the topology of the cortex exhibits to spreading of synchronised activity (Section 7.5). In a global analysis against its surrogate networks, we found that its high metastability renders

the cortex highly vulnerable to epileptic activity from random, non-hub sites. At the same time, however, the cortex also demonstrated increased resilience against the distributed stimulation of all hub nodes in comparison with its surrogates, a finding we attributed to the highly segregated and modular architecture of the cortex.

Simulations of localised, focal seizures provided further validation for the increased dynamical separateness of the topologically segregated cortical modules, effectively moderating the cortico-cortical spread of epileptic activity. All focal seizure simulations demonstrated significantly lower spread than the distributed stimulation of approximately equal numbers of random and hub regions. Among the focal seizure simulations, the cortical core was proved to be able to impose the greatest influence on the spontaneous dynamics of the rest of the network, followed by the intermediate effect of the lateral and caudal modules, and the rather low activity propagation ability of the frontal modules.

Having seen in this chapter how synchronisation dynamics on fast time scales are affected by the topology of the cortical connectivity, in the next chapter we shall investigate the patterns of inter-regional activities on slow time scales emerging on the underlying anatomical network of the cortex, that is, the relation between the cortex' structural and functional connectivities.

Chapter 8

Functional connectivity analysis

Interactions between regional resting-state activities

In the previous chapter, we studied the ways in which the anatomical connectivity shapes the dynamics unfolding on its topology in short to intermediate time scales. In this chapter, we search for statistical patterns of significantly increased or decreased interactions between inter-regional activities on longer time scales, and study how these patterns, collectively called the brain's functional connectivity, relate to their physical substrate, the structural connectivity of the cortex.

We shall assess influence of structural connectivity on cortical function by comparing it both with a simulated and an empirical functional connectivity, the latter obtained by Hagmann et al. (2008). Apart from directly comparing the two connectivity modalities (structure and function), we also attempt to characterise less direct effects of cortical network structure on its function by assessing the relationship between several spatial properties and complex network metrics of the anatomical connectivity of the cortex on the emerging dynamical patterns, represented by its functional connectivity. This latter analysis provides a direct test for one of the basic assumptions of complex network sciences, that is, that complex network metrics of topology are indicative to the functional/dynamical characteristics of the networks.

8.1 Introduction

8.1.1 Resting state functional connectivity

In the absence of any external stimulus input or motor output, that is, in its resting state, the brain exhibits a complex pattern of intrinsically generated activity (Gusnard et al. (2001), Fox and Raichle

(2007)). In contrast to the traditionally researched task-specific responses, this spontaneous activity represents an unconstrained, default brain state with nevertheless rich and active characteristic dynamics, from which any stimulus- and task-dependent activity can be initiated.

As we briefly touched in Section 1.2, by measuring the simultaneous activity of a set of brain sites, one can derive two distinctively different connectivity types: *functional connectivity* (FC) and *effective connectivity* (EC). Both modalities were designed to represent statistically significant interactions in the dynamics of brain areas under some condition, such as the resting state. However, FC, using a simpler relation model, depict those as symmetric correlations (Achard et al. (2006)), as opposed to the directed, causal connections of EC (Friston (1994)).

Correlation between structural and resting state functional connectivities of the human cortex has been investigated by several studies (eg. Skudlarski et al. (2008), Honey et al. (2009) and Honey et al. (2010)). All studies reported positive correlation between DTI and DSI derived structural connectivities and functional networks obtained by fMRI or simulations. While this correlation is particularly high at structurally directly connected brain regions, some regions have strong functional correlation even at the absence of anatomical connection, which nevertheless can partially be explained by indirect connections and spatial proximity (Honey et al. (2009)). Furthermore, despite the fact that both empirical and simulated functional connectivities exhibit some level of variability across scans and model runs (Cammoun et al. (2012), Tomasi and Volkow (2011a), Tomasi and Volkow (2011b)), all studies were in agreement on the finding that resting state functional connectivity is heavily constrained by the large-scale structural architecture of the cortex (Honey et al. (2010)).

From brain dynamics to functional connectivity

Contemporary functional magnetic resonance imaging (fMRI) techniques measure the so-called blood oxygenation level dependent signal or BOLD signal of the brain activity (Huettel et al. (2009)). The fundamental assumption behind using fMRI signals measuring the BOLD contrast is that the amount of oxygen in the blood can be used as a marker for neural activity (Friston et al. (2003)). Previous experiments, showing that neural activity and blood flow are linearly related over normal ranges (Miller et al. (2000)), provided empirical evidence that such metabolic changes picked up by the BOLD signal are indeed the result of neural activity. An important fact to keep in mind during the interpretation of BOLD fMRI, is that the signal by its nature detects major metabolic demand of the neurons, which, rather than being local spiking activity, are in fact the synaptic transmission and conductance of post-synaptic potentials, occurring at the *target sites* of the active neuron population (Friston et al. (2000)).

In recent years, the advancement and spread of fMRI imaging along with the increasing interest in the mechanistic explanation of the phenomena have generated considerable effort for developing generic hemodynamic models that mediate between synaptic activity and measured BOLD responses. The one introduced in Friston et al. (2003) and used here is comprised of two main model components: a linear dynamical model of the changes in regional cerebral blood flow (rCBF) caused by neuronal activity (Friston et al. (2000)), and the Balloon-Windkessel (BW) model (Buxton and Frank (1997), Buxton et al. (1998), Mandeville et al. (1999)) accounting for the translation from rCBF to the ”observed” (simulated) BOLD signal.

The scientific benefit of such mechanistic models is two-fold. Having passed extensive validation tests (Friston et al. (2000)), the rCBF+BW compound model is not only able to provide an explanation to the origin of the BOLD fMRI signal, thus providing a common basis to its interpretation (Friston et al. (2003)), but also serves as a model for computational research in brain activity derived functional connectivity (Cabral et al. (2011)). In the current study, we utilise this second aspect of the model.

In this section, we look at the ways structural connectivity shapes the emerging patterns of functional interactions in the human cortex in its resting state. Taking advantage of the identical cortical parcellation schemes for the two connectivities, we carry out a comparative analysis between the structural connectivity and the resting state FC of the cortex, both empirically obtained by Hagmann et al. (2008). Besides this direct, cross-modal structure–function comparison, the degree of influence of the anatomical connectivity on the emerging dynamical interactions is also assessed by comparing the empirical rsFC with its ”synthetic” counterpart, simulated by simple coupled oscillators on the cortical SC.

8.2 Methods: Functional connectivity simulation

Local neural activity is obtained by simulating time-lag coupled, non-identical and noisy Kuramoto oscillators on the anatomical connectivity of the cortex (Figure 7.1 *c*). Due to the large size of the network and the long simulation time needed, we are not able to carry out a parameter sweeping analysis and find optimal model parameters at which the simulated FC best approximates the empirical ones. Thus, we derive our working point of choice from results on the lower resolution cortical network of Cabral et al. (2011), who found that the parameter regime where the difference between the empirical and simulated FC is minimal largely overlaps with that where the simulated cortical activity exhibits its most metastable dynamics. The utilisation of these results is motivated by the fact that the obtained regime is in the physiologically plausible propagation velocity range

of 5-20m/s (Ghosh et al. (2008)), and furthermore our results on the metastable dynamics of the high resolution cortical network are in agreement with the found parameter values (Section 7.4). Therefore, to obtain the simulated functional connectivity of the cortex, we simulate regional dynamics at global coupling strength k = 20 and mean conduction delay τ = 10ms. The simulation is run for 30s, with 0.5ms integration time step.

The above local neural activity, simulated by the Kuramoto model, is then transformed into a BOLD signal on each cortical region using the Balloon-Windkessel hemodynamic model (Friston et al. (2000), Friston et al. (2003)), following the post-processing pipeline applied in Cabral et al. (2011). In the following, we briefly introduce the main steps of the processing pipeline.

The basic assumption behind the Balloon-Windkessel model, originating from interpretation of experimentally obtained BOLD fMRI signals, is that the BOLD signal indicates the variation in the firing rate of the local neuronal population. Assuming that the firing rate $r_n(t)$ of any given region n fluctuates around a fixed value, we simply approximate $r_n(t)$ by the sinusoidal relation:

$$r_n(t) = r_0 sin(\theta_n(t)) \tag{8.1}$$

where $\theta_n(t)$ is the phase of region n at time t, and r_0 is the fixed fluctuation amplitude. We stress the difference between $r_n(t)$ and f_0 in the applied modelling framework: $r_n(t)$ represents actual firing frequency or firing rate of a neuron population at region n, while f_0 denotes oscillation frequency, which is the intrinsic frequency of mean firing rate fluctuations of the regions. We use $r_0 = 1$, so that the Balloon–Windkessel model is linear and is analogue to a linear filter. This way, our results depend only on the neural activity generated by the model, and not on the non-linearities of the BOLD model (see Cabral et al. (2011) for further discussion).

In order to match the parameters at which the empirical functional connectivity (empFC) was obtained, simulated BOLD was low-pass filtered (0.25 Hz) and downsampled at 2s. After that, the global signal (average over all regions) was regressed out of the regional BOLD time series (Fox et al. (2005), Fox et al. (2009)), and finally, the correlation matrix of this time series was calculated, yielding the simulated functional connectivity (simFC).

8.3 Results: Inferring functional connections from cortical topology

8.3.1 Comparison of empirical and simulated functional connectivities

Empirical and simulated functional connectivities along with their correlation are shown in Figure 8.1. Both connectivities exhibit the tendency to organise around strongly correlated blocks of varying size along the main diagonal of their connectivity matrices, resembling the anatomical

and modular architecture of the underlying structural connectivity. Specifically, we note the high functional intra-correlation of visual lobe (red regions), as well as the similar functional correlation pattern in the first and second supermodules (top left side of the matrices) in both FC's.

Along with these similarities on the large scale, we can visually observe considerable disagreement between the individual value-pairs of the two functional connectivities. As the correlation plots show (Figure 8.1 *c* and *d*), there is a large dispersion in the corresponding entries of the two FC matrices, with most region-pairs taking very low functional correlation (red area around origin), and, especially in the simulated FC, with more region-pairs exhibiting strong positive than strong negative correlations.

Potential causes of these discrepancies between the empirical and the simulated FCs include the presumably incomplete and noisy structural connectivity (Section 2.1), the minimalistic model of regional and interaction dynamics provided by the Kuramoto model, and any further oversimplification and computational deflection introduced during the simulation of the BOLD signal and the additional post-processing steps. While, considering the extraordinarily intricate structure and dynamics of the human brain, it appears to be a naive assumption to expect very high accuracy during these simulations, the obtained results already point to the fundamental role of the cortex's anatomical connectivity and coupled oscillatory dynamics in shaping functional interactions on the large scale. We nevertheless hypothesise that ongoing improvements of anatomical tracing techniques and the utilisation of more complex computational models will certainly result in more accurate functional connectivity simulations in the future.

8.3.2 Resemblance of structural properties in the functional couplings of the cortex

An increasing amount of evidence indicates that the cortex' gross anatomical structure plays an important role in shaping the patterns of functional interactions acting on in, however, we are only beginning to discover the complex relationship between these two basic connectivity modalities (Honey et al. (2010)). Numerous studies have already found positive correlations between the anatomical and functional connections in certain parts of the brain (Greicius et al. (2009), van den Heuvel et al. (2009a)) or in the entire connectome (Skudlarski et al. (2008), Honey et al. (2009)). However, to our best knowledge, no previous work has studied the ways in which more general topological features of the connectome, such as various node-level network metrics, are reflected in its functional interaction patterns. In this section, we address exactly this question.

Beside the scientific relevance of the question, there is also a growing interest in the feasibility of "reverse-engineering" the brain from the technical side, by inferring anatomical links from functional connections (Van Dijk et al. (2010), Alexander-Bloch et al. (2012)). We believe, that

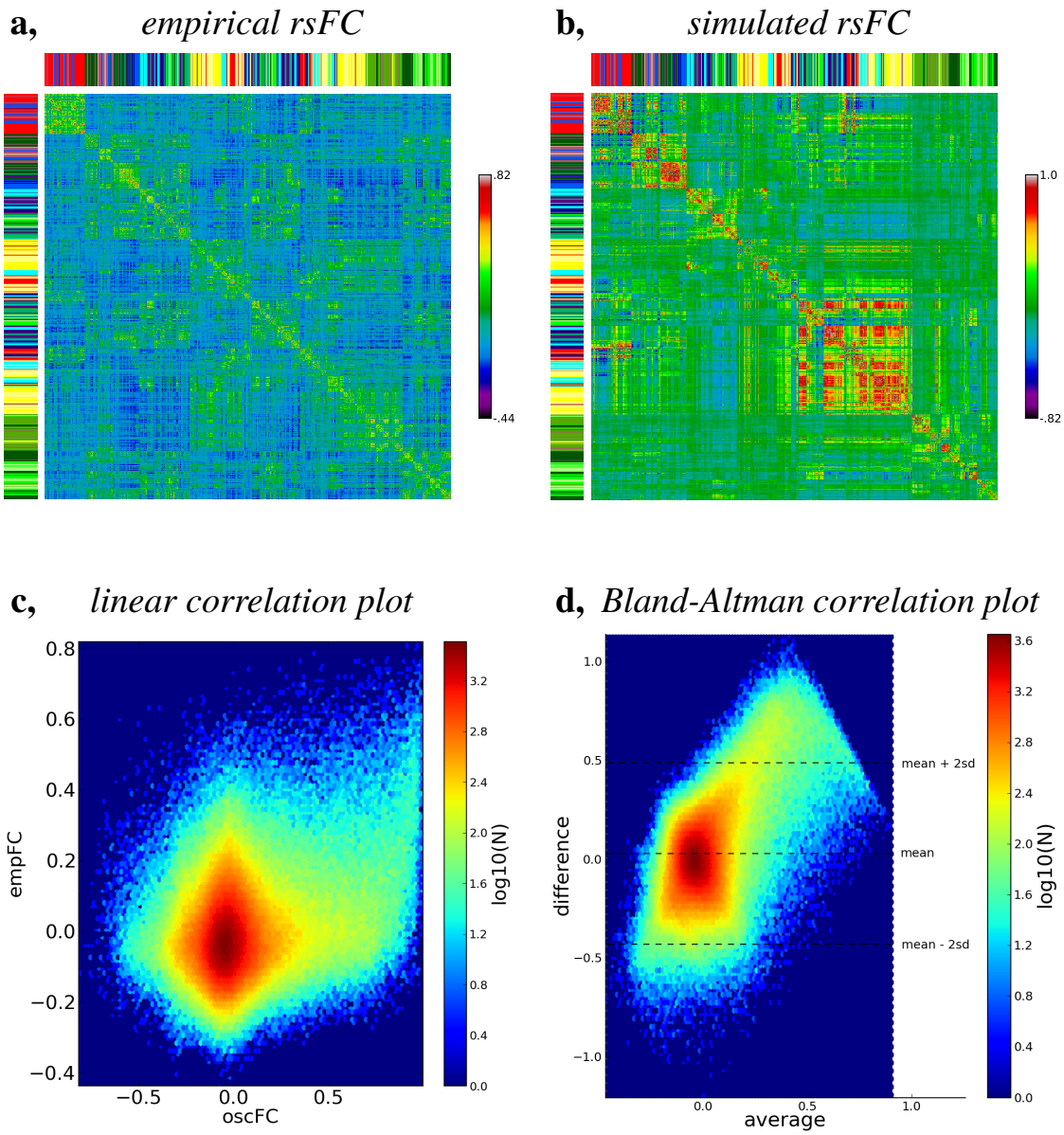

Figure 8.1: **Simulated and empirically obtained resting state functional connectivity (FC) comparison.** Top: empirical (*a*) and simulated (*b*) functional connectivity matrices. Cortical regions are ordered according to the recovered modular organisation of the structural connectivity (Section 5.3). Matrix entries represent correlation values in the pair-wise activities of corresponding regions, and are colour coded on a linear scale (see colour bars on the right side). Top and left colour stripes denote greater anatomical structures (see Figure 5.3). Bottom: Linear (traditional) and Bland–Altman mean–difference (Bland and Altman (1986)) correlation plots of the two functional connectivities.

exploring the relationship between more general structural properties and the functional links of the cortex is a crucial point for the success of such an endeavour. Furthermore, with the forthcoming analysis, we also aim to directly investigate the validity of the commonly accepted functional interpretation of various routinely applied structural measures (Rubinov and Sporns (2010)) in a concrete brain network.

Inter-relations between the empirical and simulated functional connections and the five metrics of the structural connectivity are shown in Figure 8.2. The first three, strength, efficiency and matching index, are purely topological features, while the last two, length and distance, are spatial properties of the cortex. Strength and length, being direct attributes of the structural connections, are related to functional coupling only between anatomically directly linked node pairs, while efficiency, matching index and distance are generic metrics represented and shown between all node pairs. In the following, we analyse the obtained structure–function relations one by one.

Firstly, let us investigate how direct anatomical connections translate to functional coupling (Figure 8.2, first row). In accordance with several previous studies (reviewed in Honey et al. (2010)), we detect strong positive correlations between structural and functional connections at existing anatomical links. The co-variance is present in both FC's, with the simulated one being shifted towards stronger functional correlations, presumably pointing to the lack of some inhibitory processes in the utilised dynamical model, as opposed to, for example, the model of Honey et al. (2009).

Topological efficiency (inverse path length) is generally regarded and utilised as a structural correlate to functional influence and cooperation capability (Rubinov and Sporns (2010)). How-

---

Figure 8.2 *(following page)*: **Relationship between empirical and simulated functional connectivities and various metrics of their common structural connectivity.** Each subfigure is a scatter plot showing either the relation between attributes of structural projections and functional connection strengths only between anatomically linked region pairs (first and fourth row), or the relation between a pairwise structural metric and the functional connection strength between all region pairs (second, third and fifth row). SC metrics: strength: weight of *existing* structural projections, efficiency: efficiency between *all* region-pairs, matching index: matching index of *all* region-pairs, length: projection length of *existing* structural connections, distance: distance between *all* region-pairs in anatomical space. Colours from blue (low) to red (high) represent number of node-pairs/edges in bins.

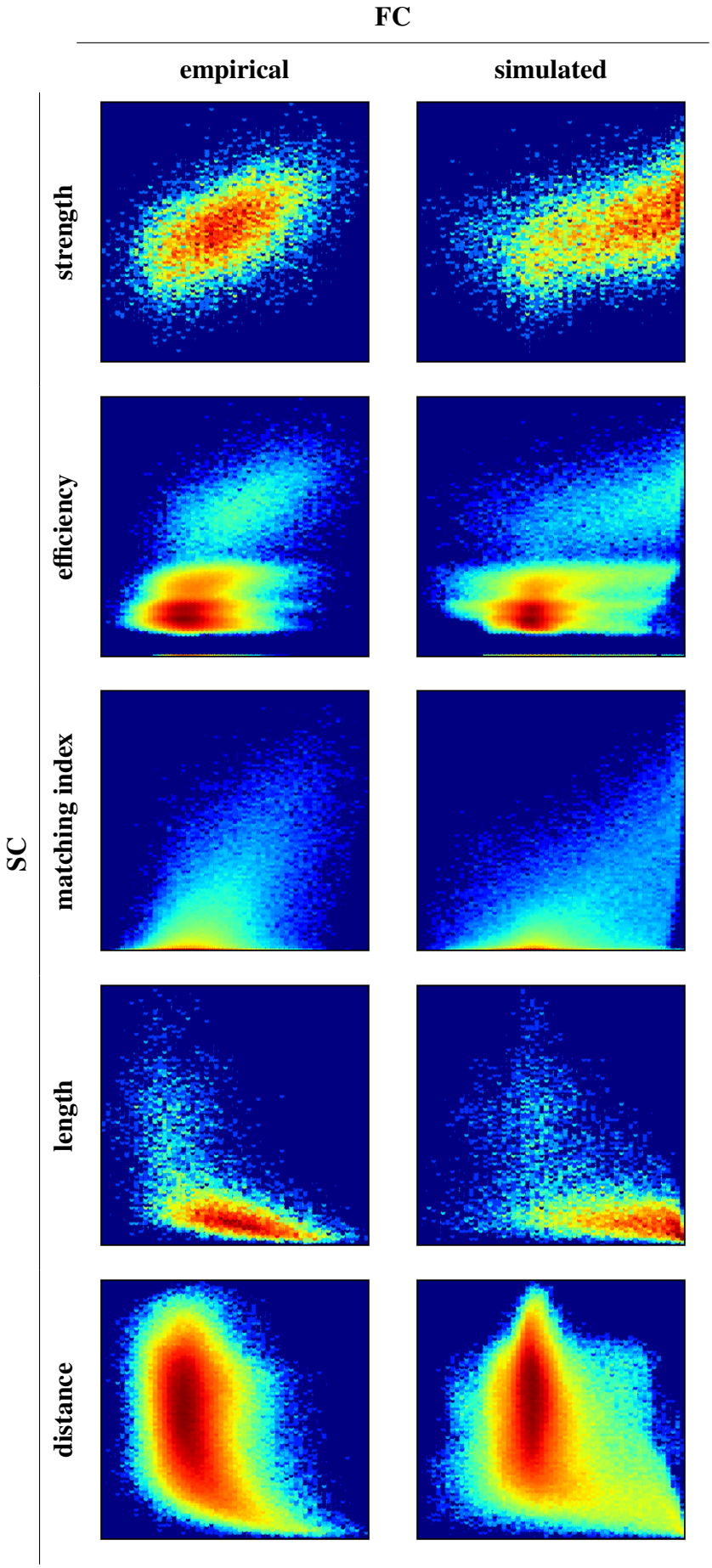
FC
empirical
simulated
SC
strength
efficiency
matching index
length
distance

ever, the relation between region–region efficiency and functional linkage exhibits a diverse pattern, being composed of multiple, partially overlapping clusters of points (Figure 8.2, second row). The diameter (length of the longest of the shortest paths) of the cortical network being 6, each of these clusters, from top to bottom, corresponds to a specific topological distance from 1 to 6 (higher to lower efficiency). The clusters are smeared and overlap because of the weighted version of the measure. Note how the most efficient, light blue uppermost cluster, representing the directly connected region-pairs, is identical to the scatter in the *strength* subfigure above.

As a generalisation of the above results on the correlation between anatomical and functional connection strength, we can observe that high structural efficiency of the directly connected regions is sufficient but not necessary for strong functional connection. Additionally, we also note that the correlation between efficiency and functional coupling sharply declines in both the empirical and simulated FC's as the anatomical linkage becomes less direct (with the increase of topological path length). These results argue against the general interpretation of efficiency as a structural measure of functional cooperation in large-scale brain networks.

Matching index measures the degree of similarity (ratio of overlap) between the connectivity fingerprints (set of neighbours) of the node pairs (Zamora-López et al. (2010)). Pairs of brain regions sharing many common neighbours are believed to fulfil similar functional roles (Passingham et al. (2002)), therefore they need to be functionally coupled. We obtain a dispersed relation between matching index and functional connections (Figure 8.2, third rows), which nevertheless reconfirms that region-pairs with similar connectivity fingerprints are more likely to functionally correlate.

Finally, the two spatial metrics we relate to functional coupling are connection length and region–region distance (Figure 8.2, fourth and fifth rows). Not surprisingly, as previously reported by Honey et al. (2009), we find that shorter projections result in strong functional correlation, as well as that spatially close region pairs tend to cooperate functionally more strongly.

Altogether these results, while cautioning against the overly broad functional interpretation of the investigated structural measures, confirm that the spatio-topological segregation of the cortical connectome significantly contribute to its functional interactions.

8.4 Overview of results

In this chapter, our aim was to assess the degree of influence of the structural connectivity of the cortex on its resting state functional connectivity. In-depth network analysis of the functional connectivity was not attempted in this study for several reasons, including i) the interpretation issues of many complex network measures developed for network structure when applied to such

abstract associations like correlation of activity (Rubinov and Sporns (2010)), ii) the ambiguity introduced by thresholding of the dense and weighted functional connectivity matrix into a binary one, and iii) the absence of null-models for functional connectivities. We note that the above issues have recently motivated research on generalising modularity and centrality metrics to densely connected functional connectivities containing negative weights (Rubinov and Sporns (2011)).

Firstly, we tested directly how well an empirically obtained rsFC can be approximated by simulating coupled Kuramoto oscillators on the anatomical connectivity of the cortex (Section 8.3.1). We observed considerable discrepancies between the empirically obtained and our simulated FC. While our rather minimalistic dynamical model certainly misses important factors that influence the emerging functional connectivity from network anatomy, the utilised structural connectivity, as the initial point of the simulations, is also necessarily imperfect due to, for instance, its limited spatial resolution and its deficiency in representing long, inter-hemispheric projections (see Section 2.1.1). Considering these points, our results report a strong structure–function correspondence by demonstrating a reasonable approximation of functional connectivity by even a simplistic dynamical model.

Having had a structural and functional connectivity dataset on the same cortical parcellation, we also took the opportunity to explicitly investigate some of the generally accepted claims about the functional relevance of structural complex network metrics in the human cortex (Section 8.3.2). In agreement with earlier results (Honey et al. (2009)), we found that while direct and strong anatomical connectivity is indicative of strong functional connections, low efficiency between region-pairs in general does not necessarily mean weak functional coupling. Similarly, high matching index (many common neighbours) result in strong functional connection, but the inverse relation is much less clear. Looking at the spatial connection length and region–region distances, we found that they are in a relatively strong negative correlation with functional connection strength. These results provide further validation to the functional influence of the both spatial and topological segregation of the cortex, but also point to the inadequacy of structural measures to accurately and reliably infer functional connections in the brain in general.

Our results are broadly in agreement with earlier studies on correlation between structural and resting state functional connectivities of the human brain. Despite the considerable technological challenge these studies require to overcome, a growing amount of experimental evidence supports the above notion of the (direct or indirect) effect of anatomical connectivity on large-scale brain dynamics (eg. van den Heuvel et al. (2008), Greicius et al. (2009), Honey et al. (2009)).

This chapter concludes the research carried out in this study, and in the next chapter we provide a summary and discussion on our results.

Part III

Epilogue

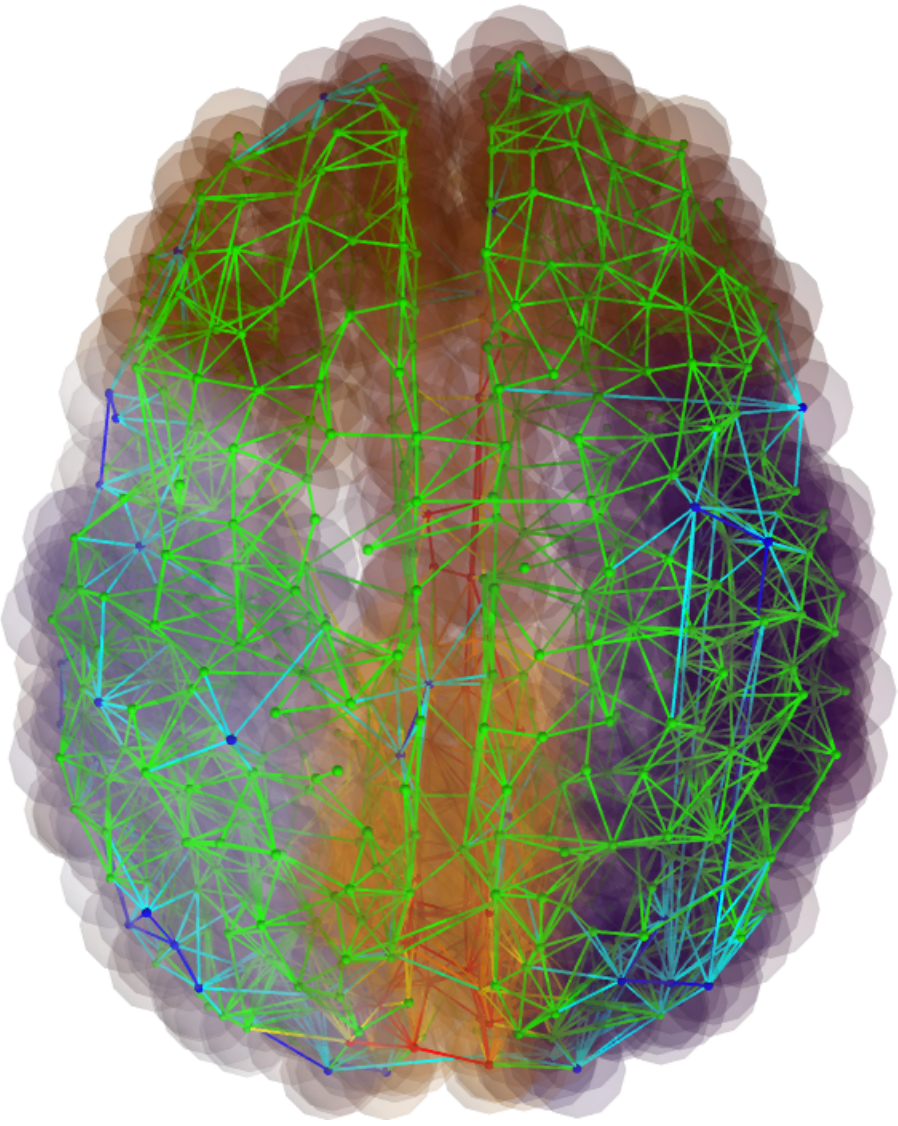

Chapter 9

Discussion

In this work, we analysed the large-scale anatomical connectivity of the human cortex in order to confirm, relate and compare the previously reported topological organisation patterns of small-worldness, modularity, hierarchy and core formation on a higher-resolution cortical connectivity network, and to then analyse the dynamical consequences of these patterns. Along the series of analyses we carried out, our aim was not only to integrate the above organisation principles into a single description of the network architecture of the cortical connectivity, but also to explore how the basic topological properties and the spatial embedding of the cortical connectivity into physical space affect the expression of these organisation principles. In this chapter, we discuss the obtained findings in the context of previous research, we give a possible explanation for the putative functional and behavioural relevance of the current results, and finish with an outlook of connectomics.

9.1 Review of results

9.1.1 The applied dataset

We started by introducing the cortical connectivity dataset used in this study (Chapter 2). Originating from the current shortcomings of the applied data acquisition technique, the analysed connectome dataset suffers from certain limitations. The most severe ones of these limitations are the absence of polarity information of the cortico-cortical connections, and the purely cortical nature of the network, excluding all thalamic and brainstem areas. We discussed how these limitations restrict our analysis and may affect our results, and why the cortical network at its currently investigated resolution can be approximately represented as a undirected (reciprocally connected) network. Then we provided an initial introduction of the cortical connectivity network

by discussing its basic topological properties.

9.1.2 Null-hypothesis networks

One of the main themes of the thesis was the question of how much and what aspects of the structural organisation of the cortex are preserved if we conserve some of its basic topological and spatial constraints but otherwise randomise its connectivity. To this end we utilised two null-hypothesis or surrogate network groups. Firstly, we analysed a set of traditional, spatially unconstrained random surrogates, that conserve the number of regions, number of connections and (binary) degree distribution of the cortical connectivity. Along with these spatially unconstrained random surrogate networks, we introduced a novel type of surrogate network, spatial surrogates, that, in addition to the properties above, also preserve the total connection length of the network globally, the sum of connection lengths of each region locally, and furthermore reasonably approximate the length distribution of the individual cortical connections. In Chapter 3, we described the purpose of these null-hypothesis networks along with their properties and generation method, and finally we evaluated the generated surrogate networks against a set of validation tests in order to verify their suitability for the current research.

9.1.3 Integration, segregation, small-worldness

In our first set of analyses, we assessed the functional integration and segregation abilities of the cortical connectivity by a set of relevant complex network measures for each phenomenon (Chapter 4). By comparing the cortical connectivity to its surrogates, we found a relatively low level of global efficiency in the cortex, significantly below that of its spatial surrogates, suggesting that long-range cortico-cortical connections are sub-optimally placed for high integration. In line with this, we also found a significantly higher level of segregation the cortical network than in its spatial surrogates, indicating that the cortex favours high segregation over integration, even when considering the already increased level of the former and reduced level of latter due to its sparse and spatial limited connectivity. Relating these measure results with those of random surrogates, we found that spatial constraints of the cortex seem to strongly contribute to its relatively low integration and extremely high segregation, together resulting in an elevated expression of small-world organisation in the cortex, compared to its spatial surrogates.

9.1.4 Hierarchical modularity

In Chapter 5 we turned to the investigation of the cortical architecture on the meso-scale, and evaluated the expression of some generic network organisation principles in the cortex, such as

hierarchical, modular, and centralised organisation patterns. The mean clustering coefficient as a function of region degree, utilised as a simple model for detecting hierarchical features, indicated the presence of a hierarchical organisation in both the cortical network and its spatially constrained surrogates, but not in random surrogates, revealing how the predominantly local connectivity and the central positioning of high degree nodes alone are suitable to foster hierarchical organisation features in the cortex.

Modularity analysis revealed that, while spatial surrogates also exhibit a considerably strong modular architecture, the modular organisation of the cortex is stronger and more refined (composed of more modules) than its connection length preserving spatial surrogates. Our findings indicate that, while basic wiring constraints of cortical regions naturally result in the tendency for cortical module formation, the long-range cortico-cortical projections appear to be more optimally placed towards a highly modular cortical architecture, than these wiring constraints alone suggest.

The large sizes of the obtained modules compared to the resolution of the cortical network under investigation allowed for the analysis of the internal topological organisation of the modules (Section 5.3). Specifically, we tested the hypothesis that these global modules, rather than having homogeneous internal connectivity (such as the models in Shanahan (2008) or Shanahan (2010)), are themselves composed of submodules of smaller size, which submodules can be divided further into sub-submodules, and so on, in other words, we searched for the cortex's multi-level, hierarchical module organisation (Arenas et al. (2006), Sporns (2006)). Topological and dynamical analysis of the large-scale anatomical connectivity of the cortex confirmed its characteristic organisation feature of being composed of relatively loosely coupled, but spatially and topologically encapsulated subunits (modules), in a repetitive manner across multiple levels. This hierarchical modular organisation of the cortical connectivity may provide the anatomical basis for the similarly organised functional connectivity of the cortex, found earlier in the cat (Zhou et al. (2007)) and the human brain (Ferrarini et al. (2009), Meunier et al. (2009b)).

9.1.5 Core formation and centralisation

While the exponential degree distribution (Hagmann et al. (2008)) and hierarchical organisation already suggested a centralised organisation of the cortical topology, in Section 5.4 we explicitly examined which, if any, parts of the cortex is located in its topological centre. Surrogate comparison revealed that the s-core of the cortex is stronger and larger than those of its spatial and random surrogates. Furthermore, confirming previous results of Hagmann et al. (2008), the s-core of the cortex was found to be spatially encapsulated at a medial-caudal location, composed by the *precuneus*, the *cingulate cortex* and the superior part of the *occipital lobe*. The cortex therefore

appears to have a spatially compact and topological highly significant s-core, optimised against its physical wiring constraints. These properties suggest high functional relevance to that core structure, and make it an appropriate candidate for some sort of putative central, global coordinator substructure of the brain (Baars (2002)).

As opposed to that, another candidate central structure, the rich-club formation of the cortex (Van den Heuvel and Sporns (2011)), while exhibiting a denser than random intra-connectedness, is formed by a relatively loosely coupled, spatially and topologically rather dispersed set of regions, therefore it appears to be a less appropriate candidate for a putative central core of the cortex.

Further investigation on the topological centralisation towards the detected s-core of the network indicated, that local s-cores in each cortical supermodule, while being the main integrator substructures within their respective supermodules, are globally less significant integrator substructures. Furthermore, these local s-cores are located in a topologically rather segregated position from the other supermodules, as opposed to the global s-core, which itself is one of these supermodular s-cores due to its modular encapsulation. These results place the s-core of the cortex into a global inter-supermodule integrator position: a spatially and topologically central structure capable of integrating and coordinating the otherwise highly segregated lateral parts of the two hemispheres.

9.1.6 Hubs regions

In Chapter 6, we analysed the topological features of a functionally potentially highly significant group of regions, the hubs of the cortex. Due to the properties and relation of the found s-core and rich-club structures (see above), we departed from the traditional connector/provincial hub categorisation scheme, and distinguished hub regions with respect to the network core, as *core hubs* or *module hubs*, depending on if they reside inside or outside of the core.

Our results about the topological properties of the two hub groups are consistent with the significant rich-club organisation and high assortativity of the cortical connectivity (compared to random surrogates). Furthermore, as an alternative to the traditional provincial/connector classes (Guimerà and Nunes Amaral (2005)), the results support the rational behind our hub categorisation scheme, that distinguishes hub regions on the basis of their relation to the structural core of the cortex. Specifically, complex network metric and motif node spectra analysis provided evidence for the remarkably high internal integratedness and global centrality of the network core, capable of acting as a central integrator 'unit' in the cortex. Additionally, the hubs in the more peripheral modules were found to be highly capable of supporting this putative function of the network core by performing a local integrator role within their individual neighbourhoods, as illustrated in Figure

5.12b.

9.1.7 Synchronizability, metastability and activity propagation

In Chapter 8, we started investigating the relevance of our structural findings on the dynamics of the cortex by assessing how synchronisation dynamics on fast time scales are affected by the topology of the cortical connectivity. Assessing the emergence of cortical synchrony from local to global levels in an abstract oscillatory model indicated a significantly lowered level of synchronizability in the cortex compared to its surrogates, presumably due to its topologically decreased integratedness and increased segregatedness. Nevertheless, the relatively high internal synchronizability of the elements of the cortical module hierarchy reinforced their increased ability for functional cooperation. Furthermore, our earlier structural results on the potentially differentiated roles of core hubs and module hubs (Chapter 6) were underscored by the finding the hubs in the cortical core are more involved in supermodular and global level synchronisation, while hubs outside of the core appear to facilitate synchronisation at the lower hierarchy levels of submodules and modules.

By simulating a physiologically more plausible coupled oscillator models, we found that the low global cortical synchrony is accompanied by a relatively high metastability, presumably facilitated by the segregated, modular nature of the network. Furthermore, this high metastability is substantially lowered after the removal of cortical hub regions, due to the decrease in inter-module connectivity. This finding points to the key role of these regions in keeping the cortical network in a presumably dynamically critical, highly metastable state, in which cortical modules, while themselves being internally highly metastable, spontaneously engage and disengage in transient coalitions of varying combinations (Shanahan (2010)). Metastability, as well as several other dynamical complexity measures, were found to be maximal at intermediate coupling strength and physiologically plausible conduction delay values (5-20 ms) (Ghosh et al. (2008)).

Simulations of localised, focal seizures provided further validation for the increased dynamical separateness of the topologically segregated cortical modules, effectively moderating the spread of epileptiform activity. All focal seizure simulations demonstrated significantly lower spread than the distributed stimulation of equal number of random and hub regions. Among the focal seizure simulations, the cortical core was proved to be able to impose the greatest influence on the spontaneous dynamics of the rest of the network, followed by the intermediate effect of the lateral and caudal modules, and the lowest propagation ability of the modules in the frontal lobe, in accordance with the findings of Vaudano et al. (2009).

9.1.8 Structure – function relationship

In our final experiments in Chapter 8, we asked the question: *How does cortical resting state functional connectivity (rsFC) relate to its structural substrate?* Our results, in agreement with the significantly positive correlation obtained in Honey et al. (2009) on the low resolution cortical connectivity, exhibited an overall similar large-scale organisation in the empirical and simulated functional connectivities, resembling the underlying structural architecture, especially considering the limitations of the dataset and the simplicity of the applied dynamical model. However, the individual region–region functional couplings demonstrated substantial differences in the two FC's, suggesting an increasing necessity of using biophysically more detailed dynamical models for simulations at the current and higher resolutions of the human connectome, such as the one used in Honey et al. (2009).

Utilising the availability of both a structural and functional connectivity dataset on the same cortical parcellation, we also took the opportunity to explicitly investigate some of the generally accepted claims about the functional relevance of structural complex network metrics in the human cortex. Our results provide further validation to the functional influence of the both spatial and topological segregation of the cortex, but also warns about the inadequacy of structural measures to accurately and reliably infer functional connections in the brain in general.

9.1.9 Summary of results

Table 9.1 summarises our results on the structural and dynamical properties of the cortex in contrast to its two surrogate types. From an abstract point of view, the need to be able to simultaneously deal with a multitude of sensory, motor and cognitive tasks necessitates the topologically lowered integratedness and elevated segregation, and the presumably related functionally favourable decreased dynamical synchronizability and increased metastability of the cortex. Furthermore, being a real complex network with a diverse and extraordinarily complex set of functions to carry out, it is not surprising that the cortex adopts, and takes advantage of, several functionally beneficial organisation patterns, such as the small-world, modular and hierarchical architectures.

Small-world architecture has been shown to naturally foster high dynamical complexity (Sporns et al. (2000)), which is one of the hallmarks of brain activity (Stam (2005)). Modularity is widely acknowledged to promote network robustness and evolvability by minimising dependencies and isolating effect of local mutations and disturbances (Sporns (2010)), and it also has been shown to increase dynamical metastability (Shanahan (2010)) thus hindering the pathological cases of prolonged synchronisation and seizures (Arthuis et al. (2009)). Hierarchically modular organisation has been found to facilitate limited sustained network activity (Kaiser et al. (2010)), it

	Structural								Dynamical		
	integration	*segregation*	*small-world*	*hierarchical*	*modular*	*s-core*	*rich-club*	*centralised*	*synchronizable*	*metastable*	*epileptic*
cortical connectome	↓	↑	↑	↑	↑	↑	↑	↑	↓	↑	↑
spatial surrogates	∼	∼	∼	↑	∼	↓	↑	↓	∼	↑	∼
random surrogates	↑	↓	n/a	∅	∅	↓	n/a	∅	↑	∅	∼

Table 9.1: **Summary of structural and dynamical features found in cortex and in its surrogates.** Symbols: ↑ : high, ∼ : moderate, ↓ : low, ∅ : nil, n/a: not applicable (random surrogate results used as baseline values for the cortex and spatial surrogates for these metrics).

hence may serve crucial role in maintaining the critical functional range the human brain operates in (Kitzbichler et al. (2009)). Combining all these findings, along with the increased rich-club and core formation tendency of the cortex, into a single description of the structural connectivity of the human cortex, our results outline a hybrid, reasonably centralised and hierarchical, but nevertheless strongly modular anatomical architecture, with a remarkably strong central network core.

9.1.10 Discussion of results in relation to other domains of connectome research

Table 9.1 demonstrates that the current study, while addressing numerous principles of the structural organisation and dynamical operation of the human cortex, utilised a wide range of complex network analysis tools. We also note, however, that several aspects of brain connectivity research, with lower or higher relevance to the investigated questions, are not covered and applied in this study. Below, we briefly discuss some of these research directions and concepts with the aim to connect them to the results of the current study.

The important questions of network growth and development have generated considerable interest not only in general complex network sciences (see Albert and Barabási (2002), Newman (2003) for reviews), but also in the neurosciences (for reviews, see Sporns (2010), Kaiser (2011), Kaiser and Varier (2011)). The role of brain's spatial embedding and wiring cost in shaping the cortical architecture was one of the main themes of the current study, and our results pointed to the fundamental, although not exclusive, impact of the wiring constraints of the cortex on its large-scale organisation features. The growth of spatially embedded networks has been investigated in a series

of studies by Kaiser et al. (Kaiser and Hilgetag (2004c), Kaiser and Hilgetag (2004b), Kaiser and Hilgetag (2007), Kaiser et al. (2009)), who proposed variants of a simple spatial growth model with developmental time-windows that are able to account for the observed small-world and modular architecture of the cortex (see Section 9.2.1), reinforcing our findings about the crucial role of basic spatial constraints on the cortical architecture. As a potential extension of these studies, it would be interesting to see how well the spatial growth models of the above studies, possibly after their appropriate customisation, are able to approximate the actual connectivity profile of the cortex in more realistic simulations that incorporate further cortical properties, such as the spatial arrangement of the cortical regions and the limited volume of the skull.

The non-local functional effects of localised lesions in brain structure have been extensively reported (e.g., He et al. (2007a), He et al. (2007b)), supporting complex network approaches in general in understanding the operation of the brain. Computational studies provide flexible tools for exploring the resilience of complex networks against random errors and targeted attacks (Boccaletti et al. (2006)), and a number of studies have investigated the possible structural (Kaiser and Hilgetag (2004a), Kaiser et al. (2007)) and dynamical/functional (Achard et al. (2006), Honey and Sporns (2008), Honey et al. (2009), Alstott et al. (2009)) consequences of various lesion scenarios in different brain networks. In the current study, we also analysed various lesioned versions of the cortical connectivity to assess the significance of its substructures in facilitating the global expression of some important network phenomena, such as global efficiency, synchronizability and metastability. The results of both our analysis and the above studies pointed to the highest vulnerability of brain networks against the loss of their highly connected hub regions, that impose the most non-local effect on the structure and dynamics of the network. In addition to investigating the effect of regional lesion scenarios, our lesion studies could be further extended by modelling the potential dynamical effect of the deactivation of certain white matter pathways (network edges), or that of the removal of various module components of the cortical network. Furthermore, cortical reconfiguration after injury may also be worthwhile studying by an appropriate adaptive network model incorporating mechanisms of neuro-plasticity.

One of the fundamental characteristics of brain dynamics is its inherently complex, metastable nature at various spatio-temporal scales (e.g., Freeman (2003), Gong et al. (2003)). Providing evidence for the behavioural and cognitive relevance of this prevalent metastable dynamics, McIntosh et al. (2008) showed that greater dynamical diversity (higher metastability) in the maturing brain can be associated with more stable cognitive and behavioural capacities. The question in turn naturally arises: What is the origin of this dynamical diversity? The concept of self-organised criticality (SOC, Bak et al. (1987), Gisiger (2001)) has been proposed as a plausible

model for dynamical variability and adaption in the brain (Chialvo and Bak (1999), Bak and Chialvo (2001)). Scale-invariant characteristics of SOC have indeed been found in the patterns of spontaneous neuronal activity (Beggs and Plenz (2003), Beggs and Plenz (2004)) as well as in MEG and fMRI signals of spontaneous brain activity (Poil et al. (2008), Kitzbichler et al. (2009)). In this study, we have showed how the hierarchically modular topology of the cortical connectivity, along with its hub and core regions, are able to provide a structural basis that facilitates the emergence of the highly metastable dynamics of the cortex. We therefore hypothesise, that elements of self-organised criticality might readily appear in the simulated dynamics of the connectome in the form of spatio-temporally scale-invariant synchronisation patterns, which claim can be directly assessed by conducting the appropriate simulations. Additionally, evidence for the existence of a critical state in cortical dynamics could be found if the cortical functional connectivity exhibits fractal-like, self-similar organisation patterns on multiple scales (Bassett et al. (2006)). The hierarchical modular architecture uncovered in the current study may provide an ideal structural substrate for the emergence of such dynamics.

Research on the above aspects of cortical architecture and dynamics would be able to complement our current results, and thus provide further insight into the organisation, dynamics and function of the human connectome.

9.2 The putative role of core and hub regions in cortical function and cognition

9.2.1 Symbiotic relationship between brain structure and function

Complex networks from broad domains exhibit adaptive properties, that is, their topological evolution is influenced by the dynamics of the network nodes (Gross and Blasius (2008)). In these ”adaptive co-evolutionary networks”, network dynamics (function) is generally shaped by structural connections on faster time scales, while structure is effectively sculpted by network activity on slower time scales.

The cortex is known to be such a network with symbiotic structure – function relationship. Numerous studies have demonstrated the important role of spontaneous neuronal activity in synaptic connectivity formation in the developing brain (Katz and Shatz (1996), Weliky and Katz (1999), Cang et al. (2005)), and we also know that the large-scale topology (Hagmann et al. (2010b), Fan et al. (2011), Echtermeyer et al. (2011b)) and functional connectivity (Fair et al. (2008), Uhlhaas et al. (2009b), Fair et al. (2010)) of the human brain continues to change dramatically during the entire human life span.

Considering the strong, characteristic network organisation features of the human cortical connectivity found in earlier studies and in the current research, an important question is ”What factors affect and guide the development of the brain’s small-world, modular, hierarchical and centralised anatomical architecture?”. Several computational studies investigated the interplay between network structure and function in various models using synchrony dependent rewiring rules (Gong and van Leeuwen (2004), Kwok et al. (2007), Rubinov et al. (2009)). In these studies, the initially random network connectivities consistently evolved towards a small-world network architecture during spontaneous activity. Additionally, Rubinov et al. (2009) observed the emergence of modular architectures with an increasing number and strength of network modules as the simulations progressed. Significant fluctuations in functional connectivity were also found in that study, which was attributed to the ”noisy dynamics of central structural nodes”, the hubs of the networks. These nodes, by providing interconnections among multiple modules, are pivotal in enabling the balance between functional segregation and integration, thus serving a key role in increasing the functional complexity of the brain (Sporns et al. (2000), see also results of current study).

The computational models of these theoretical studies propose that the spontaneous activity of neural networks on the micro-scale as well as of cortical regions on the macro-scale supports the formation of some of the prominent organisation patterns of the brain’s structural connectivity during its development, maturation, ageing. Furthermore, the highly complex and metastable dynamics of the cortex on fast time scales, enabling the continuous exploration of the repertoire of its functional micro-states (Bressler and Tognoli (2006), Honey et al. (2007)), may also account for the astounding ability of the damaged central nervous system to reorganise itself (Draganski and May (2008), Berlucchi (2011)), through activity dependent mechanisms.

Characteristic organisation patterns of the large-scale topology of the cortical connectivity may also arise as a result of evolutionary mechanisms (Kaiser and Varier (2011)). Theoretical and computational research on brain network evolution suggests the natural formation of small-world and modular architecture with highly connected hub nodes (Kaiser (2011)). Furthermore, spatial growth models also demonstrated how simple spatial rules of network growth through competition for available space and other resources can lead to the observed small-world topology of the cortex (see Section 9.1.10). Therefore it seems likely that the emergence of characteristic features of the cortical architecture is a result of the combination of evolutionary mechanisms and various spatial and activity dependent developmental processes, that, instead of acting independently, may complement or even reinforce each other in complex ways.

9.2.2 Functional accounts of the cortical core and hubs

Having found the core and hub regions at topologically distinguished positions in the cortical connectivity in Chapter 5 and 6, we focused the analysis of our simulations around the dynamical properties of these region groups. Both groups were found to significantly contribute to cortical synchronizability and metastability, and they exhibited elevated capacity for propagating synchronous activity. The finding that the hub-lesioned cortical network is less synchronizable and less metastable is intuitively explainable by the notion that hub regions are the primary facilitators of inter-module integration, as it is suggested by their high activity propagation capacity.

Several earlier studies pointed to the topologically distinguished position of the posterior parietal cortex, and specifically the precuneus. The precuneus as a strong structural hub has been identified in Gong et al. (2009) on a low resolution (78 regions) human cortex connectivity. Van den Heuvel and Sporns (2011) studied the rich-club of the human brain's structural connectivity in great depth, and revealed some level of variability in the identity of rich-club regions across the various network resolutions investigated. Considering the regional composition of the network's rich-club, Van den Heuvel and Sporns (2011) and our results disagreed in the participation of the *superio-frontal* cortex, reported only by the latter work, as well as of the *superio-temporal* and *primary visual cortex*, detected only in the current study. Despite these differences, the overlap between the two studies agree in a subset of rich-club regions, that are interestingly coincident with the regions this study distinguish as the core hub group (Figure 6.1): the *precuneus*, the *superio-parietal* cortex and the *cingulate cortex* were consistently detected as high-degree rich-club areas. The facts, that (1) these regions also make up a large part of the brain's network core, (2) they are consistently found to be strong resting-state functional hubs (Tomasi and Volkow (2011a), Tomasi and Volkow (2011b)) and therefore (3) important constituents of the default mode network (Raichle et al. (2001)), suggest that their topologically central position facilitates their distinguished functional importance in the resting state of the human brain.

Furthermore, our results about the core's *structural centrality* is in complete accordance with earlier findings on the *functional hubs* of the human brain (Tomasi and Volkow (2011a), Tomasi and Volkow (2011b)). These studies, analysing more than a thousand resting-state fMRI datasets of subjects from all around the world (Biswal et al. (2010)), identified the *precuneus*, the *cingulate cortex* and parts of the *primary visual cortex* (BA 17, 18) as the global hubs of FC, exactly the regions we found to compose the *core hub* region group: the overlap between the cortex's structural core and rich-club. Other areas found here to possess topologically high integration capacity, such as the *orbito-frontal* cortex, which contains the locally highly central s-core of the *frontal lobe*, or the superio-temporal cortex (BA 21 and 22), were also reported as global functional hub

areas during resting state brain activity by the above studies. This remarkable correspondence between structural and functional centrality provides further evidence to the notion, that patterns of dynamical interactions in the brain, that is, its functional connections, are fundamentally sculpted by its large-scale white-matter anatomy (Honey et al. (2009), Honey et al. (2010), van den Heuvel et al. (2009a)).

Several studies showed evidence for the functional influence of regions in the found cortical core to other parts of the cortex through their direct anatomical connections, as well as for their functionally intermediating role between cortical areas, that are structurally not directly connected. Direct structure – function correspondence has been investigated in van den Heuvel et al. (2008), who showed that the magnitude of the functional connection and the micro-structural organisation of the fibre tract between the *precuneus*/posterior cingulate cortex and the medial frontal cortex are significantly and positively correlated. Indirect connections between anatomy and function have been studied in Greicius et al. (2009), providing evidence for anatomically unconnected medial temporal lobe and the medial prefrontal cortex to be functionally linked by the structurally intermediating *precuneus*/posterior cingulate cortex. More generally, analysis across the whole brain revealed that a substantial proportion of strong functional connections are between structurally only indirectly linked brain areas (Skudlarski et al. (2008), Honey et al. (2009)), which, intuitively, becomes increasingly dominant in the sparser connectivity of finer and finer anatomical scales (Sporns (2010)). These findings suggest that the found globally highly coupled brain areas, the cortical core and hub structure, are not only topologically central, but also play a functionally pivotal role in coordinating distant parts of the brain.

9.2.3 Cognitive accounts of the cortical architecture

Considering the above points, the topological position and dynamical attributes of the cortical core, and in particular its anatomically most confined and prominent substructure, the *precuneus*, found here as well as in earlier studies (eg. Hagmann et al. (2008), Van den Heuvel and Sporns (2011)), suggest a distinguished functional role to that brain area, making it capable of even serving as some sort of generic coordinator region for the entire cortex (Baars (2002)). Indeed, experimental studies examining its task-dependent activation attributed a diverse set of cognitive phenomena to the *precuneus*, including episodic memory, self-referential processing, imagery (Cavanna and Trimble (2006)), and even the level of consciousness (Laureys et al. (2004)). Furthermore, deactivation or lesion of the posterior medial cortex, containing the *precuneus* and other core areas, have been shown to result in the disturbance or even loss of cognition and consciousness (Kaisti et al. (2002), Damasi (1999)). Along with these findings, as we discussed above, the *precuneus* is also identified

as a pivotal area of the brain's default mode network (DMN) (Fransson and Marrelec (2008)) with a remarkable consistency across individuals (Biswal et al. (2010)).

The *precuneus* is believed to be one of the evolutionary most recently developed areas of the human brain, with a larger relative size and more complex columnar organisation than in other primates (Cavanna and Trimble (2006)). It is also among the last cortical regions to myelinate (Goldman-Rakic (1987)). The anatomical and connectivity data available of this brain area has long been suggesting its important role in higher-order brain function, but having found its involvement in a diverse set of mental processes (see above), empirical studies were unable to pinpoint its exact cognitive function (Cavanna and Trimble (2006)). The apparently generic nature of its functional activation reinforces our finding on the topologically distinguished central positioning and putative functionally coordinating role of the *precuneus*, presumably in cooperation with the rest of the cortical core.

In line with the found topologically central and functionally distinguishable role of the cortical core, prominent theories of cognition employ the notion of *integration by convergence* on large-scale neuro-cognitive networks. In supporting functional integration across multiple cognitive domains in the brain, Mesulam (1998) have suggested the crucial role of a special set of "transmodal nodes" that are capable of binding together multiple signals from unimodal areas, and thus creating multimodal representations. Damasio (1989) proposed a related idea, that accounts the integration of multiple aspects of external and internal reality to the phase-locked co-activation of spatially distant cortical areas. According to this theory, supported by a broad range of physiological studies (Meyer and Damasio (2009)), integration is achieved by triggering and synchronising the activity of remote, distributed neural populations, which is carried out by the so-called "convergence zones" of the brain. The theory uses a hierarchical network architecture for the explanation of these processes, in which sensory stimuli of various domains from the lowest level of the hierarchy propagates through multiple levels of integration, governed by convergence zones, up to areas responsible for higher-order association in the cortex.

This model is consistent with the notion of a hierarchically segregated organisation of the brain in general, and with the hierarchical modular architecture revealed in the current study in particular. Also, the topological and dynamical properties of the distributed group of hubs in the various cortical modules, found in the current study, fit well into Damasio's theory, for these module hubs appear to be capable of coordinating the activity of their respective local neighbourhoods, and thus ensure functional integration on lower and intermediate levels of the cognitive hierarchy. Finally, our findings on the topological and dynamical features of the cortical core point to this structure as a potential convergence zone at the highest level of the neuro-cognitive hierarchy in Damasio's

model.

It is important to emphasise, that the found centralised core structure in the anatomical connectivity of the cortex and its capacity of facilitating cortical synchronisation, although being consistent with it, does not necessitate the existence of a classic ”central executive” process (e.g., Goldman-Rakic (1995)), a supervisory control of cognition over the available mental resources and decision making. The alternative notion of distributed cognitive processing, that falls closer to the complex network approach followed by this study, denies any simple one-to-one correspondence between anatomical regions and cognitive function, and instead describes specific domains of cognition as a network phenomena emerging from the cooperation of a specialised subset of regions (Mesulam (1990)). Even the distributed cognitive model of Mesulam (1998) emphasises the fundamental role of transmodal areas in coordinating the operation of large-scale neuro-cognitive networks of the brain. In that sense, the reasonable, but not complete, level of topological and dynamical centralisation of the cortical connectivity around its structural core enables the core to facilitate complex interactions between distinct cognitive subnetworks of the cortex (to ”orchestrate” cortical dynamics), as described in the model of Mesulam (1998) and found in Chapter 7, while not necessarily imposing the role of an absolute central operator (”supervisor”) of cognition on the core.

9.2.4 From resting state brain activity to behaviour and cognition

Consistent activation patterns of the brain in its resting state, its so-called default mode (Raichle et al. (2001), Gusnard et al. (2001)), is believed to serve as a physiological baseline, from where any task-dependent activity can be initiated. As opposed to this intrinsic functional connectivity of the task-independent resting state of the brain, extrinsic connectivity describes the activation patterns in the brain that are observable during task-specific processing, that is, those evoked by sensory or motor events (Raichle and Snyder (2007)). Striking observations on the brain’s intrinsic activity, such as its much higher metabolic cost than that of evoked activity, its consistency, or its coherent patterns with known brain systems (see Raichle and Mintun (2006) for a review), support the view that understanding the brain’s default mode is a key factor in bridging the gap between brain activity and cognition and behaviour (Raichle and Snyder (2007)). Accordingly, a large body of research focused on the study of the resting state activity of the brain, as a physiological baseline of brain activity of healthy subjects and various patient groups (for reviews, see Broyd et al. (2009), Northoff et al. (2010), Sutherland et al. (2012)).

Prominent areas of this network, the default mode network (DMN), are the *precuneus* and the posterior parietal cortex, along with some medial parts of the temporal and frontal cortices (Raichle

and Snyder (2007)). We know that endogenous activity of DMN far exceeds that of task-evoked activity (Raichle and Mintun (2006)), however, its functional role in cognition and behaviour is still not entirely clear. Interestingly, certain patterns of this resting state or intrinsic functional connectivity remain active during stimulus driven processing and influence on the behavioural outcome of the task. Trial-to-trial variability of simple cognitive tasks has been attributed to the spontaneous and persistent fluctuations in the baseline neural activity (Dehaene et al. (2003), Dehaene and Changeux (2005)) and in the BOLD response (Fox et al. (2006), Fox and Raichle (2007)).

Meta-analysis on the results of numerous experiments in Schilbach et al. (2008) revealed that regions of the DMN are recurrently reported to be involved in social cognitive processes, suggesting that DMN areas do not only form a physiological baseline, but also some sort of ”psychological baseline”, an internally driven cognition mode of the self and its social context. However, as several studies on sleeping humans (Larson-Prior et al. (2009)), as well as on anaesthetised primates showed (Vincent et al. (2007)), correlated default mode activity persists even in the absence of consciousness. Thus, the brain's default mode, primarily driven by its topological core, appears to be involved in both conscious and unconscious, but nonetheless fundamental mental processing, the decomposition and better understanding of which requires more detailed investigations in the future.

9.3 Proposed directions for future connectome research

Naturally, the standard models of complex network sciences and the fundamentals of the neurosciences in conjunction, often in agreement, shape the specific techniques we utilise for the analysis of brain networks. For example, the abstract concept of small-worldness has traditionally been defined in relation to random and lattice networks (Watts and Strogatz (1998)), while the diffuse nervous system of coelenterates, such as Cnidaria, has long been recognised to exhibit a characteristically regular, lattice-like pattern (Kaiser (2011)). These findings have no doubt contributed to the wide application of traditional random and lattice surrogate techniques in brain network analysis.

However, in conjunction with these traditional techniques, we argue that the utilisation of other, more constrained null-hypothesis models, incorporating not only basic topological but also spatial properties of the connectome, will help us better understand the structural organisation and functional operation of the inherently spatial brain. The spatial surrogate networks of this study were designed with that purpose, that is, to provide additional insight into the organisation features of the cortex by distinguishing the ones that appear to be at least partially spatially induced,

such as the rich-club structure of the cortex, from the ones that may be the result of some higher organisation principles and hence are potentially functionally more relevant, such as its s-core.

The results of this study raise a number of immediate questions for future research, some of which have already been proposed in Section 9.1.10. With the anticipation that the limitations of the acquisition method of the current dataset will soon be overcome, the current findings would need to be investigated in more complete and accurate connectome maps in the near future. Specifically, as a first step, the found hierarchical modular organisation, core formation and centralisation of the cortex would need to be tested on a whole brain network incorporating subcortical structures. Similar investigations could be carried out on future higher resolution brain connectivity maps, that would enable the deeper characterisation of the module hierarchy of the brain in particular, as well as the analysis of a more refined cortical parcellation in general.

Although technically it appears to be the most difficult to overcome (Jbabdi and Johansen-Berg (2011)), incorporating information about polarity (directionality) of the cortical projections would not only quantitatively enrich, but would also open up the way for qualitatively different questions to be asked and analytic tools to be applied. Among these are i) identifying chains of white-matter pathways that are in position to facilitate the effective flow of directed cortical activity, ii) assessing directed aspects of the hierarchical, modular and centralised organisation of the cortex found in the current study, such as the ratio of efferent/afferent connections of the various modules or the core, iii) performing a directed motif spectrum analysis in order to find further differences between the motif node spectra of various region groups of the brain, thus further differentiating their potential functional role, and iv) characterising the relation between directed network structure and asymmetric influence/causal interactions in large-scale network dynamics in the brain.

Even though the nature of the current study is rather abstract and theoretical, especially considering the current state-of-art in empirical systems neuroscience, some claims proposed on the basis of the findings could be tested experimentally. For example, the consistent co-activation of certain module components of the module hierarchy during spontaneous or task-specific cortical activity would provide empirical evidence for their collective significance as potential functional units of the brain. Also, although there is ample evidence for the distinguished role of the precuneus in brain function and cognition (see Section 9.2), the co-activation of the entire global structural core, along with the local s-cores found in the other three supermodules of the cortical connectome, during multiple cognitive tasks would provide evidence for the important general coordinating role these areas are capable of fulfilling functionally. Finally, our simulation results on the highly varying effect of the different entrainment locations in epileptic seizure propagation in the cortex (distributed or focal, hub regions or local modular regions) could be confirmed or revised based

on direct experimental observations. For example, an invasive experiment on model animals could compare the effects of seizures artificially evoked at various key locations in the previously mapped brain of the animal (Sheerin et al. (2004), Alexander and McNamara (2012)), while a non-invasive experiment, applicable on human subjects, could combine recent developments on modelling patient-specific epileptic networks (Murta et al. (2012)) with neuroimaging brain mapping techniques (Cammoun et al. (2012)) in order to assess the relation between the topological significance of and the epileptic danger posed by various foci.

With the ongoing developments on mapping its anatomical pathways at increasing resolutions (Cammoun et al. (2012), Toga et al. (2012)), we will soon be able to acquire more and more comprehensive and detailed, multi-scale descriptions of the topology of the human brain, "an indispensable foundation for basic and applied neurobiological research" (Sporns et al. (2005)). These structural connectivity maps of the brain will allow for the more refined characterisation of its hierarchical modular architecture, revealed in this study only on the large-scale of the human cortex, as well as for identifying their particular relevance in brain function and disorder. Furthermore, it is intuitively clear, that the strong functional connections found between structurally only indirectly linked brain areas (Skudlarski et al. (2008), Honey et al. (2009)) becomes increasingly dominant in the sparser connectivity of finer and finer anatomical scales (Sporns (2010)). Therefore we anticipate, that future research will assign increasing importance to the found globally highly coupled brain areas, the cortical core and hub structure, as those topologically central and functionally pivotal cortical regions, that coordinate integration among spatially distant and topologically segregated parts of the brain, and thus may well serve as the substrate for such high-level cognitive capacities as consciousness.

Due to ongoing technological and theoretical advancements in the past 20 years, research of the connectome has been accelerated, and complex network based study of the human brain has become the standard approach in systems neuroscience (Sporns (2010)). With the growing number of research groups joining the scientific challenge of unveiling the architectural organisation and functional operation of the brain as a whole, the coming decades promise us some major breakthroughs in the field. Among these are i) the better understanding of the relation between brain structure and function (Honey et al. (2010)), ii) the emergence of behaviour and cognition from brain dynamics and functional networks (Bressler and Menon (2010)), iii) network-level descriptions of brain dysfunction caused by various neuro-degenerative diseases and iv) the translation of that knowledge to medical applications and treatment (Bullmore and Sporns (2009)).

For that, brain imaging research needs to convey even higher resolution, more complete and more reliable connectome maps (Hagmann et al. (2010a)), traditional research themes of the brain's

structure and resting state function must be complemented by the comprehensive study of task-specific functional networks (Kitzbichler et al. (2011)), and the neurosciences ultimately need to study and understand brain networks as embodied systems being in continuous interaction with their environment (Sporns (2010)). Witnessing the pace of progress and the increasing effort invested into the field, we anticipate further rise and success of human connectome research.

Figure descriptions for part front pages

Part I: Radial representation (Appendix E) of the macaque brain structural connectivity of 880 brain sites and 6601 connections (Reveley et al. (2011)). Brain sites are represented as labels, coloured by eight greater anatomical structures (see sectors around periphery). Distance from centre indicates position in hierarchy structure. Connections are bundled along their shared hierarchical paths and colour interpolated from source site (green) to target site (magenta).

Part II: Structure and dynamics of the human cortical connectivity (Hagmann et al. (2008)), horizontal view. Left hemisphere: purely structural representation of cortical regions (blue dots) and white-matter connections (blue lines). Right hemisphere: hybrid structural – dynamical representation of white-matter connections (coloured lines) overlaid by the simulated activity of cortical regions (coloured semi-transparent circles). Colours from red (low) to blue (high) represent simulated activity (momentary phase) of one of the experiments in Section 7.4 (parameters: k=20, τ=10). For clarity, only 10% of the strongest connections are drawn for both hemispheres and inter-hemispheric projections are omitted.

Part III: Illustration of the found structural features of the cortical connectome. Dots denote brain regions, connected by 20% of the strongest white-matter projections. Dot colours: red: core region, blue: module hub region, green: crust (other) region. Colours of semi-transparent circles denote supermodule, module and submodule configuration.

Bibliography

Aboitiz, F., Scheibel, A. B., Fisher, R. S., and Zaidel, E. (1992). Fiber composition of the human corpus callosum. *Brain Res*, 598(1-2):143–153. 14

Acebrón, J. A., Bonilla, L. L., Pérez Vicente, C. J., Ritort, F., and Spigler, R. (2005). The kuramoto model: A simple paradigm for synchronization phenomena. *Reviews of Modern Physics*, 77(1):137–185. 119, 121, 127, 136

Achard, S. and Bullmore, E. (2007). Efficiency and cost of economical brain functional networks. *PLoS Comput Biol*, 3(2). 37

Achard, S., Salvador, R., Whitcher, B., Suckling, J., and Bullmore, E. (2006). A resilient, low-frequency, small-world human brain functional network with highly connected association cortical hubs. *J Neurosci*, 26(1):63–72. 156, 173

Adelstein, J. S., Shehzad, Z., Mennes, M., Deyoung, C. G., Zuo, X. N., Kelly, C., Margulies, D. S., Bloomfield, A., Gray, J. R., Castellanos, F. X., and Milham, M. P. (2011). Personality is reflected in the brain's intrinsic functional architecture. *PLoS One*, 6(11). 6

Albert, R. and Barabási, A.-L. (2002). Statistical mechanics of complex networks. *Reviews of Modern Physics*, 74:47–97. 3, 43, 172

Albert, R., Jeong, H., and Barabasi, A.-L. (2000). Error and attack tolerance of complex networks. *Nature*, 406(6794):378–382. 86, 95

Alexander, G. M. and McNamara, J. O. (2012). Vagus nerve stimulation elevates seizure threshold in the kindling model. *Epilepsia*, 53(11):2043–2052. 182

Alexander-Bloch, A. F., Vértes, P. E., Stidd, R., Lalonde, F., Clasen, L., Rapoport, J., Giedd, J., Bullmore, E. T., and Gogtay, N. (2012). The anatomical distance of functional connections predicts brain network topology in health and schizophrenia. *Cereb Cortex*. 4, 6, 9, 159

Alstott, J., Breakspear, M., Hagmann, P., Cammoun, L., and Sporns, O. (2009). Modeling the impact of lesions in the human brain. *PLoS Comput Biol*, 5(6). 132, 173

Arenas, A., Díaz-Guilera, A., and Pérez-Vicente, C. J. (2006). Synchronization reveals topological scales in complex networks. *Phys Rev Lett*, 96(11):114102–114102. 122, 125, 126, 127, 130, 135, 136, 168

Arenas, A., Diazguilera, A., Kurths, J., Moreno, Y., and Zhou, C. (2008). Synchronization in complex networks. *Physics Reports*, 469(3):93–153. 119, 122, 124, 125

Arthuis, M., Valton, L., Régis, J., Chauvel, P., Wendling, F., Naccache, L., Bernard, C., and Bartolomei, F. (2009). Impaired consciousness during temporal lobe seizures is related to increased long-distance cortical-subcortical synchronization. *Brain*, 132(Pt 8):2091–2101. 129, 136, 171

Artzy-Randrup, Y., Fleishman, S. J., Ben-Tal, N., and Stone, L. (2004). Comment on "network motifs: simple building blocks of complex networks" and "superfamilies of evolved and designed networks". *Science*, 305(5687):1107–1107. 101

Baars, B. J. (2002). The conscious access hypothesis: origins and recent evidence. *Trends Cogn Sci*, 6(1):47–52. 75, 83, 90, 169, 177

Bak, P. and Chialvo, D. R. (2001). Adaptive learning by extremal dynamics and negative feedback. *Phys Rev E Stat Nonlin Soft Matter Phys*, 63(3 Pt 1):031912–031912. 174

Bak, P., Tang, C., and Wiesenfeld, K. (1987). Self-organized criticality: An explanation of the 1/f noise. *Phys Rev Lett*, 59(4):381–384. 173

Barabási, A.-L. (2011). The network takeover. *Nature Physics*, 8(1):14–16. 3

Barabási, A.-L. and Albert, R. (1999). Emergence of scaling in random networks. *Science*, 286(5439):509–512. 3, 125

Bartos, M., Vida, I., and Jonas, P. (2007). Synaptic mechanisms of synchronized gamma oscillations in inhibitory interneuron networks. *Nat Rev Neurosci*, 8(1):45–56. 120

Bascompte, J., Jordano, P., and Olesen, J. M. (2006). Asymmetric Coevolutionary Networks Facilitate Biodiversity Maintenance. *Science*, 312(5772):431–433. 3

Bassett, D. S., Brown, J. A., Deshpande, V., Carlson, J. M., and Grafton, S. T. (2011). Conserved and variable architecture of human white matter connectivity. *Neuroimage*, 54(2):1262–1279. 13

Bassett, D. S. and Bullmore, E. (2006). Small-world brain networks. *Neuroscientist*, 12(6):512–523. 6, 50, 53, 93

Bassett, D. S., Bullmore, E., Verchinski, B. A., Mattay, V. S., Weinberger, D. R., and Meyer-Lindenberg, A. (2008). Hierarchical organization of human cortical networks in health and schizophrenia. *J Neurosci*, 28(37):9239–9248. 6, 7, 9, 23, 57

Bassett, D. S., Meyer-Lindenberg, A., Achard, S., Duke, T., and Bullmore, E. (2006). Adaptive reconfiguration of fractal small-world human brain functional networks. *Proc Natl Acad Sci U S A*, 103(51):19518–19523. 50, 174

Bassett, D. S., Nelson, B. G., Mueller, B. A., Camchong, J., and Lim, K. O. (2012). Altered resting state complexity in schizophrenia. *Neuroimage*, 59(3):2196–2207. 6, 17

Batagelj, V. and Mrvar, A. (2001). A subquadratic triad census algorithm for large sparse networks with small maximum degree. *Social Networks*, 23(3):237–243. 106

Beggs, J. M. and Plenz, D. (2003). Neuronal avalanches in neocortical circuits. *J Neurosci*, 23(35):11167–11177. 174

Beggs, J. M. and Plenz, D. (2004). Neuronal avalanches are diverse and precise activity patterns that are stable for many hours in cortical slice cultures. *J Neurosci*, 24(22):5216–5229. 174

Behrens, T. E., Berg, H. J., Jbabdi, S., Rushworth, M. F., and Woolrich, M. W. (2007). Probabilistic diffusion tractography with multiple fibre orientations: What can we gain? *Neuroimage*, 34(1):144–155. 15

Berlucchi, G. (2011). Brain plasticity and cognitive neurorehabilitation. *Neuropsychol Rehabil*, 21(5):560–578. 175

Bezgin, G., Vakorin, V. A., van Opstal, A. J., McIntosh, A. R., and Bakker, R. (2012). Hundreds of brain maps in one atlas: Registering coordinate-independent primate neuro-anatomical data to a standard brain. *Neuroimage*, 62(1):67–76. 5

Biswal, B. B., Mennes, M., Zuo, X. N., Gohel, S., Kelly, C., Smith, S. M., Beckmann, C. F., Adelstein, J. S., Buckner, R. L., Colcombe, S., Dogonowski, A. M., Ernst, M., Fair, D., Hampson, M., Hoptman, M. J., Hyde, J. S., Kiviniemi, V. J., Kötter, R., Li, S. J., Lin, C. P., Lowe, M. J., Mackay, C., Madden, D. J., Madsen, K. H., Margulies, D. S., Mayberg, H. S., McMahon, K., Monk, C. S., Mostofsky, S. H., Nagel, B. J., Pekar, J. J., Peltier, S. J., Petersen, S. E., Riedl, V., Rombouts, S. A., Rypma, B., Schlaggar, B. L., Schmidt, S., Seidler, R. D., Siegle, G. J., Sorg, C., Teng, G. J., Veijola, J., Villringer, A., Walter, M., Wang, L., Weng, X. C., Whitfield-Gabrieli, S., Williamson, P., Windischberger, C., Zang, Y. F., Zhang, H. Y., Castellanos, F. X., and Milham,

M. P. (2010). Toward discovery science of human brain function. *Proc Natl Acad Sci U S A*, 107(10):4734–4739. 7, 176, 178

Bland, J. M. and Altman, D. G. (1986). Statistical methods for assessing agreement between two methods of clinical measurement. *Lancet*, 1(8476):307–310. 12, 160

Bloom, S. A. (1981). Similarity indices in community studies: Potential pitfalls. *Marine Ecology–Progress Series*, 5(8476):125–128. 28

Boccaletti, S., Latora, V., Moreno, Y., Chavez, M., and Hwang, D. (2006). Complex networks: Structure and dynamics. *Physics Reports*, 424(4-5):175–308. 3, 23, 24, 35, 59, 60, 62, 93, 145, 173, 223

Bonifazi, P., Goldin, M., Picardo, M. A., Jorquera, I., Cattani, A., Bianconi, G., Represa, A., Ben-Ari, Y., and Cossart, R. (2009). Gabaergic hub neurons orchestrate synchrony in developing hippocampal networks. *Science*, 326(5958):1419–1424. 151

Braitenberg, V. and Schuz, A. (1998). *Cortex: Statistics and Geometry of Neuronal Connectivity*. Springer-Verlag, 2nd edition. 19, 23, 24

Breakspear, M., Terry, J. R., and Friston, K. J. (2003). Modulation of excitatory synaptic coupling facilitates synchronization and complex dynamics in a biophysical model of neuronal dynamics. *Network*, 14(4):703–732. 136

Bressler, S. L. and Kelso, J. A. (2001). Cortical coordination dynamics and cognition. *Trends Cogn Sci*, 5(1):26–36. 136

Bressler, S. L. and Menon, V. (2010). Large-scale brain networks in cognition: emerging methods and principles. *Trends in cognitive sciences*, 14(6):277–290. 4, 6, 15, 55, 182

Bressler, S. L. and Tognoli, E. (2006). Operational principles of neurocognitive networks. *Int J Psychophysiol*, 60(2):139–148. 175

Broyd, S. J., Demanuele, C., Debener, S., Helps, S. K., James, C. J., and Sonuga-Barke, E. J. (2009). Default-mode brain dysfunction in mental disorders: a systematic review. *Neurosci Biobehav Rev*, 33(3):279–296. 179

Büchel, C. and Friston, K. (2000). Assessing interactions among neuronal systems using functional neuroimaging. *Neural Netw*, 13(8-9):871–882. 5

Bullmore, E. and Sporns, O. (2009). Complex brain networks: graph theoretical analysis of structural and functional systems. *Nat Rev Neurosci*, 10(3):186–198. 6, 9, 13, 182

Burns, G. A. and Young, M. P. (2000). Analysis of the connectional organization of neural systems associated with the hippocampus in rats. *Philos Trans R Soc Lond B Biol Sci*, 355(1393):55–70. 5

Butts, D. A., Weng, C., Jin, J., Yeh, C. I., Lesica, N. A., Alonso, J. M., and Stanley, G. B. (2007). Temporal precision in the neural code and the timescales of natural vision. *Nature*, 449(7158):92–95. 118

Buxton, R. B. and Frank, L. R. (1997). A model for the coupling between cerebral blood flow and oxygen metabolism during neural stimulation. *J Cereb Blood Flow Metab*, 17(1):64–72. 157

Buxton, R. B., Wong, E. C., and Frank, L. R. (1998). Dynamics of blood flow and oxygenation changes during brain activation: the balloon model. *Magn Reson Med*, 39(6):855–864. 157

Buzsaki, G. (2006). *Rhythms of the Brain*. Oxford University Press, USA, 1nd edition. 118

Cabral, J., Hugues, E., Sporns, O., and Deco, G. (2011). Role of local network oscillations in resting-state functional connectivity. *Neuroimage*, 57(1):130–139. 16, 63, 119, 120, 121, 124, 137, 138, 142, 144, 157, 158

Cammoun, L., Gigandet, X., Meskaldji, D., Thiran, J. P., Sporns, O., Do, K. Q., Maeder, P., Meuli, R., and Hagmann, P. (2012). Mapping the human connectome at multiple scales with diffusion spectrum mri. *J Neurosci Methods*, 203(2):386–397. 6, 12, 14, 16, 18, 19, 156, 182

Cang, J., Rentería, R. C., Kaneko, M., Liu, X., Copenhagen, D. R., and Stryker, M. P. (2005). Development of precise maps in visual cortex requires patterned spontaneous activity in the retina. *Neuron*, 48(5):797–809. 174

Case, M. and Soltesz, I. (2011). Computational modeling of epilepsy. *Epilepsia*, 52 Suppl 8:12–15. 151

Cavanna, A. E. and Trimble, M. R. (2006). The precuneus: a review of its functional anatomy and behavioural correlates. *Brain*, 129(Pt 3):564–583. 177, 178

Chang, B. S. and Lowenstein, D. H. (2003). Epilepsy. *N Engl J Med*, 349(13):1257–1266. 145

Chen, B. L., Hall, D. H., and Chklovskii, D. B. (2006). Wiring optimization can relate neuronal structure and function. *Proc Natl Acad Sci U S A*, 103(12):4723–4728. 3

Chen, Z. J., He, Y., Rosa-Neto, P., Germann, J., and Evans, A. C. (2008). Revealing modular architecture of human brain structural networks by using cortical thickness from mri. *Cereb Cortex*, 18(10):2374–2381. 60

Chialvo, D. R. and Bak, P. (1999). Learning from mistakes. *Neuroscience*, 90(4):1137–1148. 174

Chiang, M. C., Barysheva, M., Shattuck, D. W., Lee, A. D., Madsen, S. K., Avedissian, C., Klunder, A. D., Toga, A. W., McMahon, K. L., de Zubicaray, G. I., Wright, M. J., Srivastava, A., Balov, N., and Thompson, P. M. (2009). Genetics of brain fiber architecture and intellectual performance. *J Neurosci*, 29(7):2212–2224. 6

Choe Y, McCormick BH, K. W. (2004). Network connectivity analysis on the temporally augmented c. elegans web: A pilot study. *Society of Neuroscience Abstracts*, 30:921.9. 218

Colizza, V., Flammini, A., Serrano, M. A., and Vespignani, A. (2006). Detecting rich-club ordering in complex networks. *Nat Phys*, 2(2):110–115. 78, 81

Conturo, T. E., Lori, N. F., Cull, T. S., Akbudak, E., Snyder, A. Z., Shimony, J. S., McKinstry, R. C., Burton, H., and Raichle, M. E. (1999). Tracking neuronal fiber pathways in the living human brain. *Proc Natl Acad Sci U S A*, 96(18):10422–10427. 5, 12

Costa, L., Francisco, A., Rodrigues, G. T., and Villas Boas, P. R. (2006). Characterization of complex networks: A survey of measurements. *Advances in Physics*, 56(1):167–242. 35, 60

Costa, L. D. F., Rodrigues, F. A., Hilgetag, C. C., and Kaiser, M. (2009). Beyond the average: Detecting global singular nodes from local features in complex networks. *Europhys. Lett.*, 87(1). 103

Crucitti, P. (2003). Efficiency of scale-free networks: error and attack tolerance. *Physica A: Statistical Mechanics and its Applications*, 320:622–642. 86

Daffertshofer, A. (1998). Effects of noise on the phase dynamics of nonlinear oscillators. *Phys. Rev. E*, 58:327–338. 121

Dale, A. M., Fischl, B., and Sereno, M. I. (1999). Cortical surface-based analysis. i. segmentation and surface reconstruction. *Neuroimage*, 9(2):179–194. 16

Daley, D. J. and Kendall, D. G. (1964). Epidemics and rumours. *Nature*, 204:1118–1118. 145

Damasi, A. (1999). *The Feeling Of What Happens: Body, Emotion and the Making of Consciousness*. Harcourt Brace, New York. 177

Damasio, A. R. (1989). Time-locked multiregional retroactivation: a systems-level proposal for the neural substrates of recall and recognition. *Cognition*, 33(1-2):25–62. 178

Damerau, F. J. (1964). A technique for computer detection and correction of spelling errors. *Communications of the ACM*, 7(3):171–176. 28

Danon, L., Díaz-Guilera, A., Duch, J., and Arenas, A. (2005). Comparing community structure identification. *Journal of Statistical Mechanics: Theory and Experiment*, 2005(09):P09008. 60, 62

Dayan, P. and Abbott, L. F. (2001). *Theoretical Neuroscience: Computational and Mathematical Modeling of Neural Systems*. MIT Press, 1st edition. 118

de Garis, H., Shuo, C., Goertzel, B., and Ruiting, L. (2010). A world survey of artificial brain projects, part i: Large-scale brain simulations. *Neurocomputing*, 74(1–3):3 – 29. 119

Deco, G., Jirsa, V., McIntosh, A. R., Sporns, O., and Kötter, R. (2009). Key role of coupling, delay, and noise in resting brain fluctuations. *Proc Natl Acad Sci U S A*, 106(25):10302–10307. 16, 119, 121, 136

Deco, G., Jirsa, V. K., Robinson, P. A., Breakspear, M., and Friston, K. (2008). The dynamic brain: from spiking neurons to neural masses and cortical fields. *PLoS Comput Biol*, 4(8). 119

Dehaene, S. and Changeux, J. P. (2005). Ongoing spontaneous activity controls access to consciousness: a neuronal model for inattentional blindness. *PLoS Biol*, 3(5). 180

Dehaene, S. and Naccache, L. (2001). Towards a cognitive neuroscience of consciousness: basic evidence and a workspace framework. *Cognition*, 79(1-2):1–37. 75

Dehaene, S., Sergent, C., and Changeux, J. P. (2003). A neuronal network model linking subjective reports and objective physiological data during conscious perception. *Proc Natl Acad Sci U S A*, 100(14):8520–8525. 180

Descoteaux, M., Deriche, R., Knösche, T. R., and Anwander, A. (2009). Deterministic and probabilistic tractography based on complex fibre orientation distributions. *IEEE Trans Med Imaging*, 28(2):269–286. 15

Dorogovtsev, S. N. and Mendes, J. F. (2001). Language as an evolving word web. *Proc Biol Sci*, 268(1485):2603–2606. 3

Douglas, R. J. and Martin, K. A. (2004). Neuronal circuits of the neocortex. *Annu Rev Neurosci*, 27:419–451. 101

Draganski, B. and May, A. (2008). Training-induced structural changes in the adult human brain. *Behav Brain Res*, 192(1):137–142. 175

Duarte-Carvajalino, J. M., Jahanshad, N., Lenglet, C., McMahon, K. L., de Zubicaray, G. I., Martin, N. G., Wright, M. J., Thompson, P. M., and Sapiro, G. (2011). Hierarchical topological

network analysis of anatomical human brain connectivity and differences related to sex and kinship. *Neuroimage*. 6

Eblen, J. D., Phillips, C. A., Rogers, G. L., and Langston, M. A. (2012). The maximum clique enumeration problem: algorithms, applications, and implementations. *BMC Bioinformatics*, 13 Suppl 10. 43

Echtermeyer, C., Costa, L. d. a. F., Rodrigues, F. A., and Kaiser, M. (2011a). Automatic network fingerprinting through single-node motifs. *PLoS One*, 6(1). 6, 103

Echtermeyer, C., Han, C. E., Rotarska-Jagiela, A., Mohr, H., Uhlhaas, P. J., and Kaiser, M. (2011b). Integrating temporal and spatial scales: human structural network motifs across age and region of interest size. *Front Neuroinform*, 5:10–10. 6, 103, 174

Engel, A. K. and Singer, W. (2001). Temporal binding and the neural correlates of sensory awareness. *Trends Cogn Sci*, 5(1):16–25. 118

Erdös, P. and Rényi, A. (1959). On random graphs, I. *Publicationes Mathematicae (Debrecen)*, 6:290–297. 3

Erdös, P. and Rényi, A. (1960). On the evolution of random graphs. *Publ. Math. Inst. Hung. Acad. Sci*, 5:17–61. 3, 125

Euler, L. (1736). Solutio problematis ad geometriam situs pertinentis. *Commentarii Academiae Scientiarum Imperialis Petropolitanae*, pages 128–140. 2

Fair, D. A., Bathula, D., Mills, K. L., Dias, T. G., Blythe, M. S., Zhang, D., Snyder, A. Z., Raichle, M. E., Stevens, A. A., Nigg, J. T., and Nagel, B. J. (2010). Maturing thalamocortical functional connectivity across development. *Front Syst Neurosci*, 4:10–10. 6, 174

Fair, D. A., Cohen, A. L., Dosenbach, N. U., Church, J. A., Miezin, F. M., Barch, D. M., Raichle, M. E., Petersen, S. E., and Schlaggar, B. L. (2008). The maturing architecture of the brain's default network. *Proc Natl Acad Sci U S A*, 105(10):4028–4032. 6, 174

Faloutsos, M., Faloutsos, P., and Faloutsos, C. (1999). On power-law relationships of the internet topology. In *In SIGCOMM*, pages 251–262. 3

Fan, Y., Shi, F., Smith, J. K., Lin, W., Gilmore, J. H., and Shen, D. (2011). Brain anatomical networks in early human brain development. *Neuroimage*, 54(3):1862–1871. 174

Feinberg, D. A., Moeller, S., Smith, S. M., Auerbach, E., Ramanna, S., Gunther, M., Glasser, M. F., Miller, K. L., Ugurbil, K., and Yacoub, E. (2010). Multiplexed echo planar imaging for sub-second whole brain fmri and fast diffusion imaging. *PLoS One*, 5(12). 15

Felleman, D. J. and Van Essen, D. C. (1991). Distributed hierarchical processing in the primate cerebral cortex. *Cereb Cortex*, 1(1):1–47. 5, 14, 218

Ferrarini, L., Veer, I. M., Baerends, E., van Tol, M. J., Renken, R. J., van der Wee, N. J., Veltman, D. J., Aleman, A., Zitman, F. G., Penninx, B. W., van Buchem, M. A., Reiber, J. H., Rombouts, S. A., and Milles, J. (2009). Hierarchical functional modularity in the resting-state human brain. *Hum Brain Mapp*, 30(7):2220–2231. 74, 168

Fischl, B., van der Kouwe, A., Destrieux, C., Halgren, E., Ségonne, F., Salat, D. H., Busa, E., Seidman, L. J., Goldstein, J., Kennedy, D., Caviness, V., Makris, N., Rosen, B., and Dale, A. M. (2004). Automatically parcellating the human cerebral cortex. *Cereb Cortex*, 14(1):11–22. 13, 14

Fornito, A., Zalesky, A., and Bullmore, E. T. (2010). Network scaling effects in graph analytic studies of human resting-state fmri data. *Front Syst Neurosci*, 4:22–22. 13, 16, 76

Fortunato, S. and Barthélemy, M. (2007). Resolution limit in community detection. *Proc Natl Acad Sci U S A*, 104(1):36–41. 62, 66, 69

Fox, M. D. and Raichle, M. E. (2007). Spontaneous fluctuations in brain activity observed with functional magnetic resonance imaging. *Nat Rev Neurosci*, 8(9):700–711. 155, 180

Fox, M. D., Snyder, A. Z., Vincent, J. L., Corbetta, M., Van Essen, D. C., and Raichle, M. E. (2005). The human brain is intrinsically organized into dynamic, anticorrelated functional networks. *Proc Natl Acad Sci U S A*, 102(27):9673–9678. 158

Fox, M. D., Snyder, A. Z., Zacks, J. M., and Raichle, M. E. (2006). Coherent spontaneous activity accounts for trial-to-trial variability in human evoked brain responses. *Nat Neurosci*, 9(1):23–25. 180

Fox, M. D., Zhang, D., Snyder, A. Z., and Raichle, M. E. (2009). The global signal and observed anticorrelated resting state brain networks. *J Neurophysiol*, 101(6):3270–3283. 158

Fransson, P. and Marrelec, G. (2008). The precuneus/posterior cingulate cortex plays a pivotal role in the default mode network: Evidence from a partial correlation network analysis. *Neuroimage*, 42(3):1178–1184. 178

Freeman, L. C. (1978). Centrality in social networks: conceptual clarification. *Soc. Netw.*, 1:215–239. 3, 37

Freeman, L. C. (1996). Some antecedents of social network analysis. *Connections.*, 19:39–42. 3

Freeman, W. J. (2003). Evidence from human scalp electroencephalograms of global chaotic itinerancy. *Chaos*, 13(3):1067–1077. 173

Fries, P. (2005). A mechanism for cognitive dynamics: neuronal communication through neuronal coherence. *Trends Cogn Sci*, 9(10):474–480. 6

Friston, K. J. (1994). Functional and effective connectivity in neuroimaging: A synthesis. *Hum. Brain Mapp.*, 2(1-2):56–78. 5, 14, 156

Friston, K. J. (2000). The labile brain. i. neuronal transients and nonlinear coupling. *Philos Trans R Soc Lond B Biol Sci*, 355(1394):215–236. 144

Friston, K. J., Frith, C. D., Liddle, P. F., and Frackowiak, R. S. (1993). Functional connectivity: the principal-component analysis of large (pet) data sets. *J Cereb Blood Flow Metab*, 13(1):5–14. 5

Friston, K. J., Harrison, L., and Penny, W. (2003). Dynamic causal modelling. *Neuroimage*, 19(4):1273–1302. 156, 157, 158

Friston, K. J., Mechelli, A., Turner, R., and Price, C. J. (2000). Nonlinear responses in fmri: the balloon model, volterra kernels, and other hemodynamics. *Neuroimage*, 12(4):466–477. 156, 157, 158

Gerhard, S. (2010). Connectome viewer. Website: `http://www.connectomics.org/viewer`. 217

Gerstner, W. and Kistler, W. M. (2002). *Spiking Neuron Models*. Cambridge University Press, 2nd edition. 119

Ghosh, A., Rho, Y., McIntosh, A. R., Kötter, R., and Jirsa, V. K. (2008). Noise during Rest Enables the Exploration of the Brain's Dynamic Repertoire. *PLoS Comput Biol*, 4(10):e1000196+. 140, 144, 153, 158, 170

Gisiger, T. (2001). Scale invariance in biology: coincidence or footprint of a universal mechanism? *Biol Rev Camb Philos Soc*, 76(2):161–209. 173

Goldman-Rakic, P. S. (1987). Development of cortical circuitry and cognitive function. *Child Dev*, 58(3):601–622. 178

Goldman-Rakic, P. S. (1995). Architecture of the prefrontal cortex and the central executive. *Ann N Y Acad Sci*, 769:71–83. 179

Gómez-Gardeñes, J., Moreno, Y., and Arenas, A. (2007). Paths to synchronization on complex networks. *Phys Rev Lett*, 98(3):034101–034101. 125

Gómez-Gardeñes, J., Moreno, Y., and Arenas, A. (2011). Evolution of microscopic and mesoscopic synchronized patterns in complex networks. *Chaos*, 21(1):016105–016105. 125

Gómez-Gardeñes, J., Zamora-López, G., Moreno, Y., and Arenas, A. (2010). From modular to centralized organization of synchronization in functional areas of the cat cerebral cortex. *PLoS One*, 5(8). 76, 119, 122, 125, 126, 130, 135, 136, 151

Gong, G., He, Y., Concha, L., Lebel, C., Gross, D. W., Evans, A. C., and Beaulieu, C. (2009). Mapping anatomical connectivity patterns of human cerebral cortex using in vivo diffusion tensor imaging tractography. *Cereb Cortex*, 19(3):524–536. 176

Gong, P., Nikolaev, A. R., and van Leeuwen, C. (2003). Scale-invariant fluctuations of the dynamical synchronization in human brain electrical activity. *Neurosci Lett*, 336(1):33–36. 173

Gong, P. and van Leeuwen, C. (2004). Evolution to a small-world network with chaotic units. *Europhysics Letters*, 67(2):328–333. 65, 175

Greicius, M. D., Supekar, K., Menon, V., and Dougherty, R. F. (2009). Resting-state functional connectivity reflects structural connectivity in the default mode network. *Cereb Cortex*, 19(1):72–78. 159, 164, 177

Gross, T. and Blasius, B. (2008). Adaptive coevolutionary networks: a review. *J R Soc Interface*, 5(20):259–271. 174

Guimerà, R. and Nunes Amaral, L. A. (2005). Functional cartography of complex metabolic networks. *Nature*, 433(7028):895–900. 93, 95, 169

Gusnard, D. A., Raichle, M. E., and Raichle, M. E. (2001). Searching for a baseline: functional imaging and the resting human brain. *Nat Rev Neurosci*, 2(10):685–694. 155, 179

Guye, M., Bettus, G., Bartolomei, F., and Cozzone, P. J. (2010). Graph theoretical analysis of structural and functional connectivity mri in normal and pathological brain networks. *MAGMA*, 23(5-6):409–421. 6

Hagberg, A. A., Schult, D. A., and Swart, P. J. (2008). Exploring network structure, dynamics, and function using networkx. In Varoquaux, G., Vaught, T., and Millman, J., editors, *Proceedings of the 7th Python in Science Conference*, pages 11 – 15, Pasadena, CA USA. 227

Hagmann, P., Cammoun, L., Gigandet, X., Gerhard, S., Grant, P. E., Wedeen, V., Meuli, R., Thiran, J. P., Honey, C. J., and Sporns, O. (2010a). Mr connectomics: Principles and challenges. *J Neurosci Methods*, 194(1):34–45. 4, 13, 14, 15, 182

Hagmann, P., Cammoun, L., Gigandet, X., Meuli, R., Honey, C. J., Wedeen, V. J., and Sporns, O. (2008). Mapping the structural core of human cerebral cortex. *PLoS Biol*, 6(7). 7, 9, 11, 12, 13, 15, 16, 52, 56, 57, 60, 63, 64, 67, 76, 77, 82, 89, 90, 93, 100, 155, 157, 168, 177, 185, 217

Hagmann, P., Cammoun, L., Martuzzi, R., Maeder, P., Clarke, S., Thiran, J. P., and Meuli, R. (2006). Hand preference and sex shape the architecture of language networks. *Hum Brain Mapp*, 27(10):828–835. 6

Hagmann, P., Kurant, M., Gigandet, X., Thiran, P., Wedeen, V. J., Meuli, R., and Thiran, J. P. (2007). Mapping human whole-brain structural networks with diffusion mri. *PLoS One*, 2(7). 11, 12, 16, 52

Hagmann, P., Sporns, O., Madan, N., Cammoun, L., Pienaar, R., Wedeen, V. J., Meuli, R., Thiran, J. P., and Grant, P. E. (2010b). White matter maturation reshapes structural connectivity in the late developing human brain. *Proceedings of the National Academy of Sciences*, 107(44):19067–19072. 6, 174

Hasenkamp, W. and Barsalou, L. W. (2012). Effects of meditation experience on functional connectivity of distributed brain networks. *Front Hum Neurosci*, 6:38–38. 6

He, B. J., Shulman, G. L., Snyder, A. Z., and Corbetta, M. (2007a). The role of impaired neuronal communication in neurological disorders. *Curr Opin Neurol*, 20(6):655–660. 173

He, B. J., Snyder, A. Z., Vincent, J. L., Epstein, A., Shulman, G. L., and Corbetta, M. (2007b). Breakdown of functional connectivity in frontoparietal networks underlies behavioral deficits in spatial neglect. *Neuron*, 53(6):905–918. 173

He, B. J., Snyder, A. Z., Zempel, J. M., Smyth, M. D., and Raichle, M. E. (2008). Electrophysiological correlates of the brain's intrinsic large-scale functional architecture. *Proc Natl Acad Sci U S A*, 105(41):16039–16044. 120

He, Y., Wang, J., Wang, L., Chen, Z. J., Yan, C., Yang, H., Tang, H., Zhu, C., Gong, Q., Zang, Y., and Evans, A. C. (2009). Uncovering intrinsic modular organization of spontaneous brain activity in humans. *PLoS One*, 4(4). 60

Heidemann, R. M., Porter, D. A., Anwander, A., Feiweier, T., Heberlein, K., Knösche, T. R., and Turner, R. (2010). Diffusion imaging in humans at 7t using readout-segmented epi and grappa. *Magn Reson Med*, 64(1):9–14. 15

Hilgetag, C. C., Burns, G. A., O'Neill, M. A., Scannell, J. W., and Young, M. P. (2000). Anatomical connectivity defines the organization of clusters of cortical areas in the macaque monkey and the cat. *Philos Trans R Soc Lond B Biol Sci*, 355(1393):91–110. 7, 23, 42, 62, 66, 74

Hilgetag, C. C. and Kaiser, M. (2004). Clustered organization of cortical connectivity. *Neuroinformatics*, 2(3):353–360. 42, 74

Holland, P. W. and Leinhardt, S. (1974). The statistical analysis of local structure in social networks. Working Paper 44, National Bureau of Economic Research. 101

Holten, D. (2006). Hierarchical edge bundles: visualization of adjacency relations in hierarchical data. *IEEE Transactions on Visualization and Computer Graphics*, 12(5):741–748. 19, 79, 229

Homae, F., Watanabe, H., Otobe, T., Nakano, T., Go, T., Konishi, Y., and Taga, G. (2010). Development of global cortical networks in early infancy. *J Neurosci*, 30(14):4877–4882. 6

Honey, C. J., Kötter, R., Breakspear, M., and Sporns, O. (2007). Network structure of cerebral cortex shapes functional connectivity on multiple time scales. *Proc Natl Acad Sci U S A*, 104(24):10240–10245. 16, 23, 42, 102, 136, 144, 175, 218

Honey, C. J. and Sporns, O. (2008). Dynamical consequences of lesions in cortical networks. *Hum Brain Mapp*, 29(7):802–809. 119, 132, 173

Honey, C. J., Sporns, O., Cammoun, L., Gigandet, X., Thiran, J. P., Meuli, R., and Hagmann, P. (2009). Predicting human resting-state functional connectivity from structural connectivity. *Proc Natl Acad Sci U S A*, 106(6):2035–2040. 4, 13, 156, 159, 161, 163, 164, 171, 173, 177, 182

Honey, C. J., Thivierge, J. P., and Sporns, O. (2010). Can structure predict function in the human brain? *Neuroimage*. 16, 156, 159, 161, 177, 182

Huberman, B. A. (2001). *The Laws of the Web*. MIT Press, Cambridge, MA. 3

Huettel, S. A., Song, A. W., and McCarthy, G. (2009). *Functional Magnetic Resonance Imaging*. Massachusetts: Sinauer, 2nd edition. 5, 156

Humphries, M. D. and Gurney, K. (2008). Network 'small-world-ness': a quantitative method for determining canonical network equivalence. *PLoS One*, 3(4). 50

Humphries, M. D., Gurney, K., and Prescott, T. J. (2006). The brainstem reticular formation is a small-world, not scale-free, network. *Proceedings of the Royal Society B: Biological Sciences*, 273(1585):503–511. 50, 52

Hunter, J. D. (2007). Matplotlib: A 2d graphics environment. *Computing In Science & Engineering*, 9(3):90–95. 228

Izhikevich, E. M. (2004). Which model to use for cortical spiking neurons? *IEEE Trans Neural Netw*, 15(5):1063–1070. 119

Izhikevich, E. M. (2010). Hybrid spiking models. *Philos Transact A Math Phys Eng Sci*, 368(1930):5061–5070. 119

Izhikevich, E. M. and Edelman, G. M. (2008). Large-scale model of mammalian thalamocortical systems. *Proc Natl Acad Sci U S A*, 105(9):3593–3598. 119

Jaccard, P. (1901). Étude comparative de la distribution florale dans une portion des alpes et des jura. *Bulletin de la Société Vaudoise des Sciences Naturelles*, 37:547–579. 28

Jang, J. H., Jung, W. H., Kang, D. H., Byun, M. S., Kwon, S. J., Choi, C. H., and Kwon, J. S. (2011). Increased default mode network connectivity associated with meditation. *Neurosci Lett*, 487(3):358–362. 6

Jbabdi, S. and Johansen-Berg, H. (2011). Tractography: where do we go from here? *Brain Connect*, 1(3):169–183. 5, 14, 15, 181

Jeong, H., Mason, S. P., Barabási, A. L., and Oltvai, Z. N. (2001). Lethality and centrality in protein networks. *Nature*, 411(6833):41–42. 3

Jirsa, V. K., Sporns, O., Breakspear, M., Deco, G., and McIntosh, A. R. (2010). Towards the virtual brain: network modeling of the intact and the damaged brain. *Arch Ital Biol*, 148(3):189–205. 119

Jones, E., Oliphant, T., P, P., et al. (2001). SciPy: Open source scientific tools for Python. 227

Jones, N. C. and Pevzner, P. A. (2004). *An Introduction to Bioinformatics Algorithms (Computational Molecular Biology)*. The MIT Press. 28

Joyce, K. E., Laurienti, P. J., Burdette, J. H., and Hayasaka, S. (2010). A new measure of centrality for brain networks. *PLoS One*, 5(8). 36

Kaiser, M. (2007). Brain architecture: a design for natural computation. *Philos Transact A Math Phys Eng Sci*, 365(1861):3033–3045. 24

Kaiser, M. (2010). Biological networks. Website: http://www.biological-networks.org/. 218

Kaiser, M. (2011). A tutorial in connectome analysis: Topological and spatial features of brain networks. *Neuroimage*, 57(3):892–907. 13, 35, 55, 62, 102, 172, 175, 180

Kaiser, M., Goerner, M., and Hilgetag, C. C. (2008). Criticality of spreading dynamics in hierarchical cluster networks without inhibition. *New Journal of Physics*, 9(5):110–110. 136

Kaiser, M. and Hilgetag, C. C. (2004a). Edge vulnerability in neural and metabolic networks. *Biol Cybern*, 90(5):311–317. 173

Kaiser, M. and Hilgetag, C. C. (2004b). Modelling the development of cortical networks. *Neurocomputing*, 58–60(0):297 – 302. 24, 173

Kaiser, M. and Hilgetag, C. C. (2004c). Spatial growth of real-world networks. *Phys Rev E Stat Nonlin Soft Matter Phys*, 69(3 Pt 2):036103–036103. 24, 173

Kaiser, M. and Hilgetag, C. C. (2006). Nonoptimal component placement, but short processing paths, due to long-distance projections in neural systems. *PLoS Computational Biology*, 2(7):e95+. 24

Kaiser, M. and Hilgetag, C. C. (2007). Development of multi-cluster cortical networks by time windows for spatial growth. *Neurocomputing*, 70(10–12):1829 – 1832. 65, 173

Kaiser, M. and Hilgetag, C. C. (2010). Optimal hierarchical modular topologies for producing limited sustained activation of neural networks. *Front Neuroinform*, 4:8–8. 136

Kaiser, M., Hilgetag, C. C., and Kotter, R. (2010). Hierarchy and dynamics of neural networks. *Frontiers in Neuroinformatics*, 4(0). 55, 56, 58, 171

Kaiser, M., Hilgetag, C. C., and van Ooyen, A. (2009). A simple rule for axon outgrowth and synaptic competition generates realistic connection lengths and filling fractions. *Cereb Cortex*, 19(12):3001–3010. 173

Kaiser, M., Martin, R., Andras, P., and Young, M. P. (2007). Simulation of robustness against lesions of cortical networks. *Eur J Neurosci*, 25(10):3185–3192. 173

Kaiser, M. and Varier, S. (2011). Evolution and development of brain networks: from caenorhabditis elegans to homo sapiens. *Network*, 22(1-4):143–147. 74, 172, 175

Kaisti, K. K., Metsähonkala, L., Teräs, M., Oikonen, V., Aalto, S., Jääskeläinen, S., Hinkka, S., and Scheinin, H. (2002). Effects of surgical levels of propofol and sevoflurane anesthesia on cerebral blood flow in healthy subjects studied with positron emission tomography. *Anesthesiology*, 96(6):1358–1370. 177

Katz, L. C. and Shatz, C. J. (1996). Synaptic activity and the construction of cortical circuits. *Science*, 274(5290):1133–1138. 174

Keller, E. F. (2005). Revisiting "scale-free" networks. *Bioessays*, 27(10):1060–1068. 3

Kitzbichler, M. G., Henson, R. N., Smith, M. L., Nathan, P. J., and Bullmore, E. T. (2011). Cognitive effort drives workspace configuration of human brain functional networks. *J Neurosci*, 31(22):8259–8270. 6, 183

Kitzbichler, M. G., Smith, M. L., Christensen, S. R., and Bullmore, E. (2009). Broadband criticality of human brain network synchronization. *PLoS Comput Biol*, 5(3). 136, 172, 174

Kleinfeld, D., Bharioke, A., Blinder, P., Bock, D. D., Briggman, K. L., Chklovskii, D. B., Denk, W., Helmstaedter, M., Kaufhold, J. P., Lee, W. C., Meyer, H. S., Micheva, K. D., Oberlaender, M., Prohaska, S., Reid, R. C., Smith, S. J., Takemura, S., Tsai, P. S., and Sakmann, B. (2011). Large-scale automated histology in the pursuit of connectomes. *J Neurosci*, 31(45):16125–16138. 4

Köbbert, C., Apps, R., Bechmann, I., Lanciego, J. L., Mey, J., and Thanos, S. (2000). Current concepts in neuroanatomical tracing. *Prog Neurobiol*, 62(4):327–351. 14

Koch, C. and Laurent, G. (1999). Complexity and the nervous system. *Science*, 284(5411):96–98. 65, 149, 151

Kötter, R. (2004). Online retrieval, processing, and visualization of primate connectivity data from the cocomac database. *Neuroinformatics*, 2(2):127–144. 13, 90, 218

Kötter, R. and Stephan, K. E. (2003). Network participation indices: characterizing component roles for information processing in neural networks. *Neural Netw*, 16(9):1261–1275. 103

Kuramoto, Y. (1984). *Chemical Oscillations, Waves, and Turbulence*. Springer-Verlag. 119

Kuramoto, Y. and Battogtokh, D. (2002). Coexistence of Coherence and Incoherence in Nonlocally Coupled Phase Oscillators. *Nonlinear Phenomena in Complex Systems*, 5(4):380–385. 139

Kwok, H. F., Jurica, P., Raffone, A., and van Leeuwen, C. (2007). Robust emergence of small-world structure in networks of spiking neurons. *Cogn Neurodyn*, 1(1):39–51. 175

Kőnig, D. (1936). *Theorie der endlichen und unendlichen Graphen*. Leipzig: Akademische Verlagsgesellschaft. 3

Lakatos, P., Karmos, G., Mehta, A. D., Ulbert, I., and Schroeder, C. E. (2008). Entrainment of neuronal oscillations as a mechanism of attentional selection. *Science*, 320(5872):110–113. 118

Lancichinetti, A. and Fortunato, S. (2011). Limits of modularity maximization in community detection. *Phys Rev E Stat Nonlin Soft Matter Phys*, 84(6 Pt 2):066122–066122. 62, 66

Larsen, R. J. and Marx, M. L. (2010). *An Introduction to Mathematical Statistics and Its Applications*. Pearson, 5th edition. 107

Larson-Prior, L. J., Zempel, J. M., Nolan, T. S., Prior, F. W., Snyder, A. Z., and Raichle, M. E. (2009). Cortical network functional connectivity in the descent to sleep. *Proc Natl Acad Sci U S A*, 106(11):4489–4494. 180

Latora, V. and Marchiori, M. (2001). Efficient behavior of small-world networks. *Phys Rev Lett*, 87(19):198701–198701. 36, 50

Laughlin, S. B., de Ruyter van Steveninck, R. R., and Anderson, J. C. (1998). The metabolic cost of neural information. *Nat Neurosci*, 1(1):36–41. 24, 46

Laughlin, S. B. and Sejnowski, T. J. (2003). Communication in neuronal networks. *Science*, 301(5641):1870–1874. 24, 46

Laureys, S., Owen, A. M., and Schiff, N. D. (2004). Brain function in coma, vegetative state, and related disorders. *Lancet Neurol*, 3(9):537–546. 177

Leergaard, T. B., Hilgetag, C. C., and Sporns, O. (2012). Mapping the connectome: multi-level analysis of brain connectivity. *Front Neuroinform*, 6:14–14. 5

Leicht, E. A. and Newman, M. E. J. (2008). Community Structure in Directed Networks. *Physical Review Letters*, 100(11):118703+. 62

Levenshtein, V. I. (1966). Binary Codes Capable of Correcting Deletions, Insertions and Reversals. *Soviet Physics Doklady*, 10:707+. 28

Luce, R. and Perry, A. (1949). A method of matrix analysis of group structure. *Psychometrika*, 14(2):95–116. 43

Lumer, E. D., Edelman, G. M., and Tononi, G. (1997a). Neural dynamics in a model of the thalamocortical system. i. layers, loops and the emergence of fast synchronous rhythms. *Cereb Cortex*, 7(3):207–227. 119

Lumer, E. D., Edelman, G. M., and Tononi, G. (1997b). Neural dynamics in a model of the thalamocortical system. ii. the role of neural synchrony tested through perturbations of spike timing. *Cereb Cortex*, 7(3):228–236. 119

Lynall, M. E., Bassett, D. S., Kerwin, R., McKenna, P. J., Kitzbichler, M., Muller, U., and Bullmore, E. (2010). Functional connectivity and brain networks in schizophrenia. *J Neurosci*, 30(28):9477–9487. 6

Mandeville, J. B., Marota, J. J., Ayata, C., Zaharchuk, G., Moskowitz, M. A., Rosen, B. R., and Weisskoff, R. M. (1999). Evidence of a cerebrovascular postarteriole windkessel with delayed compliance. *J Cereb Blood Flow Metab*, 19(6):679–689. 157

Maslov, S. and Sneppen, K. (2002). Specificity and stability in topology of protein networks. *Science*, 296(5569):910–913. 25

McAuley, J. J., Costa, and Caetano, T. S. (2007). Rich-club phenomenon across complex network hierarchies. *Appl. Phys. Lett.*, 91:084103. 78

McIntosh, A. R., Kovacevic, N., and Itier, R. J. (2008). Increased brain signal variability accompanies lower behavioral variability in development. *PLoS Comput Biol*, 4(7). 144, 173

McNaughton, B. L., Battaglia, F. P., Jensen, O., Moser, E. I., and Moser, M. B. (2006). Path integration and the neural basis of the 'cognitive map'. *Nat Rev Neurosci*, 7(8):663–678. 118

Melloni, L., Molina, C., Pena, M., Torres, D., Singer, W., and Rodriguez, E. (2007). Synchronization of neural activity across cortical areas correlates with conscious perception. *J Neurosci*, 27(11):2858–2865. 118

Meskaldji, D. E., Ottet, M. C., Cammoun, L., Hagmann, P., Meuli, R., Eliez, S., Thiran, J. P., and Morgenthaler, S. (2011). Adaptive strategy for the statistical analysis of connectomes. *PLoS One*, 6(8). 6

Mesulam, M. M. (1990). Large-scale neurocognitive networks and distributed processing for attention, language, and memory. *Ann Neurol*, 28(5):597–613. 179

Mesulam, M. M. (1998). From sensation to cognition. *Brain*, 121(6):1013–1052. 178, 179

Meunier, D., Achard, S., Morcom, A., and Bullmore, E. (2009a). Age-related changes in modular organization of human brain functional networks. *Neuroimage*, 44(3):715–723. 6, 60

Meunier, D., Lambiotte, R., Fornito, A., Ersche, K. D., and Bullmore, E. T. (2009b). Hierarchical modularity in human brain functional networks. *Front Neuroinform*, 3:37–37. 60, 74, 168

Meyer, K. and Damasio, A. (2009). Convergence and divergence in a neural architecture for recognition and memory. *Trends Neurosci*, 32(7):376–382. 178

Milgram, S. (1967). The Small World Problem. *Psychology Today*, 2:60–67. 3

Miller, K. J., Weaver, K. E., and Ojemann, J. G. (2009). Direct electrophysiological measurement of human default network areas. *Proc Natl Acad Sci U S A*, 106(29):12174–12177. 120

Miller, K. L., Luh, W. M., Liu, T. T., Martinez, A., Obata, T., Wong, E. C., Frank, L. R., and Buxton, R. B. (2000). Characterizing the dynamic perfusion response to stimuli of short duration. *Proc. ISRM*, 8:580. 156

Milo, R., Itzkovitz, S., Kashtan, N., Levitt, R., and Alon, U. (2004a). Response to Comment on "Network Motifs: Simple Building Blocks of Complex Networks" and "Superfamilies of Evolved and Designed Networks". *Science*, 305(5687). 101

Milo, R., Itzkovitz, S., Kashtan, N., Levitt, R., Shen-Orr, S., Ayzenshtat, I., Sheffer, M., and Alon, U. (2004b). Superfamilies of evolved and designed networks. *Science*, 303(5663):1538–1542. 101, 102

Milo, R., Shen-Orr, S., Itzkovitz, S., Kashtan, N., Chklovskii, D., and Alon, U. (2002). Network motifs: simple building blocks of complex networks. *Science*, 298(5594):824–827. 23, 25, 92, 101

Milton, J. and Jung, P. (2003). *Epilepsy as a dynamic disease*. New York: Springer-Verlag. 145

Milton, J. G. (2010). Epilepsy as a dynamic disease: A tutorial of the past with an eye to the future. *Epilepsy & Behavior*, 18:33 – 44. 145, 146, 153

Modha, D. S. and Singh, R. (2010). Network architecture of the long-distance pathways in the macaque brain. *Proc Natl Acad Sci U S A*, 107(30):13485–13490. 5, 76, 77, 90, 91, 218, 221

Morgan, R. J. and Soltesz, I. (2008). Nonrandom connectivity of the epileptic dentate gyrus predicts a major role for neuronal hubs in seizures. *Proc Natl Acad Sci U S A*, 105(16):6179–6184. 151

Mori, S. and Barker, P. B. (1999). Diffusion magnetic resonance imaging: its principle and applications. *Anat Rec*, 257(3):102–109. 11

Mori, S., Crain, B. J., Chacko, V. P., and van Zijl, P. C. (1999). Three-dimensional tracking of axonal projections in the brain by magnetic resonance imaging. *Ann Neurol*, 45(2):265–269. 5

Mountcastle, V. B. (1997). The columnar organization of the neocortex. *Brain*, 120 (Pt 4):701–722. 66

Murta, T., Leal, A., Garrido, M. I., and Figueiredo, P. (2012). Dynamic causal modelling of epileptic seizure propagation pathways: a combined eeg-fmri study. *Neuroimage*, 62(3):1634–1642. 182

Newman, M. E. (2004). Fast algorithm for detecting community structure in networks. *Phys Rev E Stat Nonlin Soft Matter Phys*, 69(6 Pt 2):066133–066133. 60, 69

Newman, M. E. (2006). Modularity and community structure in networks. *Proc Natl Acad Sci U S A*, 103(23):8577–8582. 60, 62, 63

Newman, M. E. J. (2002). Assortative mixing in networks. *Phys. Rev. Lett.*, 89(20):208701. 82

Newman, M. E. J. (2003). The structure and function of complex networks. *SIAM Review*. 3, 24, 35, 172

Newman, M. E. J. and Girvan, M. (2004). Finding and evaluating community structure in networks. *Phys. Rev. E*, 69(2):026113. 59, 60

Niebur, E., Schuster, H. G., and M, K. D. (1991). Collective frequencies and metastability in networks of limit cycle oscillators with time delay. *Phys. Rev. Lett.*, 67 (20):2753–2756. 136

Northoff, G., Qin, P., and Nakao, T. (2010). Rest-stimulus interaction in the brain: a review. *Trends Neurosci*, 33(6):277–284. 179

Nucifora, P. G., Verma, R., Lee, S. K., and Melhem, E. R. (2007). Diffusion-tensor mr imaging and tractography: exploring brain microstructure and connectivity. *Radiology*, 245(2):367–384. 6

Opsahl, T., Colizza, V., Panzarasa, P., and Ramasco, J. J. (2008). Prominence and control: the weighted rich-club effect. *Phys Rev Lett*, 101(16):168702–168702. 78, 79

Pan, H., Epstein, J., Silbersweig, D. A., and Stern, E. (2011). New and emerging imaging techniques for mapping brain circuitry. *Brain Res Rev*, 67(1-2):226–251. 5, 15

Passingham, R. E., Stephan, K. E., and Kötter, R. (2002). The anatomical basis of functional localization in the cortex. *Nat Rev Neurosci*, 3(8):606–616. 70, 103, 163

Pearson, K. (1901). On lines and planes of closest fit to systems of points in space. *Philosophical Magazine*, 2(6):559–572. 102

Pierpaoli, C., Jezzard, P., Basser, P. J., Barnett, A., and Di Chiro, G. (1996). Diffusion tensor mr imaging of the human brain. *Radiology*, 201(3):637–648. 14

Poil, S. S., van Ooyen, A., and Linkenkaer-Hansen, K. (2008). Avalanche dynamics of human brain oscillations: relation to critical branching processes and temporal correlations. *Hum Brain Mapp*, 29(7):770–777. 174

Prill, R. J., Iglesias, P. A., and Levchenko, A. (2005). Dynamic properties of network motifs contribute to biological network organization. *PLoS Biol*, 3(11). 103

Quilichini, P. P., Le Van Quyen, M., Ivanov, A., Turner, D. A., Carabalona, A., Gozlan, H., Esclapez, M., and Bernard, C. (2012). Hub gaba neurons mediate gamma-frequency oscillations at ictal-like event onset in the immature hippocampus. *Neuron*, 74(1):57–64. 151

Raichle, M. E., MacLeod, A. M., Snyder, A. Z., Powers, W. J., Gusnard, D. A., and Shulman, G. L. (2001). A default mode of brain function. *Proc Natl Acad Sci U S A*, 98(2):676–682. 176, 179

Raichle, M. E. and Mintun, M. A. (2006). Brain work and brain imaging. *Annu Rev Neurosci*, 29:449–476. 179, 180

Raichle, M. E. and Snyder, A. Z. (2007). A default mode of brain function: a brief history of an evolving idea. *Neuroimage*, 37(4):1083–1090. 179

Ramachandran, P. and Varoquaux, G. (2011). Mayavi: 3D Visualization of Scientific Data. *Computing in Science & Engineering*, 13(2):40–51. 228

Ravasz, E. and Barabási, A. L. (2003). Hierarchical organization in complex networks. *Phys Rev E Stat Nonlin Soft Matter Phys*, 67(2 Pt 2):026112–026112. 56, 57, 58, 93

Ravasz, E., Somera, A. L., Mongru, D. A., Oltvai, Z. N., and Barabási, A. L. (2002). Hierarchical organization of modularity in metabolic networks. *Science*, 297(5586):1551–1555. 93

Reigl, M., Alon, U., and Chklovskii, D. B. (2004). Search for computational modules in the c. elegans brain. *BMC Biol*, 2:25–25. 101, 107, 114

Reijneveld, J. C., Ponten, S. C., Berendse, H. W., and Stam, C. J. (2007). The application of graph theoretical analysis to complex networks in the brain. *Clin Neurophysiol*, 118(11):2317–2331. 6, 13

Reveley, C. M., Samu, D., Nowotny, T., and Seth, A. K. (2011). An iterative set-theoretic approach to extracting consistent anatomy from the cocomac database. Wiring the Brain, International Conference, Powerscourt, Co Wicklow, Ireland (poster). 185

Rodgers, J. L. and Nicewander, A. W. (1988). Thirteen ways to look at the correlation coefficient. *The American Statistician*, 42(1):59–66. 223

Rubinov, M. and Sporns, O. (2010). Complex network measures of brain connectivity: uses and interpretations. *Neuroimage*, 52(3):1059–1069. 22, 23, 35, 36, 42, 43, 46, 60, 62, 70, 77, 93, 98, 102, 161, 164, 214, 219, 223

Rubinov, M. and Sporns, O. (2011). Weight-conserving characterization of complex functional brain networks. *Neuroimage*, 56(4):2068–2079. 164

Rubinov, M., Sporns, O., van Leeuwen, C., and Breakspear, M. (2009). Symbiotic relationship between brain structure and dynamics. *BMC Neurosci*, 10:55–55. 65, 175

Scannell, J. W., Burns, G. A., Hilgetag, C. C., O'Neil, M. A., and Young, M. P. (1999). The connectional organization of the cortico-thalamic system of the cat. *Cereb Cortex*, 9(3):277–299. 5, 218

Schilbach, L., Eickhoff, S. B., Rotarska-Jagiela, A., Fink, G. R., and Vogeley, K. (2008). Minds at rest? social cognition as the default mode of cognizing and its putative relationship to the "default system" of the brain. *Conscious Cogn*, 17(2):457–467. 180

Schmahmann, J. D., Pandya, D. N., Wang, R., Dai, G., D'Arceuil, H. E., de Crespigny, A. J., and Wedeen, V. J. (2007). Association fibre pathways of the brain: parallel observations from diffusion spectrum imaging and autoradiography. *Brain*, 130(Pt 3):630–653. 12, 13

Schölvinck, M. L., Maier, A., Ye, F. Q., Duyn, J. H., and Leopold, D. A. (2010). Neural basis of global resting-state fmri activity. *Proceedings of the National Academy of Sciences of the United States of America*, 107(22):10238–10243. 120

Schreiber, T. (2000). Measuring information transfer. *Phys. Rev. Lett.*, 85:461–464. 136

Scott, J. (2000). *Social Network Analysis: A Handbook*. Sage Publications, London, 2nd edition. 3

Seidman, S. B. (1983). Network Structure and Minimum Degree. *Social Networks*, 5:269–287. 77

Shanahan, M. (2008). Dynamical complexity in small-world networks of spiking neurons. *Phys Rev E Stat Nonlin Soft Matter Phys*, 78(4 Pt 1):041924–041924. 93, 168

Shanahan, M. (2010). Metastable chimera states in community-structured oscillator networks. *Chaos*, 20(1):013108–013108. 93, 117, 136, 137, 138, 139, 140, 141, 142, 144, 168, 170, 171

Shanahan, M. and Wildie, M. (2012). Knotty-centrality: finding the connective core of a complex network. *PLoS One*, 7(5). 16, 75

Shannon, C. E. and Weaver, W. (1949). *The mathematical theory of communication*. University of Illinois Press, Urbana, Illinois. 224

Sheerin, A. H., Nylen, K., Zhang, X., Saucier, D. M., and Corcoran, M. E. (2004). Further evidence for a role of the anterior claustrum in epileptogenesis. *Neuroscience*, 125(1):57–62. 182

Simon, H. A. (1962). The architecture of complexity. In *Proceedings of the American Philosophical Society*, volume 106, pages 467–482. 65, 74, 149, 151

Skudlarski, P., Jagannathan, K., Calhoun, V. D., Hampson, M., Skudlarska, B. A., and Pearlson, G. (2008). Measuring brain connectivity: diffusion tensor imaging validates resting state temporal correlations. *Neuroimage*, 43(3):554–561. 156, 159, 177, 182

Soltesz, I. and Staley, K. (2008). *Computational neuroscience in epilepsy*. Academic Press, UK. 145, 153

Somogyi, P., Tamás, G., Lujan, R., and Buhl, E. H. (1998). Salient features of synaptic organisation in the cerebral cortex. *Brain Res Brain Res Rev*, 26(2-3):113–135. 66

Sporns, O. (2006). Small-world connectivity, motif composition, and complexity of fractal neuronal connections. *Biosystems*, 85(1):55–64. 23, 54, 56, 66, 69, 74, 125, 168

Sporns, O. (2010). *Netwoks of the Brain*. The MIT Press. 2, 4, 24, 50, 55, 74, 171, 172, 177, 182, 183

Sporns, O. (2011). The non-random brain: efficiency, economy, and complex dynamics. *Front Comput Neurosci*, 5:5–5. 50

Sporns, O. and Honey, C. J. (2006). Small worlds inside big brains. *Proc Natl Acad Sci U S A*, 103(51):19219–19220. 50, 53

Sporns, O., Honey, C. J., and Kötter, R. (2007). Identification and classification of hubs in brain networks. *PLoS One*, 2(10). 16, 23, 48, 92, 93, 94, 100, 102, 104, 114

Sporns, O. and Kötter, R. (2004). Motifs in Brain Networks. *PLoS Biol*, 2(11):e369+. 4, 16, 23, 24, 25, 66, 102, 114

Sporns, O. and Rubinov, M. (2010). Brain connectivity toolbox. Website: https://brain-connectivity-toolbox.net/bct/Home. 218

Sporns, O., Tononi, G., and Edelman, G. M. (2000). Theoretical neuroanatomy: relating anatomical and functional connectivity in graphs and cortical connection matrices. *Cereb Cortex*, 10(2):127–141. 7, 65, 102, 171, 175

Sporns, O., Tononi, G., and Kötter, R. (2005). The human connectome: A structural description of the human brain. *PLoS Comput Biol*, 1(4). 4, 11, 182

Stam, C. J. (2005). Nonlinear dynamical analysis of eeg and meg: review of an emerging field. *Clin Neurophysiol*, 116(10):2266–2301. 171

Stam, C. J. and van Straaten, E. C. (2012). The organization of physiological brain networks. *Clin Neurophysiol*, 123(6):1067–1087. 74

Steel, R. G. D. and Torrie, J. H. (1960). *Principles and Procedures of Statistics*. New York: McGraw-Hill. 39

Stelling, J., Klamt, S., Bettenbrock, K., Schuster, S., and Gilles, E. D. (2002). Metabolic network structure determines key aspects of functionality and regulation. *Nature*, 420(6912):190–193. 3

Strogatz, S. H. (2000). From kuramoto to crawford: exploring the onset of synchronization in populations of coupled oscillators. *Physica D: Nonlinear Phenomena*, 143(1–4):1 – 20. 127

Stufflebeam, S. M., Witzel, T., Mikulski, S., Hämäläinen, M. S., Temereanca, S., Barton, J. J., Tuch, D. S., and Manoach, D. S. (2008). A non-invasive method to relate the timing of neural activity to white matter microstructural integrity. *Neuroimage*, 42(2):710–716. 14

Sutherland, M. T., McHugh, M. J., Pariyadath, V., and Stein, E. A. (2012). Resting state functional connectivity in addiction: Lessons learned and a road ahead. *Neuroimage*, 62(4):2281–2295. 179

Szentágothai, J. (1983). The modular architectonic principle of neural centers. *Rev Physiol Biochem Pharmacol*, 98:11–61. 66

Sørensen, T. (1948). A method of establishing groups of equal amplitude in plant sociology based on similarity of species content. *Kongelige Danske Videnskabernes Selskab. Biol.*, 4:1–34. 28

Toga, A. W., Clark, K. A., Thompson, P. M., Shattuck, D. W., and Van Horn, J. D. (2012). Mapping the human connectome. *Neurosurgery*, 71(1):1–5. 7, 182

Tomasi, D. and Volkow, N. D. (2011a). Association between functional connectivity hubs and brain networks. *Cereb Cortex*, 21(9):2003–2013. 156, 176

Tomasi, D. and Volkow, N. D. (2011b). Functional connectivity hubs in the human brain. *Neuroimage*, 57(3):908–917. 156, 176

Tomasi, D. and Volkow, N. D. (2012). Aging and functional brain networks. *Mol Psychiatry*, 17(5):549–558. 6

Tononi, G., Edelman, G. M., and Sporns, O. (1998). Complexity and coherency: integrating information in the brain. *Trends Cogn Sci*, 2(12):474–484. 34

Tononi, G., Sporns, O., and Edelman, G. M. (1994). A measure for brain complexity: relating functional segregation and integration in the nervous system. *Proc Natl Acad Sci U S A*, 91(11):5033–5037. 50, 66, 74, 102

Uhlhaas, P. J., Pipa, G., Lima, B., Melloni, L., Neuenschwander, S., Nikolic, D., and Singer, W. (2009a). Neural synchrony in cortical networks: history, concept and current status. *Front Integr Neurosci*, 3:17–17. 118, 129, 145

Uhlhaas, P. J., Roux, F., Singer, W., Haenschel, C., Sireteanu, R., and Rodriguez, E. (2009b). The development of neural synchrony reflects late maturation and restructuring of functional networks in humans. *Proc Natl Acad Sci U S A*, 106(24):9866–9871. 174

Ullah, G. and Schiff, S. J. (2009). Models of epilepsy. Website: `http://www.scholarpedia.org/article/Models_of_epilepsy`. 145

Valencia, M., Pastor, M. A., Fernández-Seara, M. A., Artieda, J., Martinerie, J., and Chavez, M. (2009). Complex modular structure of large-scale brain networks. *Chaos*, 19(2):023119–023119. 60

van den Berg, D. and Van Leeuwen, C. (2004). Adaptive rewiring in chaotic networks renders small-world connectivity with consistent clusters. *Europhysics Lett*, 65:459–464. 65

van den Heuvel, M., Mandl, R., Luigjes, J., and Hulshoff Pol, H. (2008). Microstructural organization of the cingulum tract and the level of default mode functional connectivity. *J Neurosci*, 28(43):10844–10851. 164, 177

van den Heuvel, M. P., Mandl, R. C., Kahn, R. S., and Hulshoff Pol, H. E. (2009a). Functionally linked resting-state networks reflect the underlying structural connectivity architecture of the human brain. *Hum Brain Mapp*, 30(10):3127–3141. 159, 177

van den Heuvel, M. P., Mandl, R. C., Stam, C. J., Kahn, R. S., and Hulshoff Pol, H. E. (2010). Aberrant frontal and temporal complex network structure in schizophrenia: a graph theoretical analysis. *J Neurosci*, 30(47):15915–15926. 6, 52

Van den Heuvel, M. P. and Sporns, O. (2011). Rich-club organization of the human connectome. *J Neurosci*, 31(44):15775–15786. 7, 17, 48, 52, 56, 60, 64, 65, 76, 77, 82, 83, 90, 100, 169, 176, 177

van den Heuvel, M. P., Stam, C. J., Kahn, R. S., and Hulshoff Pol, H. E. (2009b). Efficiency of functional brain networks and intellectual performance. *J Neurosci*, 29(23):7619–7624. 6

Van Dijk, K. R., Hedden, T., Venkataraman, A., Evans, K. C., Lazar, S. W., and Buckner, R. L. (2010). Intrinsic functional connectivity as a tool for human connectomics: theory, properties, and optimization. *J Neurophysiol*, 103(1):297–321. 159

Van Essen, D. C. and Ugurbil, K. (2012). The future of the human connectome. *Neuroimage*, 62(2):1299–1310. 5

Van Rossum, G. (2003). *The Python Language Reference Manual*. Network Theory Ltd. 227

Vaudano, A. E., Laufs, H., Kiebel, S. J., Carmichael, D. W., Hamandi, K., Guye, M., Thornton, R., Rodionov, R., Friston, K. J., Duncan, J. S., and Lemieux, L. (2009). Causal hierarchy within the thalamo-cortical network in spike and wave discharges. *PLoS One*, 4(8). 152, 170

Verstraete, E., van den Heuvel, M. P., Veldink, J. H., Blanken, N., Mandl, R. C., Hulshoff Pol, H. E., and van den Berg, L. H. (2010). Motor network degeneration in amyotrophic lateral sclerosis: a structural and functional connectivity study. *PLoS One*, 5(10). 9

Vincent, J. L., Patel, G. H., Fox, M. D., Snyder, A. Z., Baker, J. T., Van Essen, D. C., Zempel, J. M., Snyder, L. H., Corbetta, M., and Raichle, M. E. (2007). Intrinsic functional architecture in the anaesthetized monkey brain. *Nature*, 447(7140):83–86. 180

Wang, J., Wang, L., Zang, Y., Yang, H., Tang, H., Gong, Q., Chen, Z., Zhu, C., and He, Y. (2009). Parcellation-dependent small-world brain functional networks: a resting-state fmri study. *Hum Brain Mapp*, 30(5):1511–1523. 16

Watts, D. J. (2004). The " New" Science of Networks. *Annual Review of Sociology*, 30(1):243–270. 3, 35

Watts, D. J. and Strogatz, S. H. (1998). Collective dynamics of 'small-world' networks. *Nature*, 393(6684):440–442. 3, 24, 34, 43, 50, 54, 180, 221

Wedeen, V. J., Hagmann, P., Tseng, W. Y., Reese, T. G., and Weisskoff, R. M. (2005). Mapping complex tissue architecture with diffusion spectrum magnetic resonance imaging. *Magn Reson Med*, 54(6):1377–1386. 12, 15

Wedeen, V. J., Rosene, D. L., Wang, R., Dai, G., Mortazavi, F., Hagmann, P., Kaas, J. H., and Tseng, W. Y. (2012). The geometric structure of the brain fiber pathways. *Science*, 335(6076):1628–1634. 13

Wedeen, V. J., Wang, R. P., Schmahmann, J. D., Benner, T., Tseng, W. Y., Dai, G., Pandya, D. N., Hagmann, P., D'Arceuil, H., and de Crespigny, A. J. (2008). Diffusion spectrum magnetic resonance imaging (dsi) tractography of crossing fibers. *Neuroimage*, 41(4):1267–1277. 15

Weliky, M. and Katz, L. C. (1999). Correlational structure of spontaneous neuronal activity in the developing lateral geniculate nucleus in vivo. *Science*, 285(5427):599–604. 174

White, J. G., Southgate, E., Thomson, J. N., and Brenner, S. (1986). The structure of the nervous system of the nematode caenorhabditis elegans. *Philos Trans R Soc Lond B Biol Sci*, 314(1165):1–340. 5

WHO (2009). Epilepsy. Website: http://www.who.int/mediacentre/factsheets/fs999/en/. 145

Wilson, H. R. and Cowan, J. D. (1972). Excitatory and inhibitory interactions in localized populations of model neurons. *Biophys J*, 12(1):1–24. 136

Yan, C. and He, Y. (2011). Driving and driven architectures of directed small-world human brain functional networks. *PLoS One*, 6(8). 94

Yao, Y. Y. (2003). *Information-theoretic measures for knowledge discovery and data mining*, pages 115–136. Springer. 224, 225

Yap, P. T., Fan, Y., Chen, Y., Gilmore, J. H., Lin, W., and Shen, D. (2011). Development trends of white matter connectivity in the first years of life. *PLoS One*, 6(9). 4, 6

Yendiki, A., Panneck, P., Srinivasan, P., Stevens, A., Zöllei, L., Augustinack, J., Wang, R., Salat, D., Ehrlich, S., Behrens, T., Jbabdi, S., Gollub, R., and Fischl, B. (2011). Automated probabilistic reconstruction of white-matter pathways in health and disease using an atlas of the underlying anatomy. *Front Neuroinform*, 5:23–23. 4

Young, M. P. (1993). The organization of neural systems in the primate cerebral cortex. *Proc Biol Sci*, 252(1333):13–18. 5, 218

Young, M. P., Hilgetag, C. C., and Scannell, J. W. (2000). On imputing function to structure from the behavioural effects of brain lesions. *Philos Trans R Soc Lond B Biol Sci*, 355(1393):147–161. 132

Zalesky, A., Fornito, A., Harding, I. H., Cocchi, L., Yücel, M., Pantelis, C., and Bullmore, E. T. (2010). Whole-brain anatomical networks: does the choice of nodes matter? *Neuroimage*, 50(3):970–983. 16, 22, 76

Zalesky, A., Fornito, A., Seal, M. L., Cocchi, L., Westin, C. F., Bullmore, E. T., Egan, G. F., and Pantelis, C. (2011). Disrupted axonal fiber connectivity in schizophrenia. *Biol Psychiatry*, 69(1):80–89. 6, 9

Zamora-López, G., Zhou, C., and Kurths, J. (2009). Graph analysis of cortical networks reveals complex anatomical communication substrate. *Chaos*, 19(1):015117–015117. 76, 125

Zamora-López, G., Zhou, C., and Kurths, J. (2010). Cortical hubs form a module for multisensory integration on top of the hierarchy of cortical networks. *Front Neuroinformatics*, 4:1–1. 23, 72, 76, 82, 83, 90, 125, 135, 163

Zemanova, L., Zhou, C., and Kurths, J. (2006). Structural and functional clusters of complex brain networks. *Physica D: Nonlinear Phenomena*, 224(1-2):202–212. 135

Zhan, W. and Yang, Y. (2006). How accurately can the diffusion profiles indicate multiple fiber orientations? a study on general fiber crossings in diffusion mri. *J Magn Reson*, 183(2):193–202. 14

Zhou, C., Zemanová, L., Zamora, G., Hilgetag, C. C., and Kurths, J. (2006). Hierarchical organization unveiled by functional connectivity in complex brain networks. *Phys Rev Lett*, 97(23):238103–238103. 135

Zhou, C., Zemanová, L., Zamora-López, G., Hilgetag, C. C., and Kurths, J. (2007). Structure–function relationship in complex brain networks expressed by hierarchical synchronization. *New J. Phys.*, 9(6):178+. 135, 168

Zhou, S. and Mondragón, R. J. (2004). The rich-club phenomenon in the internet topology. *IEEE Comm. Lett.*, 8(3):180–182. 78, 79, 81

Zuo, X. N., Ehmke, R., Mennes, M., Imperati, D., Castellanos, F. X., Sporns, O., and Milham, M. P. (2011). Network centrality in the human functional connectome. *Cereb Cortex*. 6, 35

Appendix A

Formal definition of applied complex network measures

Table A.1 introduces the general notation applied in this study, if not stated otherwise. Table A.2 and Table A.3 formally define the applied complex network measures. All formulae are defined for undirected networks. For a more complete collection of complex network measures relevant in the neurosciences and for further references, see Rubinov and Sporns (2010).

Notation	Definition
N	set of all network nodes
n	number of network nodes
L	set of all network links
l	number of network links
(i, j)	link between node i and node j $(i, j \in N)$
w_{ij}	connection weight of link between node i and node j
a_{ij}	connection status from node i to node j $a_{ij} = 1$ if link (i, j) exist (or $w_{ij} \neq 0$) $a_{ij} = 0$ otherwise $a_{ii} = 0$ (no self–loops)

Table A.1: Notation of basic concepts in complex network theory

Measure	Definition
Number of links	$l = \sum_{i,j \in N} a_{ij}$
Sum of weights	$l^W = \sum_{i,j \in N} w_{ij}$
Degree of node i	$k_i = \sum_{j \in N} a_{ij}$
Weighted degree of i	$k_i^W = \sum_{j \in N} w_{ij}$
Mean degree	$K_m = \frac{1}{n} \sum_{i \in N} k_i$
Connection density	$K_d = \frac{\sum_{i \in N} k_i}{n(n-1)}$
Number of triangles around i	$t_i = \frac{1}{2} \sum_{j,h \in N} a_{ij} a_{ih} a_{jh}$
Clustering coefficient	$C = \frac{1}{n} \sum_{i \in N} C_i = \frac{1}{n} \sum_{i \in N} \frac{2t_i}{k_i(k_i-1)}$

Table A.2: Formal definitions of complex network theoretical measures

Measure	Definition
Shortest path length from i to j	$d_{ij} = \sum_{a_{ij} \in g_{i \leftrightarrow j}} a_{ij}$, where $g_{i \leftrightarrow j}$ is the shortest path between i and j
Diameter	$D = \max_{\substack{i,j \in N \\ d_{ij} \neq \infty}} d_{ij}$
Characteristic path length	$L = \frac{1}{n} \sum_{i \in N} \frac{\sum_{j \in N, j \neq i} d_{ij}}{n-1}$
Global efficiency	$E = \frac{1}{n} \sum_{i \in N} \frac{\sum_{j \in N, j \neq i} (d_{ij})^{-1}}{n-1}$
Small-world index	$SWI = \frac{E}{E_{sn}} / \frac{C}{C_{sn}}$, where X_{sn} is the mean of measure X calculated to the network's (random) surrogate networks (see Section 4.5)
Betweenness centrality of node i	$b_i = \frac{1}{(n-1)(n-2)} \sum_{\substack{h,j \in N \\ h \neq j, h \neq i, j \neq i}} \frac{\rho_{hj}(i)}{\rho_{hj}}$, where ρ_{hj} is the number of shortest paths (paths with minimum lengths) between h and j, and $\rho_{hj}(i)$ is the number of shortest paths between h and j that pass through i.
Participation coefficient of node i	$y_i = 1 - \sum_{m \in M} \left(\frac{k_i(m)}{k_i} \right)^2$, where M is the set of modules, and $k_i(m)$ is the number of links between i and all nodes in module m.

Table A.3: Formal definitions of complex network theoretical measures (continued)

Appendix B

Summary analysis of various structural brain networks

The software developed during this study (Appendix D) has been tested and applied on a set of synthetic and real brain networks. As a brief summary of our results, we provide a survey of analyses of several publicly available brain networks in Table B.1.

These brain networks were acquired using different methodologies, leading to mathematically fundamentally different types of networks. Among them, we find directed and undirected networks, weighted as well as binary ones, some of them are flat (non-hierarchical), while others possess a multi-level hierarchy highly intertwined with the actual connectivity. We emphasise how the great abstraction power of graph theory and complex network science makes it able to represent, analyse and compare all these brain networks under a unified framework.

B.1 List of analysed brain maps

Below we enumerate the utilised networks along with their original publication ('reference'), the source where the datasets were actually obtained for this study ('source'), and their abbreviations in Table B.1.

Human Diffusion Spectrum Imaging

reference: Hagmann et al. (2008)

source: Gerhard (2010)

abbreviation: [Hum DSI]

CoCoMac IBM

reference: Modha and Singh (2010)

source: Modha and Singh (2010) Supp. Mat.

abbreviation: [Mac IBM]

Macaque Cortex By Kötter

reference: Kötter (2004)

source: Kaiser (2010)

abbreviation: [Mac CxK]

Macaque Cortex By Young

reference: Young (1993)

source: Sporns and Rubinov (2010)

abbreviation: [Mac CxY]

Macaque Visual Cortex

reference: Felleman and Van Essen (1991)

source: Sporns and Rubinov (2010)

abbreviation: [Mac VCx]

Macaque Visual SensoryMotor Cortex

reference: Honey et al. (2007)

source: Sporns and Rubinov (2010)

abbreviation: [Mac VSM]

Cat Thalamo Cortex

reference: Scannell et al. (1999)

source: Sporns and Rubinov (2010)

abbreviation: [Cat TCx]

C. elegans

reference: Choe Y (2004)

source: Kaiser (2010)

abbreviation: [C. Elgns]

B.2 Description of attributes and measures

Hierarchy: Properties of the hierarchy graph, if there is any. Formally, the hierarchy graph (hierarchy tree) is binary, directed acyclic graph (DAC) by its nature. Each of its nodes has zero or one parent or predecessor node (its most directly containing brain region), and can have an arbitrary number of child or successor nodes. The node not having a parent node, at the top of the hierarchy, is called the *root node*. Nodes without any child node, at the bottom of the hierarchy, are called *leaf nodes*.

- # nodes: number of nodes in the hierarchy graph, each one representing a usually anatomically defined greater structure, region or single neuron of the brain, depending on the dataset.
- # leaf nodes: number of nodes in the hierarchy graph that are at the bottom of the hierarchy, that is, are not the parent of any other nodes further down in the hierarchy.
- max depth: maximum of the distances between the root node and all the leaf nodes, giving the maximal depth of the hierarchical tree.
- mean depth: mean of the distances between the root node and all the leaf nodes.

Connectivity: Characteristics of the connectivity graph. The connectivity graph can be weighted or unweighted (binary), directed or undirected, and it can contain information about the spatial location of its nodes, and the length of its edges. Standard complex network analysis in the neurosciences currently omits self-edges (connection that links the node to itself) and parallel edges (multiple edges between the same node pair), thus these edges must be removed/aggregated prior to analysis. For a formal mathematical definition of the measures below, see Appendix A and Rubinov and Sporns (2010).

- # nodes: number of nodes in the connectivity graph, each one representing a usually anatomically defined region or neuron of the brain, depending on the resolution of investigation and the nervous system under study.
- position info: gives the kind of spatial information available for the nodes: 3 dimensional (3D), 2 dimensional (2D), or not available (n/a).
- # edges: number of edges in the connectivity graph, each one representing a traced fibre tract bundle connection between two regions, or a synaptic connection between two neurons. The presence or absence of directionality information of the edges depends on the applied data acquisition method.

- mean degree: sum of degrees over the number of nodes. It gives how many direct neighbours an average node has.
- connection density: actual over maximal connections. Describes how strongly connected the network is, on average (mean degree, compensated by the size of the network).
- reciprocal connections: ratio of reciprocal connections in directed networks. It describes the extent of directly two-way, short circuit information flow, as opposed to the longer feedback time one-way region connectivity.
- transmission coefficient (std/mean): transmission coefficient standard deviation over mean. For directed networks, transmission coefficient is the average of the afferent/efferent connections ratio, for all nodes. Nodes with high transmission coefficient are more involved in broadcasting information, while nodes with low transmission coefficient are more specialised in integrating incoming information. In networks with high deviation around their respective mean transmission coefficient ratio, there are more specialised broadcaster and integrator nodes. On the other hand, in networks with low standard deviation/mean ratio, broadcaster and integrator roles are much less clearly distinguishable among the nodes.
- diameter: the maximum distance between any two node pairs in the network. It provides a simple description about how tightly connected the network is, or how long it maximally takes for a node to transmit (receive) information to (from) the others.
- efficiency: the average inverse shortest path length. Unlike shortest path length, efficiency can be meaningfully computed on disconnected graphs (efficiency is zero between any two nodes without a route between them, while the shortest path is infinite). Generally, networks with high efficiency are more tightly coupled, and thus are able to quickly integrate information.
- surrogate network efficiency: efficiency of n=20 random surrogate networks of the brain connectivity (Chapter 3). Surrogate efficiency is used as a null-hypothesis value to indicate the significance of the network's own efficiency and small-world architecture.
- clustering coefficient: clustering coefficient, a simple, triangle-connectivity based measure of segregation. It gives the fraction of node neighbours that are also neighbours of each other for an average node. Higher clustering coefficient values indicate greater local segregation in the network.

- surrogate network clustering coefficient: clustering coefficient of 20 random surrogate networks of the brain connectivity. Surrogate clustering coefficient is used as a null-hypothesis value to indicate the significance of the network's own clustering coefficient and small-world architecture. Standard deviations in the mean surrogate clustering coefficients are negligible for all brain maps ($< 2\%$).
- small-world index: a complex network is said to have the small-world property if, despite of its large size and high clustering, there still is a relatively short path between any two nodes. That is, if the clustering coefficient of a network is significantly higher than those of its surrogate networks, while it still being able to maintain high efficiency (short characteristic path length), then we call the network small-world (Watts and Strogatz (1998)).
- betweenness centrality standard deviation/mean: standard deviation over mean of nodal betweenness centralities. The betweenness centrality of a node is defined as the fraction of shortest paths that pass through it. Nodes possessing high betweenness centrality often act as inter- or intramodular hubs, providing short connection routes between many node pair. Networks with high std/mean ratio in this metric possess clearly distinguishable hub nodes.
- innermost core #: k degree of innermost core (Modha and Singh (2010)). The kth core of the network is defined as the maximal set of nodes in which each node has at least k connections to the others in the core. The innermost core is the last, non-empty core of the network with the highest k. Networks with high innermost core numbers are integrated in a deeply nested manner, and their innermost core can act as the 'backbone' of the network. Such a network backbone is comprised of tightly coupled and thus effectively cooperating nodes, that are efficient in collecting, integrating and spreading out information from and to more peripheral nodes. Directed networks are converted to undirected for this analysis.
- nodes in innermost core %: number of nodes in innermost core proportional to the network size (see above). In general, the more nodes the innermost core is comprised of, the more uniform (homogeneous) the topology of network is, thus the less specialised its nodes are.

Table B.1: Summary of complex network metrics of some structural brain networks

Map	Hierarchy					Connectivity																							
	# nodes	# leaf nodes	max depth	mean depth	directed	weighted	# nodes	position info	# edges	mean degree	conn. density %	recipr. conn.s %	trsm. coeff. s/m	diameter	efficiency	surr. net eff.	clustering coeff.	surr. net c. c.	small-world index	btw. centr. s/m	innermost core #	nodes in i. c. %
Hum DSI	1070	998	4	2.93	-	+	998	3D	17865	17.9	3.59	n/a	n/a	6	.36	.46	.46	.05	7.40	1.81	26	11.2
Mac IBM	382	266	9	4.57	+	-	360	n/a	6602	18.3	5.11	42.2	1.08	5	.41	.43	.42	.28	1.44	2.17	29	33.9
Mac CxK	n/a	n/a	n/a	n/a	+	-	94	3D	2390	25.4	27.3	73.2	.94	4	.55	.57	.77	.65	1.15	2.60	45	36.2
Mac CxY	n/a	n/a	n/a	n/a	+	-	71	n/a	746	10.5	15.0	82.6	.32	5	.49	.52	.50	.40	1.18	1.46	16	43.7
Mac VCx	n/a	n/a	n/a	n/a	+	-	32	n/a	315	9.8	31.8	76.8	.40	3	.59	.60	.65	.65	1.02	1.28	15	40.6
Mac SMC	n/a	n/a	n/a	n/a	+	-	47	n/a	505	10.7	23.4	76.0	.65	4	.56	.58	.64	.55	1.17	1.32	18	40.4
Cat TCx	n/a	n/a	n/a	n/a	+	+	52	n/a	818	15.7	30.8	74.1	.35	3	.62	.64	.66	.61	1.07	1.30	22	46.2
C. Elgns	n/a	n/a	n/a	n/a	+	-	277	2D	2105	7.60	2.75	17.8	1.51	5	.27	.32	.28	.12	1.89	1.75	11	11.2

Appendix C

Measuring the relationship between complex network measures

In many cases, topological network properties are interrelated (Boccaletti et al. (2006), Rubinov and Sporns (2010)). Sometimes, typically for complex network metrics from the same measure group (eg. measures of integration or segregation), this relation is already evident by the nature of the measures' calculation (eg. centrality measures are usually based on node degrees and shortest paths), thus some level of dependence (overlap in information content) is *a priori* expected in those cases. On the other hand, for any given network, the relationship will also be characteristic to (influenced by) the topological properties (organisation) of *that network*. Therefore by studying the relationship between the distribution of pairs of (nodal) complex network measure values, one is able to gain insight about the *network-specific* relation of the measures, that is, how the assessed topological properties are interrelated within the network at hand.

In the current study, we use two analysis techniques to assess the relationship between complex network metrics of the human cortical network: *Pearson correlation coefficient* and *normalised mutual information* or *redundancy*. Pearson product-moment correlation coefficient (Rodgers and Nicewander (1988)), a statistical measures to assess the degree and sign of linear dependence (correlation) between two 'variables' X and Y, each represented by a set of samples, $X_1, X_2, ..., X_n$ and $Y_1, Y_2, ..., Y_n$:

$$C = \frac{\sum_{i=1}^{n}(X_i - \overline{X})(Y_i - \overline{Y})}{\sqrt{\sum_{i=1}^{n}(X_i - \overline{X})^2}\sqrt{\sum_{i=1}^{n}(Y_i - \overline{Y})^2}} \tag{C.1}$$

Pearson correction coefficient, taking its values from the interval $[-1, 1]$, measures the degree of linear dependence between the variables (sample sets) in its magnitude (absolute value) and the type of correlation (positive or negative) in its sign.

From an information theoretical point of view, complex network measure indexes of network

nodes, such as their degree centrality, clustering coefficient or s-core value, can also be interpreted as samples of an unknown distribution. Taking this approach, individual nodal measure-pairs represent corresponding observations of two stochastic processes, between which various types of (stochastic) relationships can be tested, such as (dis)similarity, divergence, dependency, one- or two-way association, or redundancy.

Taking two stochastic variables (observation vectors), X and Y, with value sets (domains) V_X and V_Y, and their individual and joint probability density functions (normalised distributions) $p(x)$, $p(y)$ and $p(x, y)$, their $I(X, Y)$ mutual information can be calculated (estimated) by

$$I(X,Y) = H(X) + H(Y) - H(X,Y), \tag{C.2}$$

where $H(X)$ is the entropy of X:

$$H(X) = -\sum_{x \in V_x} p(x) * log(p(x)), \tag{C.3}$$

and $H(X, Y)$ is the joint entropy of X and Y:

$$H(X,Y) = -\sum_{x \in V_X} \sum_{y \in V_Y} p(x,y) * log(p(x,y)), \tag{C.4}$$

Mutual information measures the dependence between two stochastic variables, that is, how much uncertainty is reduced about one variable by knowing the value of the other (Shannon and Weaver (1949)). Being a symmetric, dimensionless quantity (usually measured in bits), high mutual information indicates high dependence (large reduction in uncertainty), while zero mutual information means that the two variables are independent.

By considering the limits of the $H(X, Y)$ mutual information:

$$min(H(X), H(Y)) \quad \leq \quad H(X,Y) \quad \leq \quad H(X) + H(Y) \tag{C.5}$$

$$\Downarrow$$

$$0 \quad \leq \quad I(X,Y) \quad \leq \quad min(H(X), H(Y)) \tag{C.6}$$

one can use a normalised variant of mutual information

$$R(X,Y) = \frac{I(X,Y)}{min(H(X), H(Y))}. \tag{C.7}$$

which is also referred to as the normalised redundancy between X and Y (Yao (2003)). By applying the above normalisation, we gain a dependency metric which is independent of the individual entropies of the stochastic variables (in our case, complex network measures), consequently making direct comparison between the redundancies of various pairs of network measures possible. We

note, that, as the above formulation implies, normalised redundancy "is the degree of deviation of the joint distribution from the independence distribution" (Yao (2003)). It is also important, that both Pearson correlation coefficient and normalised redundancy are dimensionless, scale-invariant measures: they detect statistical relation patterns insensitively of the magnitudes of the sample sets. These properties make both measures capable of comparing various complex network metrics.

As an illustration of the above introduced measures, Pearson correlation coefficients and normalised redundancies between some representative variable-pairs are shown on Figure C.1. In each column, a set of n=1000 values (observations) of x stochastic variable are drawn from a well-characterised distribution: uniform, normal and exponential (see bottom labels). In each row, the corresponding n=1000 values of 'variable' y are calculated using the values of x (see labels on left side), resulting in a distribution of variable-pairs with known interrelation. Given the observation vectors of x and y, Pearson correlation coefficients (C) and normalised redundancies (R) are calculated, and linear regression line (red lines) is fitted to each data set.

We note, that while the Pearson correlation coefficient is generally more noise-tolerant than normalised redundancy (see especially second and third rows), it measures strict linear dependency, and therefore in some cases fails to detect more complex relations between the sample sets (see fourth row). Also, the existence of some 'residual' redundancy at the case of independent relation (fifth row), which is due to binning errors unavoidable introduced during the probability density function estimation of the variables. In the current study, the k bin size was determined from the number of samples n by the widely applied simple rule of thumb $k = \sqrt{n}$.

Figure C.1 *(following page)*: **Illustration of statistical dependence on representative variable-pairs.** In each column, n=1000 values (observations) of x were taken and scatter-plotted against their corresponding y values in each subfigure. C: Pearson correlation coefficient, R: normalised redundancy, red line: linear regression. Columns from left to right: uniform distribution, normal distribution, exponential distribution. Rows from top to bottom: linear (identical) relationship, noisy linear relationship, noisy polynomial dependence, sinusoidal relationship and independence. $U(a, b)$: uniform distribution in the $[a, b]$ interval.

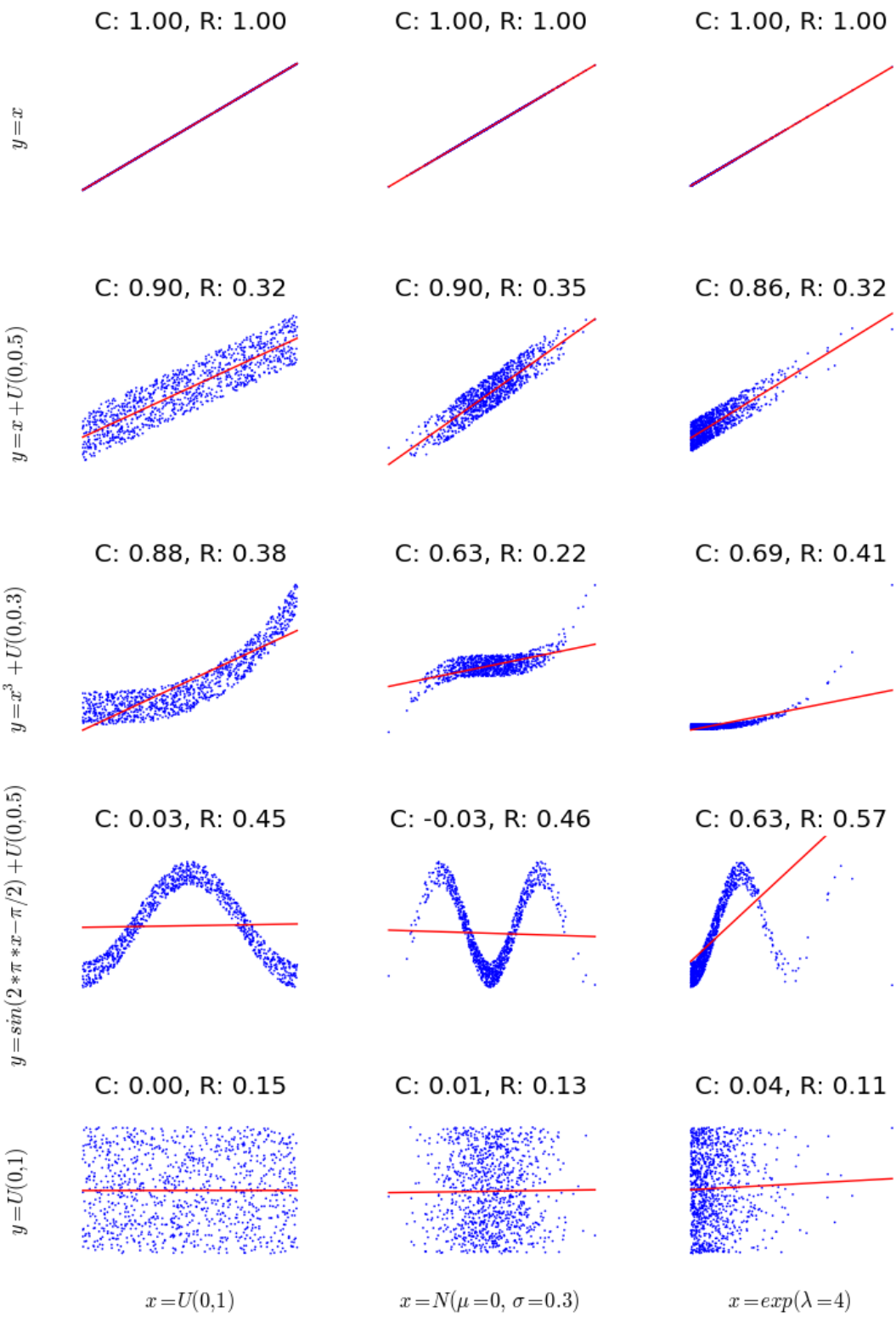
C: 1.00, R: 1.00
C: 1.00, R: 1.00
C: 1.00, R: 1.00
$y = x$
C: 0.90, R: 0.32
C: 0.90, R: 0.35
C: 0.86, R: 0.32
$y = x + U(0,0.5)$
C: 0.88, R: 0.38
C: 0.63, R: 0.22
C: 0.69, R: 0.41
$y = x^3 + U(0,0.3)$
C: 0.03, R: 0.45
C: -0.03, R: 0.46
C: 0.63, R: 0.57
$y = sin(2 * \pi * x - \pi/2) + U(0,0.5)$
C: 0.00, R: 0.15
C: 0.01, R: 0.13
C: 0.04, R: 0.11
$y = U(0,1)$
$x = U(0,1)$
$x = N(\mu = 0, \sigma = 0.3)$
$x = exp(\lambda = 4)$

Appendix D

Utilised software packages

The entire project was carried out in the Python programming environment (Van Rossum (2003)). In the following, we enumerate the several specialised Python software packages that were utilised for the various aspects of the work. These packages were integrated into a generic complex network analysis package composed of some 20 thousand lines of code, incorporating a graphical user interface, and capable of analysing, simulating and visualising networks of various properties and attributes (see Appendix B).

The NetworkX package (Hagberg et al. (2008)) was used for the representation and manipulation of the studied networks, as well as for calculating the various complex network measures in Section 4.2, 4.3 and Appendix B. Whenever it was possible, we used the NetworkX implementation of the investigated complex network measures in the rest of the work too. Due to the lack of their implementation in NetworkX, however, the following algorithms and metrics were programmed by the author in Python: network rewiring algorithm (Alg. 1), Sørensen distance (Eq. 3.1), leverage centrality (Eq. 4.2), regional specialisation measure (Eq. 4.7), small-world index (Eq. 4.8), hierarchical organisation analysis (Section 5.1), modularity calculation (Eq. 5.1), flat and hierarchical module detection (Section 5.2 and 5.3), intra- and inter-module connection density (Section 5.3.3), matching index (Section 5.3.3), symmetry (Section 5.3.3), s-core detection (Section 5.4.2), weighted rich-club detection (Eq. 5.2), modular s-core dispersion (Eq. 5.4), participation coefficient (Section 6.2), and motif counting and analysis (Section 6.3).

The numeric and scientific computation capabilities of the NumPy and SciPy packages (Jones et al. (2001)) were utilised throughout the work, from representing and manipulating vectors and matrices to performing statistical tests and calculating Fast Fourier Transformations. All the simulations and the subsequent analysis of the simulated regional time-series activities in Chapter 7, as well as the calculation of the rCBF signal and the Balloon-Windkessel model in Chapter 8, were implemented by the author in Python, building upon the functionalities provided by the

NumPy and Scipy packages.

The graphical package Matplotlib (Hunter (2007)) was used for creating the two dimensional plots of the thesis, including the hierarchical radial visualisation of the networks (Appendix E) and most of their projection images.

Figure 7.10 and the front page images of Part II and Part III are actual projections of three dimensionally rendered images, and were created with the MayaVi package (Ramachandran and Varoquaux (2011)).

The illustrations in Figure 5.1A, Figure 5.2, Figure 5.5 and Figure 5.10 were drawn manually with the image drawing software Inkscape (`http://inkscape.org/`).

This document was edited in Emacs (`http://www.gnu.org/software/emacs/`) and typeset by LaTeX 2_ε (`http://www.latex-project.org/`).

Appendix E

Abstract visualisation of large networks

Effective visualisation of large complex networks is a challenging task, which, however, can serve as an invaluable tool for gaining insight into and for the better understanding of such networks. In the context of brain networks, often not only the sheer size of the connectivity network, but also the various auxiliary data make it extremely difficult to present the observer with all the available information on a single, yet accessible image. Such additional information can include: name and spatial position of regions (nodes), direction, weight and length or trajectory of connections (edges), and further hierarchical relations among the different levels or resolutions of the network.

Besides the standard 2D projected visualisations of the brain, the ”abstract” (non-spatial) layout utilised in this work (front page figure of Part I, Figure 2.3 top, Figure 5.11 bottom and Figure 6.1 middle) is called hierarchical radial tree, and was developed by Holten (2006). We implemented the layout in Python for the current project, making it capable of visualising directed or undirected, weighted or unweighted networks generically, possessing balanced or unbalanced hierarchy structure. The basic idea behind this layout is that both the hierarchy structure (inclusive relations) and the connectivity (adjacent relations) of a network can be visualised on a single image, the former being depicted by the radial distances of the nodes from a common centre point (the origo), while the latter is made accessible by effectively ”bundling” the edges that run along the same ”path segment” in this hierarchical layout (Holten (2006)). Our implementation has some 20 adjustable parameters to manipulate the positioning and colouring of the network’s nodes and edges on the layout, as well as to select only a subset of those to be drawn.